Multi-body dynamics analysis and experimental investigations for the determination of the physics of drivetrain vibro-impact induced elasto-acoustic coupling

By

M.T. Menday

BSc (Hons.), MSc, CEng, MIMechE

A thesis submitted in partial fulfilment of the requirements for the award of the degree
Doctor of Philosophy of Loughborough University

Loughborough University

April 2003

Abstract

A very short and disagreeable audible and tactile response from a vehicle driveline may be excited when the throttle is abruptly applied or released, or when the clutch is rapidly engaged. The condition is most noticeable in low gear and in slow moving traffic, when other background engine and road noise levels are low. This phenomenon is known as clonk and is often associated with the first cycle of shuffle response, which is a low frequency longitudinal vehicle movement excited by throttle demand. It is often reported that clonk may coincide with each cycle of the shuffle response, and multiple clonks may then occur. The problem is aggravated by backlash and wear in the drivetrain, and it conveys a perception of low quality to the customer.

Hitherto, reported investigations do not reveal or discuss the mechanism and causal factors of clonk in a quantitative manner, which would relate the engine impulsive torque to the elastic response of the driveline components, and in particular to the noise radiating surfaces. Crucially, neither have the issues of sensitivity, variability and non-linearity been addressed and published. It is also of fundamental importance that clonk is seen as a total system response to impulsive torque, in the presence of distributed lash at the vibro-elastic impact sites.

In this thesis, the drivetrain is defined as the torque path from the engine flywheel to the road wheels. The drivetrain is a lightly damped and highly non-linear dynamic system. There are many impact and noise emitting locations in the driveline that contribute to clonk, when the system is subjected to shock torque loading.

This thesis examines the clonk energy paths, from the initial impact to many driveline lash locations, and to the various noise radiating surfaces. Both experimental and theoretical methods are applied to this complex system. Structural and acoustic dynamics are considered, as well as the very important frequency couplings between elastic structures and acoustic volumes.

Preliminary road tests had indicated that the clonk phenomenon was a very short transient impact event between lubricated contacts and having a high frequency characteristic. This indicated that a multi-body dynamics simulation of the driveline, in conjunction with a high frequency elasto-acoustic coupling analysis, would be required. In addition, advanced methods of signal analysis would be required to handle the frequency content of the very short clonk time histories. These are the main novelties of this thesis.

There were many successful outcomes from the investigation, including quantitative agreement between the numerical and experimental investigations. From the experimental work, it was established that vehicle clonk could be accurately reproduced on a driveline rig and also on a vehicle chassis dynamometer, under controlled test conditions. It then enabled Design of Experiments to be conducted and the principal causal factors to be identified. The experimental input and output data was also used to verify the mathematical simulation. The high frequency FE analysis of the structures and acoustic cavities were used to predict the dynamic modal response to a shock input. The excellent correlation between model and empirical data that was achieved, clearly established the clonk mechanism in mathematical physics terms. Localised impact of meshing gears under impulsive loads were found to be responsible for high frequency structural wave propagation, some of which coupled with the acoustics modes of cavities, when the speed of wave propagation reached supersonic levels. This finding, although previously surmised, has been shown in the thesis and constitutes a major contribution to knowledge.

Keywords:

impact dynamics, drivetrain dynamics, clonk phenomenon, high frequency noise and vibration monitoring, multi-body dynamics, elasto-acoustic coupling, ARMA, wavelet analysis, BEM, FEA, component mode synthesis

To Catherine

ACKNOWLEDGEMENTS

The author would like to acknowledge the support of the Ford Motor Company for this project, and other ongoing research projects, with Loughborough University.

In particular I would like to acknowledge the support and encouragement given to me by my managers Dr Heinz Foellinger and Mr Tony Weatherley at Ford.

I am indebted to my fellow engineers at Ford who have conducted many tests and have provided me with the necessary data to support this thesis. Unfortunately, there are too many to mention by name.

Dr Homer Rahnejat has been my supervisor at Loughborough University and has been a fantastic support to me throughout this period, and also for my earlier M.Sc at Bradford University.
I welcome this opportunity to put on record my appreciation of his help and advice and encouragement.

My thanks also go to Stephanos and Max in the PG office, for their help.

In conclusion, I would like to thank Catherine and our sons Roger and Stephen for their understanding and shared pleasure, and are probably as surprised as I am that this thesis has finally been completed.

TABLE OF CONTENTS

Nomenclature

a	: Radius of hollow tube
a_k	: The auto-regressive coefficients
A	: Cross-sectional area
b_k	: The Moving Average coefficients in chapter 3, and predictor in chapter 4
c	: Damping coefficient, except in chapter 5: speed of sound
c_k	: Coefficients of corrector in chapter 4
C	: Constraint function
$[D]$	: Structural damping matrix
e	: Exponential function, 2.73
E	: Expectation in chapter 3, elsewhere modulus of elasticity
E^*	: Effective (reduced) modulus of elasticity
f	: Frequency
$f(t)$	: Time history
f_c	: Coincidence (critical) frequency
f_r	: Ring frequency
F_q	: Generalised force
$F(\omega)$	: Fourier coefficient
h	: A coefficient or a division, and gap in chapter 5, except for tubes, representing thickness
I	: Mass moment of inertia
j	: Complex number $\sqrt{-1}$
$[J]$	: Jacobian matrix
k	: Stiffness, except in chapter 5: acoustic wave-number
K	: Kinetic energy
L	: Length of Eulerian beam
m	: Mass
M	: Momenta

n	: Input to filtration process in chapter 3
m, n	: structural wave-numbers
N	: Number of samples for a random process
N_s	: Number of given data segments
p	: Auto-regression order in chapter 3, sound pressure in chapter 5
q	: Order for the Moving Average process
p, q	: Acoustic wave numbers
q_j	: Generalised Eulerian co-ordinates
R	: Radius
$R_{xx}(\tau)$	: The auto-regression function
s	: Scaling factor in inertial sub-matrix
S_p^{fb}	: Sum of the forward or backward squared prediction errors
t	: time
T	: Period
U	: Potential energy
v	: Velocity
V	: Volume of acoustic cavity
$w(x)$	: Wavelet
$x(t)$	: Time series function
$\tilde{x}$	: Reversal of x
x^*	: Complex conjugate of x
x^T	: Transpose of x
$\lVert x \rVert$	: Euclidean norm of x
x,y,z	: Cartesian co-ordinates
α	: The unspecified element of a vector or a matrix
δ	: Hertzian contact deflection
δ_m	: Delta function
$\varepsilon_p(n)$	: Prediction error of the AR order p
$\varepsilon_p^b(n)$	: Backward prediction error for order p
γ_p, γ'_p	: Forward and backward reflection coefficients for order p

λ	: Lagrange multiplier
ν	: Poisson's ratio
ρ	: Density
$\rho(f)$	: Power Spectral Density
σ^2	: Prediction error variance estimate
∇_a	: Gradient with respect to the vector parameter a
ω	: Angular frequency
ψ, θ, ϕ	: Euler angles

GLOSSARY OF TERMS

ADAMS	Automatic Dynamic Analysis of Mechanical systems
ARMA	Auto Regressive Moving Average
BEM	Boundary Element Method
CAD	Computer Aided Design
CAE	Computer Aided Engineering
Clonk	An onomatopoetic word for the effects of torsion shock
CMS	Component Mode Synthesis
CWT	Continuous Wavelet Transform
DAE	Differential Algebraic Equation
DOE	Design of Experiments
DOF	Degrees of Freedom
DMF	Dual Mass Flywheel
DFT	Discrete Fourier Transform
EHL	Elasto Hydrodynamic Lubrication
FEA	Finite Element Analysis
FFT	Fast Fourier Transform
FWD	Front Wheel Drive
GRF	Global Frame of Reference
I Mech Eng	Institute of Mechanical Engineers
JSAE	Japanese Society of Automotive Engineering
LH / RH	Left Hand / Right Hand
LPRF	Local Part Reference Frame
MATLAB	Matrix Laboratory
MBD	Multi-Body Dynamics
MT75	Manual Transmission (5 speed)
NOF	Nodal Degrees of Freedom
NVH	Noise, Vibration and Harshness
PSD	Power Spectral Density
RWD	Rear Wheel Drive

SACHS	Supplier name for clutches and couplings
SAE	Society of Automotive Engineers (USA)
SEA	Statistical Energy Analysis
SGF	Supplier name for rubber coupling
SHM	Simple Harmonic Motion
SIMULINK	Simulation and Link
STFT	Short Time Fourier Transform
VER	Vehicle Evaluation Rating

ABAQUS
PATTRAN
ABAQUS
SYSNOISE FE / Software / Tools.
IDEAS
NASTRAN
FORTRAN

LIST OF FIGURES

LIST OF TABLES

Chapter 1

Introduction

1.1 Driveline clonk in motor vehicles. Problem Definition.

Clonk (sometimes referred to as *clunk*) is an unacceptable audible and tactile driveline response from the driveline, which may occur under several different driving conditions, as follows:

Tip-in clonk may occur, when the throttle is rapidly applied from coast.
Tip-out (or *back-out*) *clonk* may occur, when the throttle is abruptly released from drive.
Clutch engagement clonk may occur after gear selection, if the clutch is rapidly engaged. This happens on pull away, but it is more noticeable during low speed creep manoeuvres.
Shift clonk may occur during a gear up-shift.
Clonk may also occur, when a road input accelerates through a driveline backlash.

The throttle-induced tip in and tip out clonks, and shift clonks, *are not* affected by the clutch or its actuation. By comparison, clutch engagement clonk *is* directly affected by the clutch.

In all of the above driving conditions, the resulting torsional impulse delivered to the driveline gives rise to a short duration vehicle jerk and an accompanying metallic clonk or thud noise. Clonk may or may not accompany low frequency vehicle longitudinal fore and aft motion, referred to as *shuffle*, which is the fundamental rigid body torsional mode of the drivetrain.

If the vehicle is exposed to shuffle, which is a relatively lightly damped mode of vibration, having many cycles of oscillations, then it is probable that multiple clonks would occur with every shuffle cycle. This happens every time the alternating torque passes through a lash zone. There could be 5 or 6 clonks, when a shuffle mode is excited.

The audible clonk signal is seen as a high frequency component, which is attached to the lower frequency tactile shuffle carrier wave.

Figure 1.1 shows actual vehicle data that was recorded during an in-gear braking manoeuvre below the idle engine speed without clutch slip. This induced an 8 Hz shuffle response. As a result clonk may occur each time the shuffle transient passes through zero lash torque.

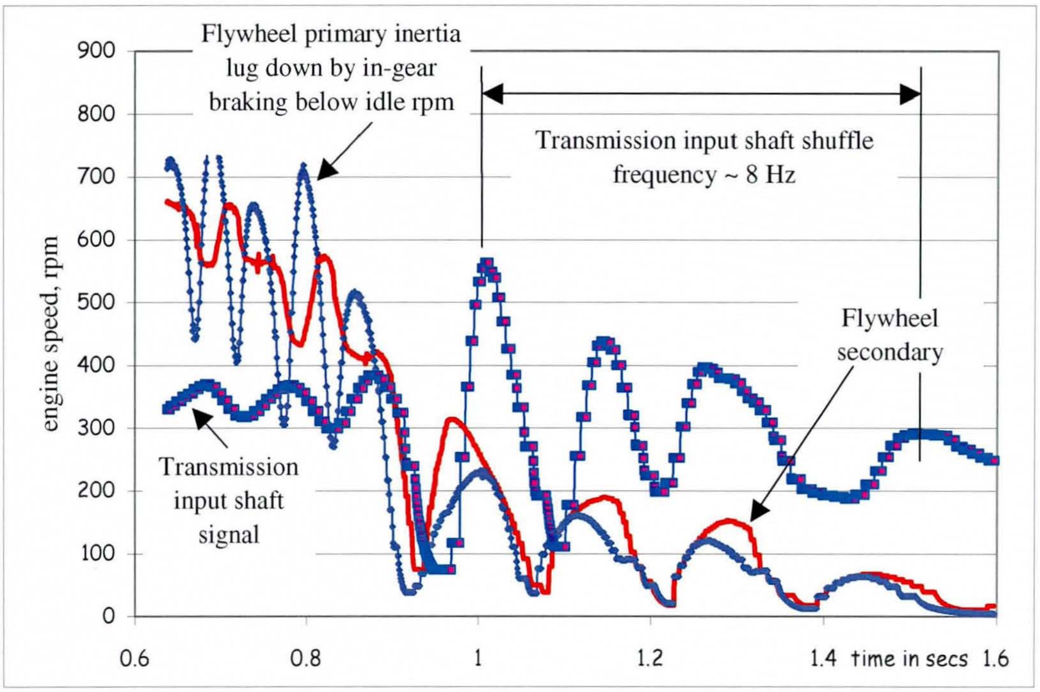

Figure 1.1: Shuffle induced by in-gear braking

The presence of backlash in the driveline also causes the shuffle mode to have a higher initial overshoot response and a slower transient decay, when torque excites the mode.

Shuffle and clonk are two *error states* of the vehicle driveline dynamic system.

Shuffle may be readily excited, if a multiple gear up-shift is made, which pulls the engine speed down into the shuffle frequency domain.

Figure 1.2 is the actual vehicle data collected during normal use. Each data entry is a point in time. The effects of the 5 gears are clearly identifiable. The 1st gear is less well-defined due to the need for clutch slip modulation.

The speed drop-down is illustrated in the following gear speed structure, where a typical up-shift from 2nd gear to 5th gear could result in an engine speed of 1000rpm sufficient to excite shuffle.

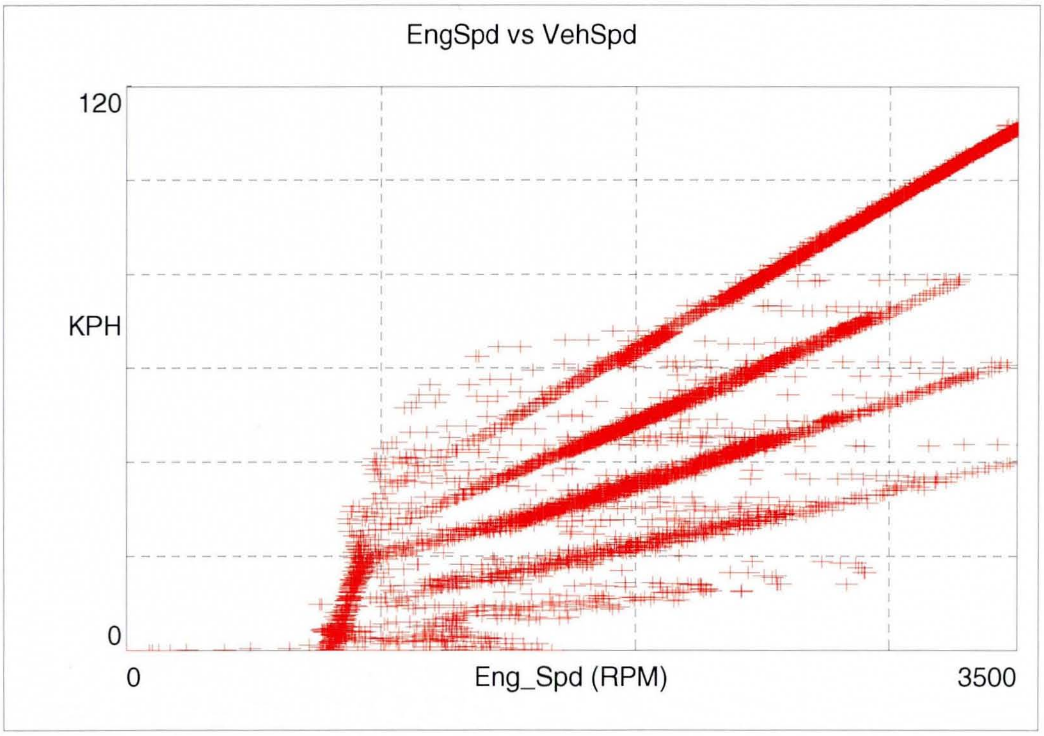

Figure 1.2: Measured engine speed variation in different gears

The clonk noise complaint is usually most noticeable in low gear and whilst driving at low road speeds, when engine and road noises are at a reduced level. However, clonk is not so readily excited, even in a complaint vehicle, at higher engine speeds and when engaged in higher gears.

Driveline clonk is not a new phenomenon. However, it is more noticeable for several reasons:

- Vehicles are more responsive with higher torque rise rates
- Lubrication fluids are less viscous and operate at higher temperatures
- The output power-to-weight ratio has increased over time
- Materials are lightweight and have much less inherent damping
- Background noise levels are much lower
- Customer expectation is much higher

Surprisingly the generation of clonk noise in a vehicle is little understood and there is little published data.

- It is believed to be multi-sourced and to have multiple vibration and noise propagation paths.
- It is thought that its originating source is impact-induced through backlash in gearing and/or splined connections, but the extent of sensitivity is not fully understood.
- It is not known if there are potential root causes other than backlash.
- It is not known how or if clonk varies with vehicle model variants - suspension, engine type, body, powertrain, etc.
- The variability between nominally identical vehicles is not fully understood.
- The effect of piece-to-piece variation in manufacture and assembly is not investigated to any great detail.
- It is not clear what effect, if any, wear of load bearing members has on the deterioration of the clonk response.
- The relationships between backlash, engine torque characteristics, and vehicle model type are not yet established.
- The relationships between functional and component variability in the driveline are not understood.

Clonk is a function of many parameters including backlash, torque rise rate, clutch engagement rate, speed differences during torque engagement, inertial loading, and several other factors. Clonk will not occur in a driveline with overall zero backlash.

Therefore, clonk will not occur when applying torque from a drive condition, when the entire driveline lash has already been taken up. Of course it is not possible to build and to operate a driveline with no backlash. It should also be noted that lash clearance between impacting bodies is a prerequisite for component assembly and durability. Thus, it is necessary to find a way to manage clonk in the presence of lash.

It has been established that the subjective variation of clonk between production vehicles of nominally identical build specification is surprisingly large. It has also been established that different customers with different driving styles, will excite driveline clonk to a greater or less extent *even in the same complaint vehicle.* One reason for perceived clonk variation is simply that the initial lash conditions at each lash site are different every time a driving manoeuvre is made, which itself is a variable factor.

This knowledge raises the possibility that, if the underlying causal mechanism and aggravating factors are fully understood, it should be possible to establish design guidelines that would robustly prevent customer complaint.

1.2 Aims of this investigation

Vehicle noise, vibration and harshness (NVH) problems such as clonk are difficult to predict and to manage, due to:

- the system complexities,
- the numerous non linear factors,
- the redundancies in the system,
- the *noise factors*, (those that are of a semi-random nature and are not readily controllable, but can affect performance),
- the interactions of the numerous vehicle sub-systems,
- the variability issues in powertrain constructions,
- the design compromises that are often required

As a consequence, it is often necessary to resolve NVH concerns by the late and costly addition of design palliatives.

Typical clonk palliation may include throttle damping, torque rise rate control, backlash control, driveline compliance, clutch slip control, and engine management. Sometimes the effectiveness of the palliation is compromised by lack of package space, weight limitations, manufacturing and assembly issues, available time, dynamic interaction, and many other factors. As a result, the added value from NVH palliation can sometimes be disappointing and not very cost effective.

Therefore, the overall aim of this thesis is to understand the sensitivity of the driveline to clonk and the factors that affect it (backlash, torque rise rates, clutch engagement rates, etc), and to identify robustness criteria, which achieve product quality by minimising the causes of variation without necessarily eliminating them. If backlash is a cause of clonk it may not be necessary to reduce it. Effects of backlash should be managed in the knowledge of how the noise is generated.

Thus, clonk is one of the driveline error states. It is desirable to seek and to maximise the driveline system functionality - which is to deliver torque to the road wheels - at the expense of the error states.

This thesis intends to show how a robustness philosophy and appropriate methods of analysis may be applied to driveline clonk to help avoid palliation or to maximise its effectiveness.

There are specific aims and objectives within this research. They are:

- To carry out a fundamental study of the driveline clonk phenomenon through combined experimental investigation and numerical predictions.
- To highlight the source(s) that contribute to the clonk problem, including the investigation of the following:
    - The impact mechanism through impulsive action in load bearing members such as meshing gears and spline joints.

- o Multi-body analysis, including the effect of component flexibility/compliance, to investigate the effect of impact(s) within the overall system and its modes of propagation.
- o Mechanism of structural wave propagation in drive train components.
- o An elasto-acoustic coupling study, leading to sound radiation from structures and cavities in the system.
- o Verification of hypotheses and numerical predictions with experiment. Use of component and rig and vehicle test data to support verification.

1.3- The Research Approach

The research study reported in this thesis, focuses on causal excitation and local driveline response factors within the clonk frequency range and assumes insignificant contributions from vehicle body and suspension. This assumption sets the boundary limitation for the development of mathematical simulation and experimental rig-based investigations, which by this virtue can be more readily created and to be offered for correlation studies.

An assumption has been made that the clonk phenomenon is based on torque factors alone. Therefore, bending has not been considered either in experiments or in simulation.

For the experimental investigations several approaches have been taken. These include vehicle-based tests on a chassis dynamometer, a floor mounted driveline rig, and component modal testing. A number of key factors have been considered in the development of the rig. These are discussed in some detail in Chapter 3. An outline of the important requirements for such a rig is given.

An applied torque pulse, being representative of the vehicle condition with throttle tip in, must be applied to the driveline rig. This impulsive action will accelerate through a backlash zone of minimal resistance at the first impact site. The torque path will continue to the succeeding lash sites as each lash gap is closed by impact. Clearly, there will be multiple sequential impacts along the driveline at each lash zone along the torque path, until the torque would finally accelerate the vehicle inertia and the total driveline lash will then be considered to be closed. In the experimental rig, the rear axle may be clamped in order to investigate the effect of reflected waves, which are thought to be troublesome. This variation between the rig and the vehicle calls for some rig-to-road vehicle correlation studies to be carried out.

The driveline has numerous locations where backlash may be observed. Therefore, the rig must incorporate all such zones. These include:

- *At the clutch disc*: A very low rate predamper spring with a wide operating angle is be fitted to the clutch disc to control transmission idle rattle, and this is in effect a major source of driveline lash.
- *Lash clearance between the clutch disc hub splines and the transmission input shaft*: Spline clearance is required at this location to allow free translation of the disc and to avoid clutch drag during gear shifting and clutch disengagement. However, the shaft diameter is usually only 25 mm, hence the desired longitudinal spline clearance will result in a high level of angular free play (backlash).
- *Lash clearance between meshing gears*: This occurs in the transmission after the synchronisation cones have allowed engagement.
- *Lash clearance in universal joints.*
- *Lash clearance between the drive pinion gear and the crown wheel at the rear drive axle.*
- *Lash clearance in the drive axle between the side gears the drive axle half-shaft spline engagement:* A similar condition exists here as that described above for the clutch hub spline.

At each lash zone there are dry or greased or oil lubricated contacts, and these may also be contaminated by debris or heat effects, giving rise to different energy transfer conditions and contact times, at each lash zone.

Lash magnitudes are a function of normal piece-to-piece production variation, and also a function of normal wear in service. It is for these reasons that driveline clonk is considered to be a system problem, since there are multiple noise sources in the driveline.

Any fundamental investigation of the clonk problem necessitates the use of extensive numerical predictive methods. This is particularly true, because the phenomenon occurs over a very short transient time of the order of a few milliseconds. Furthermore, the physics of the problem, from the point of induction by impulsive action and short impact duration, through to structural wave propagation and acoustic radiation is not fully understood. Hence, this thesis presents a multi-disciplinary and detailed numerical analysis of the problem, which together with the experimental investigations facilitates a detailed understanding of the dynamics of the problem.

The numerical work includes:

- Multi-body dynamic analysis of the drivetrain system to include rigid body inertial degrees of freedom in a detailed mechanism model, based upon constrained Lagrangian dynamics.
- The inclusion of an impact model to represent the onset of impulsive action, which is based upon Hertzian impact dynamics.
- The incorporation of component flexibility through the use of the component mode synthesis technique with the super-element finite element analysis to investigate the mechanism of structural wave propagation in thin elastic members.
- The above models are combined to create an elasto-multi-body dynamic predictive tool for the system.
- The use of super-element finite element analysis, as well as boundary element method to represent acoustic cavities in the driveline system, such as the thin walled hollow driveshaft tubes.

The above combined analysis commences from the point of impact with localised Hertzian deformation, leading onto structural wave propagation superimposed upon the rigid body motion of the drivetrain system, which in turn excites the acoustic modes of the above-mentioned cavities through structural-acoustic coincidence.

1.4. Structure of the thesis

A roadmap of the thesis shows the study areas by Chapter number, which are as follows: (See table 1.1)

- Research studies.
- Subjective studies.
- Objective studies.
- Modelling studies.

Thesis roadmap

Study	RWD commercial vehicle		FWD passenger car
	2-piece driveline	**3-piece driveline**	
Subjective evaluation	*Road test*		*Road test. Chassis dynamometer used for Design of Experiments subjective testing*
Objective evaluation	*Static floor mounted driveline rig used for Design of Experiments.*	*Dynamic driveline rig to be used for Design of Experiments. (Rig is under construction and is not reported in the thesis)*	*Road test (noise and vibration). Component NVH. Chassis dynamometer DOE testing used for Design of Experiments testing.*
Modelling - rigid body	*ADAMS multi-body analysis of driveline with clutch impact*	*ADAMS low frequency multi-body analysis of driveline with gear impact.*	
Modelling - finite element	*Structural modal analysis of driveshaft tubes with ramp torque input.*	*High frequency modal analysis of drive shaft and acoustic cavity, coupled with the ADAMS model.*	

Table 1.1: A "roadmap" to the structure of the thesis

Chapter One provides an introduction to the problem investigated in this thesis, with clear aims and specific objectives. An outline of research methodology is also provided.

Chapter Two provides a review of literature pertinent to the various aspects of the undertaken investigation. The review includes the works reported on driveline clonk, where a dearth of previous investigations is clear, and related subjects. The survey is necessarily wide ranging due to the multiplicity of interacting phenomena, such as impact dynamics, multi-body approaches, component mode synthesis, signal acquisition and processing methods for high-frequency short-lived transient events.

Chapter Three is concerned with the experimental investigation and measurement of clonk at the vehicle and rig level. It provides detailed considerations in rig design, as well as methods of actuation, data acquisition and processing. Both commercial vehicles and passenger cars, and front and rear wheeled derivatives, are considered. Clonk is measured in the vehicle whilst on the road. This is correlated to a driveline rig, which is used to reliably capture experimental data. A front wheel drive vehicle is also set up on a chassis dynamometer to conduct a DOE-Design of Experiments.

The design and objectives of the floor mounted driveline rig are considered. This includes the method of torque pulse application, the torque reaction, and the rig measurements.

An experimental Design of Experiments orthogonal test matrix is established in order to evaluate the effects that various factors have on the generation of clonk.

Chapter Four describes the multi-body dynamics theory used in the thesis. It gives an overview of the constrained Lagrangian dynamics for the generation of equations of motion for an assembly of components in the system model, as well as the formulation of holonomic and non-holonomic constraint functions that represent the joints and attachments in the system model. The method of solution is described for a set of Differential-Algebraic Equation (DAE) set. Issues related to numerical simulation exercises such as numerical error control and convergence criteria are also highlighted.

The chapter proceeds to describe the specific drivetrain model(s) created in multi-body formulation, with a description of the geometrical and physical data for a number of pertinent driveline configurations.

Chapter Five considers the numerical analysis of driveline impact dynamics. It focuses on the impact phenomenon in meshing gears with backlash. Assumptions made are described and the inclusion of the impact model within the multi-body model of the drivetrain system is explained. This chapter also considers component elastic compliance theory applied to drive shafts and the associated modal behaviour obtained through component mode synthesis. Furthermore, it considers the acoustic emission from radiating surfaces in the driveline, and also the internal acoustic cavity modes of the transmission and drive shafts. Frequency coupling of the structural and acoustic components in the driveline is described.

Chapter Six is concerned with the theoretical and experimental results and the correlation between them. The chapter provides the numerical predictions by the elasto-acoustic-multi-body model, being the amalgamation of all the theoretical models described in the previous chapters to form a multi-physics framework for the numerical analysis. The results obtained in this chapter and those previously reported in the preceding parts of the thesis are compared with the experimental findings, both for rig-based and on-road vehicles, in order to validate the model(s) as well as to gain a fundamental understanding of the interacting phenomena, which is the overall aim of the research study.

Chapter Seven provides the concluding remarks, highlights the novel aspects of the reported research, the contributions made to knowledge, a critical assessment of the approach undertaken in the thesis, and it proposes several pertinent areas for future work.

Chapter 2

Literature Review

2.1. Introduction

As described in chapter 1, driveline clonk occurs when a torque pulse is applied to the driveline, and this is caused by an abrupt use of the throttle and/or clutch or even road inputs. Elastic impact then occurs at every location in the driveline, where there is a clearance between bodies in contact in the torque path.

The end result of this Dirac type torque pulse is to generate high frequency waves in lowly damped structures. These waves are responsible for the high frequency clonk noise. The emission is aggravated, when there is frequency coupling between the structural and acoustic eigenmodes of the driveline system, mainly occurring at the bell housing and the hollow drive shafts.

The perception of clonk is that it is extremely variable, due to many factors. It is sensitive to driving style, the gear selected, road speed, drivetrain combination, and many other factors. But it may be summarised as an event that occurs when the excitation energy is matched to the system characteristics.

The phenomenon must, therefore, be captured at the *system* level, even though there are many initial impacts at the *component* level. This means that in order to fully understand the clonk mechanism it is necessary to generate a system level model simulation of the impact and then to examine the dynamic repercussions through the system.

A further requirement is that the numerical model generation must be fully supported by experimental data to confirm the validity of the mathematical model. This is especially important when one considers the extremely short duration of the event, which is of the order of only milliseconds.

Hence, the literature review focuses on both experimental and theoretical aspects of the investigation, as well as the noise generation mechanism that arises from impact-induced wave propagation.

2.2 Review of literature pertaining to driveline dynamics and impact

As a result of this literature survey, several benefits should accrue:

- An awareness of the analytical and experimental techniques, and their benefits and limitations, with general regard to torsional vibration analysis in drivelines.
- An awareness of the specific information available with regard to the NVH (Noise, Vibration and Harshness) phenomenon of driveline clonk. Additionally, an awareness of the key parameters that have been found by others to be influential in the examination of clonk, so that these could be considered in this thesis.
- An awareness of the applicability of Quality Engineering methods, particularly Taguchi type controlled designed experiments, and the understanding of dynamic factor contribution to driveline clonk.
- The need to first identify the prime causal reasons for functional variability and then to identify design control factors to shift the system gains and hence achieve the desired targets. The literature survey would help to identify these causal factors.

A definition of driveline clonk:
A short duration audible transient response. Usually the result of a load reversal, and in the presence of backlash (Krenz, 1985).

This thesis considers the driveline clonk mechanism, and the many driveline factors that need to be considered in the noise generation. Many coincident impacts will occur when demand torque is transmitted along the driveline and through several lash zones. As a consequence, this thesis considers the following items are a summary of the important interrelated subject areas in the study of driveline impact:

- Elastic contact under a steady applied load.

- Elastic impact under dry contact conditions.
- Transient elastohydrodynamic (EHL) lubrication.
- Elastic wave propagation following impact.
- Structural multi-body dynamic analysis of the driveline.
- Pulse tailoring of the input signal.
- Elasto-acoustic coupling and frequency coincidence.
- Design of Experiments methodology, as applied to time-dependent events.
- Signal analysis of transient impacts, hidden in unwanted noise.
- Finite element modelling and eigenmode analysis of acoustic cavity volumes.
- Finite element modelling and eigenmode structural analysis of thin walled cylindrical shells.
- Acoustic radiation and efficiency of excited thin walled shells.

Krenz (1985) has given one of the most descriptive accounts of driveline clonk. He defined clonk and shuffle as a vehicle transient response to a driveline torque reversal that can occur during throttle tip-in from coast to drive, and throttle tip-out from drive to coast. In the presence of lash, the engine speed changes with respect to the rest of the driveline during a torque reversal. When all the lash is taken up, a torque pulse is generated which is transmitted to the vehicle through the drive wheels and suspension.

Note: Tip-in is the so-called fast application of throttle pedal. Tip-out or back out is an abrupt throttle pedal release.

Lash is the initial clearance between parts before they impact. Lash will have a zero magnitude with tip-in from drive (i.e. a preloaded system), and it will be a maximum when driving from coast.

Driveline backlash may be described as the summation of lashes at each contact zone in the driveline, including the major lash effect of the clutch disc low rate predamper springs.

This thesis focuses on the impacts at each lash point, and the contribution of the many potential driveline impacts to the overall radiated clonk noise.

There are many lash locations in a geared driveline system, and each lash point has an associated pair of impacting inertias. The lash zones in a Rear Wheel Drive (RWD) driveline are:

- The clutch disc hub spline lash clearance to the transmission input shaft.
- The clutch disc low rate predamper springs - the largest single lash source.
- The transmission free play between gears in mesh and transmitting torque.
- The universal joint spline free play.
- The final drive lash between pinion and crown wheel.
- The half-shaft spline lash.

All of the above lash zones are subjected to degradation, which is wear and time related. This increases the lash travel and reduces the lash drag, both of which degrade clonk.

Richards (1981) concluded that noise due to backlash alone was due to very short impact times and to the high frequencies associated with the impact, arising out of lack of cushioning lubrication and surface roughness.

The driveline torque versus time profile (torque rise rate) is a useful way of explaining the event sequence during throttle tip-in or tip-out (see Figure 2.1)

At t=0 the throttle is applied while the vehicle is in coast (negative torque). As the air / fuel mixture to the engine increases, the axle torque increases until it reaches zero. At this point the axle torque remains at zero, whilst the engine accelerates through the backlash with little or no resistance (Krenz, 1985).

Lash is assumed by Krenz (1985) to have zero resistance and is accumulated at the final drive axle from where the major impact occurs, although this is a simplification.

Krenz (1985) wrote: 'after the lash zone, a positive torque transient occurs. The initial torque rise rate that is the most steep, generates the high frequency metallic noise, if any.'

Shuffle is the first torsion driveline mode and it may be easily identified and simulated using a 2 or 3 degrees of freedom mathematical model. The lowest shuffle frequency, dependent on driveline gearing, is approx. 2,5 Hz which equates to a 400 ms cycle period. It is fundamentally related to the side shaft torsion stiffness.

A vehicle shuffle mode may be excited by a short torque transient or an impulsive road input, and will worsen in the presence of driveline lash. Shuffle may be lightly damped and multiple shuffle cycles may occur after excitation. Clonk on the other hand, requires the presence of lash, and a zero lash driveline is not likely to clonk (Hrovat, 1989). Shuffle can readily be identified with a simple two or three degree of freedom model, because it is the fundamental driveline torsion eigen-frequency.

Shuffle may be minimised if iteration is used to find the optimum input torque pulse shape that optimises the active system parameters. This process works only if backlash is absent (Tobler and Tsangerides, 1985).

Krenz (1985), and others (Tobler, 1983, Ambrosi and Orofino, 1992, and Biermann and Hagerodt, 1995, 1997, 1999) have also studied the relationships between audible clonk and shuffle. The first swing on the torque transient, which can be 2-3 times greater than steady state torque, is the basic clonk response. This is perceived as a short duration jerk and may be accompanied by a low frequency boom or thud sound (Krenz, 1985).

Backlash is the link between shuffle and clonk. Backlash aggravates shuffle but is not necessarily the root cause; backlash aggravates clonk and is probably the root cause. Hence, it is possible to generate a shuffle response with minimum audible clonk. It is also possible to generate a single audible clonk without the associated shuffle.

Reference has been made in the literature to a high frequency metallic noise, and also to a low frequency thud. The first may be the noise perceived by the driver when the door window is lowered, and the clonk impact noise is then airborne directly from the driveline impact zones.

The driver may also perceive the low frequency thud with the windows closed, and the clonk noise is then said to be structure borne. Both noise conditions may emanate from the same noise site(s).

Following the initial clonk response a low frequency torque variation occurs. This is the shuffle response, which is perceived as a fore and aft surge, which may last up to a second.

A study by Steinel (1990) showed that a multiple sequence of clonks with associated shuffle would be more readily achieved on a downhill test when the lightly damped shuffle mode would persist longer. Their study also showed that clutch torsion damping in the disc hub springs was not effective against shuffle, but a viscous damper would be effective. However, this adversely affected gear shiftability due to the increased inertia to be synchronized in the transmission. They observed that the main cause of shuffle was engine management.

Krenz (1985) made an important and interesting - but not substantiated - observation on the relationship between clonk and lash:
Clonk severity increases with driveline lash but not necessarily in a linear manner. If one accepts that minimal lash is an assembly and design requirement for a geared system, then the study of clonk then becomes one of how best to manage the lash and impact variations from location to location in the driveline, and from vehicle build to build.

Krenz (1985) suggested that clonk control had been managed in the past by the use of tighter lash controls and optimum clutch disc tuning, but this was no longer effective due to;

- Lower levels of driveline torsion compliance.
- Customer requirement of 'fun to drive' throttle response.
- Transmission idle rattle control mandated the use of low rate clutch disc predamper springs with wide-angle characteristics.
- The increasing uses of responsive fuel injection systems.
- (In the case of auto transmissions), the introduction of lock up clutches with direct drive.

Krenz (1985) made several clonk prevention design suggestions, but without a verification of their effectiveness:

- To minimise the engine torque rise rate at the flywheel.
- To minimise driveline lash (however, no suggestion was made as to how transmission idle rattle would be palliated without use of predamped clutches).
- To optimise driveline compliance to reduce the severity of impact responses. This could reduce clonk, but insufficient damping would then worsen the shuffle response.

The balance between compliance / damping / engine performance / rattle / clonk was delicate, and Krenz (1985) warned that even optimum tuning may not be a feasible option.

Krenz (1985) proposed several palliative actions for clonk attenuation:

- Use of a throttle dashpot to increase torque rise time. It is known that this was effective against shuffle, but was not proven against clonk.
- Use of compliant elastomeric driveline couplings (although it was doubted if the necessarily low rate coupling would have sufficient capacity to prevent lock up under normal driving conditions).
- Progressive throttle linkage (but this gave a consequent loss of customer 'fun to drive' responsiveness).
- Controlled clutch slip engagement. This was attractive and had proven merit, but electronic clutch control systems were costly.
- Ignition spark retard

In summary, Krenz (1985) had submitted one of the few surveys that described the specific features of clonk, albeit without significant analytical justification or experimental verification.

Subjective benchmarking of competitor power trains had identified that some transmissions were much more sensitive to *rattle* than others (Biermann and Hagerodt, 1995, 1997, 1999). In addition, the associated flywheel angular acceleration levels were much higher, adding to the rattle levels.

This had mandated the use of low rate clutch disc predamper springs to palliate the idle speed rattle. This in turn had subjectively worsened clonk. As a result it became necessary to further understand the clonk concern and the principal clonk contributors in the driveline, and Aachen University was commissioned to conduct some basic research in 1995.

This study is believed to be the first attempt to understand the generic behaviour of driveline clonk (Biermann and Hagerodt, 1997, 1999). The front wheel drive (FWD) driveline, from flywheel to wheels, was mounted in a test fixture. The transmission was compliantly mounted and the wheels were rigidly fixed.

An impulsive shock torque was applied to the transmission input shaft by means of an instantaneous release of a torque preload to the system. The fixed wheels provided the torque reaction. The transmission housing was partially cut away to allow access for instrumentation to the shafts and gears for lash measurements.

A microphone was positioned near to the transmission housing, and noise recordings were also taken with a binaural head at the driver's head location.

The rig noise recordings were found to correlate to the vehicle condition for clonk.

A mathematical simulation with four degrees of freedom was employed by Biermann and Hagerodt (1997, 1999) to identify the driveline natural torsion mode shapes and frequencies, and to assist with the test results.

- The first eigenvector corresponded to the shuffle mode, and the shuffle mode frequencies for each selected gear were evaluated.

- Lash was introduced to the model and the effect was to superimpose a higher frequency (ca. 55 Hz) on to the shuffle carrier wave frequency. This was identified as transmission gear rattle between the non-load carrying gears in mesh.

- For all transmissions, the clonk frequency range was found to be 500 - 3000 Hz. The clonk duration was approximately 125 ms. A clear relationship between transmission housing acceleration and the impacting pulses was noted.

- The effective 'rotating impulses' and the corresponding equivalent sound pressure ratios were calculated and were found to have a linear relationship. This fact, and the observed correlation between impulses and housing acceleration data, indicated that the impulsive nature of the driveline impacts provided the mechanism for the perceived clonk.

The following influential factors were observed by Biermann and Hagerodt (1995, 1997, 1999):

- The effective rotational impulse of the final drive (FWD) was significantly the major contributor to clonk.
- The transmission housing cut-out (for instrumentation) had an insignificant effect on escaping clonk noise.
- The deletion of the clutch predamper was *very* significant, reducing clonk by up to 7dB(A) on the rig.
- Stiffer / hollow side shafts increased back out clonk by 3 dB (A) on the rig.
- Lower levels of clonk were recorded in the higher gears.

Using basic physics, since rotational impulse equated to the product of inertia and angular velocity, it was proposed that:

- Decrease the *inertia* of impacting components - to reduce the sound level *magnitude*. The transmission having the highest inertia was caused by the greatest separation between main shaft and countershaft.
- Decrease the torque pulse:
- By matching the system with regard to clutch characteristics,
- By increasing the driveline damping,
- By increasing the transmission component and housing damping, and

- By effective lash 'bridging' - to shorten the sound *duration.*

Both *magnitude* and *duration* were considered to contribute to perceived audible clonk, although the balance was not defined.

A linear relationship was found between excitation torque preload and the clonk response within the range of tests.

The final drive was considered to be *the decisive contributor to clonk*, due to the high inertia and rotational impulse compared with the other driveline components in impact. Not known, was the influence of final drive lash. Clonk was significantly improved on the rig (duration and magnitude were reduced) by the deletion of the clutch predamper, although it was acknowledged that this action would worsen rattle. Not studied, was the effect of a more gradual transition from low rate predamper to main damper or a progressive reduction in predamper spring travel.

The Aachen investigation pioneered a greater generic understanding of the clonk phenomenon than had previously been achieved.

2.3- System level driveline analysis

According to Newton's Second Law of motion the rate of change of momentum of a body is proportional to the force acting on a body and is in the direction of the applied force – this may be applied to a vibrating system using differential equations of motion to describe the system.

A vibrating system has n degrees of freedom if n independent co-ordinates are required to define the natural movements of the system. As a result, an n degree of freedom system will require n differential equations to define the motion. Solution of the n equations will yield n natural frequencies / eigenfrequencies of the system, and their associated mode shapes (eigenvectors) (Norton, 1989, Shearer *et al*, 1967). For large displacement low frequency systems the modal definition may be readily achieved with a low n; for small displacement higher frequency systems with complex phase relationships, a much higher n is required. Hence the computation effort goes up rapidly with n.

The differential equations may be derived from Newton's laws of motion and are characterised by mass /spring/damper values in the case of interconnected rigid bodies. It is normal to simplify the system under investigation and to reduce the number of equations to be solved.

Figure 2.2 shows schematically how a multi-modal mechanical system nay be represented by a series of mass/spring/damper elements and how they may be coupled by damping factors. This is a mutually inclusive concept. In other words, a mathematical model may be constructed to simulate a mechanical vibrating system; additionally a system may be built and tested to yield an output which may be translated back into mass/spring/damper elements.

The governing equations are *second order*, because acceleration is the second derivative of displacement with respect to time and it is the highest derivative in the equations of motion.

The vibrating system may be assumed to be *linear* if:

- The stiffness term in the differential equation follows Hooke's linear elastic law, so that the deflection is proportional to applied force, and
- The damping term in the differential equation assumes that velocity is proportional to force. This is known as *viscous* or ideal damping.

Solution of the ***n*** linear ordinary differential equations of motion with constant coefficients of stiffness and damping is much easier than the solution of non-linear equations. For this reason it is advisable to linearise the stiffness and damping functions if possible, although usually the non linearities peculiar to the driveline are too discontinuous to be linearised. The response of vibrating structures is considered later in the study. It is useful to visualise the structure as a summation of discrete vibrating systems each having its own stiffness and damping functions, linear or non-linear (See Figure 2.2)

Impacting energies will excite this structure into numerous resonances. When forced and damped, the linear system response will be composed of *steady state* and *transient* elements. The transient response is due to an asymptotically stable point *attractor,* which is independent of initial conditions. When the forcing function is a step input, the time domain response of the linear system is very similar to that of the *shuffle* mode. It has an initial rise time to overshoot, then decays through periodic cycles to a steady state, which is dependent on system damping.

By way of illustration, figure 2.3 shows a shuffle response with damping. The shuffle is excited by tip-in from drive and so backlash effects are not considered.

By comparison, Figure 2.4 shows a shuffle response including backlash effects, by a tip-in from coast or overrun. Note the overshoot magnitudes.
Both Figures 2.3 and 2.4 illustrate the effects of torque ramp times on the shuffle response.

Figure 2.5 shows a comparison between a slow and fast torque ramp, on the shuffle response.

The non-linear behaviour is so-called, because the damping and / or stiffness coefficients in the equations of motion are *not* linear. The driveline may be represented by a series of interconnected masses, springs and dampers and these are fundamentally non-linear. This means that normal solution methods cannot be applied. It also means that proportionality does not apply, and the response may change radically with a change to the forcing function. Linear systems harmonically forced will respond at the same frequency, but non-linear systems may respond at non-sinusoidal oscillations. The steady state response of non-linear systems depends on initial conditions, whereas the linear system does not. Typically, the initial conditions in an actual drive environment are never the same, and so the behaviour is not predictable.

The resonance of linear systems is directly related to stiffness and inversely related to mass. By comparison, the non-linear system resonance, is dependent on the non-linear restoring spring force, which may have a *hard* or *soft* characteristic. The non-linear system resonance may have two levels of resonant amplitude response at the same frequency in a region of instability that is influenced by initial conditions (Cook, 1986).

Such non-linear system characteristics are important in driveline NVH, particularly shuffle and rattle. The effects of these non-linearities on excitation of the clonk response are of particular interest, and also on the subsequent ability to predict the clonk response.

A non-linear vibrating system with *hard* springs will exhibit the so-called *jump* phenomenon when excited. For any given excitation frequency the non-linear system will have two different response magnitudes at resonance, dependant on initial conditions. The response may *jump* between the two response states (Cook, 1986, Stoker, 1950, and Broch, 1984). In comparison, the conventional linear system will respond at resonance at the same frequency as the excitation and will have a single valued response.

A non-linear system with the *hard* spring will have a resonance that *increases* with frequency; the soft spring resonance *decreases* with frequency.

This resonance phenomenon is pertinent to the study of non-linear dynamics of a driveline. The implication for the driveline, is that perceived functional variation may be caused in part by the *jump* factor. It has a somewhat limited contribution in a clonk study because one is mainly concerned with the physics of localised impact and not on the subsequent global system vibration behaviour. However, one must consider the *initial condition* variation of a non-linear system. The initial conditions of displacement and velocity are probably not known - when the clutch or throttle is actuated - and yet the motion of non-linear systems depends crucially on this information.

Excitation of shuffle and clonk in a vehicle may also depend critically on engine and road speed conditions when the torque pulse is applied. The response depends heavily on this, Figure 2.6 illustrates the shuffle effect by gear and by engine speed. Shuffle is measured by the driver seat longitudinal acceleration.

Chaotic behaviour in some non-linear systems is characterised by very large response differences to very small changes in initial conditions. This generates an uncertainty for prediction. The subject is considered not to be of significant relevance to clonk but is more relevant to other driveline system NVH concerns such as shuffle and judder, and particularly gear rattle.

From the above, it may be seen that lumped parameter modelling is a suitable method for capturing the forced responses of non-linear systems (such as drivelines) and to conduct parameter optimisation in the non-linear zones of interest. However, the study of higher frequency radiated clonk noise is best conducted by the use of finite element FE or boundary element BEM methods to examine structural and acoustic behaviours, and to evaluate their contributions to structure borne sound transmission.

The approved solution method is to subject a lumped parameter model to a 'real' torque pulse and then to use the lumped parameter signal to drive the FE/BEM models of the radiating noise surfaces in the system, and to couple the structural dynamics to the outer noise field.

Tsangerides, Tobler and Heerman (1985) have made important torsion driveline analytical contributions, which specifically addressed transient responses to shock inputs in the presence of a lumped lash in a RWD (rear wheel drive) model simulation.

Their model was of the *lumped parameter* type - component inertias connected in series and parallel by stiffness and damping elements - and backlash was effectively included by using zero rated springs. Some of the model data was empirical. They defined *tip-in jerk* as *the rate of change of vehicle acceleration which may / may not be accompanied by an audible sound.*

Tip-in jerk was primarily caused by impacts between inertial components in a drive train separated by backlash. Their model was used to investigate, amongst others, the influence of lumped driveline lash on tip-in response, and they concluded that tip-in jerk, surge, and overshoot (dynamic reactions) became progressively more severe when the lash was increased. The model also agreed with other investigators, that fast torque ramp times excited worst-case shuffle response.

Their model did not, however, consider total lash greater than 8 degrees (and the clutch disc predamper alone has more than 8 effective degrees of lash).

Their model was not a predictor of audible clonk. It was used to model shuffle. They made an implicit assumption that audible clonk was related to tip-in jerk.

Morimura *et al* (1985) have confirmed that modification of the clutch disc characteristic would reduce the shuffle response.

The use of mathematical simulations to understand the dynamic torsion behaviour of lightly damped non-linear systems with lash and subjected to impulsive torque inputs, is a fairly well understood technique. Torsion impulses from the engine may be reacted at the road wheels / tyres as a tractive force, at the engine mounts to resist the roll couple, and at the rear suspension mounts longitudinally. These models are essential indicators of whole system torsion behaviour. They cannot police the movements of impacts along the driveline, and the impact energies that are locally dissipated by torsion pulses.

Hawthorn (1995) used a lumped parameter driveline model to investigate back-out shuffle. His model was then used to conduct parameter optimisation studies, and he concluded:

- A torque ramp time 0,3 seconds was critical to minimise shuffle excitation,
- He established a lash threshold. Lashes beyond this threshold caused further increases in the shuffle response. Below this threshold the shuffle was not affected.
- Stiff clutch main damper springs in conjunction with compliant drive shafts gave a low initial response but a slow decay rate.
- Conversely, soft clutch springs in conjunction with stiff drive shafts gave high initial response but a rapid decay rate.

Rooke, Crossley, and Chan (1993) generated a low order of freedom driveability model, which achieved good shuffle correlation in terms of frequency damping and overshoot. With zero driveline lash - effectively simulated by a tip-in from drive - the shuffle responses for two torque rise rates were compared (See Figures 2.3 and 2.4).

When the ramp time was the inverse of shuffle frequency the response appeared to be highly damped. (Hawthorn had also indicated that shuffle response was strongly related to the ramp time). The effect of driveline lash - lumped at one location - was to significantly increase the initial peak overshoot response.

An interesting characteristic emerged when the model predictions for backlash effects were compared for short and optimum ramp times, showing the significantly increased overshoot with backlash. This is shown in figure 2.7 and 2.8.

In other words, backlash alone had a major effect on shuffle response even when the impulse excitation was minimised.

It was suggested that shuffle response was largely determined by flywheel inertia, gear ratio, and driveline compliance, and was highly sensitive to lash in the system. Shuffle mode damping was best achieved by attention to clutch and half shaft characteristics, and at the road to tyre interface.

Figure 2.5 showed that the initial jerk rate, which was also claimed by Krenz (1985) to be a significant clonk factor, produced a higher overshoot for the system with backlash. Similarly, Hrovat (1989) concluded that increased lash led to increased longitudinal accelerations but without significant changes to system damping decay.

Loos and Laermann (1993) used a driveline model to conclude, as others have done, that minimum shuffle response is achieved when the torque rise time was equal to the inverse of the shuffle frequency. This is in line with the responses of non-linear systems to impulsive inputs. They found that repeating the shuffle mode during testing was difficult, due to the sensitivity of driveline response to short duration pulse excitation.

Petri and Heldingsfeld (1989) observed that '.if the system mode (shuffle) was excited, the so-called tip in/out effect with a hard metallic clunk noise could be experienced. These were seen as acceleration peaks at the input shaft and differential.'

It is clear that these and other review sources: Laschet (1994), Ambrosi and Orofino (1992), Chisolm and Worthington (1987), Chan and Crossley (1993), Kim (1987), LUK Buhl (1990), Mo *et al* (1996) and Gizard *et al* (1990) have used simplified lumped parameter models, some with non-linearity, to achieve a shuffle simulation, but low order degree of freedom lumped parameter studies fail to provide an explanation for the audible clonk mechanism and its sensitivity to tip in and back out, and the variability from vehicle to vehicle, and driver to driver.

Fothergill and Swierstra (1992) concluded that modification to clutch and drive shaft stiffness characteristics was effective in raising the modal frequency and thus to reduce the subjective discomfort. The human body is particularly sensitive to longitudinal oscillations in the shuffle frequency range 3-6 Hz.

They suggested that the only way to avoid a compromise solution was to use a closed loop *feedback control system*, which modified excitation forces as soon as the shuffle response was detected.

Tobler (1983) stated that:

- Clonk and shuffle could not be improved by engine mounting.
- The first few degrees of driveline lash produced the worst degradation.
- Lash reduction alone would not fix clonk; it was one ingredient in an overall clonk strategy.
- Clutch modulation eliminated shuffle and could improve clonk, dependant on the tuning.
- Tip in from a slight drive when compared to tip in from coast/over-run, showed a significantly different response, indicating that lash was a predominant cause of clonk, and it also worsened shuffle.

Without backlash, which is the major source of non-linearity in the driveline, the shuffle response was characteristic of a normal 2nd order linear system forced by a step input.
(i.e. the response had a steady state component and a transient component)

Lash is also a factor in transmission gear rattle, albeit in different ways:

- Backlash in the driveline when it is in the torque path, leads to shuffle and clonk excitation.
- Backlash in non-transmitting gear pairs in the transmission, in conjunction with low drag torque due to low viscosity lubrication, causes transmission gear rattle only.

2.4 Elasto-acoustic emission.

In driveline clonk we are concerned with two conditions of dynamic coupling:

- The elastic coupling between the applied torsion impulse and the associated structural response. In other words the excitation of shuffle. It has been seen that the shuffle frequency range for a given vehicle is ca 3-7 Hz dependent on gearing, and so pulse durations of 150 to 330 ms would align with the shuffle mode.
- The elasto acoustic coupling between the already excited structures and the subsequent noise emission due to either internal or external acoustic coupling. Here we are concerned with pulse durations of only 0.5 to 2.0 ms. This is now considered in more detail.

2.4.1. Structural response characteristics.

Arnold and Warburton (1949) have defined thin cylindrical shell vibration mode patterns. An infinite number of axial (*m*) vibration modes are theoretically possible, each with a corresponding number of circumferential (*n*) forms. To define a mode, the *m* and *n* values must be specified. Arnold and Warburton used the energy equation to develop complicated cubic equations, the roots of which defined the *(m, n)* eigenmodes.

Forsberg (1964) used a method outlined by Flugge in 1934 and he concluded, as did Warburton, that for any given set of values of *(m, n)* there were three natural frequencies corresponding to three mode shapes.

Santiago and Wisniewski (1989) used FE analysis to compute the natural frequencies of a clamped cylinder. Their results confirmed the work of Arnold and Warburton (See Figure 2.9)

When the resonant structural modes of a thin walled cylinder are the dominant sources of sound, standing waves will be set up in the axial *and* circumferential *and* radial directions, and some modes will radiate noise more efficiently than others. Normally these are the flexural modes. The *radiation ratio* from mode to mode may vary significantly.

Radiation ratio is the efficiency with which a structure radiates sound compared with a piston of the same surface area vibrating at the same condition. The piston has unity radiation ratio.

A typical schematic of radiation ratio for a pulsating resonant cylinder is shown in Figure 2.10 with some accompanying explanatory notes. Below a critical frequency, it can be seen that the lower order circumferential modes are more efficient sound radiators than the higher order modes.

2.4.1.1 Structural modal density (of cylindrical tubes)

The mechanical excitation of plates or panels results in most of the radiated sound being produced by resonant plate modes (Szechenyi, 1971). Sound radiation depends upon the number of possible vibration modes that can exist within a given frequency bandwidth. This is the definition of structural modal density.

Norton (1989) reported a simple estimation method derived by Heckl (1962) for cylindrical shells. There are large numbers of axial mode orders, and hundreds of natural frequencies of a cylinder that may be excited into resonance - the modal density of lightly damped cylindrical shells is generally very high.

Rennison and Bull (1977) developed modal density look-up characteristics to show the build up of modal density with frequency. They investigated the effect of material changes, wall thickness changes, and end fixings, on the modal behaviour.

The modal density for brass was twice that of a comparable steel cylinder. Substantial changes in damping occurred when end fixings were revised from free to clamped, especially for the low order m modes. This is a significant conclusion for drive shaft design. Structural damping improvements by end fixing revisions could be achieved with little cost or weight penalties.

Szechenyi (1971) proposed a simplified equation for modal density and radiation efficiency of unstiffened cylinders, these being the two parameters required in order to determine the acoustic radiation into or out of a cylinder due to resonant vibration. The mode-by-mode analysis of the vibration behaviour of cylinders with high modal density was considered to be too difficult; statistical methods were used instead. Non-dimensional wave number diagrams were established using natural frequency equations, to enable modal density and radiation efficiencies to be directly measured graphically.

Clarkson and Pope (1981) used experimental methods to excite a cylinder and evaluate the modal density profile, and then compared it to the predictions of Szechenyi (1971). They concluded that the modal density was a maximum at the cylinder ring frequency and that the measured modal density distribution conformed to Szechenyi (1971).

2.4.2. Acoustic response characteristics

When sound waves propagate within the confined spaces of a duct or cylinder, the wave propagation can either be parallel to the cylinder walls or at some angle to them.

The former type of wave propagation (longitudinal) is a low frequency *plane wave*, and the acoustic pressure is constant across any given cross section. The latter types (radial) are referred to as *higher order acoustic* modes, and acoustic pressure is not constant across the cross section, it varies with distance across the cylinder, and with the angular position. The pressure gradient is normally extremely high.

For the purposes of defining the sound field inside a shell at cavity resonance, the structural walls may be assumed to be rigid to allow sound wave reflection. Solution of the Helmholtz wave equation will then yield the spatial pressure distribution (acoustic mode) within the hard cavity boundary.

Modal analysis of acoustic cavities works well at low frequencies when the standing waves are well separated on the frequency scale; but at higher frequencies the acoustic modes are much closer together and they are highly coupled. The transition frequency between these frequency ranges may be more readily evaluated when modal density is plotted against frequency for a given cavity.

The internal acoustic modes for a cylindrical shell may be described as (p, q) type configuration, where p is the number of plane diametral nodal points, and q is the number of cylindrical nodal points concentric to the cylinder axis.

As an example, and using the empirical formula suggested by Norton (1989), the following acoustic mode patterns and frequencies for an 80 mm inside diameter cylinder (equivalent to the dimensions of the vehicle drive shaft tube) may be evaluated as follows:

(p, q)	Frequency (Hz)	(p, q)	Frequency (Hz)
1, 0	2520	4, 0	7291
2, 0	4193	1, 1	7312
0, 1	5246	5, 0	8778
3, 0	5763	2, 1 etc	9191 etc

Table 2.1: The first four acoustic modes fall within the clonk frequency range.

2.5. Contact and impact theories.

This thesis is concerned with impacts in a vehicular driveline that may occur due to a clearance or backlash between mating parts, during the process of transmitting torque.

As a result of an impact, the resulting energy may be fed into nearby noise emitting structures, which may then resonate with the applied energy and in turn radiate noise through elastic wave propagation.

The technical literature review yielded very little which was specifically pertinent to driveline clonk. There were very few references to an analytical assessment of the mechanism. Therefore, it was necessary to consider the physics that govern elastic contact and impact, the dynamic effects of high-energy impact, the possible resonance conditions that may be excited, the elastic wave propagation, and finally the acoustic radiation from the wave motion. Simultaneously, as the elastic material conditions were considered, it was also necessary to consider the lubrication effects in the contact zone under transient loading.

The very short time duration of the impact and the subsequent noise radiation was of the order of milliseconds and it was necessary to follow an engine torque pulse from the flywheel to the rear wheels, passing through all the elastic contact zones that generated impact conditions, and to construct a multi-body simulation.

Statics, *kinematics* and *dynamics* are all important branches in the field of *mechanics:*
Viz, Mechanics is concerned with motion or change in the position of objects.
Statics is concerned with conditions for which there are no apparent motions.
Kinematics is concerned with the geometry of the motion with out regard for the inertial properties of the objects.

Finally, *dynamics* is concerned with the causes of motion, translation and rotation, for which Newton's 2^{nd} law of motion may normally be applied.

For the purposes of this thesis, one may consider the problem of driveline clonk to be primarily in the field of vibro-dynamics.

In addition there was an essential need to consider other scientific fields. In particular:

Elasticity, which is concerned with the resistance of materials to deformation caused by external forces, and the ability of the materials to elastically recover to their original shape and property when the force has been removed.

Hydrodynamics, which is concerned with the dynamics in a fluid film that separates two bodies in motion.

Structural dynamics, which is concerned with the high frequency modal behaviour of lightly damped thin walled structures, especially when they are readily excited into resonance by the application of impulsive forces.

Acoustic emission, which is concerned with the radiation of sound pressure from the vibrating surfaces.

2.5.1. Introduction to impact

The root cause of driveline clonk is *impact*. This is now considered in more detail. The force transient in impact causes sudden changes of velocity in the colliding bodies and these are normally the measured characteristics of impact.

If the force transients could be readily measured in an impact experiment, then the solution to an impact problem may be achieved by integration of the equation of motion. Of course the force transients are not normally easy to measure in impact.

As a result of impact, the energy is partly converted into elastic deformation and partly into kinetic energy (rigid body motion), dependant on the nature of the impact.

Both the local and global elastic deformations due to impact are significant and are strongly dependent on the m_1/m_2 mass ratio (the impacting and impacted masses). One can observe that when the mass ratio m_1/m_2 is large, the loss of kinetic energy during impact is small, and the local and global deformations are insignificant. When the mass ratio is small, and when m_1 is smaller than m_2, the loss of kinetic energy is larger, and the local deformation is more significant.

A high-speed impact with a low mass ratio will cause significant local deformation.
A low-speed impact with a high mass ratio will cause significant global deformation.

It is particularly interesting to investigate the impact of gear teeth in the driveline. A gear tooth is analogous to a cantilever beam. When an impact is made to a cantilever beam, most of the impact energy is converted to local elastic deformation, and only a small amount is converted to rigid body motion. By comparison, an impact to a free-free simply supported beam will produce elastic deformation plus rigid body motion, by virtue of the lower flexural resistance.

It has been assumed that the applied forces produce an elastic response within the bounds of Hooke's law. If the impact forces are higher than the ability of the structure to elastically contain it, then the dynamic behaviour may become plastic and wave propagation may be stifled. In addition, if the pulse duration of the impact is much shorter than the fundamental period of elastic wave vibration of the gear tooth, then local plasticity will result and wave propagation will not readily occur. Therefore, one should check for these two conditions; does the material behave elastically within Hooke's criterion under impact, and is the duration of impact short in comparison to the gear tooth natural bending frequency?

If the pulse duration of the impact is much shorter than the fundamental period of elastic wave vibration of the gear tooth, then one may conclude that gear tooth resonance is not of consequence and that the impact energy will be largely applied to rigid body motion and to the onwards transmission of vibration energy.

2.5.2. Hertzian contact theory

Newtonian impact is concerned with velocity changes in each of the bodies as a result of a Dirac type impact, and these are only dependent on the initial velocities and on the magnitude of the masses in contact. Newtonian impact makes no allowance for elastic deformation.

Hertz (1881) assumed that the loading rate in elastic contact was sufficiently slow for the stresses to be in equilibrium with the loads at all times. When the applied force was removed, the body returned to its original state in accordance with Hooke's law of elasticity. If the applied forces exceeded the yield strength of the material, then plasticity occurred and the original state was not regained. By comparison the Hertz model of *impact* was characterised by forces of large magnitude in conjunction with an event of extremely short duration. One may refer to *contact* as an event of longer duration with the applied force maintained in contact during the duration of the event.

Note, this thesis shall refer to *impact* in both translation and angular terms. Hertz (1881) considered elastic impact as a collision between bodies that were elastic at the location of contact, but otherwise moved as rigid bodies. The impact and subsequent local elastic deformation was considered to be concentrated in the so-called mass-less Hertzian spring, and all other parts of the impacting bodies were unaffected by the collision.

For the case of two *elastic spheres* in collision and with a circular contact area, it may be shown that;

Total contact force, $F = k\delta^{\frac{3}{2}}$, where K is a constant and is a function of E and R, and δ is local elastic displacement.

The derivative $\frac{\partial F}{\partial \delta} = \frac{3k\delta^{0.5}}{2}$, which is the local stiffness for a value of δ.

If Newton's 2nd law is applied, then after integration and the use of boundary conditions, one arrives at Hertz' famous elastic impact time equation.

Hertz (1881, 1896) found the total impact time $t \sim \frac{2.94\delta}{V}$, where V is the relative velocity of the bodies before impact, and δ is the local elastic deformation.

For spheres of similar sizes and properties, the impulse function and the duration of impact is normally very long compared to the wavelength of the lowest dominant mode of the impacting spheres. As a result we can expect that vibration will not be excited, in line with the Hertz assumptions that elastic wave propagation from impact may be ignored, and that all impact energy would be returned through elastic recovery.

The Hertzian impact theory has two potential shortcomings that render it less accurate for the impact of gear teeth, but it nevertheless will suffice as a reasonable first approximation. The first shortcoming is that in many gear-meshing contacts the area of the highly loaded conforming contact (as in helical gears of transmission) may be comparable in dimensional terms to the principal radii of mating solids at the contacting region. This means that the semi-infinite elastic half-space assumption made by Hertz to simplify an analytical solution, does not necessarily hold true for helical gears. The second shortcoming is that load bearing and transfer surfaces such as the meshing gears are normally lubricated, whilst the Hertzian theory applies to the contact/impact of dry smooth surfaces.

There is another consideration, that of the elasticity and size of the bodies in contact.

If the impacting mass is small and elastic compared to the impacted mass, then rebound may occur immediately after impact. If the impacting mass is large and elastic compared to the impacted mass, then rebound may not occur immediately after impact. If both are inelastic then they may *adhere* after impact regardless of size. As a result, one may consider a range of collisions, from *elastic* to *inelastic*.

Perfectly elastic impacts occur typically with materials such as glass and steel. The work done during impact is stored as strain energy, there is no conversion to heat energy, and no energy is ideally used to overcome internal friction. The bodies regain shape immediately after separation. The coefficient of restitution e, is nearly equal to unity. As the speed of impact increases and the elastic impact approaches plastic conditions, the value of coefficient of restitution drops.

By comparison, *perfectly inelastic* impacts occur typically with materials such as lead. The work done during impact is used to overcome internal friction with a consequent heat energy increase. The bodies do not regain their shape, they may adhere, and the post impact kinetic energy levels are lower. The coefficient of restitution is now much lower than for elastic impacts, and reduces further with impact velocity. Hence, there are extreme conditions of attraction and repulsion following impact, which are functions of not only the masses and velocities in contact but also the elastic body's moduli of elasticity. In other words, there are *global* and *local* conditions to consider.

2.5.3. St Venant theory of wave propagation

If the forces acting on a small portion of the surface of an elastic body are replaced by another statically equivalent system of forces acting on the same portion of the surface, this redistribution of loading will produce substantial changes in the stresses locally, but will have a negligible effect on the stresses at distances which are large in comparison to the linear dimensions of the surface on which the forces are changed.

St Venant proposed that an impact between elastic bodies would be of finite time duration and the collision energy would give rise to elastic wave propagation at the impact sites in each departing body following impact. The duration of the impact would be a function of the time for the wave to travel out and back from the impact.

By comparison, the Hertzian impact theory was primarily concerned with the local elastic deformation at the impact site. It assumed that the coefficient of restitution was unity and that the impact was perfectly elastic.

Love (1892) reported on the work of Sears and Wagstaff, who investigated both impact theories. Sears experimented with the impact of longitudinal rods and concluded that the Hertzian impact theory was appropriate at the ends of the rod in contact, whilst the elastic strain behaviour at the centre of the rods was in line with St Venant theory. Wagstaff experimented with the impact of rods having rounded ends, to establish the relationships with impact time. He showed that for a sufficiently large length-to-diameter ratio, the time duration was independent of impact velocity.

2.5.4. Lubricated contact

The inclusion of lubricated impact dynamics into the complex multi-body approach was seen as being outside the scope of this investigation and a new dedicated research undertaking in this respect is needed. However, the effect of lubricated contacts on the local deformation of impacting solids was investigated in the literature review, and as an initial precursor for future research.

It has been well established both theoretically and experimentally that machine elements having concentrated contact and also in relative motion, will be separated by a coherent liquid lubricant film. If the contact load is high enough to locally distort their surfaces and to increase the lubricant viscosity in the gap between them, then elastohydrodynamic lubrication (EHL) will result. This condition can occur in engineering applications such as between rolling elements and their races in ball and roller bearings, between pairs of teeth in spur gears, and between splined connections. Practical evidence that EHL does indeed occur is shown in the complete absence of wear of lubricated parts, evidence that the parts are separated by a lubricant film even when under load. The formulae obtained from numerical solutions to the EHL problem are therefore a useful design tool and the most useful is the prediction of the minimum lubricant film thickness.

EHL in general occurs in heavily loaded contacts, and the pressures in these contacts are sufficiently high to cause significant elastic deformation of the lubricated surfaces together with a very large increase in the viscosity of the lubricant fluid. Thus from a mathematical point of view, EHL is concerned with the simultaneous solutions of the Reynolds equation for fluid film lubrication and the elasticity equations for coincident deformation of the bounding surfaces for incremental time during the contact cycle.

In short the mechanism of EHL is a combination of hydrodynamic action of the fluid as originally described by Reynolds (1886), and the elastic deformation of contiguous surfaces in contact as expounded by Hertz (1881, 1896). The combined effect of these two mechanisms, which generated a protective lubricant film, was in fact finally proposed by Ertel and Grubin (1949) and later confirmed by Petrusevich (1951) to signal the birth of EHL.

Since the 1950's a considerable amount of work has been carried out in the field of tribology, particularly EHL. The most pertinent contributions for the impact dynamics phenomenon related to conditions typical of meshing teeth impact, leading to problems such as driveline clonk. We may consider clonk to be a transient EHL problem of normal impact through a lubricant film and having a squeeze film motion, rather than the entrainment of a fluid into the contact by relative motion of the surfaces. The EHL condition for surfaces having relative sliding motion is a separate problem. The normal impact problem is assumed to be quasi-static, and the governing equations of the impact must be resolved for extremely small increments of time, also with due regard for ongoing parameter changes during the contact cycle. This is the case as the sudden applied torque through small lash zones (clearances) introduces a high approach velocity, which dominates the kinematics of contact. Therefore a fundamental understanding of lubricated impact dynamics was required.

In an experimental investigation, Safa and Gohar (1986) carried out an interesting experiment to investigate the normal approach problem. They used a small Manganin pressure transducer to measure the pressure distribution in the contact between an impacting steel ball on a glass plate covered by an oil droplet. They found that the pressure distribution obtained was similar to those obtained theoretically elsewhere under a steady state EHL rolling contact, but the magnitude was far higher due to the force of the normal impact. From the shape of the pressure gradient time trace, they showed that *no* metal-to-glass contact occurred and the oil film always separated the surfaces. They also showed that *dimples* were formed in each surface during the latter stages of the approach.

Dowson and Wang (1994) carried out a numerical analysis of the same problem, and under identical conditions to those of Safa and Gohar (1886). They found very good agreement with the experimental findings of the latter. It became clear that the extent of deformation increased (i.e. the dimple) under lubricated conditions and the contact force was larger due to lubricant reaction than those under dry impact. There was an exponential relationship between pressure and viscosity such that at high pressures the lubricant temporarily became an elastic solid. This demonstrated that the impact time also increased and so more energy was dissipated. In general however, the behaviour of the impact did not greatly deviate from the Hertzian investigation. The latter may then be applied, as in this thesis, to investigate the resulting wave propagation. Other similar lubricated impact dynamics studies have been carried out by Hoglund and Larson (1994,1995) and more recently by Al-Samieh and Rahnejat (2002), the latter obtaining very close agreement with the experimental work of Safa and Gohar (1986).

2.6. Acceleration and ringing noises due to impact

Norton (1989) reported on the work of Richards *et al* (1979 to 1986) on impact.

It was argued that when two bodies were impacted together, two distinct processes would create a noise. They were *acceleration noise,* and *ringing noise* Richards *et al* (1979b).

The first event following impact was acceleration noise, and this was due to a rapid change in velocity of the moving part during the impact and this gave rise to a pressure perturbation. This was not dependent on damping or vibration isolation.

Ringing noise followed the acceleration noise and this was due to sound radiation from vibrating modes of the attached structure.

Acceleration noise arising from impact is a function of impact duration, size factor, area in contact, and impact velocity Richards *et al* (1979a, 1979b). Acceleration noise is only developed during the contact time. The dominant acceleration noise mechanisms are those that relate to very short impact times and in association with free backlash. The impacting bodies are solid elastic. The shorter the contact time the greater the radiated noise energy. In general, however, the contribution from acceleration noise is small. By comparison ringing noise, which follows the acceleration noise, is due to sound radiation from vibrating modes of the attached structure and is the major impact noise contributor. The ringing continues until all the impact energy has been radiated as sound or has been absorbed into the structural damping system Richards *et al* (1979b).

Ringing noise is a function of structural damping, the vibration energy propagation rate, Young's elastic modulus of the structure, the radiation efficiency of the structural panels likely to flexurally vibrate, the surface areas and velocities, and the vibration amplitudes. (Richards *et al* 1979) Hence we would expect a small ringing noise contribution from solid inert bodies in impact.

Richards *et al* (1979a, 1979b) developed empirical formulae for the prediction of noise generated by impact, so that design action could be taken early in a programme to avoid costly palliation later on. It was found that for bodies with 'sufficiently compact' dimensions, the acceleration noise and structural ringing noise were of a similar order. Richards (1981, 1983). However, if the local flexural modes were excited into resonance by the impact, then radiation energy was significantly higher than the energy radiated during the time of impact. The reason for this was the much longer time taken for the lightly damped structure to radiate the noise energy by ringing, or for the ringing to be structurally damped, or for the vibration energy to be channelled to other parts of the structure (Richards *et al* (1983)). If *no* internal structural damping or leakage of vibration energy to ground could occur, then all the vibration energy must be radiated acoustically.

In a lightly damped structure such as the aluminium clutch housing and the thin walled steel drive shafts, for example, very little impact energy would convert into heat through structural damping, and most of the impact energy would radiate as sound until the energy had been fully dissipated. The thin walled transmission bell housing for example, is cast in aluminium which intrinsically has much less structural damping than the housings that were previously produced in cast iron.

Figure 2.11 schematically shows one of many possible pulse exchanges in the driveline due to lash. The impact in the lash zone generates a short (1 to 2 ms) pulse of airborne noise, which is dependent on contact conditions. The impact energy is dissipated into the surrounding and supporting structure, and this may take 30 to 50 ms dependent on structural damping and on the vibration paths.

This has been measured on test and supports the corresponding work at Aachen University (1995) mentioned earlier.

When both acceleration and ringing noises are significant in an impact process, it is necessary to confirm which is dominant, in order to take appropriate design actions. The fraction of ringing energy radiated as structure borne sound will depend on the ratio of acoustic to structural damping, and on the rate of propagation into the floor and other parts of the surrounding structure.

The impulsive noise from impacts must necessarily consider in some detail, the structural response characteristics that are associated with the impact. Resonant structural modes will probably be much more responsible for most of the sound radiation compared to non-resonant forced modes, which are much less effective noise radiators.

Richards *et al* (1983, 1984) reported that noise reduction of impacts primarily depended on a reduction in excitation levels, and also by increased impact duration, both of which had the effect of achieving lower acoustic radiation efficiencies at lower structural response frequencies.

In general, softening the impact was a more effective way of reducing impact noise than by adding structural damping. This is an important conclusion for driveline impact analysis.

Richards *et al* (1981) examined the motions of a solid mass striking one side of plate which had a viscoelastic damping layer. They observed that for the same impulse applied to both sides of the plate:

- The ball peak acceleration levels were greatly reduced when impacting the resilient side of the plate.
- The plate peak acceleration levels were reduced in sympathy.
- The plate vibration reflected the longer impact time.

- As a result the emitted noise was lower due to the reduced radiation efficiency at lower plate frequencies.

They concluded that detuning the frequency of excitation from the response represented the best impact noise control method available.

The following Table 2.2 serves to illustrate how difficult this is. The pulse content in the frequency domain would need a significant shift in order to clearly separate the excitation from the various responses.

In an analysis of backlash in industrial machines, Richards (1981) suggested that the increased impact noise associated with machine *wear*, was a function of:

- The increased energy transfer from impact zone to the radiating structure, and
- The increased ringing time over which the deceleration occurred.

Hence, the use of thick cold lubricating oils can have significant effects on both of these effects. The main purpose of the low viscosity oil was to increase the contact time at the end of the lash travel; and surface velocities would be relatively unaltered. Noise reduction was again achieved by a reduction of acoustic radiation efficiency associated with the increased contact time.

The important implications for driveline impacts with backlashes at several locations, is that backlash *damping* or *lash rate* was likely to be a critical parameter and would have a controlling influence on the softening of impacts. The same lash rate benefits could also be achieved by increased *drag torque* and the use of *thick low viscosity* oil to increase contact time and reduce contact forces.

Richards *et al* (1983) investigated the ringing noise of milk bottles in crates due to impact, and its elimination by the use of plastic containers (stillages). He posed the question: Was the noise reduction achieved by vibration damping, or was the noise mechanism due to softened impacts and lowered excitation frequency with a subsequent noise reduction? He concluded that noise reduction was due to the softened impacts. Lightly damped structures will have high modal densities in the frequency range of interest, so that softened impacts would excite fewer resonant modes.

Piston slap was another quoted example (see Richards, 1981), where noise reduction was aimed at reducing the impulse magnitude, to excite the lower frequency and lower radiative modes at the most relevant part of the structural response.

Several damping devices were available. The effective treatment would be that which controlled the ringing time and hence the ringing noise, and would depend on a judicious application of isolation techniques based on knowledge of the energy transfers in the structure.

Shope *et al* (1984) reported that a conventional cardboard tube liner had been installed in a large diameter aluminium drive shaft to attenuate tube surface resonance and thereby to reduce gear noise and rattle. However, it is not clear whether the desired effect was the result of acoustic or structural damping or both. It is known that drive shaft shielding is a very effective rattle palliative. It is an attractive possibility that inert drive shafts may resolve both rattle and clonk, or at least provide the adjustment potential necessary for optimal control.

2.6.1. Acceleration noise

Airborne sound, which is radiated as a result of impact, depends on the surface area, the mean velocity magnitude, and contact time. The dominant acceleration noise mechanisms were those, which related to very short impact times *in association with backlash* and gear clashing. Richards *et al* (1981), (1986).

The peak sound pressures arising from impact are predictable. These would vary inversely as the cube of the impact time, and directly as the impact velocity (Richards and Cuscheri,1983).

To show the importance of increased contact time, Norton (1989) empirically derived the relationship between radiated noise energy and the non-dimensional contact time relationship.

Once the non-dimensional contact time had exceeded unity, the acceleration noise rapidly ceased to be of any significance (see figure 2.12 and the accompanying explanation).

This relationship could be used to compare the noise radiation potential of the clutch bell housing and the drive shaft tubes. The bell housing probably had the greater propensity to radiate more impact noise, for the same given contact time.

In metal to metal impacts of thin walled structures which became resonant as a result of the impact, it was estimated by Richards (1979a, 1979b) that only about *one five thousandth* of the hammer kinetic energy was radiated as acceleration noise. The remaining energy was converted to structure borne ringing noise.

2.6.2. Ringing noise

Structure borne noise is generated and radiated from body structural vibration. Bending / flexural plate waves are by far the most significant for sound radiation because particle velocity is normal to the direction of wave propagation, Norton (1989) although in the clonk frequency range the driveshaft flexural vibration modes are not as predominant as the more complex combined circumferential and radial modes.

Bearing in mind that a linear resonance occurs when the excitation frequency *coincides* with the natural structural frequency, the structural modes thus excited are responsible for most of the sound radiation. Many natural frequencies may be excited and they resonate with the applied force. Sound radiation depends on the number of possible vibration modes within a given frequency bandwidth, known as modal density.

With regard to the excitation of responsive structures, Roy and Ganesan (1995) investigated the transient response of a cantilever beam to impulsive loading for various loads, load locations, and values of damping. In summary, they concluded:

When the impulse time was increased i.e. by a 'softer' impact, the first structural mode contribution was predominant and the higher order modal contributions were less significant. When the impulse duration was reduced i.e. by a 'harder' impact, the response contribution of the higher order modes was increased. The explanation, though not offered, is due to the frequency domain characteristics of the impulse.

When three levels of damping were tested, the deflection responses were again predominantly governed by the first mode.

When the nodal point of excitation was moved, additional higher order modes were excited. Their conclusions added support to the work of Richards.

2.7. Noise palliation

Norton (1989) reviewed the effects of internal stiffeners versus diaphragms to control noise radiation from thin walled cylindrical shells. A comparison of the measured sound pressure at a set distance from the resonating cylinder, for three test conditions, was made:

- A cylinder without structural stiffeners and without diaphragm (baseline).
- A cylinder with stiffeners and without diaphragm.
- A cylinder with diaphragm and without stiffeners.

The diaphragm was found to be a more effective noise attenuator than the ring stiffeners, particularly for the lower structural modes. Both the diaphragm and stiffeners, in turn, significantly reduced noise radiation.

This result demonstrated that the structural treatment of drive shaft tubes could be an effective means of controlling the dissipation of structure borne energy.

Richards, Carr and Westcott (1983) conducted a similar study of impacts between a plain cylinder, and another cylinder keyed by a wedge to achieve a structural discontinuity. The keyed cylinder responded to impact at a much lower frequency and the decay time was much shorter.

In this case, structure borne sound conveyed energy from the vibration source to a surface, from whence it was radiated into a fluid / air. It was found that the coupling at the two interfaces - driving and receiving - was as important as the noise propagation process itself.

Junger and Feit (1972) summarized the control of structure-borne sound as follows:

At the source:

- Reduce the power of the source of excitation.
- Isolate the vibration path between source and structure.
- Use resilient layer on impacting surfaces.
- Reduce the velocity of the impacting masses.
- Ensure the vibration source is remote from where low noise levels are required.
- Strengthen the structure at the point of excitation.

Along the vibration path:

- Isolate the source along the path by a structural discontinuity, structural separation, dynamic separation or material changes

At the receiver:

- Radiating surfaces to be covered with a damping layer.
- Reduce surface vibrations with damping material especially if the material could be tuned to the operating environment.

2.8. Elasto-acoustic coupling and coincidence.

Coincidence occurs when the wave speed of a flexural structural wave equals that of an acoustic wave of the same frequency travelling in air Norton (1989). Note that coincidence does not compare modal shapes, only modal frequencies.

Acoustic standing waves that are sustained within the enclosed fluid volume may be coupled to the structural panel modes. The coupling may be resonant or non-resonant.

Coupled structural-acoustic modal behaviour dominates the sound transmission in relation to cylindrical shells (Norton, 1989).

As stated before, externally radiated sound from a cylindrical shell is predominantly determined by coincidence of the higher order acoustic modes inside the shell, and resonant flexural modes in the pipe wall in the axial and circumferential directions. The condition of coincidence for a no-flow closed cylindrical shell may be illustrated by superimposing the acoustic and structural modal behaviour (see Figure 2.13).

It can be seen that coincidence can occur between the (m, 1) structural mode and the (1, 0) and (1, 1) acoustic modes, and also coincidence can occur between the (m, 2) structural mode and the (2, 0) acoustic mode.

- When there is both wavelength and frequency matching in coincidence, the pipe wall is driven at or near resonance and damping could then have a large effect.
- When there is poor frequency matching the pipe wall response is forced by the high response of the sound field and damping may then have only a little effect.

The importance of coincidence analysis is to recognise the existence of the many possible modal configurations in the acoustic and structural domains, and the noise radiation effects when they are coupled by coincidence. In the case of a lightly damped driveshaft tube, the effect of coincidence on externally radiated noise is not yet fully understood. There is also the question of coincidence coupling not only between the interior cavity and the cylindrical surface resonance, but also the next coupling between the structure and the exterior noise field.

Dowell, Gorman and Smith (1977) examined the effects of interior sound fields separated by a flexible wall, by using a theoretical model. The equations of motion of the containing structure were linked to the acoustic model to allow an examination of the relationship between structural and acoustic fields at resonance.

Some of their more important and relevant conclusions were:

- In most cases the structural wall resonant frequencies were unchanged by the cavity resonances.
- The cavity sound pressure levels were much higher than the external sound pressures when the acoustic mode and structural mode frequencies coincided.
- The cavity acted as a vibration absorber for the structural wall, when the external exciting frequency was equal to the cavity resonant frequency.
- Cavity wall absorption/damping had the effect of decreasing the internal sound pressure field, but was the least effective for the lower order acoustic modes.

Hutchins (1990) investigated the effects of violin cavity resonances on radiated sound and concluded that cavity mode pressures and the corresponding decrease in tonal quality could be most affected by two mechanisms:

- By opening a series of small holes in the ribs.
- By damping the acoustic modes with foam plug inserts.

Both mechanisms had the same effect of shifting the acoustic cavity mode frequencies. The study concluded that violin playing quality and radiated sound was significantly affected by the strong interactions between resonances of the mechanical structure and the cavity modes.

The implications of this piece of research was that awareness of acoustic cavity modes and the relationship with the containing structural characteristics is of potential significance (but not yet proven) to the study of radiated clonk especially from the clutch bell housing and the drive shaft tubes.

2.9 The loudness of impulsive sounds

It is necessary to refer to the perceptive loudness of impulsive sounds. The ear is known to be an energy sensitive device, which responds to impulsive sounds by averaging over a certain time.

Investigators using psycho-acoustical experiments have attempted to determine the link between the loudness of pulses of different duration, and that of the steady sound (Broch, 1969). They have reported different relationships with different assumptions of ear averaging time.

An idealisation has been made which investigated by how much the sound pressure level would have to be increased in order to be perceived to be as loud as a continuous sound. The breakpoint, or effective averaging point of the ear, was found to be approximately 100msec.

It has been concluded that for pulse durations greater than a certain value - considered to be this effective averaging time of the ear - the impulse was judged to have the same loudness as that of the *steady* sound. Below this value, the *level* of the impulse had to be increased to be perceived to be as loud as the steady sound.

Interestingly, multiple event structure borne clonks are typically of the same duration as the effective averaging time of the ear (i.e.100ms)

Noise *annoyance* is related to loudness and frequency, and intermittent noises are more annoying than steady state noises. Broch (1969). Noise annoyance is also related to noise location; it is more annoying if the noise source is mobile or if the source cannot be located. Clonk is such a noise, and it occurs in the most sensitive frequency band for the ear.

2.10. FEA and BEM methodology

The boundary element method BEM is a computational method for solving the acoustic wave equation, and is especially helpful when the acoustic domain has an irregular boundary.

The BEM is different to the finite element analysis FEA approach. When applying the BEM to the acoustic domain eigenvalue problem, only the domain boundary needs to be discretised. When the FE approach is used to solve the 3D wave equation for an acoustic domain, the resulting matrix is sparse and the boundary conditions are much more tedious to set up.

The BEM has been extensively used in coupled structure-acoustic analysis, both for the internal and external sound fields. For example, BEM has been applied to the analysis of low frequency interior boom in a car body, and to identify the contributions to boom from each part of the vibrating body structure. Those parts of the structure that make a positive contribution to noise at the occupant head position, must be identified using the method so that palliation may be effectively applied (Pates et al ,1995).

In addition, transfer function analysis may be used to identify those structural areas that make negative contributions to interior noise at the occupant head locations so that 'blanket' palliation may be avoided.

The coupled analysis may also be used when considering exterior noise radiation from structures. For example, airborne noise transmission from the tyre to the driver's ear has been studied using BEM models of the tyre wall (Kim *et al*, 1997). Particular attention was paid to the inner cavity resonances of the tyre, and the vibration characteristics of the tyre at the cavity frequencies. Another example of this approach using FEM and BEM was the coupling analysis between the vehicle body structure and the internal sound pressure field in the low <200 Hz audible boom range (Soi *et al*, 2001).

2.11. Signal analysis of transient events

The purpose of signal analysis is to extract useful information from the measured transient signal in order that the physics of the mechanism under investigation, and ultimately the root causal factors, may be identified.

Signal data is normally collected in the time domain and then transported to the frequency domain, since it is the frequency components that provide most insight into the multi-body behaviour of a system. When the data is periodic and of finite duration the analysis by Fourier transform is reliable. When the data is not periodic but transient the duration is short and the signal changes rapidly. Fourier analysis is no longer a reliable method of analysis.

Driveline clonk is a very short transient event that requires careful measurement and analysis, so that data extraction may be used to correlate the model assumptions. A feature of high frequency clonk behaviour is that it is often associated with a low frequency shuffle motion of the vehicle. These events must be separated.

Clonk noise is emitted from high frequency structural waves that propagate from the impact site and shortly afterwards are reflected from a local physical boundary. Hence there is a need to consider both the frequency and time content of the transient signal.

2.11.1. Fourier analysis FFT

Joseph Fourier pioneered frequency analysis. Fourier analysis breaks down a continuous signal into its constituent sinusoids of different frequencies. It transforms the time based data into frequency based data so that further investigative analysis in the frequency domain may be made. In other words, it transforms data from *amplitude/time* domain, to the *amplitude/frequency* domain.

$$F(\omega)=\int_{-\infty}^{\infty} f(t)e^{-j\omega t}dt$$ where f(t) is the original time signal.

and F(ω) are the Fourier coefficients.

Hence, the transform is the sum over all time of the time signal multiplied by the complex exponential.

However, Fourier analysis has two limitations when applied to transient event data:
First, if the signal data is non-stationary and it contains important time information, then the time data will be lost in the transformation to the frequency domain. In other words, it might be important to know *when* a frequency based event occurred. Second, Fourier sinusoids are used for continuous signals, but are not really suitable for transients or abrupt signal changes.

2.11.2. Short time Fourier analysis STFT.

In 1946 Dennis Gabor used a windowing technique to analyse a small part of the signal each time. Thus he mapped from an *amplitude/time* to a *frequency/time* domain, and was able to preserve the time information. This overcame the inherent disadvantage of Fourier signal analysis.

The precision of the method was however, related to the window size. A window size was applied to the total signal so that it was useful at some frequencies but not at others.

2.11.3. Wavelet analysis.

Wavelet analysis has taken the STFT process a little further, by the use of a *sliding* or variable window. Long time interval windows may be used for low frequency data, and short time intervals for high frequency data content.

Wavelet analysis uses *wavelets* (as opposed to the use of sinusoids in FFT) to break down a transient signal. Wavelets are themselves transients, so they are better configured for transient analysis, and there are a number of wavelet families that have been defined and are already available as support tools.

The analysis is similar to FFT, as follows:

$$CWT(scale, position) = \int_{-\infty}^{\infty} f(t)\psi(scale, position)dt$$

where the continuous wavelet transform CWT is the sum over all time of the signal f(t) multiplied by the wavelet function.

Each coefficient is multiplied by the appropriate wavelet to yield the constituents of the original transient signal $f(t)$. It can be seen that this is similar approach to that used in Fourier transforms.

Fourier analysis consists of decomposing a signal into many sinusoids of different frequencies; the sinusoids used in Fourier analysis are smooth functions of infinite time. By comparison, wavelet analysis considers the signal to be represented by wavelets, which have finite time and zero value and are irregular and asymmetric. Wavelet signatures are readily available to use in transient signal analysis, the so-called Haar / Daubechies / Biorthogonal / Coiflets / Symlets / Morlets / Mexican Hat / and others.

As already stated, the Wavelet transformation is suitable for analysis of transient signals with discontinuities, and it is especially useful if time information is required. For example, it was successfully used in the analysis of vehicle crash data by Cheng (2002), and Gearhart (1999). The Wavelet analysis identified when every minor collapse in the vehicle structure occurred and this was essential when constructing a mathematical CAE crash model.

Wavelet transform is particularly well suited to the analysis of transient wave propagation (Onsay, 1995). Since the physical phenomenon and the wavelet representation are well matched. The method is very suitable for transient analysis of both elastic wave motion and acoustic wave motion. Hence, the wavelet transform may be applied to clonk signal analysis, since it is aligned to the transient characteristic, and it preserves the time information that allows the impulse analysis of the structural and acoustic wave propagation and wave reflection. The Daubechies wavelet family is coded from db1 to db10, and the db9 and db10 wavelets are suitable for clonk analysis.

2.11.4. ARMA-Auto Regression Moving Average-modelling analysis

The approach taken here is to generate a data based model of the transient time signal, and then to interrogate the model structure to determine the defining parameters of the system.
Error terms that arise from differences between the measured output and the predicted output are used to optimise the model with each time increment.

The ARMA approach isolates and windows the main spectral contributions in a transient signal.

The ARMA model takes the definition ARMA (*p, q*) where *p* is the order of regression and *q* is the order of the moving average.

Once the (*p, q*) parameters of the ARMA model have been identified then the spectral estimate can be made. The *p* value defines the mode number in the signal.

The ARMA model has two subsets, the AR and MA, i.e. the autoregression and moving average groups. The AR expresses a time series as a function of its past values with an error term. The order refers to the number of past values that are used in the autoregression. The MA similarly expresses the time series as a moving average with a defined order. The estimation of the AR parameters $[a_1, a_2, a_3, \ldots a_p]$ involves the solution of the matrix equation using Burg's method, and maybe independently conducted from the MA parameters. MA parameters $[b_1, b_2, b_3, \ldots b_q]$ may be estimated using Shank's method. The process is detailed by Vafaei *et al* (2001).

2.12 Summary of the impact theories and the application to driveline clonk.

Impact noise control is a study of the energy transfer paths from an impulsive process, and the isolation of these paths from any highly radiating flexural vibrations. Contact time is directly related to elastic deformation and inversely proportional to relative velocity at impact. Increasing contact times by the use of these two factors or by any other means, will reduce ringing noise as well as the initial acceleration noise peaks. Ringing noise occurs from the excitation of structural modes of vibration and may also be associated with acoustic coupling. The resonant behaviour must be measured and analysed using appropriate spectral analysis methods, such as ARMA and Wavelet. These are strong conclusions from the driveline clonk study.

The driveline lash characteristics are piecewise linear, where the transition from a very low torsion stiffness rate to a high rate (as in a *hard* clutch disc) is instantaneous. (See later Figure 2.14). This transition is severe and it is sometimes referred to as a *stiff* system, having widely split eigenvalues.

It would appear therefore, that a higher initial lash drag rate followed by a more gradual engagement of the higher rate spring, and with higher disc hysteresis levels, would soften the impact and increase the impact time in line with the suggestions by Richards *et al* (1981).

A lower oil or grease viscosity would have similar effects on impact time and pulse severity. For example, a clutch with a viscous damper in series with it, has been found to be very effective against the onwards transmission of impulsive forces to the driveline.

2.13- Closure

- Increased contact times at impact will reduce the ringing noise and achieve lower acceleration noise peaks.
- Isolation devices for the energy path between the impact site and the nearby resonant structures should be identified.
- If impacts are softened then noise radiation is lowered due to the lower efficiency of sound radiation at lower response frequencies. This is generally a more effective way of reducing impact noise than by the addition of damping to impulsively excited structures.
- Increased structural damping of structures will attenuate noise radiation.
- Increased structural bulk (the volume to surface area ratio) will reduce the acceleration noise component.
- Introduction of resilience in impacts - if possible - will reduce velocity levels and increase contact times. This process will detune the response from the excitation.
- Increased drag torque will achieve increased contact times.
- Reduction in oil or grease viscosity will cushion impacts and increase contact times and thereby reduce acoustic radiation efficiency.
- The radiation efficiency of structures has a very important relationship to flexural vibration.
- Increased backlash rate (drag) may be more effective than backlash angle to soften impacts and to increase contact time. This also means that manufacturing control of backlash would be unnecessary.
- Structural resonant modes are responsible for most of the impact noise radiation and should be controlled. Non-resonant forced modes are much less effective noise radiators.

- Lightly damped structures may have a high modal density in the clonk frequency range of interest.
- The modal characteristics of thin walled cylinders are - perhaps surprisingly – complex and lightly damped with high inter-modal coupling.
- There is an opportunity for simultaneously improving rattle and clonk palliation by shielding the drive shaft tubes or reducing their activity. Both rattle and clonk noises are radiated from the drive shaft tubes. They have similar impact mechanisms.
- Clonk is a system problem evidenced by the numerous impact sites and by the interactions with the neighbouring structure at each site.
- Driveline inertias are coupled by extremely non-linear spring elements, which complicate the transmission of energy pulses down the driveline from site to site.
- The variation of body sensitivity to clonk is not known and is not included in this study.
- Lumped parameter modelling will be a useful tool for tuning the driveline system behaviour and for examining parameter change effects, which would otherwise be more difficult in an experiment. For example, the examination of alternative clutch disc characteristics may be readily evaluated using a mathematical simulation.
- Finite element modelling of thin walled structures in the driveline will be useful in understanding the noise radiation from resonant surfaces. Ideally, the FE model should be driven by the output of the tuned lumped parameter model.
- The acceleration noise efficiency of impacted bodies is logarithmically related to the non-dimensional contact time, which is itself inversely proportional to cube root of the body volume and directly proportional to impact time.
- The damping properties (due to internal slip mechanisms) of aluminium, steel, and cast iron are different by factors of 10.

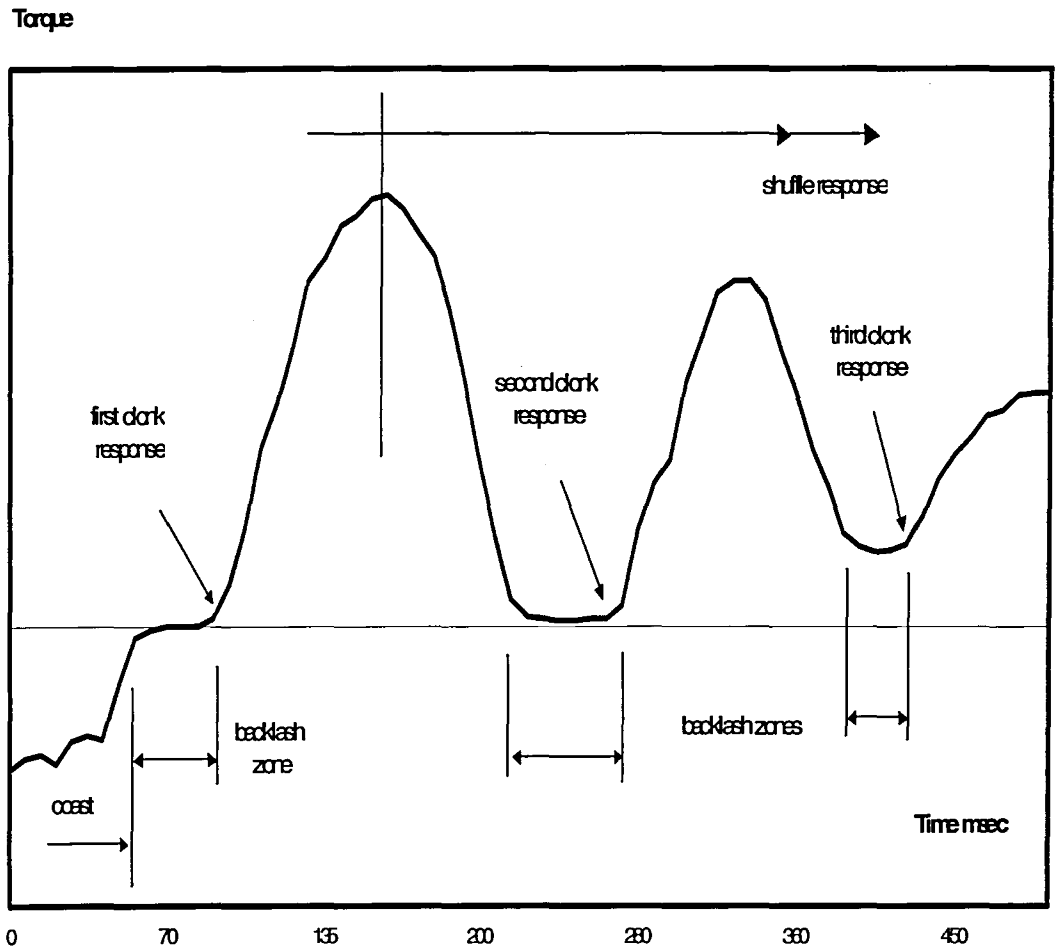

FIGURE 2.1. Typical torque variation with time during vehicle shuffle

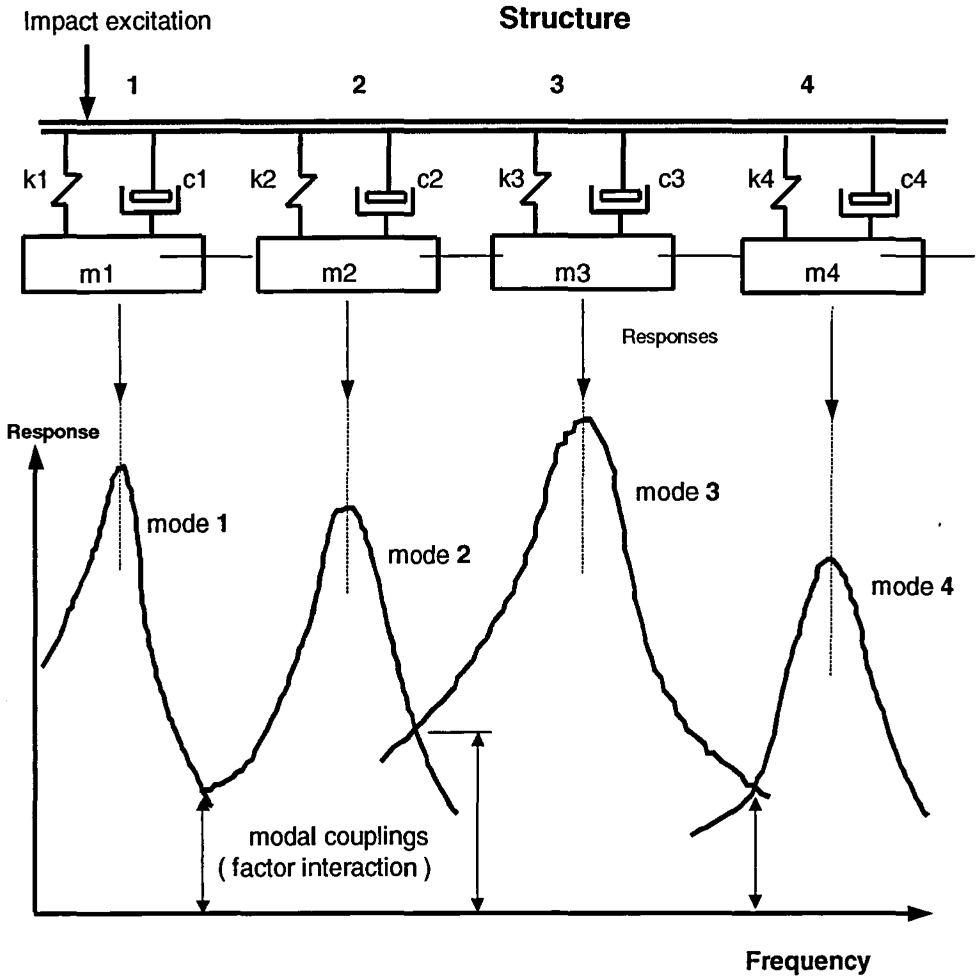

To show schematically how the structural modes may be excited by impact and how each mode is not only configured by its own (k,c,m) parameter values, but each each mode is also affected by coupling between the neighbouring modes.

FIGURE 2.2 The impact response of a multi modal system and the factor coupling interactions

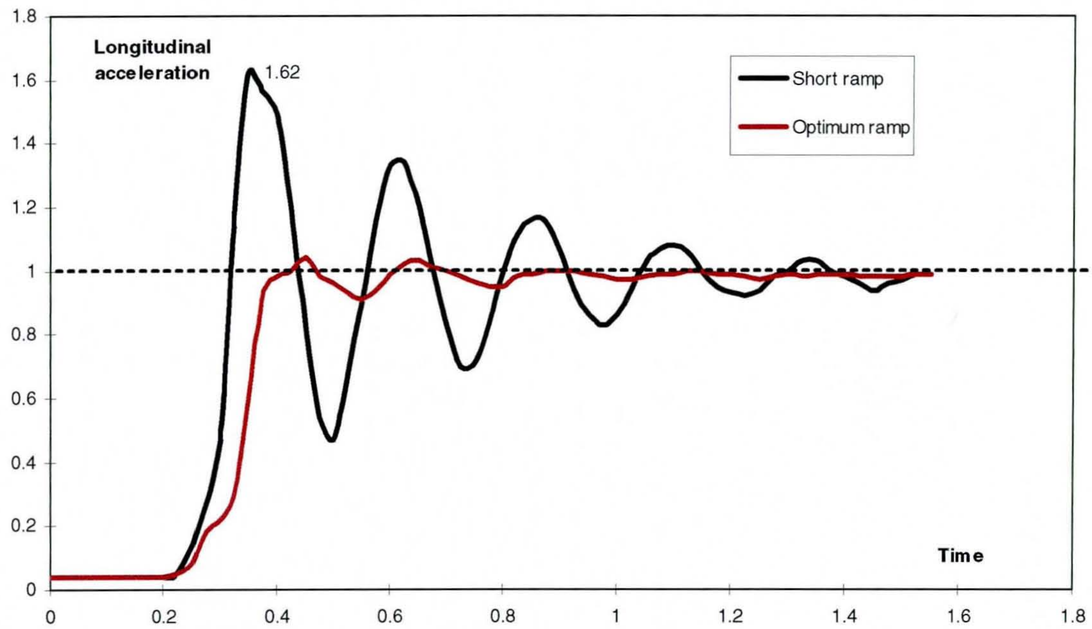

FIGURE 2.3 Typical vehicle shuffle response from drive i.e. not including the effects of backlash

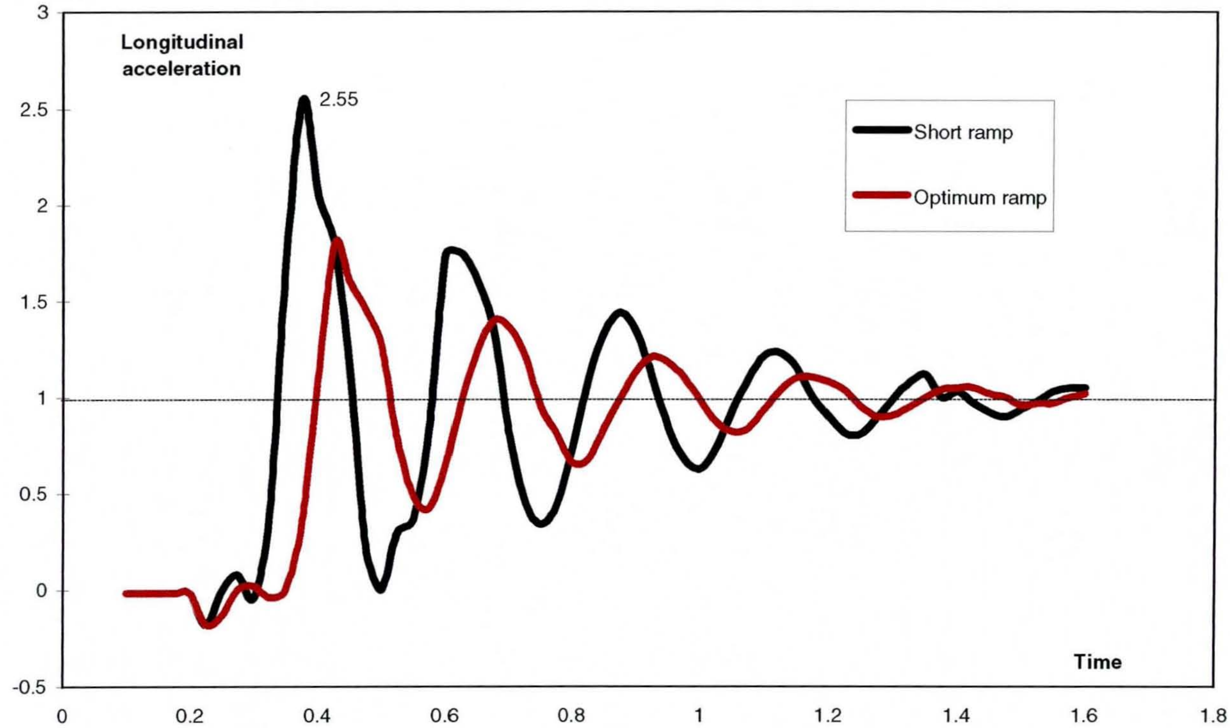

FIGURE 2.4 Typical vehicle response from coast i.e. *including* the effects of backlash

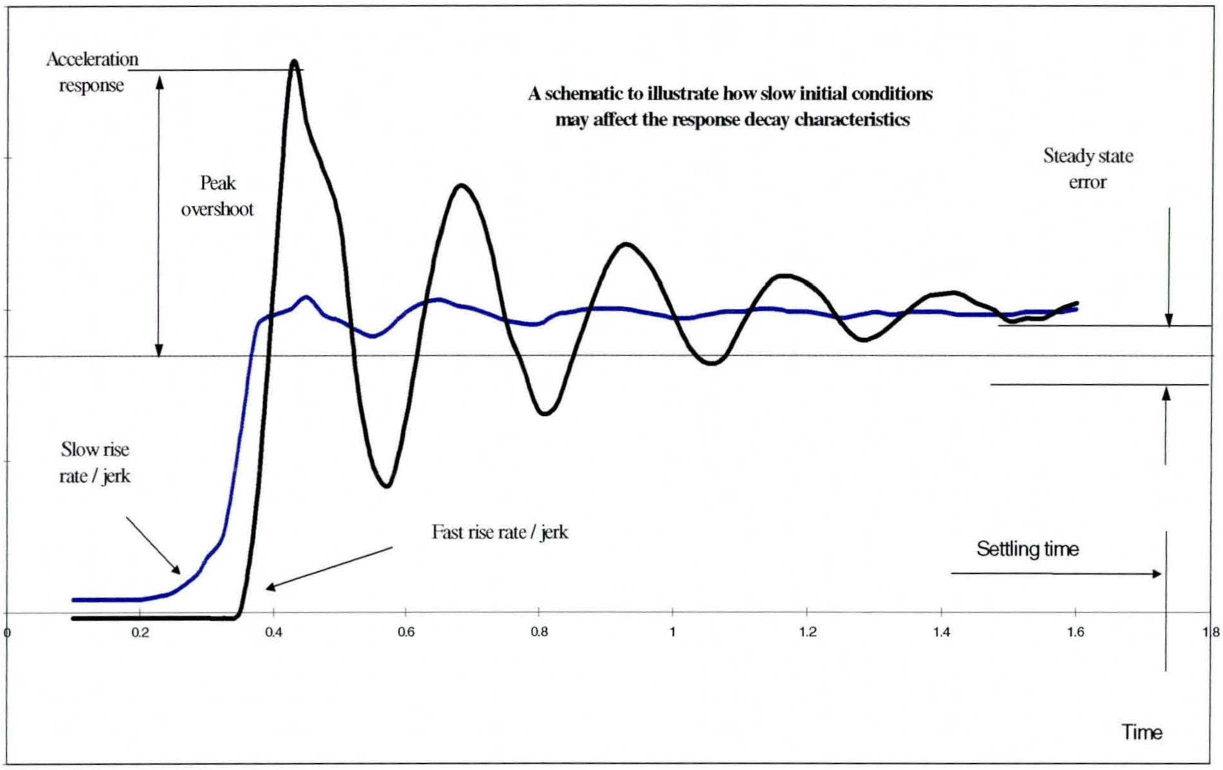

Figure 2.5. To illustrate the effects of initial conditions on response

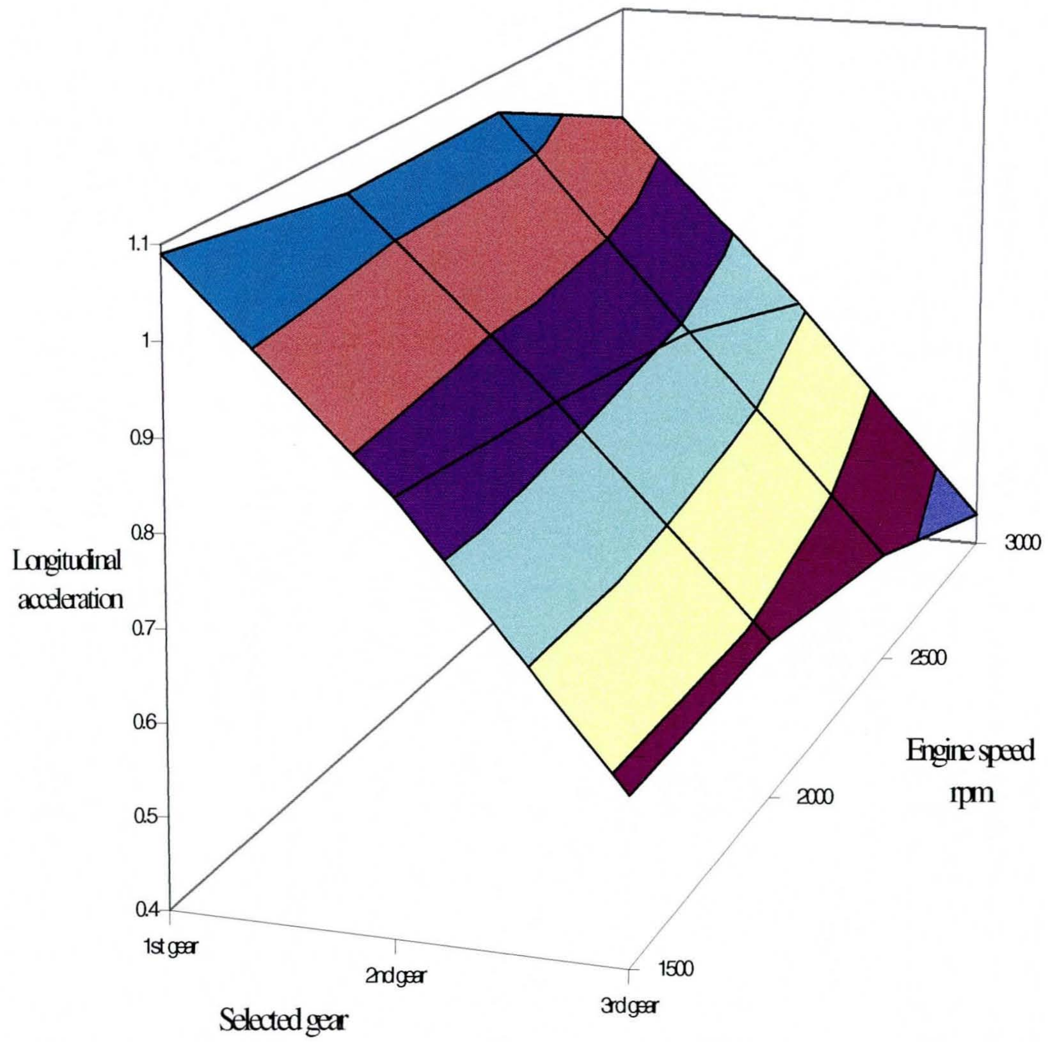

FIGURE 2.6. Shuffle response by gear and engine speed

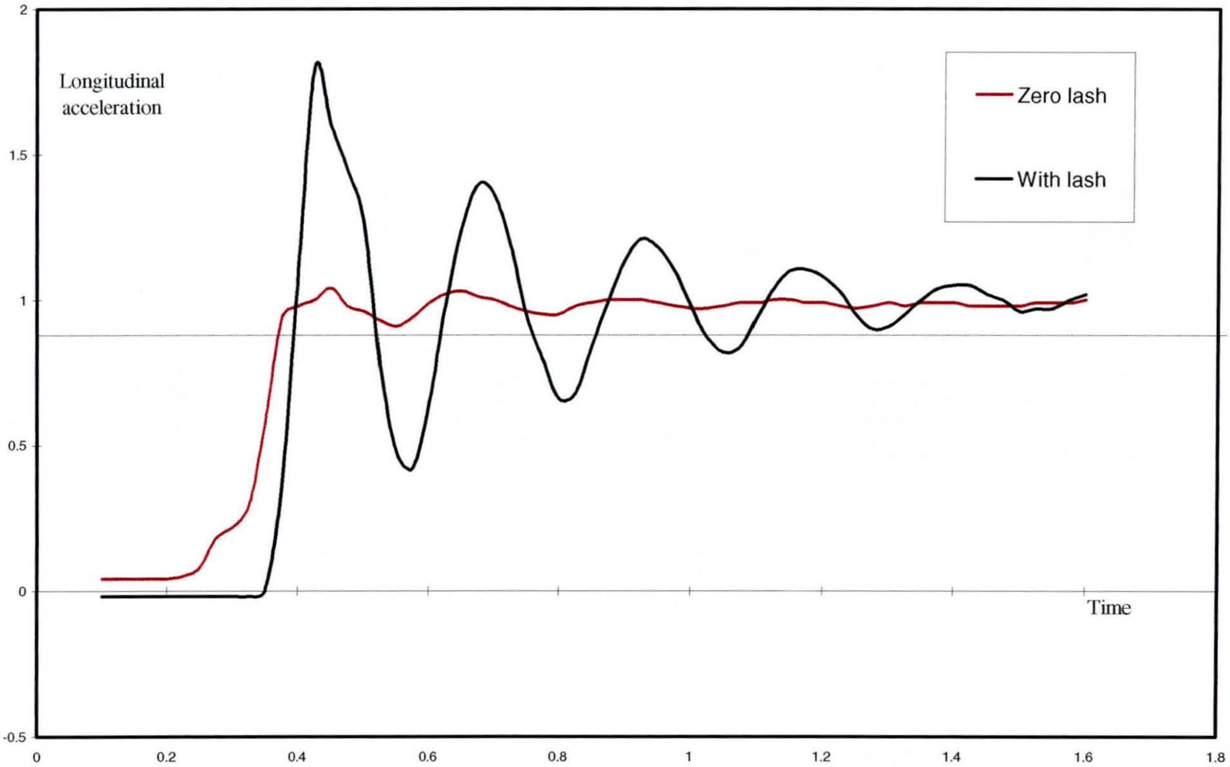

FIGURE 2.7 Shuffle response to optimum ramp impulses, with and without lash effects.

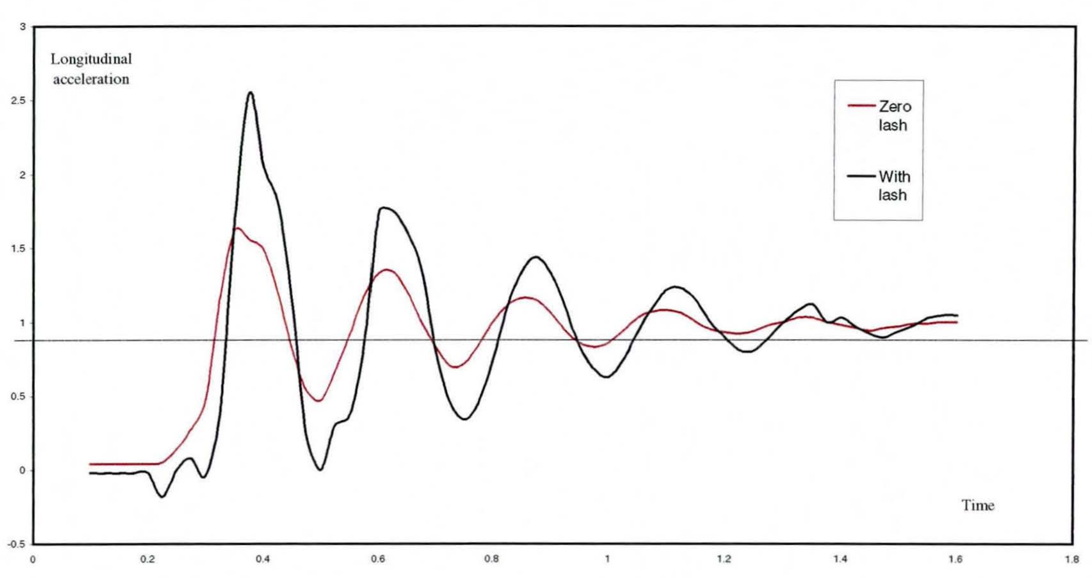

Figure 2.8 Shuffle response to short ramp impulses, with and without effects of lash

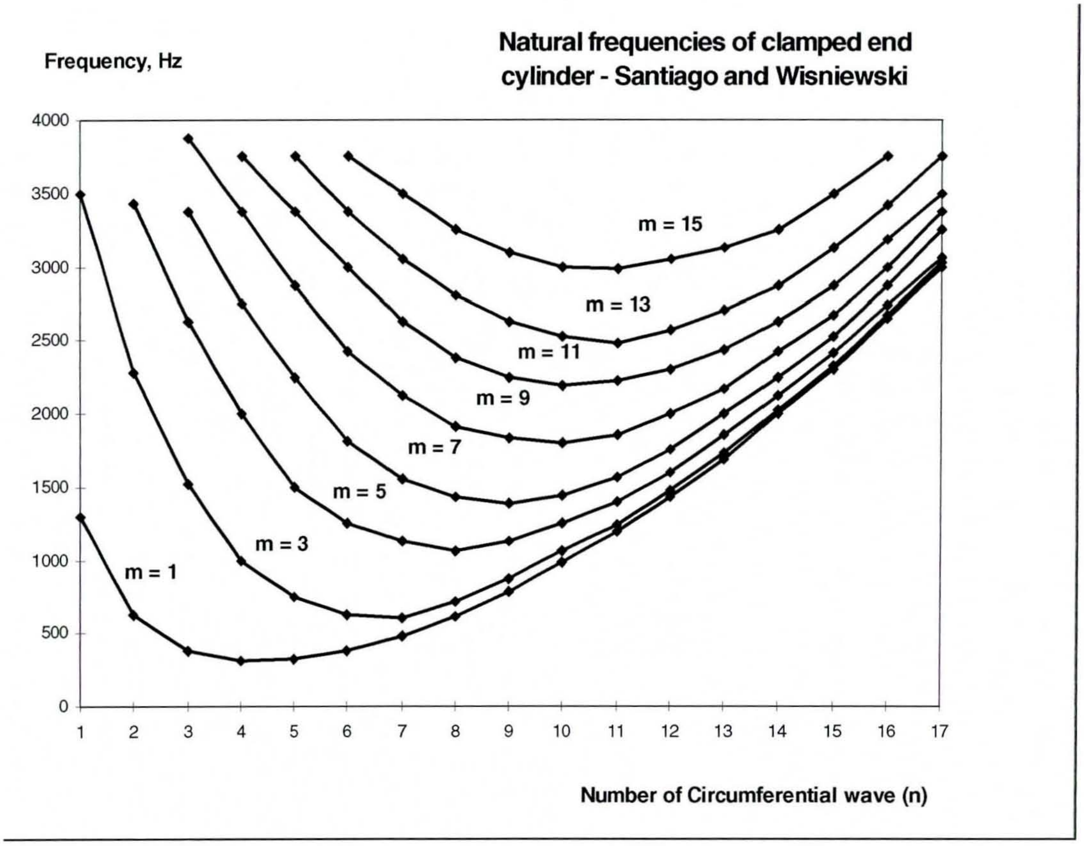

where :
Length between clamped ends = 800 mm
Inside diameter of cylinder = 305 mm
Wall thickness = 1.02 mm

Source : Convergence of finite element frequency predictions for a thin walled cylinder.
Authors : Joseph M. Santiago and Henry L. Wisniewski.
Computers and Structures 1989

FIGURE 2.9 Natural structural frequencies of a thin walled cylinder

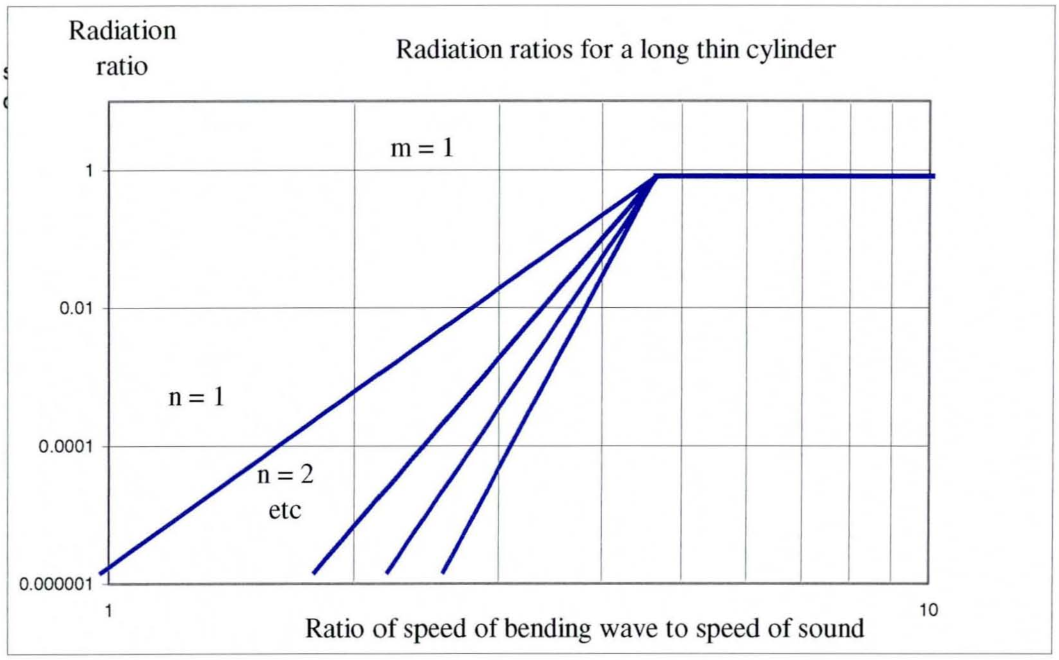

Reference : M.P.Norton. *Fundamentals of noise and vibration analysis for engineers* Camb Univ Press 1989

Resonant structural modes radiate noise very efficiently. When the flexural bending wave speed of the cylinder is equal to the speed of sound, the radiation ratio is unity. Radiation ratios help to estimate radiated noise levels from resonant surfaces.

The above diagram gives radiation ratio for **m**, i.e. number of *half* waves along the axis, and for **n**, i.e. the number of *full* waves around the pipe circumference.

The resonant peristaltic motion of the driveshaft tube in the clonk frequency range produces radiation ratios close to unity.

In other words the tubes radiate noise very efficiently, dependant also on their modal patterns.

FIGURE 2.10 Radiation ratios for a long thin cylinder

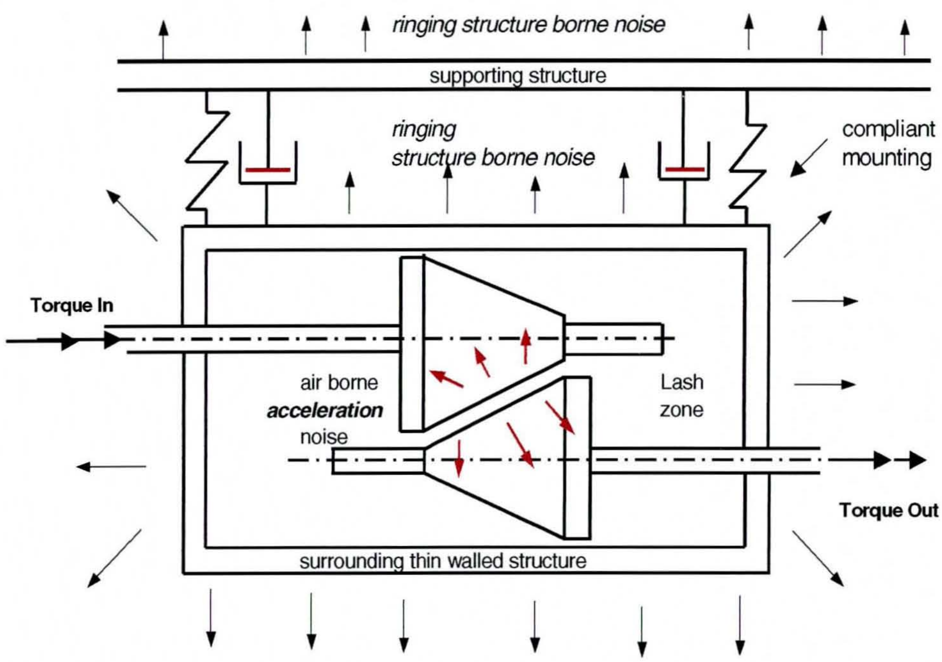

FIGURE 2.11
The impact mechanism and the dissipation of impact energy into the surrounding structure

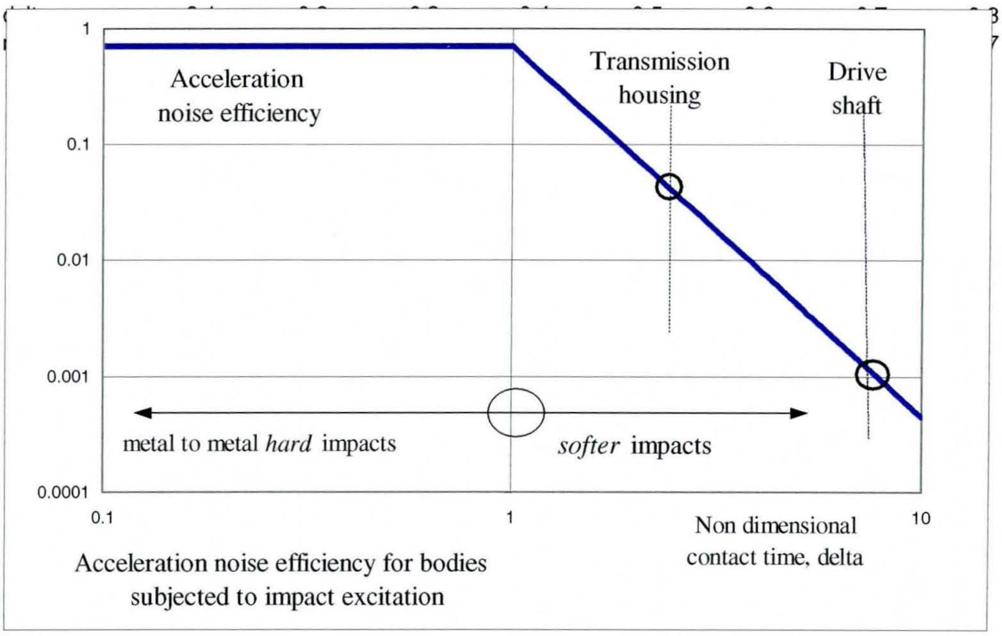

Ref : M.P.Norton. *Fundamentals of noise and vibration analysis for engineers.* Camb Univ Press 1989
If the impacted body is brought to rest in a finite time, most of the energy would be returned to the body but some would be radiated as sound.
Non-dimensional contact time is given by delta = c.t/cube root of V
where t = duration of impact
c = speed of sound
V = volume of single body
Acceleration noise efficiency is the ratio of actual noise radiated during impact, to that which would be radiated instantaneously. It is a function of the contact time.
For most metal to metal impacts delta <1.0 and acceleration noise is then significant.
It is highly desirable therefore, to increase contact times to reduce acceleration noise by preloading, by dense or cold fluid lubrication, etc

Richards [28] provided two empirical equations for the sound pressure developed during impact.Hence if both acceleration and ringing noise are present the dominant component may be estimated by considering the following :
Acceleration noise is calculated using the empirical graph and energy equations [28],
Ringing noise is evaluated from the product of radiation ratio, fluid density, speed of sound, radiating surface area of the structure, and vibrational velocity squared [28].

The above graph shows the importance of increasing *delta* in impacts by reducing body volume and increasing contact time.
For a **2 ms** impact time, the MT75 housing acceleration noise efficiency is much higher than that of the driveshaft tube, due to the relative volume difference. See above.
Note, for a **1 ms** impact, the acceleration noise efficiency for MT75 would be unity.
This is perfect noise radiation.

FIGURE 2.12 Acceleration noise efficiency for bodies subjected to impact excitation.

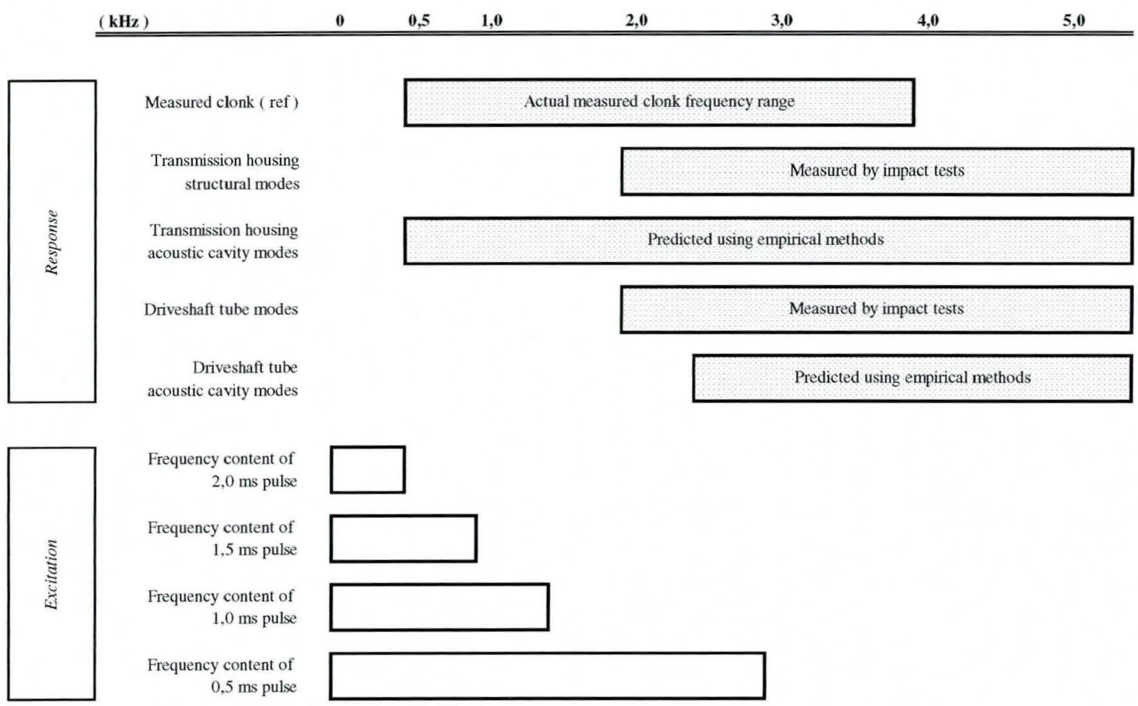

TABLE 2.2. Frequency chart

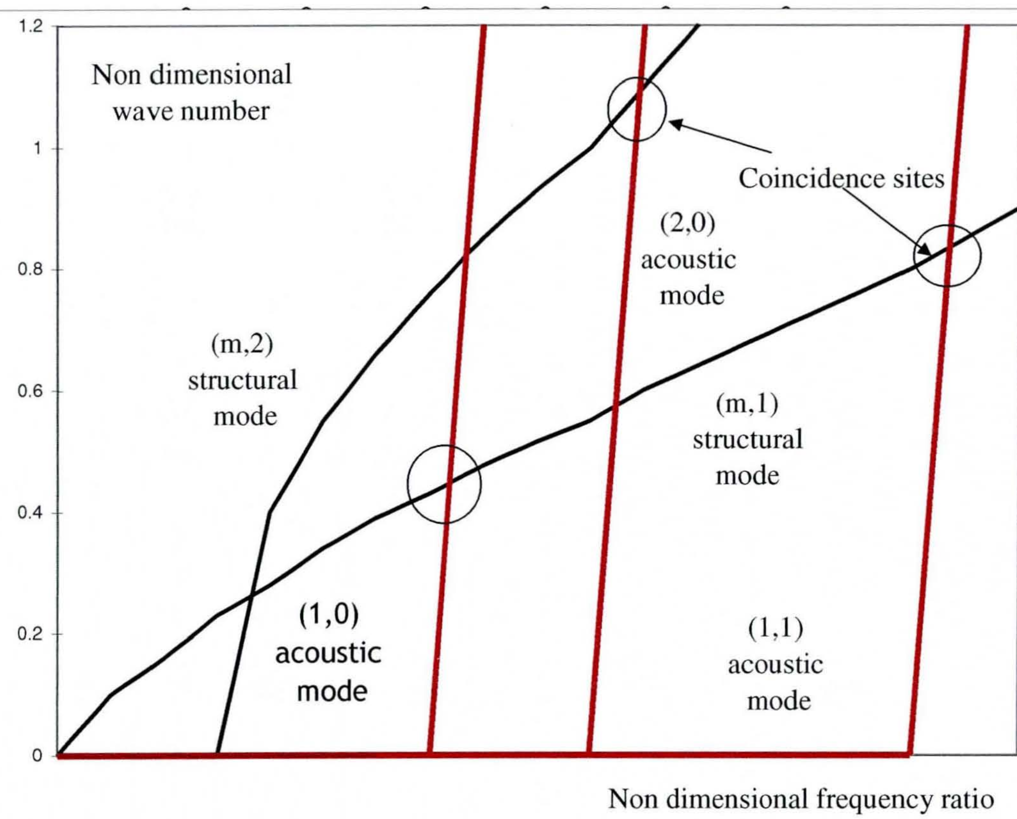

Showing coincidence between the structural pipe modes and the no flow internal acoustic modes

Reference : M.P.Norton.
Fundamentals of noise and vibration for engineers
Camb Univ Press 1989

Showing the coincidence conditions between the structural pipe modes and the internal no flow acoustic modes.

Coincidence is shown to occur between the (m,1) structural modes and the (1,0) and (1,1) higher order acoustic modes.

Coincidence is also shown between the (m,2) structural modes and the (2,0) higher acoustic mode.

Only a few acoustic modes occur in the shaft tubes in the clonk frequency range, and so there is little coincidental coupling with the tube structure.

FIGURE 2.13 Coincidence between structural pipe modes and no flow internal acoustic cavity modes.

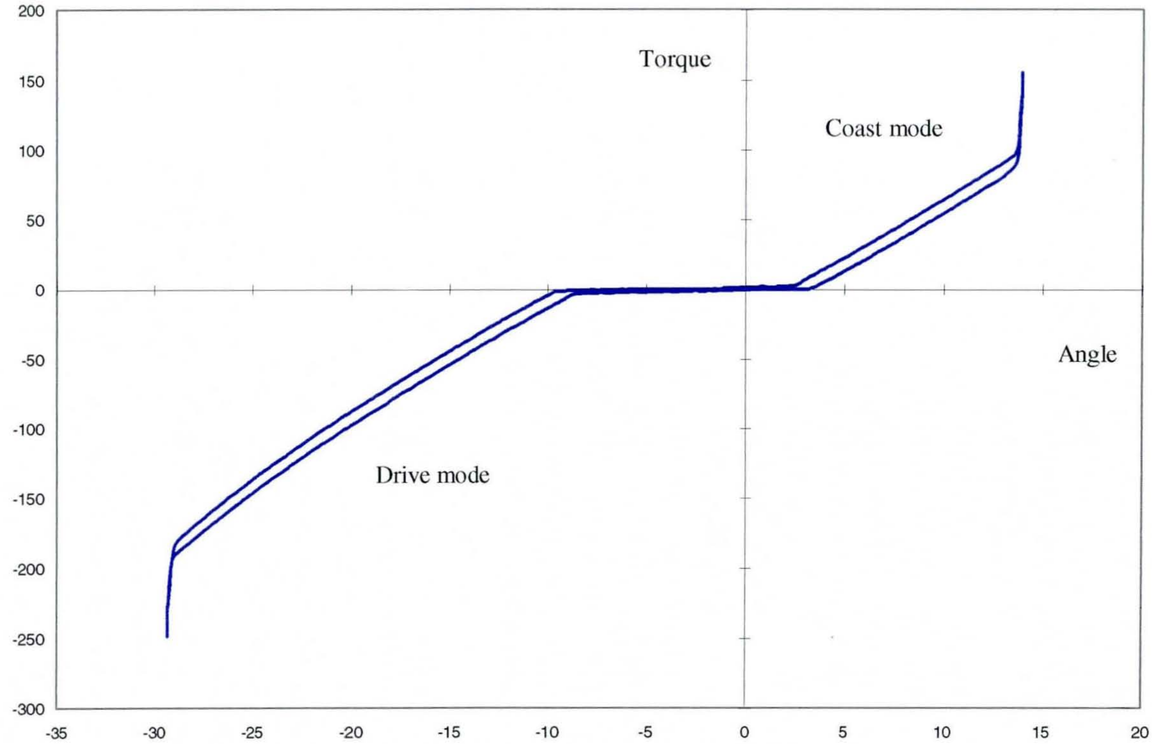

FIGURE 2.14 Non-linear characteristics of clutch disc with predamper

Chapter 3

Experimental investigations and signal analysis

3.1 Introduction

Table 1.1 in Chapter 1 provides a "roadmap" to the structure and contents of this thesis. It shows that a combined numerical prediction and experimental investigation is carried out to gain a fundamental understanding of the clonk phenomenon, with one major objective being the determination of the important design factors within the drivetrain system that most profoundly affect clonk. The ultimate aim ensuing from such a detailed investigation is to find a root cause solution to the problem, and in the medium term to be able to recommend cost effective palliative measures.

The fundamental study of the clonk concern necessitated a replication of the "problem vehicle" conditions with a representative laboratory-based experimental rig, which would enable investigations to be carried out in a repeatable manner and under controlled conditions. The piece-to-piece variations in manufacture and assembly of drivetrain components are unavoidable, particularly when dealing with tight tolerances and backlash in geared and splined components. These problems, and variations in driver-to-driver behaviour makes vehicle testing rather subjective as far as a fundamental physical study is concerned. However, rig-based studies also have some limitations, including imposed boundary conditions and to some extent the lack of "real world" noise factors. This makes rig-to-vehicle correlation studies a critical issue from the automobile manufacturer's viewpoint, since the outcome of the rig-based studies should lead to practical solutions for customer concerns.

Clonk is a major concern in powertrain engineering and affects all makes of vehicles, as well as across the range of vehicle types and models, from small saloons to light trucks. Therefore, the experimental vehicle work has been carried out for several configurations to obtain statistically significant results. The generic nature of a solution emanating from a fundamental investigation is another key desired outcome. Therefore, the investigations must include all vehicle models which experience the problem, and in all possible configurations.

A range of experimental techniques has been employed in order to cross correlate the findings, and to highlight the most suitable methods for given conditions. For instance, various signal processing techniques have been employed to deal with the high frequency transient signal. They included FFT, PSD, ARMA and Wavelet analysis, each of which is suited to a particular form of information or testing method. The high frequency vibro-impact problem was investigated at the system level (*in situ* in the vehicle on the road, and on a vehicle chassis dynamometer, and with a driveline rig), In addition the problem was investigated at the component level, where the behaviour of sub-systems and components was closely monitored.

This Chapter describes the experimental investigations and the techniques used in both subjective as well as objective studies. Chapter 6 provides the results of the experimental findings.

To gain a fundamental understanding of the clonk phenomenon it is important to ascertain the validity of the generally regarded postulate that impulsive loading of the drivetrain system through sudden demand in output torque or abrupt changes of the same is responsible for the elasto-acoustic coupling of thin walled volumes through impact dynamics in load bearing surfaces. Although the phenomenon is observed and surmised in literature, a fundamental proof of the postulate requires conformance of axiomatic proof (through experimentation) with mathematical proof (through the use of numerical techniques). The latter are developed in some detail in Chapters 4 and 5. Chapter 6 shows the conformance of the mathematical investigations with the experimental findings, thus providing a proof of the above postulate and the underlying physics of motion of the clonk problem.

Table 1.1 illustrates the structure (i.e. a roadmap) of the numerical and experimental investigations reported in this thesis

3.2 *Statistically designed experiments*

If a test is conducted on a system or a design with the purpose of evaluating a change to a function, and this test involves the collection of data for the purpose of making that judgement, then one is deemed to have conducted an *experiment* (Grove and Davis, 1992). And what is meant by the *Design* of Experiments? This means that the experimentation must be conducted in a controlled manner; to a predetermined test plan. The success of the experimentation is based on the use of statistical methods to confirm if the *factor effects* are statistically significant in the presence of *noise*, or not. In this case, noise refers to any cause of variation in the function of a part or system, whether the variation is caused through manufacturing or by the customer use or the environment. If a product or process functions as intended against a background of noise, then it is said to be robust (Grove and Davis, 1992).

3.2.1. *Background to DOE*

The Design of Experiments (DOE) is a process, whereby certain key system factors (parameters) are selected for study and are deliberately varied in a controlled fashion for the purpose of observing the effects of such action.

More often than not in the past, such an experiment may have involved changing only *one factor* at a time; so-called because the study would have involved holding all other factors constant, whilst only one was changed, in the belief that this would be the only way to precisely measure the effect of a change. This approach suffered from two main disadvantages:

- Changing one factor at a time was extremely time consuming,
- There was no opportunity for evaluating any factor interactions.

DOE should be used, when the system to be analysed is complex, and when there are many potential causal factors. It may be used in physical experiments or in analytical experiments, when a mathematical simulation of the system may be applied. It would *not* be appropriate for a new design concept.

A very useful way of determining the most relevant system factors is to conduct a brainstorm with contributions from all the appropriate technical specialists. Such a process uses a Cause and Effect fishbone structure.

For driveline clonk, the Cause and Effect fishbone would appear as shown in figure 3.15

Another useful technique is to identify the contributing factors at each operating level of the system, for example:

Driveline clonk = function (torque rise rate, backlash, engine speed differential, clutch engage rate, throttle demand, ***drive shaft dynamics***, transmission oil viscosity, *etc*)
Of which;

Drive shaft dynamics = function (***structural modal density***, acoustic modal density, torque pulse characteristic, modal damping, *etc*)
Of which;

Structural modal density = function (drive shaft tube wall thickness, tube diameter, tube length, material properties, *etc*)

Using this logical procedure, it is then possible to select the factors for DOE and to ensure that they are included in model and experimental parameterisation.

DOE may be applied to any process or system that has measurable inputs and outputs and has known control factors. Sir Ronald Fisher pioneered DOE in 1935 in his book *The Design of Experiments*. He used the approach to investigate the effects on agricultural yield when subjected to varying farming methods.

The technique later gained wider popularity and moved from agriculture into other process systems such as the chemical and pharmaceutical industries, where it was relatively easy to collect data and to analyse the results and implement process efficiencies.

In the 1980's the Japanese electronics and automobile industries realised the potential of the DOE methodology and along with the availability of personal computers, they enthusiastically adopted DOE to improve their product quality.

The champion of the Japanese enthusiasm for DOE was Dr Taguchi, who widened the appeal of the DOE methodology. He introduced the principles of robust product design and improved customer satisfaction, along with significant cost benefits. Taguchi also had a different approach to DOE than that adopted by Fisher.

Taguchi advocated that cross-functional teams of specialists should be used to identify by brainstorming the most likely control factors to include in an experiment, and to make the experiment more meaningful and time effective. Taguchi suggested that all processes and design functions should be considered in terms of an energy flow from input to output.

DOE is a significant subject area in its own right. For the purposes of this thesis, the outlying principles and methodology of DOE will be discussed, and how they shall be applied to the multi-faceted problem of driveline impact dynamics.

3.2.2 Introduction to DOE methodology

The Design of Experiments is a systematic test approach, which seeks to identify the contribution to the yield of a complex process or function, from a number of pre-assigned factors. It would not be advisable to apply the DOE process to a simple function or process having only a few control factors.

By contrast, DOE is most suitable when applied to multi-factored complex systems, when robust system performance is required, when factor contribution must be sorted into order, when optimisation is required, and when parameter and tolerance design studies are being performed.

DOE is a controlled series of tests, which are conducted in line with a predetermined test matrix. This matrix identifies for each test run, the factors and the levels at which the factors are to be set.

When there are many potential system factors under consideration, a *screening* experiment is first conducted, the purpose of which is to identify the *significant* from the *trivial* factors that have the most effect on the system or process output. A follow up experiment may then be conducted with a reduced number of factors, and perhaps with three or more levels, to identify the factor *settings* that optimise the system output. When factors are set at three or more levels, it becomes possible to gain information about non-linear effects, albeit at the expense of *confounding* and the need for an additional number of test runs.

Confounding or *aliasing* occurs when it is not possible to separate the effects of one factor from another, or to separate factor effects from factor interaction effects. This is the penalty for conducting a reduced DOE test plan.

For example, an optimisation DOE matrix could be run with each of k factors at two setting levels. Such a test would require 2^k possible test combinations, which would be configured in a *Full Factorial* test matrix. Hence, if 7 factors were each set to two factor levels, then a total of 2^7=128 test combinations in a Full Factorial matrix would be necessary, which would allow each of the factors to be investigated, at all setting levels in combination. For a factor with two level settings, it is assumed that the extremes are linearly related. In most cases, the factors in driveline dynamics have non-linear characteristics.

Such a Full Factorial test is time and resource consuming. The number of test runs grows geometrically with the number of factors. A more efficient test procedure is the Fractional Factorial matrix. The fractional factorial matrix will deliver useful (but not accurate) information from more factors, but with fewer test runs. It is a matter of balancing the quality and resolution of test information, against the time and cost to conduct the experiment.

Fractional experimentation reduces the number of tests, but then introduces *confounding*. Confounding is the term used to describe when main factor effects and interaction effects and higher order effects cannot be separated. In many cases the higher order effects are minimal (buried in the *noise* of the experiment) and fractional experimentation may then be justified.

Resolution: The concept of resolution is a description of what is lost in a test matrix, when a fractional factorial matrix is used to reduce the number of test runs.

Resolution *3*: No main factor effects are aliased with other main effects.
The main effects are aliased with two factor interactions.
Two factor interactions may be aliased with each other.

Resolution *4*: No main effects are aliased with other main effects.
No main effects are aliased with two factor interactions.
Two factor interactions may be aliased with other two factor interactions.

Resolution *5*: No main effect or two-factor interaction is aliased with any other main effect or two-factor interaction.

Two factor interactions may be aliased with three factor interactions.

3.2.3. Example: A 2-level full factorial test plan

For the case, where 3 factors A, B, and C, each at 2 levels (at HIGH and LOW levels) are considered a full factorial experiment results in 2^3 combinations.

The DOE test matrix would be as follows:

	Factor A	Factor B	Factor C	System yield
Run 1	LOW	LOW	LOW	
Run 2	HIGH	LOW	LOW	
Run 3	LOW	HIGH	LOW	
Run 4	HIGH	HIGH	LOW	
Run 5	LOW	LOW	HIGH	
Run 6	HIGH	LOW	HIGH	
Run 7	LOW	HIGH	HIGH	
Run 8	HIGH	HIGH	HIGH	

The system response variable (yield) would be measured for each of the runs 1 to 8 in the matrix. The runs would also be in random order.

Fitting a prediction equation to the test data results in the following first order yield response model as:

$$Y = \mu + \beta_1(A) + \beta_2(B) + \beta_3(C) + \beta_{12}(A.B) + \beta_{13}(A.C) + \beta_{23}(B.C) + \beta_{123}(A.B.C) + \varepsilon$$

where Y is the system yield.

A, B, and C are the main factors in the DOE matrix.

A.B and A.C and B.C are two-way interactions.

A.B.C is three-way interaction.

$\beta_{i,j}$ is a linear coefficient.

μ is the mean value.

ε is experimental error.

This equation would be used to predict the system yield for factors set at any other levels

The 8 run matrix experiment may also be simply represented as an eight-sided cube as follows, where each corner represents a response for each test run in the matrix.

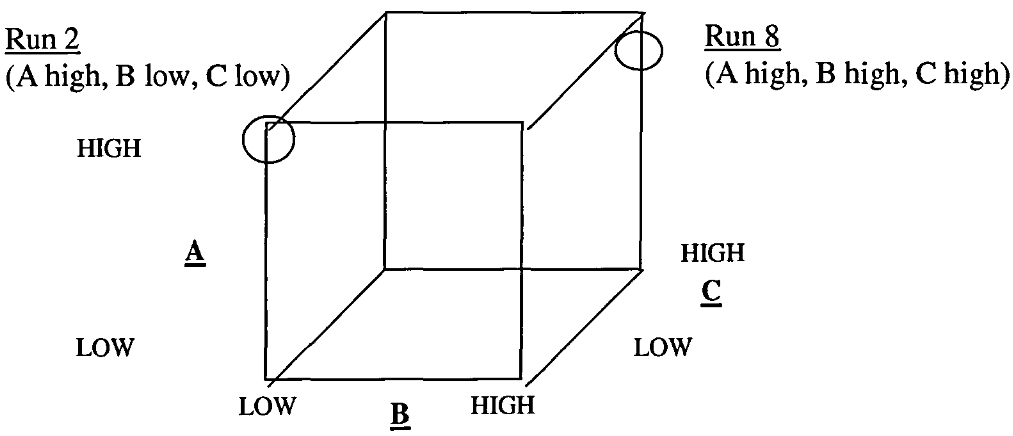

3.2.4. Factors A, B, C in 8 test runs with factor interactions

	Factor A	Factor B	A.B	Factor C	A.C	B.C	A.B.C	OUT -PUT
Run 1	-	-	+	-	+	+	-	6.2
Run 2	+	-	-	-	-	+	+	7.1
Run 3	-	+	-	-	+	-	+	9.5
Run 4	+	+	+	-	-	-	-	7.5
Run 5	-	-	+	+	-	-	+	13
Run 6	+	-	-	+	+	-	-	12.1
Run 7	-	+	-	+	-	+	-	12.9
Run 8	+	+	+	+	+	+	+	15.1

$$\text{Effect of factor A} = \frac{(7.1 + 7.5 + 12.1 + 15.1)}{4} - \frac{(6.2 + 9.5 + 13 + 12.9)}{4}$$

$$\therefore A = 10.45 - 10.4 = 0.05$$

which is the average of four effects, one for each of the four combinations of B and C.

Similarly, effect of factor B = 11.25 – 9.6 = 1.65

effect of factor C = 13.275 – 7.575 = 5.7

The same procedure is applied to the factor interactions, for instance:

$$\text{Effect of A.B} = \frac{(6.2 + 7.5 + 13 + 15.1)}{4} - \frac{(7.1 + 9.5 + 12.1 + 12.9)}{4}$$

A.B = 0.05, which is the interaction of A.B measured over the average of C

Similarly, A.C = 0.6 and B.C = -0.2

The three way interaction A.B.C = -1.5, which is half the difference between the interaction B.C for A_{HIGH}, and the difference between B.C for A_{LOW}.

Therefore, in this fictitious example, factor A is not significant compared to B and C, but the three-way factor interaction A.B.C is relatively significant.

Note in this trivial example, all the factors and the factor interactions are not confounded, and their contributions are clearly separated. However, in the following example the 5 test factors (A, B, C, D, E) are confounded in 8 test runs. We cannot separate the main factor effect from the interaction, and the interactions are also confounded. Hence, this is a Resolution 3 array.

	A B.E	B A.E	E A.B C.D	C D.E	A.C B.D	B.C A.D	D C.E	YIELD
Run 1	-	-	+	-	+	+	-	
Run 2	+	-	-	-	-	+	+	
Run 3	-	+	-	-	+	-	+	
Run 4	+	+	+	-	-	-	-	
Run 5	-	-	+	+	-	-	+	
Run 6	+	-	-	+	+	-	-	
Run 7	-	+	-	+	-	+	-	
Run 8	+	+	+	+	+	+	+	

3.2.5. Steps in setting up a Design of Experiments

Step 1: Define the problem clearly.

>> Choose a multifunctional team.

>> Establish the objectives of the experiment.

Step 2: Selection of control factors and factor levels.

>> Use of Cause and Effect charts/Pareto charts/etc.

>> Establish how the factors are controlled and measured

>> Set the factor levels as wide as possible.

Step 3: Selection of the output variable.

>> Does it provide information about the problem?

>> Is it measurable and repeatable and with what accuracy?

>> Is the output stable over time? Is it in statistical control?

Step 4: Choice of the experimental design matrix and sample size.

>> Balance between accuracy and resource.

Step 5: Perform the experiment and collect data.

>> Perform a pilot run.

>> Accuracy of measurement.

>> Repeatable test conditions.

>> Consider data variability.

Step 6: Data analysis.

>> Eliminate the statistically insignificant factor effects and rerun with only the significant factors and interactions.

>> Use graphical and numerate methods.

Step 7: Results and conclusions.

Step 8: Achieve the objective stated in step 1.

3.2.6. Application of the DOE methodology to driveline impact

The driveline is a complex interactive system with many potential clonk causal factors. Hence, DOE would be a suitable diagnostic tool.

The driveline is a mechanical system that can be modelled using MBD code, and then this could also be submitted to DOE analysis. In fact if the model is parameterised, it makes DOE analysis easier.

DOE clonk studies may be conducted at different system levels:

At the macro level, e.g. The flywheel to the rear road wheels,

At the micro level: The gear tooth impact.

The hollow cylinder (driveshaft)

The choice of the clonk output variable (the Quality metric) can be critically important:

External clonk noise, perhaps at the driveshaft or transmission?

Internal noise as perceived at the driver's ear position?

Structural vibration at the driveshaft or transmission?

The output variable is time dependent. This means that it would be more appropriate and of more value, to consider the total clonk time response than the single peak value recorded in the time response.

Following the previous point, it is important to ensure that if a factor has a positive effect in the clonk frequency range, that it does not have a negative effect outside the clonk range.

It is very important that every test run is fully repeatable and is made with the same initial conditions, because the driveline system is very non-linear and very sensitive to changes in initial conditions.
Some calculations must also be made to account for the following, in order to be able to draw meaningful conclusions from the tests:

Only one vehicle tested, with only one set of vehicle conditions.
Only one testing engineer be in charge of data collection.
Only one set of measuring equipment to be employed.
Effects of day to day variation be taken into account.
Variation in initial test conditions, as already mentioned.
Stability of 'noise' factors during test (oil temperature, ambient temperature, etc).
Choice of test control factors and settings:

The final DOE result is completely dependent on the initial choice of factors and settings.
Some of the test factors are very non-linear. Backlash is the biggest discontinuity.

3.3 Road testing ~ RWD commercial vehicle

Manufacturing and assembly plant quality audits by the plant test drivers, had identified a significant clonk subjective variability in production off-line vehicles. This was partly due to the driveline response sensitivity to driving styles (See Figure 3.1).

Shuffle ~ low frequency pitching mode ~ was found to be significantly dependent on driving conditions and driving style. Clonk was particularly noticeable, when excited by the shuffle mode.

The clonk response at different vehicle speeds was rated subjectively, and found to be worse at lower speeds and in lower gears (See Figures 3.2 and 3.3).

Microphones were placed at the transmission, at the rear axle, and at the driver's head.

The 1/3rd octave noise recordings due to back-out throttle in 2nd gear at low speeds are shown in Figure 3.4. This figure shows:

- The clonk frequency range was 500 - 4000 Hz (approx.) as measured at the transmission and at the rear axle.
- Noise levels from the transmission were higher than those from the axle. This was in accordance with subjective evaluations. The microphone was placed at the rear of the transmission and near the driveshaft.
- The interior noise level spectra showed a flatter profile, showing how the metallic airborne noise from gear impact at the axle and transmission is 'converted' to a lower frequency structure-borne noise.

3.3.1 Commercial vehicle jack up test

The test vehicle was jacked up under the rear axle. The handbrake was lightly applied to give some torque resistance. The 2nd gear was selected and the clutch was quickly engaged. The clonk response was subjectively rated to be the same as when driving on the road. It appeared to source from the transmission. No data was collected.

This test gave subjective support to the proposal that the actual vehicle driveline should be monitored in the test lab. It was essential that the same problem condition as experienced on the road should be repeatable under controlled conditions in the test laboratory.

3.3.2 Road testing ~ FWD passenger car

An interior microphone was placed in the car at the passenger head location, and an exterior microphone at the driveshaft. The engine speed was also recorded. A typical output is shown in Figure 3.5.

A number of driving manoeuvres were experimented to best excite clonk. The most reliable and repeatable manoeuvre was rapid clutch engagement at low vehicle speeds and in low gear and with no throttle. It was called the 'car park' manoeuvre. This manoeuvre consistently gave unacceptable clonk.

3.4. Chassis dynamometer testing

The chassis dynamometer offered the opportunity to study vehicle dynamics and NVH under realistic and controllable test conditions on the ‘rolling road’. The disadvantage when testing driveline clonk is that other unwanted noises are also recorded, engine noise and road noise for example.

3.4.1. Chassis dynamometer testing with a FWD vehicle

The FWD passenger vehicle was installed on a vehicle dynamometer (the engine was used to drive the rolling road), and the same driving method to induce clonk as had been used on the road, was then applied on the dynamometer. The data was recorded at the head and shaft locations. There was no subjective difference between the clonk on the road and the clonk on the dynamometer.

The purpose of this dynamometer test was to confirm that the clonk phenomenon could be reproduced under controlled conditions, and then to conduct a Design of Experiments (DOE) on the vehicle, whilst on the dynamometer rig.

Note that the DOE testing had also been conducted on the commercial vehicle, but on a so-called static test rig (with no motored condition). It had been evident that the lightly damped thin walled structures (transmission housing and driveshaft tubes) were resonant in the clonk frequency range and so modal data was needed. This data had been obtained on the rig.

The intention with the passenger car was to conduct a similar factor analysis, this time on the rolling road and using DOE methods, in order to understand the FWD clonk factor contribution and the various factor interactions. Other noise factors were measured and held constant during the tests.

The selected control factors were as follows:

- Clutch pedal engage rate
- Engine speed at engagement
- Transmission oil viscosity
- Drive shaft type
- Clutch disc type

All of these factors were set at two levels during the test as follows:

- Clutch pedal engagement rate: Fast and slow
- Engine speed at engagement: Above and below the idle rpm
- Transmission oil viscosity: Thin and thick
- Driveshaft type Solid and tubular
- Clutch disc type With and without predamper springs

By definition, clutch pedal engagement rate is a noise factor. Since its effect was considered to be significant, its contribution was tested with a view to considering how it might be later converted to a control factor. For example, a hydraulic restrictor could be employed.

The measured and recorded noise factors during the DOE were as follows:

- Transmission oil temperature.
- Test room environment

The DOE orthogonal test matrix was a 16 run random sequence with no confounding of the factors and factor interactions. This meant that the effect of each and every factor and factor interaction was not complicated (confounded) by another neighbouring factor. The DOE test array is shown in Figure 3.6

Several output data channels were measured simultaneously in the time domain for each test condition:

- Interior noise at the passenger head location, using a dummy head
- Exterior noise near the driveshaft location
- Laser speed signals from the driveshaft
- Engine speed
- Time

Sometimes the factor effects could be different at various locations and this was the purpose of taking several output data recordings for each factor setting.

The data was also analysed in different ways. The factor effects were calculated:

- Using only the peak response value
- Using the complete time domain signal response

The response signals for each test run were collected several times to check for the repeatability of data.

It was also necessary to take account of whether the vehicle was statistically representative of the production volume, whether there was repeatability in the measuring equipment, and whether the test method was repeatable.

This ultimately allowed for factor identification process; those that made significant clonk contribution, even after other noise factors had been taken into account, and due allowance was made for the single test sample/vehicle.

With regards to the method of analysis, if DOE factor effects are based on <u>peak</u> signal values, this may or may not be appropriate for clonk. This is an impulsive and transient noise with a frequency range in the most sensitive part of the human ear audible range.

It was decided to also analyse the complete response spectrum for each test run, and not just the peak. This had several advantages:

- It was a more appropriate metric for audible clonk, since the ear has a slow filter process for transient sounds of less than 100-msec, and so peak value readings were probably less reliable indicators
- It was then possible to compare the factor contribution for each spectral line and test whether it was significant against background 'noise'. The factor effect could be insignificant, significant but negative, or significant and positive.
- It was possible to determine if the factors were effective inside the clonk frequency range, and whether they would have any detrimental effect outside the clonk range.
- If the factor settings resolved or improved clonk, but also simultaneously introduced another NVH concern, it would still be possible to revise the factor settings and achieve a smaller clonk improvement and with nil adverse NVH effects outside the clonk frequency range. In other words to exercise compromise. For example, it might be found that deletion of the clutch disc predamper would improve clonk, but worsen idle gear rattle in another frequency range. In this case, a compromise may be made, for example to reduce but not eliminate the predamper characteristic. Another example, a chosen factor might be set to a level that improved driver's head noise but this worsened the passenger head noise.

3.5. *Driveline rig testing (RWD)*

It was very important that the clonk experimentation should be reliably conducted:

- With absolutely repeatable test conditions.
- With responses which truly reflected the effects of factor changes alone, and not those of any other peripheral factors (including test methods).
- With no environmental or human error affects.

A static driveline rig would offer the opportunity for controlled testing in a quiet environment with repeatable test conditions. This would not be achieved in a fully dressed vehicle on the road with tyre noise, wind noise, etc masking the data. A static rig would also allow modal data to be collected and to get a much better insight into the clonk phenomenon.

3.5.1. Commercial vehicle 2 piece driveline rig test (RWD)

Requirements of a driveline rig:

- To collect test data and then verify the mathematical simulation
- To enable clonk to be reproduced in a clean and quiet environment on a static rig
- To conduct a design of experiments
- To locate the major clonk noise sources in the driveline
- To examine the factor influences as suggested by a team of cross functional experts
- To study the structural responses of the system under impact
- To better understand driveline sensitivity to clonk

3.5.2. Rig boundary

- To include flywheel / clutch / transmission / two piece driveshaft / rear axle assembly including hubs and drums. (i.e. the system rig to include all lash zones in the driveline).
- Transmission to be fixed via compliant mounts to the floor.
- Bell housing, drive shafts, and axle, to be mounted to bedplates and to the floor.
- Input torque to be applied directly to the flywheel, with the engine disconnected.
- No connections to a body.
- Torque reactions from the driveline fixing locations, to the floor.

The driveline layout is shown schematically in figure 3.7.

The actual rig is shown in figure 3.8, which depicts the experimental static drive train rig. The rig includes a flywheel, clutch system, transmission, a two-piece drive shaft with the centre journal bearing, the differential and the rear axle assembly including hubs and drums. Therefore, it includes all the lash zones in the drivetrain system. The transmission casing is fixed to the ground through compliant mounts, and the bell housing, the driveshafts and the rear axle are mounted upon bedplates fixed to the ground. The driveshaft assembly's universal joint angles are set to nominal with no suspension test latitude. The clamped clutch transmits the flywheel impulse torque to the transmission input-shaft via the torsion friction disc springs, when a preload torque is released. The transmission is engaged in the second gear.

3.5.3. System and subsystem functions

Torque developed by the engine is used to accelerate the flywheel and to overcome the torsion drag in the driveline such that sufficient tractive effort at the road wheels is achieved to provide the desired vehicle motion.

Each sub-system in the driveline makes a functional contribution to the system design intent of torque transfer. The output of each subsystem is an input to the next downstream subsystem, viz.

- The engaged / clamped clutch transmits the flywheel torque to the transmission input shaft via the torsion springs in the clutch disc. Driveline shuffle and clonk occur when the clutch is engaged.
- The disengaged / slipping clutch transmits slip torque after gear selection through the clutch disc springs. There are two torque paths through the clutch. These are:
  - From the flywheel face to the transmission input shaft splines, via the pressure plate assembly and then via the clutch disc.
  - From the flywheel face to the transmission input shaft splines, via the clutch disc. The friction material is fully clamped.
- The transmission assembly provides gear ratio selection dependent on driving conditions. It transmits torque to the drive shaft assembly.
- The driveshaft assembly consists of universal joints, slip splines to allow for suspension movement, and is restrained by support bearings to the body. It transmits torque from the transmission output shaft to the driving pinion gear in the rear axle assembly.

  The rig driveline angle is set to nominal with no suspension test latitude.
- The axle differential splits the torque to each road wheel. The differential gear assembly ensures that inner and outer road wheels rotate at the same speed appropriate to the corner or surface being travelled. Torque flow is from the pinion gear to the road wheels via the crown wheel gear reduction and through the side gears splined connections to the half shafts, which then transmit the driving torque to the wheels.

Each of the sub-system functions include backlash and are, therefore, essential components of the rig. The presence of backlash will cause the input / output relationship to be non- linear. (The ideal system will be linear and contain no backlash)

3.5.4. Description of test method (RWD)

The IKA University of Aachen experience with FWD driveline clonk had indicated, that the application of torsion impact to the driveline by the instantaneous release of a preload torque, was an effective method of generating an impulsive sound (Biermann and Hagerodt, 1997, 1999). It was repeatable, simple, and cost effective, and this system was adopted in the test rig. The input shaft was strain gauged to record the torsion pulse applied.

The literature survey had suggested that structural response was a major contributor to impact ringing noise. Accordingly, the test accelerometers were placed not only at the sub-system output points but also at equi-spaced structural locations to gather modal response data due to impact. All the response signals were simultaneously recorded. Microphones were placed at the transmission and at the axle housing thus copying the vehicle test set up.

3.5.5. The test input.

In general, it is not practicable to reproduce the actual shock environment in a test. It is better to ensure that the *effects* of the test shock are similar to the shocks in practice, and to ensure that these shock effects are completely reproducible for the purposes of comparison of test results with other factor levels.

A comparison of repeated pulse inputs is shown in figure 3.9 to illustrate rig repeatability. This requires that the shock pulse is simple, well-defined, and repeatable. More important, the associated frequency spectrum is repeatable. The measured peak acceleration responses to repeated input conditions were found to have identical responses.

The response of the system to impact is a function of the torque rise pulse shape, the pulse duration, and the system characteristics.

A shock *impulse* contains, theoretically, the energy spread over all the frequencies from zero to infinity. It has infinite force over an infinitesimally small duration. It therefore, has the capacity to excite any modal system through an infinite spectrum.

By comparison, a real shock *pulse* has finite duration, and the time is short compared to the frequency range of interest of the system under study. The input energy spectrum will ensure that all the resonant dormant modes of the system will be excited.

The torsion pulse applied to the driveline rig had a duration that varied between 80ms and 180ms, dependent upon the test conditions (i.e. the factor levels selected). Coincidentally, this pulse duration was ideal excitation for the shuffle mode, but the pulse generated by lash take-up in the driveline was of the order of 1-2 *ms*, which was sufficiently short to excite the much higher frequency clonk modes.

The specified preload torque was applied to the system to take up the entire lash in the system and to compress the clutch springs. This preload torque was then held on a low inertia disc brake. The stored energy was instantaneously released, when required, in the form of a ramp saw-tooth pulse. The accelerometer and noise recordings were simultaneously made with the torque release.

Figure 3.10 shows a typical surface response in time and frequency domain. It shows a 1-2 *ms* impact followed by approximately 30 ms of driveshaft tube *ringing*.

This system of excitation had several attractions:

- Quietness of operation (no spurious background noise)

- Negligible added inertia to the driveline rig system.
- Compact, simple, cost effective.
- Highly repeatable.
- No damping or frictional drag during pulse release.

Several torsional rebounds followed the first pulse application. Only the first of these rebounds was considered in the analysis.

3.5.6. Torsional hammer (an alternative method of input shock)

A torsion impact hammer had been developed by Stone (1994) to apply an impact *during rotation.*

The hammer system was attached to the input shaft of the system under test. When required, two sliders of equal mass are released from the axis of rotation and they accelerated radially outwards. At the end of their travel they each impacted a stop, which imparted a sharp pulse to the system. This is perhaps a more realistic method than that used in the static application of torque in the clonk study, but there are several disadvantages with the torsion hammer:

- There was a significant added inertia to the system.
- There was a risk of lack of repeatability.
- There would be a rebound at the end of the mass slider travel.
- The two impacts may not be coincidental at the end of the slider travel.
- Costly and lacked compactness.
- Noisy.

3.5.7. Description of the experimental rig

There have been only few investigations of drivetrain structural-acoustic response. A recent experimental investigation by Biermann and Hagerodt (1995) has shown that repeatable clonk conditions can be achieved and measured by experimental rigs that include all elements of a drivetrain system, subjected to an instantaneously released preload torque. Their experiments, carried out for a front wheel drive system, have pointed to a cost-effective way for the investigation of clonk. Their approach is extended in this paper to study the clonk response of a two-piece rear-wheel driveline system.

The experimental investigation must consider the movements of every transmission and structural component along the torque path when excited by a torsion input. As high frequency vibrations are responsible for the clonk response of the system, monitoring of accelerations of structural elements are required at a multitude of locations.

A specified preload torque was applied via a low inertial disc brake system to the drivetrain rig to take up all the lash elements and to fully compress the clutch disc springs. The stored energy was then instantaneously released in the form of a ramp saw tooth pulse. The duration of the torsion pulse was varied between 80-180 *ms* as required, inducing a generated lash take up of the order of 1-2 *ms*, of sufficiently short period to excite the higher frequency structural modes. The 1-2 *ms* impact was followed by approximately 30 *ms* of drive shaft tube ringing. The input ramp torque was found to be repeatable and reproducible.

The cycle can repeat itself (be it at lower oscillation levels) as cycles of shuffle, the frequency of which is around 3-7 Hz in this case.

Calibrated piezo-accelerometers were located and adhered at the various locations as shown in figure 3.7. In order to place an accelerometer pick-up at the ring gear position, the axle was tested without lubrication. Microphones were also placed at the transmission and the rear axle locations. Twelve channel data acquisition was carried out at a data sampling rate of 12500 samples per second, corresponding to a time interval of 0.008 *ms*. This was sufficient sampling frequency to capture high frequency structural modal behaviour.

3.5.8. Rig to road clonk correlation

Very good correlation of 0.93 was found for the noise responses between the rig and road conditions (see figure 3.11).

Third octave analysis used in figure 3.11 can be of value, when it is required to correlate vibration spectra with noise spectra, and where a simple spectrum comparison is needed.

3.6 Component modal impact testing

Additional impact tests were conducted to add to the knowledge taken from road and rig testing and to confirm that clonk radiated noise was related to structural modal behaviour (see figure 3.14, discussed later).

3.6.1. RWD transmission housing modal impact response

The transmission was mounted to a solid block to replicate the normal assembly condition to the engine. A metallic hammer head was used to excite the structure. The response at randomly spaced locations on the housing was recorded for each hammer blow. The excitation point was the same for all impacts. All of the eight impact responses are shown in figure 3.12.

The response spectra showed the major modal areas to be spaced 500-600 Hz apart and all modes were lightly damped. The Aluminium transmission housing wall thickness is only 3,0 mm.

The modes are especially active around 5000 Hz.

3.6.2. FWD driveshafts modal impact response

A ring with extended flange was clamped to the driveshaft and a hammer blow struck on the flange to induce a torsion impact to the tube. Figure 3.13 shows the spectral modal response.

3.6.3. RWD driveshaft tubes modal impact response

The RWD driveshaft tube was impacted on the surface and the accelerations were recorded. The driveshaft tube is steel and has a wall thickness of 1,5 mm and outer diameter of 90,0 mm. The modes were extremely active especially above 3000 Hz. Only one impact location was used, and it may be assumed that more modal activity would have been 'uncovered' had other impact locations been used. This shaft was then filled with foam to evaluate damping properties. This achieved a satisfactory improvement. A thin steel sheet was then spiral wound on to the tube, greatly increasing the effective wall thickness and inertia. This achieved another improvement.

Figure 3.14 shows the spectrum of vibration of a driveshaft tube, obtained by the above mentioned component testing. Note that there are many spectral contributions, with significant amplitudes at frequencies above 1500 Hz. Some attenuation is observed by palliative measures indicated on the figure, but such measures do not remedy the clonk response to an appreciable extent. Later results obtained from the driveline rig indicate that these modes are excited through testing at the system level.

3.7. Signal analysis methods

It has already been stated that experimental data acquisition is normally in the time domain, and this must be transformed into the frequency domain to be a useful diagnostic tool. Transient non-periodic data is difficult to transform due to the short time available for data collection and because normal transformation is best suited to periodic data.

If sampling frequency rates of >12500 Hz are used then modal information up to 6000 Hz may be safe by applying the Nyquist sampling theorem.

3.7.1. Fast Fourier Transform (FFT)

Estimation of Power Spectral Density (PSD), or simply the spectrum of discretely sampled deterministic or stochastic processes, is usually based upon procedures that employ Fourier transformation. This approach is computationally efficient in many applications, but there are some inherent limitations. The most prominent shortcoming of this approach is that of frequency resolution; the ability to distinguish between the spectral contributions. The other limitation is due to the implicit windowing of the sampled data, which occurs when processing with Fast Fourier Transformation (FFT). Windowing can manifest itself as "leakage"; the spectral domain energy in the main lobe of a spectral response leaks into side-lobes, obscuring and distorting other spectral contributions which may be present there. These limitations become significant whilst studying short transient response of systems, particularly at high frequencies. One can then conclude that for "stiff" systems with widely split eigen-values spectral decomposition techniques based upon FFT are unsafe.

3.7.2. Auto Regression Moving Average method (ARMA)

For the case of stationary processes, the auto-correlation function can provide the basis for spectral analysis, rather than the random process *x (t)* itself. Therefore:

$$R_{xx}(\tau) = E[x(t+\tau)x^{*}(t)] \tag{3.1}$$

The auto-correlation function $R_{xx}(\tau)$ for a stochastic wide sense discrete process x_n is defined in this paper as the expectation of the product $x_{n+k}x_n^{*}$, where x_n is assumed to have a zero mean value. The Wiener-Khinchin theorem relates the auto-correlation function via the Fourier transform to the Power Spectral Density (PSD), $\rho(f)$, as:

$$\rho(f) = \int_{-\infty}^{\infty} R_{xx}(\tau) e^{-j2\pi f\tau} d\tau \tag{3.2}$$

In practical circumstances one does not usually know the statistical auto-correlation function. Thus, an additional assumption is often made, by considering the random process as ergodic in the first and second moments. This property permits for the substitution of time averages for ensemble averages. For an ergodic process, therefore, the statistical auto-correlation function may be represented as:

$$R_{xx}(\tau) = \lim_{T\to\infty} \frac{1}{T} \int_{-T}^{T} x(t+\tau)x^{*}(t)dt \tag{3.3}$$

An obvious companion auto-correlation estimate, based upon the above equation is the unbiased estimator:

$$R_{xx}(m) = \frac{1}{N-m} \sum_{n=0}^{N-m-1} x_{n+m} x_n^* \qquad (3.4)$$

for *m=1,2,........M,* where $M \leq N-1$.

The negative lag estimates are determined from the positive lag estimates in accordance with the conjugate symmetric property of the auto-correlation function of a stationary process, as:

$$R_{xx}(-m) = R_{xx}^*(m) \qquad (3.5)$$

The auto-correlation estimate proposed by Jenkins and Watts (1968) and Parzen (1961, 1968) tends to have a lesser least square error than equation (3.4) and is employed in the current analysis as:

$$R_{xx}(m) = \frac{1}{N} \sum_{n=0}^{N-m-1} x_{n+m} x_n^* \qquad (3.6)$$

where: *n=0,1,2,3,......M*

3.7.3. The Burg's Method

The Burg's method (Burg, 1975, 1981) is based on the Levinson recursion and the lattice structure for the model and has proven to be effective in a number of practical applications.

The Burg procedure is a recursive procedure, where at each step in the recursion process a single reflection coefficient is estimated. The p^{th} reflection coefficient is chosen in order to minimise the sum of the forward and backward squared prediction errors.

$$S_p^{fb} = \sum_{n=p}^{N_s-1}\left(\left|\varepsilon_p[n]\right|^2 + \left|\varepsilon_p^b[n]\right|^2\right) \tag{3.7}$$

It should be noted that the forward and backward prediction problems are statistically identical and that there is no reason to favour one over the other in estimating the prediction error. Therefore, both ε_p and ε_p^b should be included for the minimisation criterion.

The Burg's method can be derived as follows:

Consider running the p^{th} order forward and backward over the available data in order to generate the error terms needed in equation (3.7). According to the lattice equation, these terms satisfy the order recursions as:

$$\begin{bmatrix} \varepsilon_p[p] \\ \varepsilon_p[p+1] \\ \cdot \\ \cdot \\ \cdot \\ \varepsilon_p[N_s-1] \end{bmatrix} = \begin{bmatrix} \varepsilon_{p-1}[p] \\ \varepsilon_{p-1}[p+1] \\ \cdot \\ \cdot \\ \cdot \\ \varepsilon_{p-1}[N_s-1] \end{bmatrix} - \gamma_p^* \begin{bmatrix} \varepsilon_{p-1}^b[p-1] \\ \varepsilon_{p-1}^b[p] \\ \cdot \\ \cdot \\ \cdot \\ \varepsilon_{p-1}^b[N_s-2] \end{bmatrix} \tag{3.8}$$

And:

$$\begin{bmatrix} \varepsilon_p^b[p] \\ \varepsilon_p^b[p+1] \\ \cdot \\ \cdot \\ \cdot \\ \varepsilon_p^b[N_s-1] \end{bmatrix} = \begin{bmatrix} \varepsilon_{p-1}^b[p-1] \\ \varepsilon_{p-1}^b[p] \\ \cdot \\ \cdot \\ \cdot \\ \varepsilon_{p-1}^b[N_s-2] \end{bmatrix} - \gamma_p^* \begin{bmatrix} \varepsilon_{p-1}[p] \\ \varepsilon_{p-1}[p+1] \\ \cdot \\ \cdot \\ \cdot \\ \varepsilon_{p-1}[N_s-1] \end{bmatrix} \tag{3.9}$$

Where:

$$\varepsilon_p = \begin{bmatrix} \varepsilon_p[p] \\ --- \\ \\ \\ e_p^f \end{bmatrix} \; ; \; \varepsilon_p^b = \begin{bmatrix} e_p^b \\ \\ \\ ------ \\ \varepsilon_p^b[N_s-1] \end{bmatrix} \; ; \; e_p^f = \begin{bmatrix} \varepsilon_p[p+1] \\ \varepsilon_p[p+2] \\ . \\ . \\ . \\ \varepsilon_p[N_s-1] \end{bmatrix} \; ; \; e_p^b = \begin{bmatrix} \varepsilon_p^b[p] \\ \varepsilon_p^b[p+1] \\ . \\ . \\ . \\ \varepsilon_p^b[N_s-2] \end{bmatrix}$$

Since $\gamma'_p = \gamma^*_p$, the lattice relations (3.8) and (3.9) can be written as:

$$\varepsilon_p = \begin{bmatrix} \times \\ -- \\ \\ \\ e_p^f \end{bmatrix} = e_{p-1}^f - \gamma_p^* e_{p-1}^b$$

$$\varepsilon_p^b = \begin{bmatrix} e_p^b \\ \\ \\ -- \\ \times \end{bmatrix} = e_{p-1}^b - \gamma_p e_{p-1}^f \tag{3.10}$$

With these definitions and relations, equation (3.10) can be expressed as:

$$S_p^{fb} = \left\|\varepsilon_p\right\|^2 + \left\|\varepsilon_p^b\right\|^2$$

$$\ldots\ldots = (e_{p-1}^f - \gamma_p^* e_{p-1}^b)^{*T}(e_{p-1}^f - \gamma_p^* e_{p-1}^b) + (e_{p-1}^b - \gamma_p e_{p-1}^f)^{*T}(e_{p-1}^b - \gamma_p e_{p-1}^f)$$

$$\ldots\ldots = (1+\gamma_p\gamma_p^*)(\left\|e_{p-1}^f\right\|^2 + \left\|e_{p-1}^b\right\|^2) - 2\gamma_p^*(e_{p-1}^f)^{*T} e_{p-1}^b - 2\gamma_p(e_{p-1}^b)^{*T} e_{p-1}^f$$

Then using the expressions in a scalar form of the complex gradient provides the necessary condition:

$$\nabla_{\gamma_p^*} S_p^{fb} = \gamma_p \left(\left\| e_{p-1}^f \right\|^2 + \left\| e_{p-1}^b \right\|^2 \right) - 2 (e_{p-1}^f)^{*T} e_{p-1}^b = 0$$

Or

$$\gamma_p = \frac{2 (e_{p-1}^f)^{*T} e_{p-1}^b}{\left\| e_{p-1}^f \right\|^2 + \left\| e_{p-1}^b \right\|^2} \qquad (3.11)$$

The form of this equation guarantees that the estimated reflection coefficient satisfies the condition $|\gamma_p| \leq 1$.

These are iterated for $p = 1,2,3,........, P$, when starting from the initial conditions:

$$\begin{bmatrix} \times \\ -- \\ \\ \\ \\ \\ e_0^f \end{bmatrix} = \begin{bmatrix} e_0^b \\ \\ \\ \\ \\ -- \\ \times \end{bmatrix} = \begin{bmatrix} x[0] \\ x[1] \\ . \\ . \\ . \\ . \\ x[N_s - 1] \end{bmatrix} \qquad (3.12)$$

The algorithm is quite simple in this form. At each stage of iteration the reflection coefficient is formed from equation (3.11). The vectors are then combined as in (3.10), the elements denoted by $\times$ are omitted, and the steps are repeated. Thus, the vectors e_p^f and e_p^b decrease in size at each iteration. An estimate for the prediction error variance can be computed by the additional recursion:

$$\sigma_{\varepsilon p}^2 = (1-|\gamma_p|^2)\sigma_{\varepsilon p-1}^2 \tag{3.13}$$

and then the MA coefficients can be computed from the recursion:

$$a_p = \begin{bmatrix} a_{p-1} \\ \\ \\ -- \\ 0 \end{bmatrix} - \gamma_p^* \begin{bmatrix} 0 \\ -- \\ \\ \\ \tilde{a}_{p-1}^* \end{bmatrix} \tag{3.14}$$

3.7.4. The Shanks' Method

This next procedure is due to Shanks (1967) and the combination of this with the least squares procedure for finding the AR parameters is sometimes referred to as the Shanks' method. The goal is to represent the given data in the form:

$$X(z) \approx \frac{B(z)}{A(z)} \tag{3.15}$$

where, $A(z)$ has already been determined using the Burg's method. Define :

$$H_A(z) = \frac{1}{A(z)} \quad \text{and} \quad X(z) \approx B(z)H_A(z) \tag{3.16}$$

Let $h_A[n]$ be the sequence corresponding to $H_A(z)$. This sequence is actually the impulse response, corresponding to the partial system $1/A(z)$. The approximation problem can now be thought of as shown in Figure below.

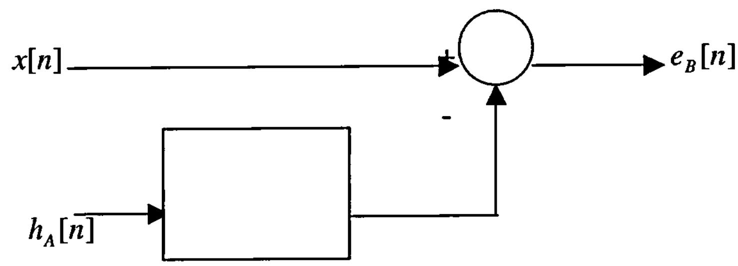

The error in the signal domain is given by

$$e_B[n] = x[n] - h_A[n] * b[n] \tag{3.17}$$

If the filter B(z) is chosen in order to minimise the sum of squared errors, then:

$$S_B = \sum_{n=0}^{N_s-1} |e_B[n]|^2 \tag{3.18}$$

In fact, this is exactly the least squares' Wiener filtering problem. The problem can be represented as:

$$H_A b \overset{ls}{=} x \tag{3.19}$$

$$\text{where: } H_A = \begin{bmatrix} h_A[0] & 0 & . \; . \; . & 0 \\ h_A[1] & h_A[0] & . \; . \; . & 0 \\ . & . & & . \\ . & . & . \; . \; . & . \\ . & . & & . \\ h_A[Q] & h_A[Q-1] & & h_A[0] \\ . & . & & . \\ . & . & . \; . \; . & . \\ . & . & & . \\ h_A[N_S-1] & h_A[N_s-2] & . \; . \; . & h_A[N_s-Q-1] \end{bmatrix} \qquad (3.20)$$

and:

$$x = \begin{bmatrix} x[0] \\ x[1] \\ . \\ . \\ . \\ x[Q] \\ . \\ . \\ . \\ x[N_s-1] \end{bmatrix} \qquad (3.21)$$

and b=0. As an alternative the lower limit in (3.18) can be set to Q, in which case equations (3.20) and (3.21) will be missing from the first Q rows. The solution is then obtained as:

$$b = H_A^{-1} x \qquad (3.22)$$

The terms needed in the sequence; $h_A[n]$ can be obtained from the recursive difference equation:

$$h_A[n] = -a_1 h_A[n-1] - ....a_P h_A[n-P] + \delta[n] \tag{3.23}$$

Alternatively, it may be feasible to find the roots of $A(z)$ and develop an analytic expression for $h_A[n]$ (at least for some simple cases).

3.7.5. Wavelet analysis

The Fourier transform of a time-based signal breaks it down into constituent sinusoids of different frequencies. However, in the transformation process when the time domain is mapped to the frequency domain, the time information is lost, and so the event timing from the time history is lost. For stationary signals (i.e. those not in the time domain), this is not a significant loss, and FFT is an acceptable method of frequency analysis. This is not the case for transient signals, when time-based information may be needed, and when constituent sinusoids are not best suited to the analysis.

As a natural consequence of this limitation, Alfred Haar in 1909 introduced the idea of wavelets for transient signal analysis.

In 1946, Gabor adapted the FFT technique to window the time signal at small increments of time. The process was called STFT (Short Time Fourier Transform) and used a discrete Fourier transform to map from the time signal domain to a 2D domain of frequency and time. This gave limited time event information dependent on the size of the domain window. A disadvantage was that the window was the same for all frequencies, and so could not discriminate between coupled modal activities.

Morlet in 1982 introduced a further improvement in wavelet analysis, which offered an opportunity to analyse transient time domain data by the use of a *variable* window. Long time windows were used for low frequency data, short time windows were used for high frequency data.

In particular, wavelet analysis is ideally suited to 'window in' on a transient event in a signal, and by using a suitable wavelet transient function to represent the discontinuity. This would normally be beyond the useful scope of FFT analysis, which is best suited to continuous data. Wavelet analysis decomposes a signal using a set of wavelets, and is able to extract transient events that may be otherwise buried in noisy time based data. The wavelet function is wide at low frequencies (which change more slowly with time), and narrow at high frequencies

Wavelets are irregular and asymmetric short-time transients, of which there are several families.

With wavelet analysis, an arbitrary square integrable function can be decomposed into, or constructed from, shifted and dilated versions of another square integrable function. Therefore, for a particular application, there may exist optimal wavelet representations that would behave better than others. Given that for a complex vibration signal a suitable wavelet form is identified, one may be able to narrow around a given frequency range (Li and Ma, 1997). This is particularly useful in the cases of localised effects, where resonant frequencies become dominant with given events (Mallat, 1989).

It is possible to decompose any arbitrary signal $f(x)$ into its Wavelet components. The approach is the same as in harmonic analysis, except that instead of breaking a signal down into harmonic functions of different frequencies, the signal is broken down into Wavelets of different scale (different level) and different positions along the abscissa. For example, consider a finite length of a signal $f(x)$, assumed to be known over the interval $0 \leq x < 1$. The signal may be represented as a constant level (for all the Wavelets level less than zero), plus Wavelets of all levels above zero, thus:

$$
\begin{aligned}
f(x) &= a_0 + a_1 w(x) \\
&+ a_2 w(2x) + a_3 (2x-1) \\
&+ a_4 w(4x) + a_5 w(4x-1) + a_6 w(4x-2) + a_7 w(4x-3) \\
&+ a_8 w(8x) + a_9 w(8x-1) + a_{10} w(8x-2) + \ldots\ldots\ldots\ldots
\end{aligned} \tag{3.24}
$$

$$f(x) = a_0 + \sum_{j=0}^{\infty} \sum_{k=0}^{2j-1} a_{2^j+k} w(2^i x - k) \qquad 0 \le x \prec 1 \qquad (3.25)$$

The discrete wavelet transform (DWT) is an algorithm for computing a_0, a_{2^j+k}, when $f(x)$ is sampled at equally spaced intervals over $0 \le x \prec 1$. The DWT algorithm was first proposed by Mallat (1989) and is called the Mallat's pyramid algorithm or sometimes as the Mallat's tree algorithm.

The Wavelet ''level'' is determined by the number of Wavelets fitting into the unit interval $x = 0$ to 1. At level zero, there is $2^0 = 1$ Wavelet, whilst at the level 1 there are $2^1 = 2$ Wavelets, and so on.

Wavelet analysis involves a fundamentally different approach. Instead of seeking to break down a signal into its harmonics, which are global functions that continue indefinitely, the signal is broken down into a series of local basic functions called Wavelets. Each Wavelet is located at a different position on the time axis and is local in the sense that it decays to zero, when sufficiently far from its centre. At the finest scale, Wavelets may be very short indeed and at a coarse scale, they may be very long (Misiti *et al*, 1997).

Wavelet analysis has demonstrated that it can be particularly powerful in the analysis of vehicle crash testing. The decomposition of the crash time traces by wavelet analysis not only identifies the dynamic response to structural impact but also identifies the time sequence of collapse. As a result it is then a matter of representing the crash structure by a mechanical MBD model, which if configured correctly, will follow the same time sequence of collapse as the actual vehicle. The model can then be used to highlight the part(s) of the structure that are most influential on the collapse mechanism.

The wavelet analysis is similarly well suited as a tool for the study of transient structural and acoustic wave propagation that arise from impact forces. The method is powerful, because it transfers 2D frequency and time data from the measured time history, and the time component may be used to study the propagation in some detail. As already mentioned, wavelet analysis is able to extract such a transient wave signal from a noisy background.

There are many built in wavelet functions available for wavelet analysis in software packages. In this analysis the Wavelet form *'db10'* has been employed (Strang and Nguyen, 1995). This form has a very close similarity to the clonk time history profile.

3.8. Closure

- Experimental studies have identified the clonk frequency range for FWD and RWD variants.
- Good correlation between the road tests and component and rig tests, all identifying resonant behaviour in the clonk frequency range.
- Elasto-structural / acoustic mode coupling in the presence of lash, was considered to be a fundamental causal factor.
- ARMA analysis also identified/confirmed these modal frequencies.
- Mode shape analysis on RWD 2-piece system identified complex structural modal shapes ~ radial/circumferential /axial
- Extremely high structural and acoustic modal density of the cylindrical tubes in the clonk range.
- Transmission housing and driveshaft tube structural modes are very lightly damped.
- Use of metal hammer impact on thin walled structures (housing and shafts) was also used to excite structural modes and support the evidence from the rig and road vehicle.

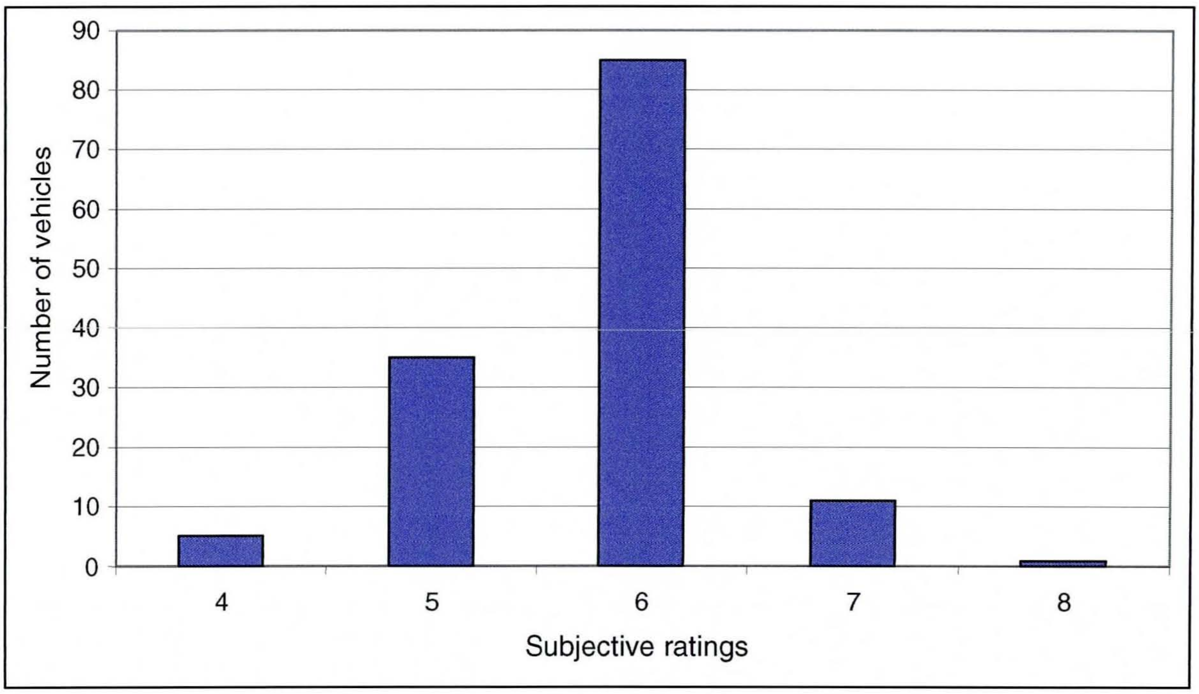

Figure 3.1 Rated subjective variability of clonk in production vehicles

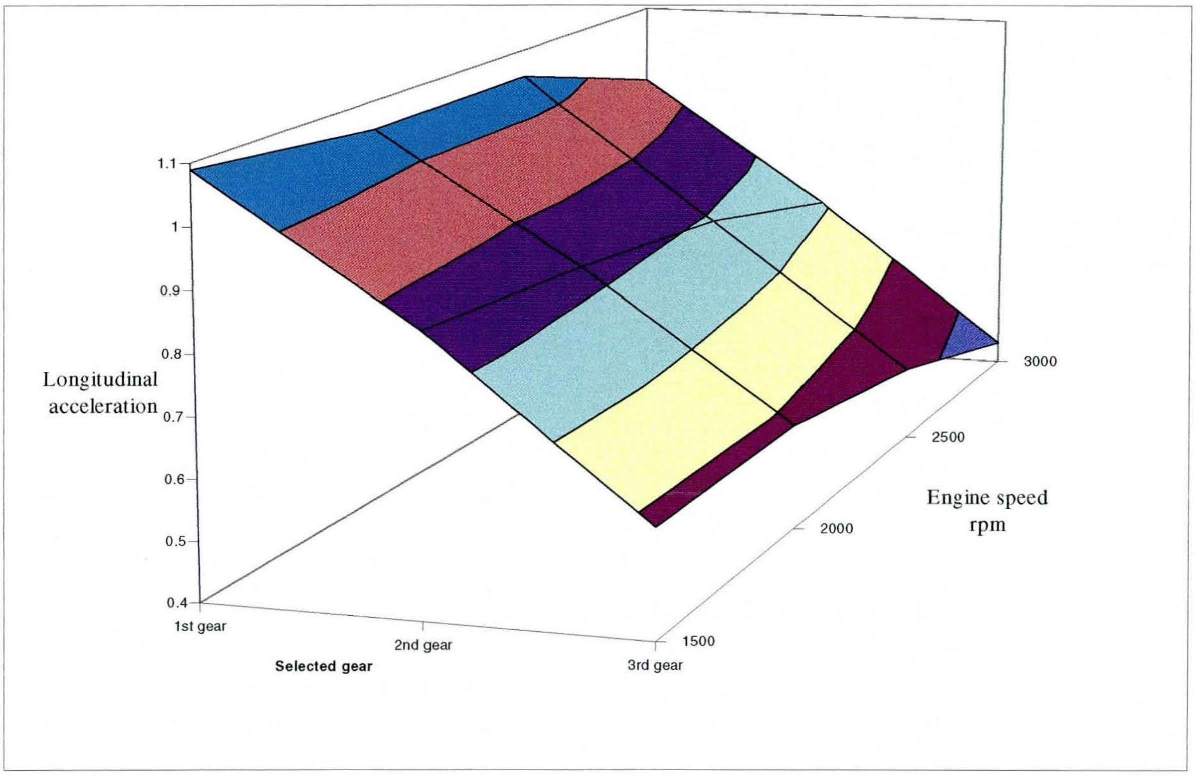

Figure 3.2 Shuffle response by gear and engine speed

Subjective rating	1	2	3	4	5	6	7	8	9	10
Evaluation	Not acceptable		Poor		Border line	Acceptable	Fair	Good	Very Good	Excellent

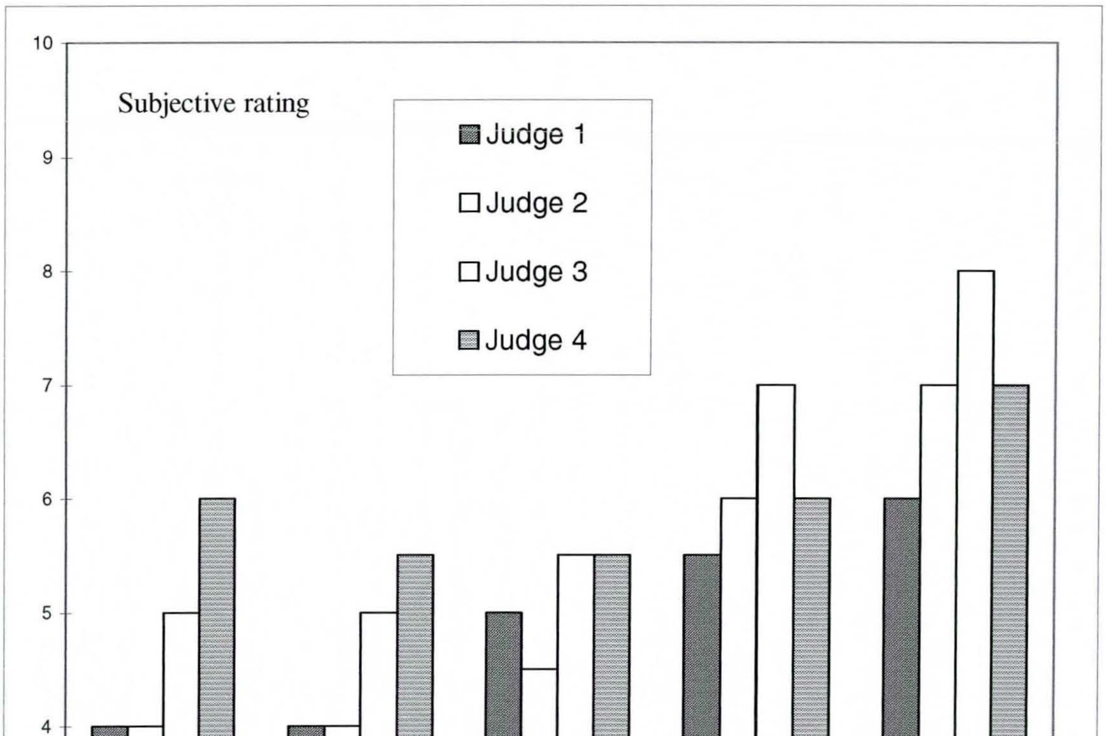

Figure 3.3 Clock subjective ratings versus engine speed

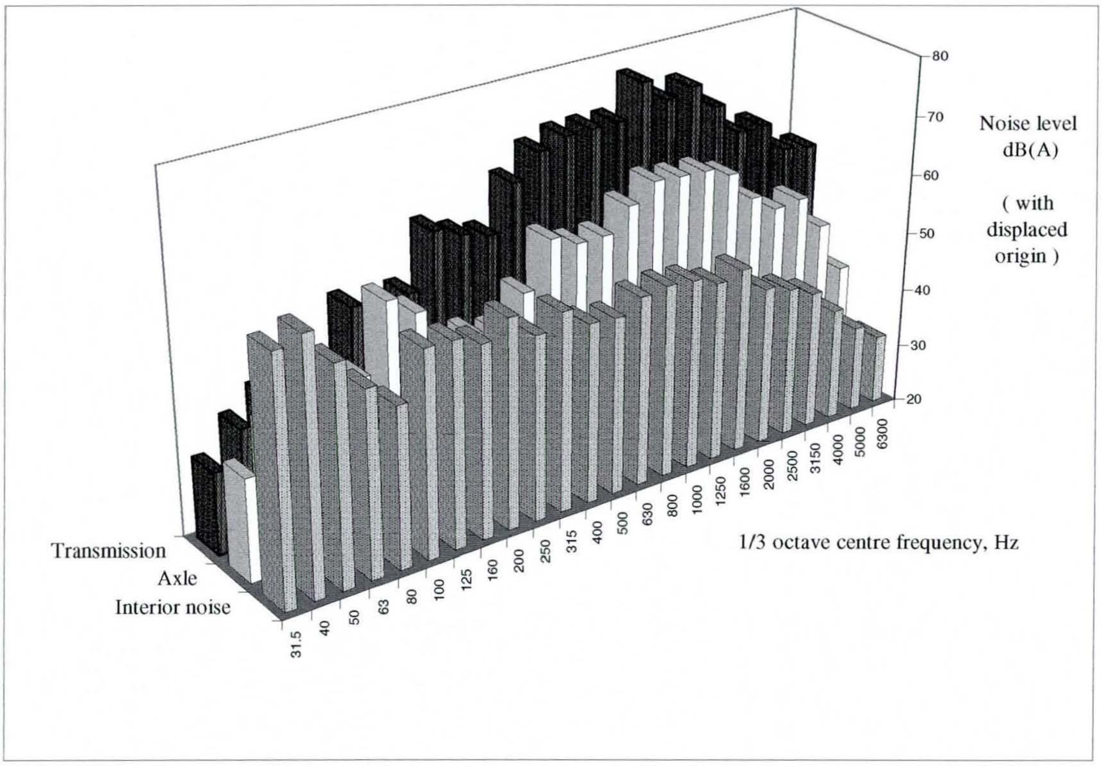

Figure 3.4 Driveline clonk in 2nd gear on the road

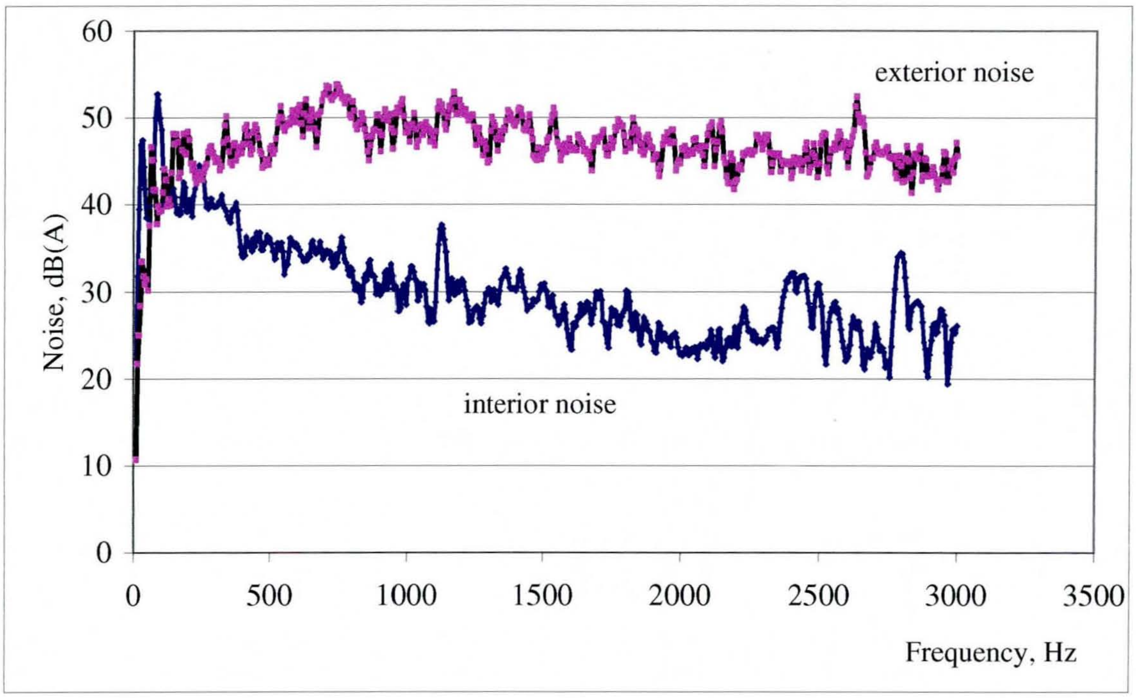

Figure 3.5 Passenger car FWD clonk

RUN	A	B	C*D*E	C	A*C	B*C	A*B*C	D	A*D	B*D	A*B*D	C*D	B*E	B*C*D	A*B*C*D	YIELD	
			A*B				D*E				C*E			A*E	E	Exterior noise	Interior noise
1	Minus	Minus	Plus	Minus	Plus	Plus	Minus	Minus	Plus	Plus	Minus	Plus	Minus	Minus	Plus		
2	Plus	Minus	Minus	Minus	Minus	Plus	Plus	Minus	Minus	Plus	Plus	Plus	Plus	Minus	Minus		
3	Minus	Plus	Minus	Minus	Plus	Minus	Plus	Minus	Plus	Minus	Plus	Plus	Minus	Plus	Minus		
4	Plus	Plus	Plus	Minus	Minus	Minus	Minus	Minus	Minus	Minus	Minus	Plus	Plus	Plus	Plus		
5	Minus	Minus	Plus	Plus	Minus	Minus	Plus	Minus	Plus	Plus	Minus	Minus	Plus	Plus	Minus		
6	Plus	Minus	Minus	Plus	Plus	Minus	Minus	Minus	Minus	Plus	Plus	Minus	Minus	Plus	Plus		
7	Minus	Plus	Minus	Plus	Minus	Plus	Minus	Minus	Plus	Minus	Plus	Minus	Plus	Minus	Plus		
8	Plus	Plus	Plus	Plus	Plus	Plus	Plus	Minus	Minus	Minus	Minus	Minus	Minus	Minus	Minus		
9	Minus	Minus	Plus	Minus	Plus	Plus	Minus	Plus	Minus	Minus	Plus	Minus	Plus	Plus	Minus		
10	Plus	Minus	Minus	Minus	Minus	Plus	Plus	Plus	Plus	Minus	Minus	Minus	Minus	Plus	Plus		
11	Minus	Plus	Minus	Minus	Plus	Minus	Plus	Plus	Minus	Plus	Minus	Minus	Plus	Minus	Plus		
12	Plus	Plus	Plus	Minus	Minus	Minus	Minus	Plus	Plus	Plus	Plus	Minus	Minus	Minus	Minus		
13	Minus	Minus	Plus	Plus	Minus	Minus	Plus	Plus	Minus	Minus	Plus	Plus	Minus	Minus	Plus		
14	Plus	Minus	Minus	Plus	Plus	Minus	Minus	Plus	Plus	Minus	Minus	Plus	Plus	Minus	Minus		
15	Minus	Plus	Minus	Plus	Minus	Plus	Minus	Plus	Minus	Plus	Minus	Plus	Minus	Plus	Minus		
16	Plus	Plus	Plus	Plus	Plus	Plus	Plus	Plus	Plus	Plus	Plus	Plus	Plus	Plus	Plus		

Figure 3.6 DOE test array for FWD classis dynamometer clonk investigation

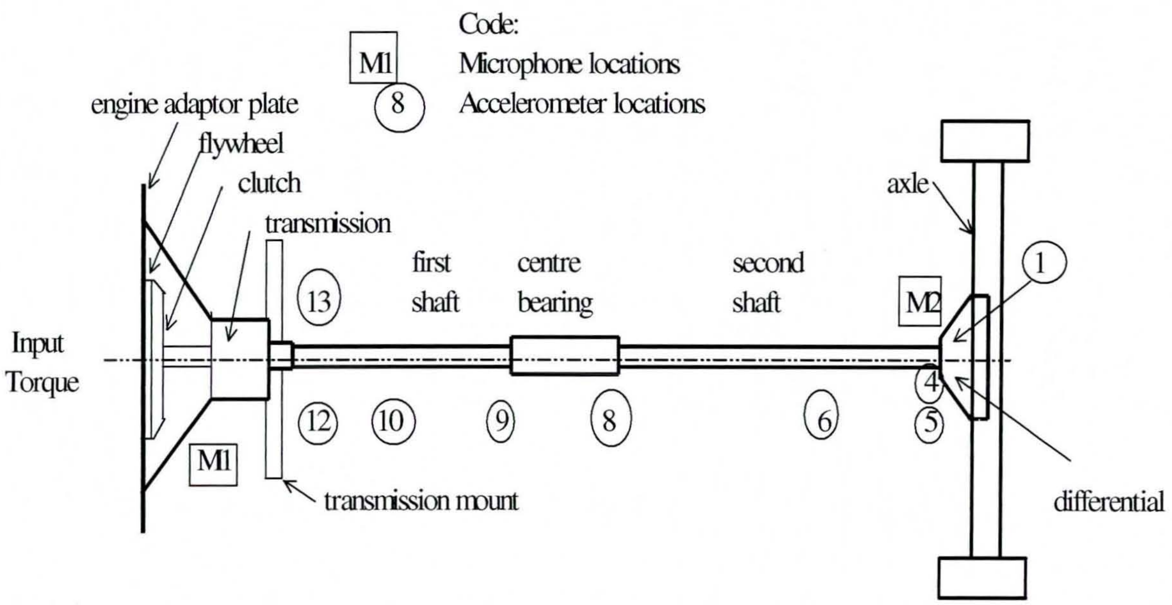

Figure 3.7 Schematic of RWD two piece driveline clonk rig

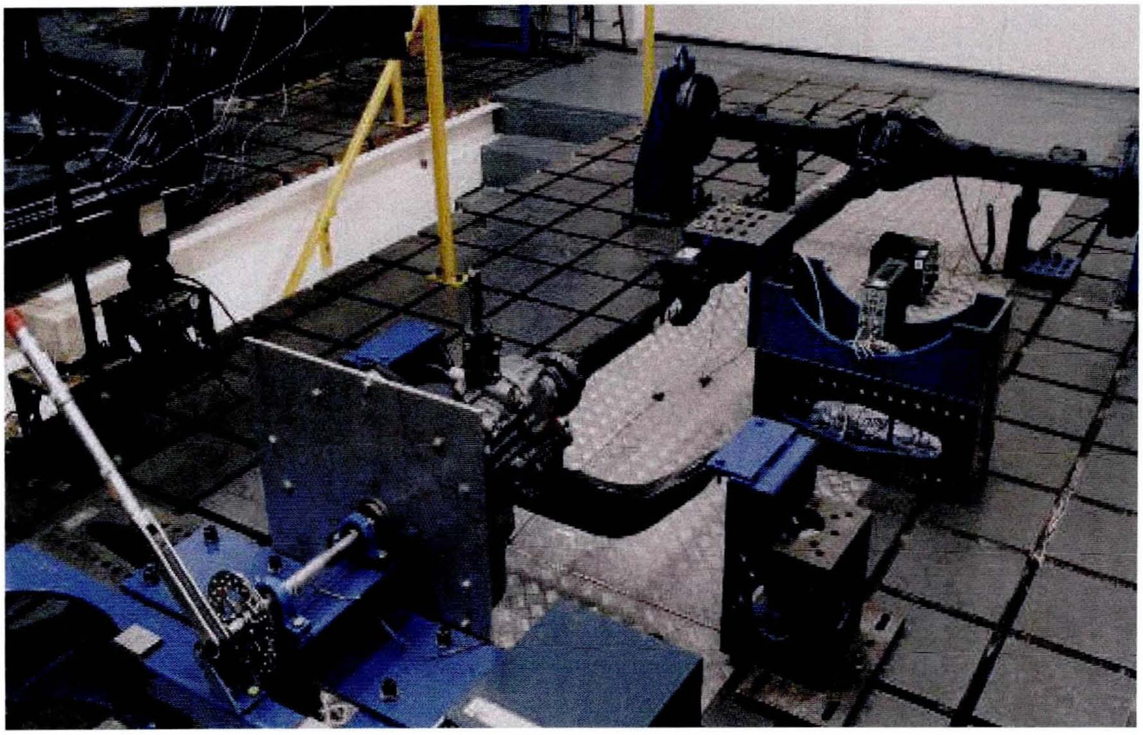

Figure 3.8 Two-piece driveshaft system clonk rig

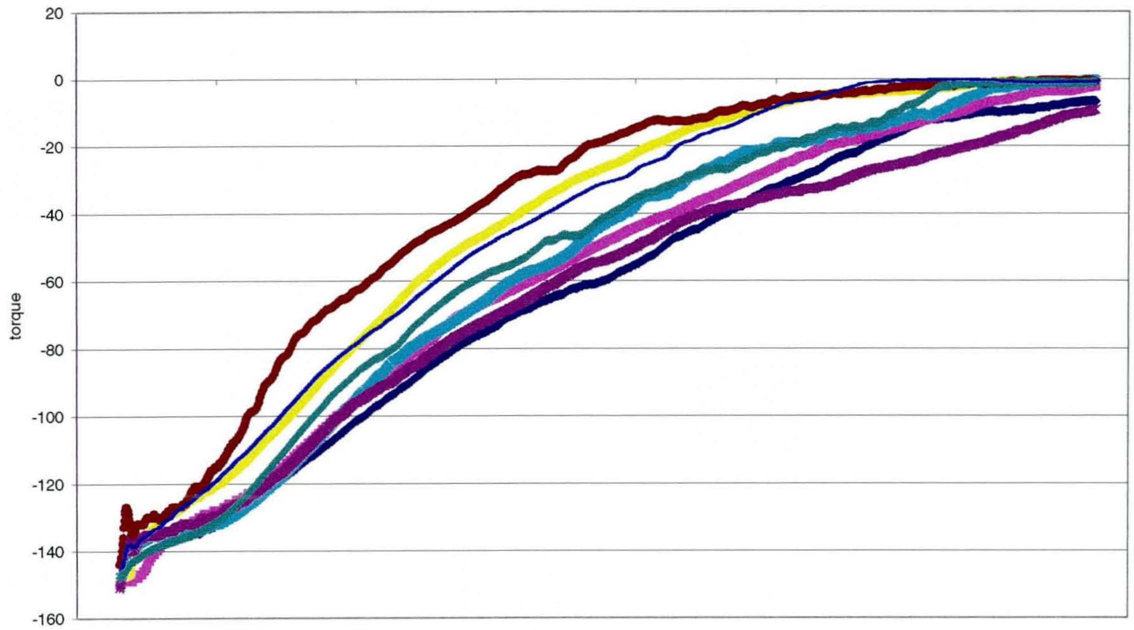

Figure 3.9 Rig torque rise rate comparison

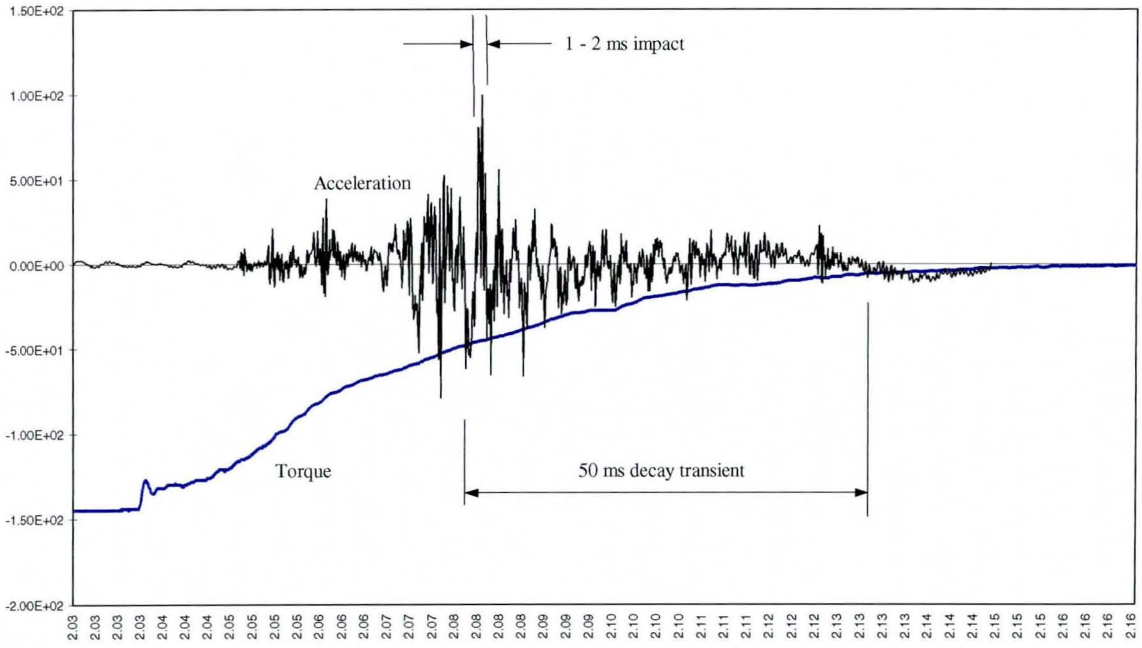

Figure 3.10 Profile of input torque release and the corresponding surface at 1st shaft centre

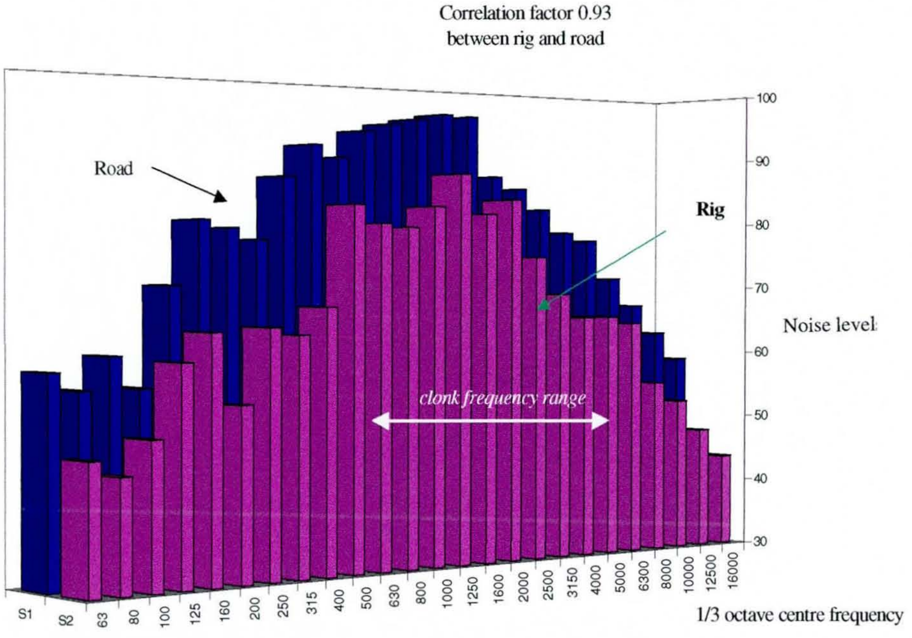

Figure 3.11 Comparison of clonk noise at transmission bell housing for road and rig

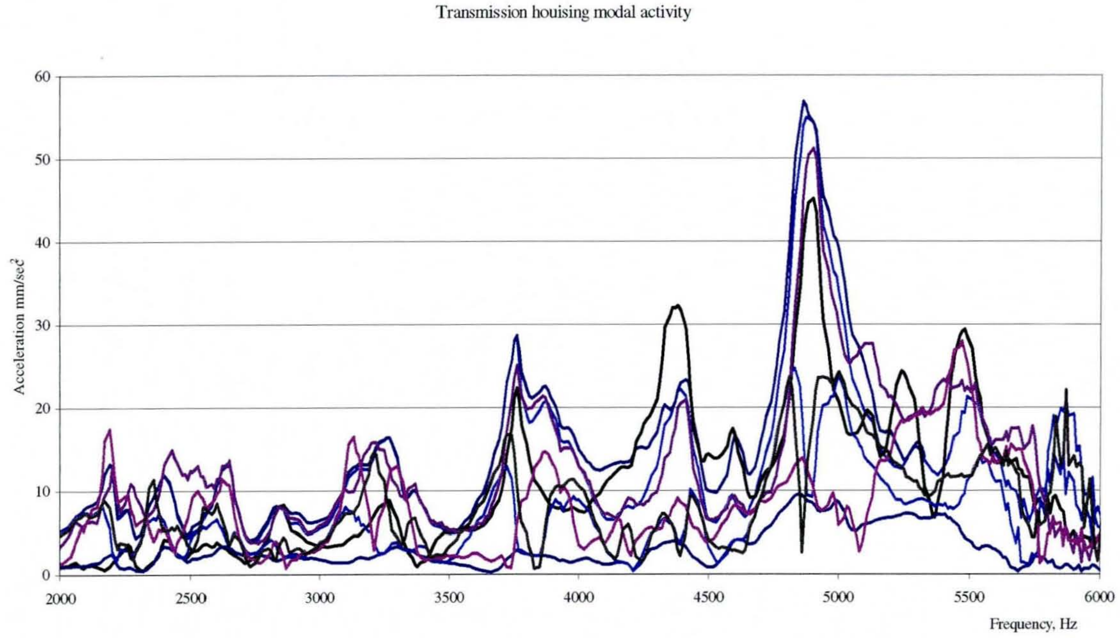

Figure 3.12 Modal activity of transmission housing when impacted by hammer at 8 pickup locations

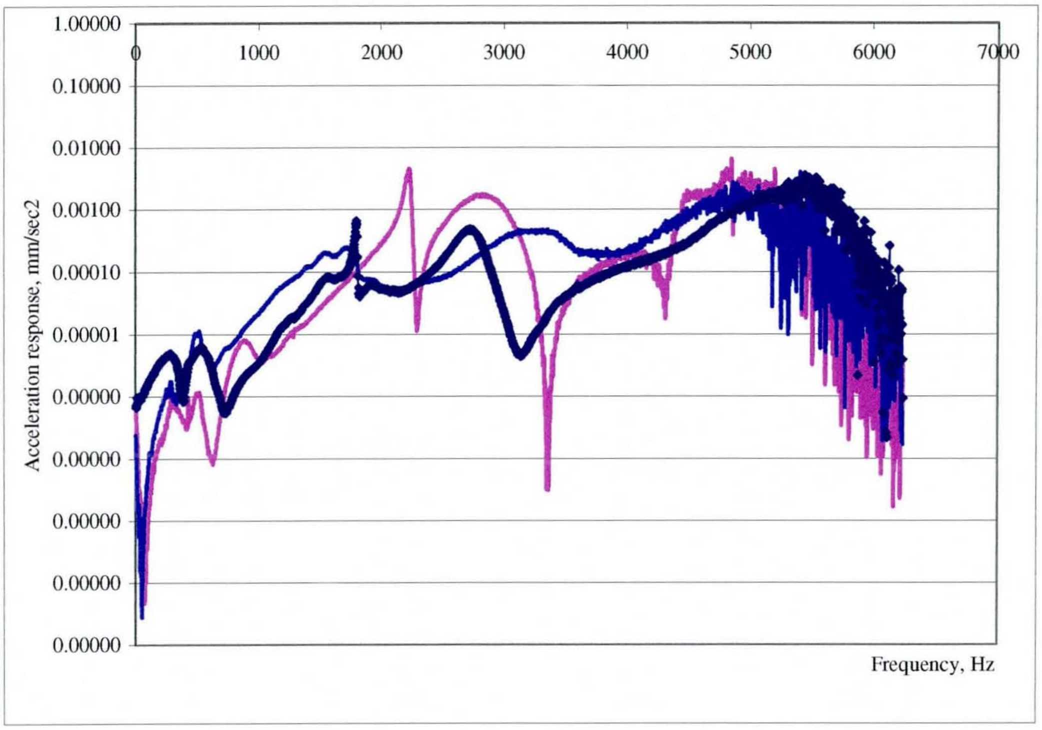

Figure 3.13 FWD impact response

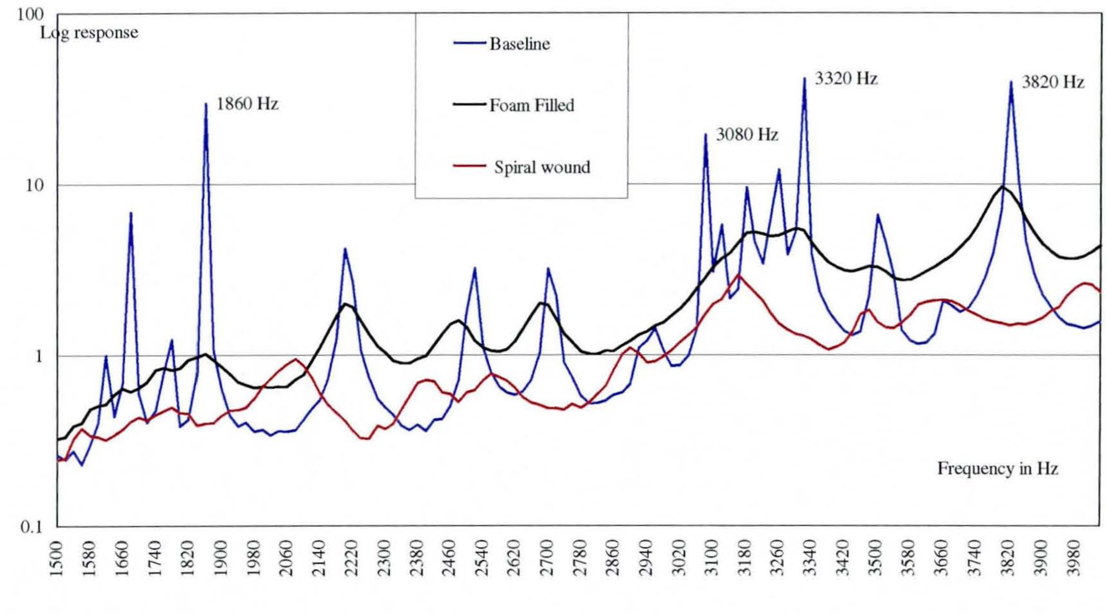

Figure 3.14 Impact response comparisons of driveshaft tube with different damping methods, in the clonk frequency range

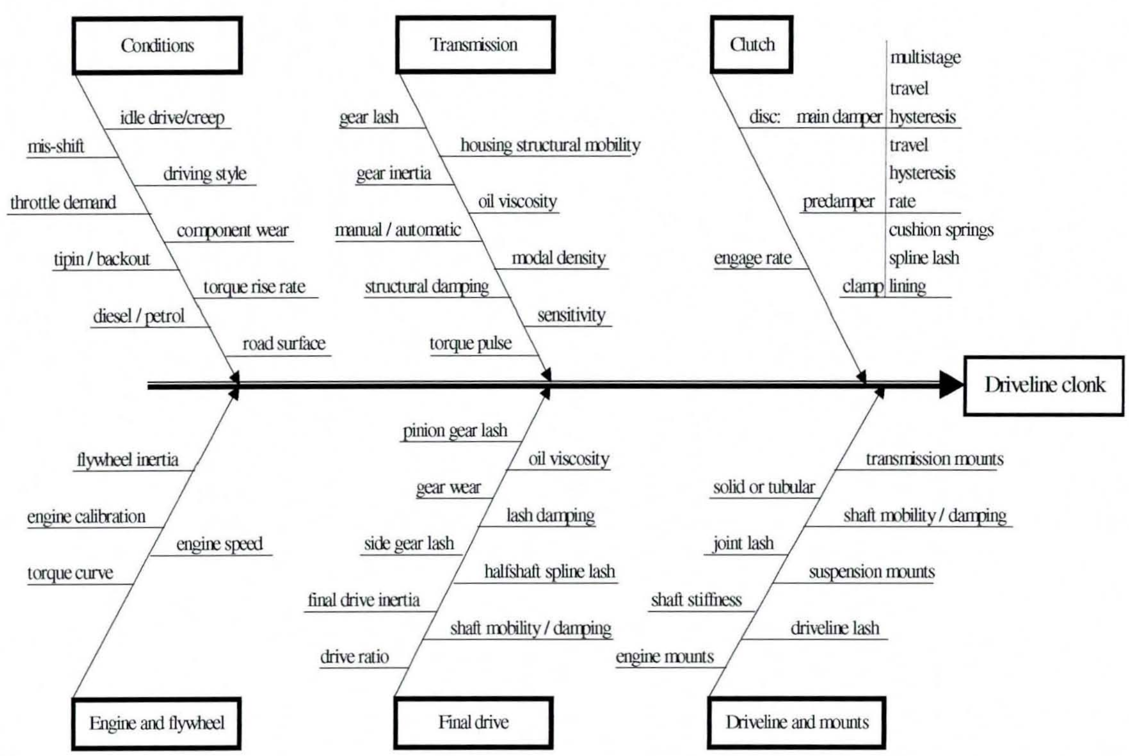

Figure 3.15 Cause and effect fishbone for driveline clonk

Chapter 4

Multi-body dynamics theory and drivetrain modelling

4.1 Introduction.

The prototype phase has become one of the most time intensive periods within the development cycle of a product. Many vehicle manufacturers are replacing hardware prototypes by *virtual prototypes* (i.e. the use of computer models to enable accurate representation of system behaviour). Computer models are simplified representations of real systems, usually embodying some assumptions. Therefore, virtual prototyping depends on the particular application and on the appropriate and justified use of adopted assumptions. Virtual prototyping simulations enable scenario building investigations at much reduced costs, when compared to comparable physical prototypes. Alternative designs can be evaluated, and the necessary time to bring a new product to the market may be shortened by the elimination of many iterations of laboratory testing and prototype fabrication.

In particular, in complex investigation of vehicle noise, vibration and harshness (NVH) studies, there is a demand for analysis tools to be sufficiently detailed and allow the broadest spectrum of users to employ their capabilities effectively. Virtual prototyping tools are in the form of powerful computer-based software packages that provide modelling and simulation environments for their users. The tools must be user friendly. This means that the model input parameters should represent real physical data such as geometrical dimensions, masses, moments of inertia, stiffness and damping coefficients.

Multi-body dynamics (MBD) is the physics of interaction of an assembly of rigid or flexible inertial bodies/parts, held together by some form of constraints or restraints like joints, couplers, gears, bearings, bushings. Furthermore, other forms of constraints arise from pre-specified motions that ensure inertial components in an assembly of parts follow a pre-defined type of motion. The overall behaviour of a multi-body system is, therefore, influenced by its individual inertial elements which may exert forces upon each other, and/or when exposed to external force excitation (Rahnejat, 1998). Since the combination of constraints, restraints, applied forces/torques, and the inertia of the parts, govern the overall motion and response of the multi-body system, it is necessary to devise a method of formulation and solution in order to obtain and to understand the resulting dynamic behaviour. The methodology is based upon constrained Lagrangian dynamics, and the solution method is adopted for a mix of differential-algebraic equation set (DAE). The equations of motion are partial differentials, whereas the constraint functions are usually algebraic expressions.

The results obtained from multi-body dynamic analyses are usually in the form of displacements, velocities, accelerations and reaction forces/torques (Chace, 1984). These time-domain outputs can be converted into frequency signals to obtain the spectra of individual vibration of parts in the system. Based on this, the designers can make modifications to multi-body mechanisms to guard against resonant conditions, when prevailing operating conditions may coincide with the fundamental natural frequencies of the overall system or its components. Furthermore, the reaction force output from the system allows for better component design in terms of reducing stress levels, thus increasing the life of parts under cyclic loading variations.

Unlike linear system dynamics problems, for complex non-linear multi-body systems, where many interactions between the parts may take place (for example, in vehicular powertrain systems) the number of factors affecting the design process may be quite significant. Hence, for such systems, it would not be cost effective to carry out "what if" scenarios on full size physical prototypes, since a large number of such prototypes might be required in order to obtain the desired goal. The reasons for using such powerful virtual prototyping tools described above have been highlighted by Ambrossi *et al* (1989).

Sophisticated modelling environments are now available as virtual prototyping tools, such as ADAMS, DADS, A-GEM, SIMPACK, VAMPIRE, and others. The work highlighted in this thesis is a model of a vehicular drive train system developed in ADAMS, which is an acronym for Automatic Dynamic Analysis of Mechanical Systems (Ryan, 1990, Ryan and Steigerwald, 1988). The modelling procedure in ADAMS is based on constrained Lagrangian dynamics and is outlined later in this chapter.

4.2 Theory of multi-body system dynamics

The dynamics of many assembled real systems, such as vehicle systems are quite complex in nature. In particular, such systems often include non-linear characteristics such as sources of compliance (as in stiffness and damping). An assembly of parts or components, having relative degrees of freedom with respect to one another, introduces constraints that are also represented by complex non-linear functions. The set of equations; the equations of motion, the algebraic constraint functions and applied forces/torques, require matrix formulation for simultaneous solution. Often the resulting matrices are quite large in size, when the model is complex, and in a Jacobian form will include many zero entries. The solution methodology, therefore, requires handling of large sparse matrices that cannot easily be inverted, to obtain the solution vector. In addition to this, the nature of the non-linear dynamic problem is such that in many cases a large range of response frequencies may exist. Thus, a suitable formulation and solution method must be employed in order to obtain the required system response in small discrete steps of time (Rahnejat, 1998, and Orlandea, 1999).

A multi-body system may comprise many inertial members, each of which can possess six unconstrained degrees of freedom in the three dimensional space. Each part can rotate and translate about and along the three mutually perpendicular axes (X, Y and Z); the three dimensions of space respectively that define the Cartesian co-ordinates. Since a multi-body mechanism is designed to provide a certain type of motion(s), the parts have to be constrained to one another in order to achieve the desired and intended functions (Rahnejat, 1998). If the constraints employed are such that all the degrees of freedom within the multi-body mechanism are removed such that for a given input there remains a prescribed output, a kinematic system would result. On the other hand, if one or more degrees of freedom exist, a dynamic mechanism is obtained. It should be noted, that as the degrees of freedom of a mechanism increases, the non-linear characteristics of the multi-body system may also increase. This can result in quite complex multi-body dynamic systems, which may include many sources of compliance such as flexible parts, non-linear stiffness, and damping characteristics. Hence, to formulate and to solve all the equations for an overall non-linear dynamic multi-body system would be a tedious and a lengthy process (Rahnejat, 2000). Therefore, the Lagrange's equation for constraint systems is used, which employs the fundamentals of dynamics to simplify the formulation procedure. The method of formulation lends itself to the automatic generation of equations of motion for all individual parts in a multi-body system separately (Ryan and Steigerwald, 1988). The integrity of the multi-body system as a whole is then assured by the inclusion of constraint functions that describe the joints, restraints and applied forces and torques between the neighbouring parts (Ryan, 1990, and Ryan and Steigerwald (1988).

The equations of motion for every part in the multi-body mechanism are then expressed in a single matrix format (the matrix is commonly known as the Jacobian matrix), which is often very large in size and consists of many zero entities. The solution procedure, therefore, requires the simultaneous solution of these equations by applying numerical methods which use simple but effective matrix manipulation techniques outlined by Cholesky (see Rahnejat, 1998) , to handle large sparse matrices that cannot easily be inverted, to obtain the solution vector (Ryan and Steigerwald, 1988, and Orlandea *et al*, 1978).

It must be noted that the position and orientation of a part can be obtained relative to another part, but if both the bodies are in motion, then the results can be somewhat difficult to understand. Therefore, Lagrangian dynamics uses the ground as the fixed datum and sets up all the equations of motion in the Global Reference System (GRF). Hence, to summarise the above explanations, the position and orientation of a part relative to the GRF can be expressed in the form of generalised co-ordinates as (see figure 4.1):

$$\{q_j\} = [x \quad y \quad z \quad \psi \quad \theta \quad \phi]^T \tag{4.1}$$

where $j = 1,...,6$ and corresponds to each co-ordinate in the vector set.

The translation velocity of the part with respect to a Local Part Reference Frame (LPRF) is located at the centre of its mass and is given by the time derivative of the position vector $\vec{R}_G$, relative to the Global Reference Frame. This can be written as:

$$\frac{\partial[\vec{R}_G]}{\partial t}=\frac{\partial}{\partial t}\left[x.\vec{i}+y.\vec{j}+z.\vec{k}\right] \tag{4.2}$$

Or in a matrix form as:

$$\left[\dot{\vec{R}}_G\right]=\left[\vec{i} \quad \vec{j} \quad \vec{k}\right]\{\dot{x} \quad \dot{y} \quad \dot{z}\}^T \tag{4.3}$$

The angular velocity of the body can be determined by the time derivatives of the Euler angles. Therefore, the rotational velocities in terms of Euler co-ordinates are given by the rate of change of these three angles about their respective axes (Rahnejat, 1998). This is shown in Figure 4.2.

Where: $\frac{\partial\psi}{\partial t}=\dot{\psi}$ - about the initial R-axis (parallel to the z-axis)

$\frac{\partial\theta}{\partial t}=\dot{\theta}$ - about the current position of the P_1-axis (parallel to the x_1-axis)

$\frac{\partial\phi}{\partial t}=\dot{\phi}$ - about the current position of the R_2-axis (parallel to the z_2-axis)

Therefore, if ω is termed as the general overall angular velocity of the part, it can be expressed in its component form as:

$$\omega=\omega_x+\omega_y+\omega_z \tag{4.4}$$

where ω_x, ω_y and ω_z are the angular velocity components in the GRF, about the X, Y and Z-axis respectively. These angular velocity components are obtained by the following transformation:

$$\begin{bmatrix}\omega_x\\ \omega_y\\ \omega_z\end{bmatrix}=[T]_V\{\dot{\psi} \quad \dot{\theta} \quad \dot{\phi}\}^T \tag{4.5}$$

where $[T]_V$, is the angular velocity transformation matrix (used to express LPRF's angular velocity in GRF). This transformation is given by:

$$[T]_V = \begin{bmatrix} S\theta S\phi & C\phi & 0 \\ S\theta C\phi & -S\phi & 0 \\ C\theta & 0 & 1 \end{bmatrix} \tag{4.6}$$

where $C \equiv Cos$ & $S \equiv Sin$

When the transformation in equation (4.6) is carried out, the following relationships are obtained:

$$\omega_x = \dot{\psi} S\theta S\phi + \dot{\theta} C\phi \tag{4.7}$$

$$\omega_y = \dot{\psi} S\theta C\phi - \dot{\theta} S\phi \tag{4.8}$$

$$\omega_z = \dot{\psi} C\theta + \dot{\phi} \tag{4.9}$$

4.2.1 Lagrangian Equation of Motion For Constrained Systems

The Lagrange's equation for constrained systems generates six differential equations of motion for each part within a mechanism for each of the six independent degrees of freedom and is given by the generalised vector co-ordinate set $\{q_j\}$. The Lagrange equation is composed of the following:

- Energy (which accounts for both the rotational and translation kinetic energy)
- Momenta (which accounts for the momentum of the parts)
- Kinematic relations (in terms of position and orientation)
- Applied kinetics (which comprise applied forces and torques, these include system restraints such as restoring forces of compliant members)
- Constraint functions (which formulate the reaction forces due to constraints)

Using the above-mentioned entities, Lagrange's equation for constraint systems can be formulated as follows (Rahnejat, 1998):

$$\frac{d}{dt}\left[\frac{\partial K}{\partial \dot{q}_j}\right]-\frac{\partial K}{\partial q_j}-F_{q_j}+\sum_{i=1}^{n}\lambda_i\frac{\partial C_i}{\partial q_j}=0 \qquad (4.10)$$

The force kinetics in the above equation is determined by the rate of change of potential/strain energy, as described by Euler: $F_{qj}=-\frac{\partial U}{\partial q_j}$.

Hence, the equations of motion are set up by resolving for the individual entities in the Lagrange's equation (4.10) for every co-ordinate in the generalised co-ordinate vector set. This is explained in the following sections.

For an unconstrained part in the three-dimensional space six equations of motion would result when $q=\{x,y,z,\psi,\theta,\varphi\}^T$, where $\vec{x}$, $\vec{y}$, $\vec{z}$ are the position vectors and φ, γ, ϕ are the first, second and third Euler angles in body 3-1-3 set of rotations, using Eulerian transformations. For constrained systems such as the parts in the drive train model, some of the equations of motion are represented by zero entries in the final Jacobian matrix.

4.2.2 Kinetic energy

The total kinetic energy, K, of a body in motion is given by its translational and rotational kinetic energy components. Hence, the translation components of kinetic energy are given by:

$$\begin{bmatrix} K_x \\ K_y \\ K_z \end{bmatrix}=\frac{1}{2}m\begin{bmatrix} v_x & v_y & v_z \end{bmatrix}\begin{Bmatrix} v_x & v_y & v_z \end{Bmatrix}^T \qquad (4.11)$$

where m, is the mass of the body and $\lfloor v_x \quad v_y \quad v_z \rfloor = \lfloor \dot{x} \quad \dot{y} \quad \dot{z} \rfloor$. Therefore, the resultant kinetic energy can be defined as:

$$K=\frac{1}{2}mv^2=\frac{1}{2}m\left[\dot{x}^2 \quad \dot{y}^2 \quad \dot{z}^2\right] \qquad (4.12)$$

Similarly, the rotational components of the kinetic energy are given by:

$$\begin{bmatrix} K_{rx} \\ K_{ry} \\ K_{rz} \end{bmatrix} = \frac{1}{2} \begin{bmatrix} I_{xx} & 0 & 0 \\ 0 & I_{yy} & 0 \\ 0 & 0 & I_{zz} \end{bmatrix} [\omega_x \quad \omega_y \quad \omega_z] \{\omega_x \quad \omega_y \quad \omega_z\}^T \tag{4.13}$$

Therefore, the total angular kinetic energy can be expressed as:

$$[K_r] = \frac{1}{2} I\omega^2 = \frac{1}{2}\left(I_{xx}\omega_x^2 + I_{yy}\omega_y^2 + I_{zz}\omega_z^2\right) \tag{4.14}$$

where I, is the moments of inertia matrix and ω is the overall angular velocity of the part.

4.2.3 Momenta

The general momenta of a body is given by the term: $\frac{\partial K}{\partial \dot{q}_j}$ in the Lagrange equation (4.10), and is denoted by M_{q_j} here. Hence:

$$M_{q_j} = \frac{\partial K}{\partial \dot{q}_j} \tag{4.15}$$

The momenta can be further broken down into their translation and rotational components. Therefore, expressing the translational momenta in its component form yields the equations (4.16)-(4.18) by differentiating the translational kinetic energy equation (4.12) with respect to the individual co-ordinates of the generalised vector co-ordinate set:

$$M_x = \frac{\partial K}{\partial \dot{x}} = m\dot{x} \tag{4.16}$$

$$M_y = \frac{\partial K}{\partial \dot{y}} = m\dot{y} \tag{4.17}$$

$$M_z = \frac{\partial K}{\partial \dot{z}} = m\dot{z} \tag{4.18}$$

The rotational components of the momenta are obtained in a similar manner. The angular velocity components in the rotational kinetic energy equation (4.14) are replaced by their respective components in terms of $\lfloor \dot{\psi} \quad \dot{\theta} \quad \dot{\phi} \rfloor$. Thus, after simplification, the following expressions are obtained:

$$M_{\psi} = \frac{\partial K}{\partial \dot{\psi}} = I_{xx}\dot{\psi}S\theta S\phi + I_{yy}\dot{\psi}S\theta C\phi + I_{zz}C\theta \qquad (4.19)$$

$$M_{\theta} = \frac{\partial K}{\partial \dot{\theta}} = I_{xx}\dot{\theta}C\phi - I_{yy}\dot{\theta}S\phi \qquad (4.20)$$

$$M_{\phi} = \frac{\partial K}{\partial \dot{\phi}} = I_{zz}\dot{\phi}^2 C\phi \qquad (4.21)$$

The above three equations give the angular momenta of a part in motion relative to fixed frame of reference (Rahnejat, 1998, and Ryan, 1990).

4.2.4 Force kinetics

The applied kinetic terms in the Lagrange's equation is used to formulate the generalised forces acting on an element such as contact forces, which would be a consequence of applied forces or torques, or body forces. Therefore, if a generalised force *F* acts on a body, then the components of this force along any co-ordinate direction of the generalised vector co-ordinate set $\{q_j\}$ can be expressed as:

$$F_{q_j} = \left[\frac{\partial \vec{R}_G}{\partial q_j}\right].F \qquad (4.22)$$

where, $\left[\frac{\partial \vec{R}_G}{\partial q_j}\right]$ is the differential with respect to a co-ordinate in the generalised vector co-ordinate set. The result of the differential is only the unit vectors $\lfloor \vec{i} \quad \vec{j} \quad \vec{k} \rfloor$, which specify the direction in which the applied force acts with respect to the GRF. Hence, if there is a force applied in the *x* direction, then the generalised force component along this direction would be given by a vector dot product operation as:

$$F_x = \left[\frac{\partial \vec{R}_G}{\partial x}\right].F = F.\vec{i} \qquad (4.23)$$

A similar method can be applied to account for the generalised forces in the other co-ordinate directions. If the force applied does not exist in a certain direction, then the scalar product in equation (4.23) equates to zero.

For each part of the multi-body drive train model, a set of equations of motion is established using the Lagrange's equation for constrained systems (i.e. equation (4.10)).

4.2.5 Constraint Functions

To evaluate the last term in the Lagrange's equation, which accounts for all the joint reaction forces in a multi-body system, the constraint functions; C_i, for every joint in the mechanism need to be determined. It must be noted that a constraint function is only to be formulated when a degree of freedom is removed from a part, which in turn depends on the type of joint used to constrain the system (Rahnejat, 1998, Ryan and Steigerwald, 1988). Therefore, for example, if a joint between two parts removes five degrees of freedom from the mechanism, then five constraint functions are formulated to account for this. There are a host of joints in the drive train model, described in this thesis. Constraint functions for all these types of joints and others are provided in Rahnejat (1998).

4.2.6 The Jacobian Matrix

The set of differential equations of motion described above, scalar constraint functions, the applied forces and force characteristics and the various sources of compliance, must be resolved for each small step of time. The vector of unknowns includes the system state variables: position, velocity and acceleration of all parts, and the Lagrange multipliers representing the joint reactions. Thus, in matrix form, the set of simultaneous equations are represented as:

$$[J]\{q,\lambda\}^T = \{F_q\} \tag{4.24}$$

where $[J]$ is the Jacobian matrix, $\{q,\lambda\}^T$ is the required solution vector for all small time steps, dt, and $\{\vec{F}_q\}$ is the vector of applied forces. The Jacobian matrix is of the following form:

$$[\mathbf{J}] = \begin{bmatrix} \left[\frac{\mathbf{s}}{\mathbf{dt}} \frac{\partial \mathbf{K}}{\partial \dot{\mathbf{q}}} + \frac{\partial \mathbf{K}}{\partial \mathbf{q}} \right] & \left[\frac{\partial \mathbf{C}}{\partial \lambda} \right] \\ \left[\frac{\partial \mathbf{C}}{\partial \mathbf{q}} \right] & [0] \end{bmatrix} \tag{4.25}$$

where $[J]$ is the Jacobian matrix, s is scaling factor (taken as 1 in all the analysis carried out in this thesis), K represents the kinetic energy, C represents the constraint function, q is the vector of generalised co-ordinates, λ represents the Lagrange multiplier, and t is the time.

The Jacobian matrix, as shown in equation (4.25) consists of a number of sub matrices, relating to the mass/inertial contributions, constraint functions and the corresponding joint reactions, given as Lagrange's multipliers. The Jacobian matrix contains many zero entries, and is thus referred to as sparse (Rahnejat, 1998, and Orlandea, 1999). The Jacobian matrix is also quite large in size, as it embodies appropriate coefficients for 6 equations of motion for every drive train component, and for all the formulated constraint functions. In fact, fewer than 10% of all the elements of the matrix are usually non-zero. The solution to equation (4.24) is obtained in small variable time steps, *dt*, by employing the predictor-corrector technique, and the Newton-Raphson method for the solution of non-linear simultaneous equations, and step-by-step integration using a "stiff" algorithm for widely split eigenvalue problems.

4.2.7 The Solution Methodology

The Jacobian matrix contains a mix of linear and non-linear algebraic equations (i.e. constraints functions and generalised forces) and differential equations of motion. The Jacobian matrix for a multi-body system is usually a very large square matrix. Therefore, it is difficult, if not impossible, to invert such a matrix in order to solve the simultaneous set of equations given by equation (4.24). Thus Cholesky's factorisation process is used for this purpose. The sets of equations in most multi-body systems are non-linear in nature. Therefore, Newton-Raphson iteration method is employed for the solution of these non-linear equations. The vector of the state variables includes a set of derivatives, usually of the first order since the problem is normally presented in first order form, using the following substitutions:

$$\varsigma = \frac{dq}{dt} \tag{4.26}$$

$$\varsigma' = \frac{d^2q}{dt^2} \tag{4.27}$$

where q is the generalised co-ordinate set (i.e. the state variables), ς is the vector of the state variables in the first order formulation, ς' is the vector of the state variable derivatives and t is time.

This means that the state variables and the state variable derivatives in each time step must be evaluated by the process of discretisation of the differential equations of motion, using a time stepping integration method. This process is carried out using recursive backward difference formulae in a predictor-corrector procedure, also employing the Gear integration algorithm (Gear, 1971a, Gear 1971b, Rahnejat, 1998).

4.2.8 LU Decomposition (Cholesky factorisation)

For a set of linear equations that has to be repeatedly solved with different inhomogeneous terms, the LU decomposition is recommended (Nakamura, 1991). The LU decomposition represents the replacement of the Jacobian matrix by a product of two triangular matrices, known as the lower and the upper triangular matrices. In the lower triangular matrix all the non-zero elements occupy the triangle on or below the diagonal, whilst in the upper triangular matrix all such terms reside on or above the diagonal. Therefore:

$$[L]\cdot[U] = [J] \tag{4.28}$$

where *[J]* is the Jacobian, *[L]* is the lower matrix and *[U]* is the upper matrix.

Thus, the equation (4.24) becomes:

$$[J]\cdot\{q,\lambda\}^T = ([L]\cdot[U])\cdot\{q,\lambda\}^T = [L]\cdot\left([U]\cdot\{q,\lambda\}^T\right) = \{F_q\} \tag{4.29}$$

Equation (4.29) may then be represented by a pair of matrix equations. The first step is solving for the $\{V\}$ vector as indicated below:

$$[L]\cdot\{V\}=\left\{F_q\right\} \tag{4.30}$$

and afterwards by solving:

$$[U]\{q,\lambda\}^T=\{V\} \tag{4.31}$$

This set of matrix equations is sufficient for the solution of a linear system. However, the set of equations in the multi-body systems described in this thesis is non-linear, requiring the use of the Newton-Raphson method.

4.2.9 The Newton - Raphson Method

The Newton-Raphson method can be employed for the solution of a system of non-linear equations. This method is based upon the approximation of a characteristic curve $f(q,\lambda)$ with a straight line near the point of solution, where $f(q,\lambda)=0$.

$f(q,\lambda)$ is the solution curve for the problem at hand. The solution is obtained by an iterative process, where current values for the characteristic curve are obtained from previously determined solutions, and the gradient of the curve in the vicinity of the point of solution is derived, as (Rahnejat, 1998):

$$f(q,\lambda)_{n+1}\approx f(q,\lambda)_n+\frac{\partial \mathrm{f}}{\partial q}\cdot\nabla q_{n+1} \tag{4.32}$$

$$[J]=\frac{\partial \mathrm{f}}{\partial q} \tag{4.33}$$

$$\nabla q_{n+1}=q_{n+1}-q_n \tag{4.34}$$

where f is the solution curve, *[J]* is the Jacobian and ∇q_{n+1} is the vector of backward difference.

The historical data in the above equations are obtained by approximating the solution trend from previous known values using polynomial fits in the predictor-corrector procedure, based on Newton interpolations.

4.2.10 The Newton Interpolations

A set of data points can be interpolated using polynomial, spline or rational functions, Fourier series or other possible ways. Polynomial interpolation uses a polynomial to fit a given set of points. The most important one-dimensional interpolation schemes are the Lagrange interpolation, Newton interpolation, Lagrange interpolation using Chebysev points, Hermite interpolation or a cubic spline interpolation (Nakamura, 1991).

The predictor-corrector procedure described later uses Newton interpolation because the order of the polynomial can be changed easily and the evaluation of the errors can be obtained easily.

There are two versions of the Newton interpolations: the Newton forward interpolation and the Newton backward interpolation.

A function f, can be represented by a set of discrete points (x_n, f_n). A subset of these points can be selected. The set (i.e. $n = 0,1,2,3$ or $n = 3,4,5,6,7$) has $m+1$ points (m being 3 and 4 respectively in this example). An interpolation polynomial function $p(x)$ has to be found to fit the given points (see Figure 4.3) (Nakamura, 1991, Centea, 1996).

The forward differences $\Delta^n f_n$ are defined in Nakamura, 1991 as:

$$\Delta^0 f_n = f_n \tag{4.35}$$

$$\Delta f_n = f_{n+1} - f_n \tag{4.36}$$

$$\Delta^k f_n = \Delta^{k-1} f_{n+1} - \Delta^{k-1} f_n \tag{4.37}$$

where, f_n is a function given by a set of consecutive data points (x_n, f_n), n is a point within a specific set of points, k is the order of forward difference with $0 \le k \le m$ and $m+1$ is the number of points in the selected set.

The backward differences $\nabla^n f_n$ are defined as:

$$\nabla^0 f_n = f_n \tag{4.38}$$

$$\nabla f_n = f_n - f_{n-1} \tag{4.39}$$

$$\nabla^k f_n = \nabla^{k-1} f_n - \nabla^{k-1} f_{n-1} \tag{4.40}$$

where, f_n is a function given by a set of consecutive data points (x_n, f_n), n is a point in a chosen set of points defined within the total number of given points, $m+1$ is the total number of points within the selected set and k is the order of backward difference with $0 \le k \le m$.

The equivalence relationship between the forward difference and the backward difference is given in Nakamura, 1991 by:

$$\nabla^k f_k = \Delta^k f_{n-k} \tag{4.41}$$

The Newton forward interpolation formula defines an interpolation function f as:

$$p(x) = p(x_r + s \cdot h) = \sum_{k=0}^{m} \binom{s}{k} \Delta^k f_0 \tag{4.42}$$

where, p is the value of the function which has to be found by interpolation, x_r is the abscissa of the first point in the selected set, h represents the constant distance between any two consecutive points on the abscissa ($h = x_1 - x_0 = x_2 - x_1$ - see figure 4.3), and s is the local co-ordinate defined as:

$$s = \frac{x - x_r}{h}, \quad 0 \le s \le k \tag{4.43}$$

where, subscript r is the order of the first abscissa from the selected set of data points, x is the current abscissa and h is the constant interval along the abscissa.

The Newton backward interpolation formula is defined as:

$$p(x) = p(x_n + s \cdot h) = \sum_{k=0}^{m} \binom{s+k-1}{k} \cdot \nabla^k f_n \tag{4.44}$$

where, p is the value of the polynomial function which has to be fitted by interpolation through the given points, x_n is the abscissa of the last point in the selected set, h represents the constant distance between any two consecutive points on the abscissa and s is the local co-ordinate defined as:

$$s = \frac{x - x_n}{h}, \quad -k \le s \le 0 \tag{4.45}$$

where, n is the order of the last abscissa point from the selected set, x is the current value and h is the constant interval.

The backward differences can, therefore, be expressed in terms of forward differences as:

$$p(x) = \sum_{k=0}^{m} \binom{s+k-1}{k} \cdot \Delta^k f_{n-k} \tag{4.46}$$

where, $p(x)$ is the interpolation polynomial, s is the actual co-ordinate defined in equation (4.45), k is the counter and n is the order of the point from which the backward interpolation commences.

Both the forward and the backward Newton interpolations are mathematically equivalent. The selection of one or the other expression depends on how the formulae are applied. The predictor-corrector procedure uses the Newton backward interpolation, because data points are all in the backward position.

4.2.11 Predictor-corrector method

A predictor-corrector method consists of a predictor step and a subsequent corrector step in each time interval. The predictor provides an estimate for the solution vector at the new point, whilst the corrector improves the accuracy of the solution. A polynomial is fitted to the previous solutions and interpolation is carried out to obtain the slope at various points.

The interpolation polynomial p is fitted to the function ς' defined in each time step (the abscissa x is the time t in a dynamic system) at points n, n-1.,.n-m and may be written, using the Newton backward interpolations formula as (Nakamura, 1991) (see equation (4.46):

$$p_m(t) = \sum_{k=0}^{m}(-1)^k \binom{s+k-1}{k} \cdot \Delta^k \varsigma'_{n-k} \tag{4.47}$$

where, p is the polynomial interpolated function, $\binom{s+k-1}{k}$ is the binomial coefficient, $m+1$ is the number of points within the chosen set of points, k is the loop counter, $\Delta^n \varsigma'_{n-m}$ is the forward difference term and s represents the local co-ordinate defined by substituting the abscissa x in equation (4.45) with the time t:

$$s = \frac{t - t_n}{h} \tag{4.48}$$

where, t is the time at the point where the interpolation polynomial has to be found and t_n is the abscissa of the last used point.

By using the Runge-Kutta method, in order to calculate the following point ς_{n+1} at $t_{n+1} = t_n+h$ with a known value of ς_n, the following integral should be evaluated (Nakamura, 1991):

$$\varsigma_{n+1} = \varsigma_n + \int_{t_n}^{t_{n+1}} f(\varsigma, t) \cdot dt \tag{4.49}$$

Substituting the equation (4.47) into equation (4.49), the Adams-Bashford predictor formula for m^{th} order is obtained as:

$$\varsigma_{n+1}^{p} = \varsigma_n + h\left[b_0 \cdot \varsigma_n' + b_1 \cdot \Delta\varsigma_{n-1}' + \cdots + b_m \cdot \Delta^m \varsigma_{n-m}'\right] \tag{4.50}$$

where, the superscript p represents the predictor phase, $b_0 ... b_n$ represent the polynomial coefficients and the vector ς is given by a set of already calculated points..

The polynomial coefficients b_k in equation (4.50) are defined as:

$$b_k = \int_0^1 \binom{s+k-1}{n} \cdot ds \tag{4.51}$$

where, s is the local co-ordinate, k is the counter and n represents the point of interest.

The first few values of b_n, calculated in Nakamura, 1991 are:

$$b_0 = 1 \tag{4.52}$$

$$b_1 = \frac{1}{2} \tag{4.53}$$

$$b_2 = \frac{5}{12} \tag{4.54}$$

$$b_3 = \frac{3}{8} \tag{4.55}$$

$$b_4 = \frac{521}{720} \tag{4.56}$$

The corrector formula may be derived in the same manner. The polynomial interpolation for the slope in this phase is given by the following relationship:

$$p(t) = \sum_{k=0}^{m} \binom{s+k-2}{k} \cdot \Delta^k \varsigma'_{n+1-k} \tag{4.57}$$

where, p is the polynomial interpolated function, $\binom{s+k-2}{k}$ is the binomial coefficient, $m+1$ is the number of points of the chosen set of points, k is the loop counter, $\Delta^n \varsigma'_{n-m}$ is the forward difference term and s represents the local co-ordinate defined by substituting the abscissa x in equation (4.45) with the time t defined in equation (4.48).

The Newton backward difference formula, fitted in the case of the corrector, using forward integration differences is, therefore, obtained as:

$$\varsigma^c_{i+1} = \varsigma_i + h\left[c_0 \cdot \varsigma'_{i+1} + c_1 \cdot \Delta\varsigma'_i + \cdots + c_m \cdot \Delta^m \varsigma'_{i-m}\right] \tag{4.58}$$

where, the superscript c represents the corrector phase and c_n represents the polynomial coefficients defined as:

$$c_k = \int_0^1 \binom{s+k-2}{k} \cdot ds \tag{4.59}$$

where, s is the local slope.

The first few values of c_n follow from Nakamura as:

$$c_0 = 1 \tag{4.60}$$

$$c_1 = -\frac{1}{2} \tag{4.61}$$

$$c_2 = -\frac{1}{12} \tag{4.62}$$

$$c_3 = -\frac{1}{24} \tag{4.63}$$

$$c_4 = -\frac{19}{720} \tag{4.64}$$

The advantage of the predictor-corrector methods is their computational efficiency (Nakamura, 1991), being evaluated in a fewer number of steps (regardless of the order of the predictor-corrector method) as required by the fourth order Runge-Kutta method. Furthermore, the technique permits detecting at each step the local error with a small computational effort.

The disadvantage of the method is that it cannot start by itself, because of the need to use previous data points. Therefore, an assumption/guess value is required to initiate the process. Another method like Runge-Kutta may be used to start the iterative process.

4.2.12 Gear Stiff Integration

Stiff differential equations frequently arise in representation of physical systems due to the existence of greatly differing time constants. A system is "stiff", when its largest inactive eigenvalue is much larger that its largest active eigenvalue.

A numerical integrator approximates the solution by a polynomial that satisfies the system governing equations at discrete time intervals. The error of integration during one integration step is related to the first omitted derivative in the truncated Taylor series that represents the polynomial. Therefore, fixed step size integrators can behave well with systems having close eigenvalues. When the smallest eigenvalue is active, costly unnecessary computation can result. The step-size Gear-type integrators (Gear, 1971b) allow the integration step size to be automatically altered according to an estimate of the local truncation error, making them particularly suitable and fast in dealing with stiff systems.

The Gear stiff integrator used in ADAMS is called Gstiff. It stores the information relating to the "historical" polynomial as the analysis moves in time in the form of a Nordsieck vector, which is a particular form of representation of the Taylor series. Every time a new value is calculated, a corresponding error is also calculated (Rahnejat, 1998). If the estimated error is greater than specified error tolerance, a new smaller time step is used and the value obtained is better fitted to the curve.

4.2.13 Integration error control

Each integration step consists of two phases: predictor and corrector. The predictor uses the previous values of each variable to predict the value of the variable at the end of the current integration time step. The corrector uses the predicted values as the initial guesses to solve the system state equations using Newton-Raphson iterations.

The integrator error is the difference between the solution of a differential equation and its direct analytical solution. The difference between analytical solution and the numerical approximation at any time, t, is called the "Global Integration Error", where the "Local Integration Error" is the error which occurs during a single integration step time, *dt* (Boysal, 1995, Boysal and Rahnejat, 1997).

Using the information about the numerical method an upper bound for the Local Integration Error can be estimated. The argument related to Gstiff integrator controls the integration error associated with the state variable ς. The integration error for state variable derivates, $\dot{\varsigma}$, will be less than or equal to *error/dt,* where *dt* is the integration step size. The integration for acceleration and forces will be the order of $\leq error/dt^2$. These integration error limits apply to the solution approximation to the differential and algebraic equations by Taylor series polynomial for the predictor phase. According to Taylor's remainder theorem, the principle term in the local truncation error in an interval of time *dt* is:

$$\mathbf{R}_k \leq \varsigma^{k+1} \cdot \hat{\mathbf{t}} \cdot \frac{\mathbf{dt}^{k+1}}{(\mathbf{k}+1)!} \tag{4.71}$$

where, *k+1* indicates the $(k+1)^{th}$ derivative term with respect to time and $\hat{\mathbf{t}}$ is a multiplier maximising the value of ς^{k+1}. During the corrector phase the integrator ensures that the largest change in a variable will not exceed *error/1000.*

Two methods used to ensure the satisfaction of the upper limit are (Boysal, 1995):

1. The absolute method:

$$\text{if } \nu_c \leq 1 \text{ then } \chi \leq \frac{error}{1000} \tag{4.72}$$

2. The relative method

$$\text{if } \nu_c > 1 \text{ then } \frac{\chi}{\nu_{max}} \leq \frac{error}{1000} \tag{4.73}$$

where, ν_c is the absolute value of the corrected variable with the largest change during an iteration, ν_c is the largest past value of ν_c and χ is the absolute value of change in ν_c.

4.3. Description of the multi body driveline models.

4.3.1. Driveline background

The Rear Wheel Drive (RWD) vehicle driveline is a lightly damped non-linear system with many degrees of freedom. The driveline is defined as the collection of parts between the flywheel and the road wheels. The subsystems are connected together in a multi body series of elements that are highly non-linear. There is a complicated interaction between the elements due to gear meshing, spline movement, backlash, friction contact in the clutch, and rubber compliance in the drive.

When engine and road inputs are applied to the driveline system, rapid changes in the driveline response can take place. These rapid changes excite the higher frequency structural modes in the driveline, particularly at the drive shaft and transmission bell housing.

Driveline clonk is generic. It is equally likely to cause problems on FWD or RWD, on vehicles with petrol or diesel engines, drivelines having ***n*** shafts, or under certain driving conditions. In other words, it is sensitive to many factors. It is also known that the problem demonstrates a natural variation from vehicle to vehicle, even when comparing vehicles of identical build specifications. Furthermore, it is known that this is more related to driving style than to part or vehicle variation. The *magnitude* of the problem may also change if, for example, the driveshaft is made of aluminium.

This thesis considers both the FWD and RWD driveline configurations, and different capacity engines, and it considers two and three piece drivelines. This diversity of approach is considered to be important in order to compare and confirm the clonk mechanism and causal factors.

In addition it considers component testing, rig testing, chassis dynamometer testing, and road testing.

This was a deliberate attempt to expose the problem in as many ways as possible in order to understand the underlying phenomenon.

If a short duration impulsive torque is applied to a FWD or RWD driveline it will excite a response in the system across the frequency range. Impulse torque conditions will occur when the throttle is rapidly applied from coast, or when the throttle is rapidly released from drive. Impulse torque conditions also occur when the clutch is rapidly engaged after a gearshift or when manoeuvring. In either case, the effect of the impulse torque supplied to the driveline is to excite a low frequency condition known as shuffle, and a high frequency condition known as clonk.

Shuffle is particularly evident at low speeds and in low gear. It is the first torsional mode of the driveline and the driver experiences this mode as a longitudinal jerk, referred to as shunt.

The high frequency clonk noise may be heard coincident with the shuffle cycles of vibration, and when backlash in the driveline is taken up by the torque surge over a very short time period. Clonk may be heard with or without shuffle, and whenever the torque travels through the system backlash. It is particularly noticeable in low gears and at low speeds, when background engine and road noises are minimal.

The high frequency 1000 to 5000 Hz clonk response may be clearly seen on the much lower (4 to 8 Hz) shuffle frequency carrier wave, when it has been taken from an instrumented test vehicle. This high frequency characteristic is common to both the hollow large diameter tubes on RWD and the smaller diameter shafts on FWD vehicles.

In order to study shuffle, a multi body dynamic driveline model is required. In fact, a lumped mass model with 4 or 5 degrees of freedom will clearly demonstrate the low frequency shuffle condition.

By comparison, in order to specifically study high frequency clonk, an FE model of the noise emitting parts of the driveline is required.

This thesis presents two driveline simulation models (a 2-piece and a 3-piece driveline simulation) and an experimental back up rig, which was used for CAE model verification.

A simple two-piece driveline ADAMS model, and a corresponding driveline test rig, were set up to evaluate shuffle and clonk. Furthermore, a short test was conducted on a vehicle with one rear wheel jacked up and with the handbrake lightly applied. The 2nd gear was selected and the clutch was abruptly engaged. The clonk response was subjectively rated to be the same as that heard when driving on the road. It appeared to emanate from the transmission. No data was collected. The purpose of this short static test was to confirm that clonk could be excited with a stationary vehicle. It was, therefore, confirmed that a static driveline rig could be expected to behave in a similar manner, with the advantage that experimentation would then be conducted in a controlled environment.

This driveline clonk test rig was fully described in Chapter 3.

- The rig consisted of flywheel/clutch assembly/transmission assembly/two-piece drive shaft/rear axle/wheel ends including hubs and drums and half shafts. All the system lash zones were included.
- The flywheel and clutch and transmission input shaft were rigidly mounted to the floor.
- The two-piece drive shaft was compliantly mounted at the centre bearing.
- The transmission was compliantly mounted.
- The wheel ends were rigidly fixed to the ground.
- The torque was applied to the flywheel by winding up the driveline torque through the clutch springs and then by an abrupt release.
- Microphone and piezo-accelerometers were used to capture the system response to the applied torque pulse.

4.3.2. Multi-body model constraints and definitions

4.3.2.1 Parts

A rigid body is referred to as a *part*. Each part has six DOF (explained later) and so it will be necessary to solve six equations of motion to define the part motion.

In an MBD system, the constituent parts are modelled according to Lagrange's definition, to establish the equations of motion. There is no coupling between each part except by the use of constraint functions, which describe the joints between neighbouring parts.

In an MBD system there are also *constraints*, which often have non-linear characteristics.

4.3.2.2. Constraints.

A constraint represents idealised connections.

A constraint removes movement (one or more degrees of freedom dependent on type of constraint) between parts ***i*** and ***j*** in specified directions.

Types of constraints:

Fixed joint: A fixed joint locks two parts together so that they cannot move with respect to each other. The two parts are defined as one.

It has 3 translational and 3 rotational constraints.

Revolute joint: A revolute joint allows the rotation of one part with respect to another about a common axis. In other words, this is a hinged joint.

It has a mixed translational and rotational constraint.

Spherical joint: A spherical joint allows full freedom of rotation movement as would a ball and socket joint. It has a mixed translational and rotational constraint.

Universal joint: A universal (Hooke) joint allows rotation of one rigid body to be transferred to another rigid body. It is particularly useful when defining the motion between two shafts in a driveline that are permitted to articulate at the connection.

It has 3 translational and 1 rotational constraints.

Translation joint: A translation joint allows one part to translate (not rotate) along a vector with respect to another part.

Cylindrical joint: A cylindrical joint allows one part to rotate and translate with respect to another along their shared axis.

Coupling joint: A coupling joint allows two or three joints to be coupled together. It relates the translation / rotation motion of the coupled joints by the use of linear scaling. It is useful for belt drives, pulleys, chains, etc.

4.3.2.3. *Restraints*

A restraint resists movement by its compliance, i.e. it is not rigid.

4.3.2.4. *Applied Forces*

A force or torque may be externally applied to a multi-body (MBD) system. It may also be considered as an internal force or torque arising from internal interactions.

4.3.2.5. *Degrees of freedom in the MBD system driveline model*

The degree of freedom (DOF) of any multi-body system is the minimum number of independent coordinates that is required to fully define the position of all parts of the system at any time.
For example:

A simple pendulum has one DOF.
Two masses connected in series is a two DOF system.
A freely floating rigid body in 3D space is said to have 6 DOF.

Each degree of freedom (DOF) in a mechanical system represents at least one equation of motion that must be solved.

Joints in a multi-body model may be prescribed to constrain motion. Some joints constrain more degrees of freedom than others. Hence the real number of degrees of freedom in a model is the total number of co-ordinates that defines the system, less the number of constraints imposed on the system.

The number of DOF of the multi body driveline model is obtained using the Gruebler-Kutzbach (G-K) expression as: $\mathrm{DOF} = 6(\text{number of parts} - 1) - \sum \text{constraints}$

The parts count in the multi-body system (in the above expression) includes the ground, but because this does not contribute to the degrees of freedom of the model, it is deducted in the Gruebler-Kutzbach (G-K) equation.

The general rules that may be applied for rigid bodies regarding system DOF are as follows:

If the number of DOF $< \mathbf{0}$, then the system is *over constrained.* It cannot be resolved.
If the system is over-constrained, then there will be a redundancy in the system. The normal explanation given is a hinged door. Although multiple hinges on a real door are in line to provide rotation control, in the model this would be a redundancy. In this case the code will identify the redundant constraint and delete it from the equation set, and the system will nevertheless behave in a characteristic manner.

If the number of DOF $= \mathbf{0}$ then the system is *kinematic.*
Kinematics is the *description* of body motion without consideration of the causes of motion. However, it is not necessarily safe to ignore inertia and damping effects in an MBD system.

If the number of DOF $\geq \mathbf{0}$ then the system is *dynamic.* This is the case for the two ADAMS models that have been constructed for driveline clonk. Dynamics considers the kinetics and kinematics of a system. It considers the forces and interactions that lead to system motion. The fundamental principles governing dynamics are based on Newton's three laws of motion
The G-K equation will always yield a positive DOF result, if the system is not over-constrained.

4.3.2.6. DOF in the 2-piece driveline model

For the 2-piece driveline model, the number of parts was 14 and the number of constraints was 76:
Using G-K equation, the number of independent DOF in the model was $6(14-1)-76=2$ DOF
The two DOF for the 2-piece driveline model (in its rigid-body form) were:

- The axial float of the rear torque tube/differential/axle with respect to flywheel / transmission / front torque tube, and
- The longitudinal oscillation of the vehicle body with respect to the ground.

The model compliances included the clutch cushion and diaphragm springs, and the pressure plate cover and strap stiffnesses. The model stiffnesses included the rear axle half-shafts and the longitudinal stiffness of the tyre to road contacts at each wheel. No allowance was made to include backlash, or the equivalent, in the 2-piece driveline model.

Figure 4.15 is a schematic representation of the simple 2 DOF model. Note that the motions jacking and rotation are the prescribed kinematic conditions. The 2 DOF already mentioned are vehicle shunt, (1) in figure 4.15, and rear tube float (2).

4.3.2.7. DOF in the 3-piece driveline model

For the 3-piece driveline model, the number of parts was 41 and the number of constraints was 235: Hence, the three-piece driveline model has 240 – 235 = 5 rigid body DOF.
The 5 degrees of freedom for the 3-piece driveline model are shown in figure 4.14, as follows:

- Transmission input shaft and main shaft rotation
- Transmission counter shaft rotation
- Rotation of the three-piece driveshaft assembly, including the axle drive pinion
- Translational motion of the slip spline
- Crown wheel rotation and all subsequent rotational parts to the wheels

4.3.3 2-piece RWD elasto multi body driveline model.

This multi-body model was set up to conform to most of the test conditions that were employed on the test rig, and to recreate the low frequency response characteristics.

The model comprised a number of parts with appropriately constrained functions. Where appropriate the element stiffnesses were included.

The clutch subsystem was kept simple, due to the fact that the clutch was fully clamped in the test rig study, when the torque was applied. Hence, the clutch cushion springs and the diaphragm springs and the pressure plate cover, were lumped together.

The transmission subsystem was represented with appropriate stiffness and configured to be in second gear (when shuffle and clonk are most evident) by a suitable coupling ratio. The transmission subsystem was represented by two masses, the input shaft was connected to the clutch model, and the output shaft was connected by a revolute joint to the driveshaft.

The plunging motion of the rear drive shaft was defined by the use of a splined member. The universal joints with appropriate cross-piece orientations were used to allow freedom of angular movement between transmission output shaft and the axle pinion shaft.

The differential was grounded via a translational joint to allow driveshaft angulations and to allow the shuffle mode dynamics. This is achieved by moving the translational joint, similar to a jacking-up test at the shuffle frequency.

The vehicle body had a translation joint to ground in order to allow modelling of the rear axle compliance and the longitudinal tyre contact patch stiffness.

The vehicle body also had a translation joint to the transmission in order to allow for the axial body motions to take place with respect to the drive train. This enables the inclusion of the vehicle inertia into the model dynamics.

There was a cylindrical joint between the flywheel and the vehicle body to ensure that they could float with respect to each other.

One of the rear wheels was locked and the torque flow was through the other halfshaft to the ground.

It can be seen that the ADAMS model was not set up entirely in line with the rig conditions.

Figures 4.4-4.6 show the various assembled parts of the multi-body model.

4.3.3.1. Description of modelled Parts

Table 4.1 lists the **12** component parts of the two-piece driveline model, and their respective masses and moments of inertia.

TWO PIECE DRIVELINE MODEL
MASS AND INERTIA PROPERTIES

Ref	Part description	Mass (kg)	Inertia $kg.m^2$ I_{xx}	I_{yy}	I_{zz}
1	Flywheel and pressure plate assembly	18.65	0	0	$2.94E^{-01}$
2	Clutch friction disc	1.45	0	0	$1.00E^{-05}$
3	Clutch hub	1	0	0	$1.00E^{-05}$
4	Transmission input shaft	5.98	$1.92E^{-03}$	$7.27E^{-02}$	$7.27E^{-02}$
5	Transmission output shaft	0.86	0	0	$3.65E^{-04}$
6	Drive shaft spline	1.63	0	0	$4.49E^{-04}$
7	Drive shaft tube	3.42	0	0	$1.91E^{-03}$
8	Rear axle differential	13.79	0	0	$2.65E^{-02}$
9	LH half shaft	2.75	0	0	$6.45E^{-03}$
10	RH half shaft	2.75	0	0	$6.47E^{-03}$
11	LH wheel and drum and tyre assembly	40	$3.22E^{-02}$	$5.93E^{-02}$	$3.22E^{-02}$
12	RH wheel and drum and tyre assembly	40	$3.22E^{-02}$	$5.93E^{-02}$	$3.22E^{-02}$

Table 4.1 : Parts in the 2-piece drivetrain model

4.3.3.2. Model constraints

Table 4.2 defines the **17** component parts and constraints of the driveline model.

ASSEMBLY CONSTRAINTS IN THE VEHICLE MODEL

Ref	Part i	Part j	Constraint type	Number of constraints
1	Flywheel and pressure plate assembly	Ground	Revolute joint	5

2	Clutch disc	Flywheel and pressure plate assembly	Fixed joint	6
3	Clutch hub	Clutch disc	Revolute joint	5
4	Clutch hub	Transmission input shaft	Revolute joint	5
5	Transmission input shaft	Transmission output shaft	Revolute joint	5
6	Transmission output shaft	Drive shaft spline	Universal joint	5
7	Drive shaft spline	Drive shaft tube	Translation joint	5
8	Drive shaft tube	Pinion shaft	Universal joint	5
9	Pinion shaft	Rear axle differential	Revolute joint	5
10	Rear axle differential	RH Half shaft	Revolute joint	5
11	Rear axle differential	LH Half shaft	Revolute joint	5
12	Rear axle differential	Ground	Translation joint	5
13	LH Half shaft	LH wheel and drum and tyre	Fixed joint	6
14	RH Half shaft	RH wheel and drum and tyre	Fixed joint	6
15	#10 (pinion)	#12 (RH diff)	Coupler joint	1
16	#10 (pinion)	#11 (LH diff)	Coupler joint	1
17	#4 (hub)	#6 (input shaft)	Coupler joint	1

Table 4.2: Constraints in the 2-piece drivetrain model

4.3.3.3. Applied forces and torques

Table 4.3 defines the 3 forces' and torques' locations in the driveline model, both external and internal. The magnitude and duration of each torque is shown.

EXTERNAL EXCITATION

Ref	Force / torque	Position of application	Magnitude	Duration
1	Vertical motion at differential	#12 in table	SHM	One cycle
2	Torque on flywheel and pressure plate assembly	Flywheel and pressure plate assembly	SHM	Engine torque

Table 4.3: External excitation in the 2-piece drivetrain model

The clutch disc spring characteristic is critical to the transfer of engine excitation into the driveline model. The clutch torsion stiffness is given as 19.4 Nm/degree.

4.3.4. The three-piece RWD elasto-multi body drive line model.

Figures 4.7-4.13 show the ADAMS model construction for the three-piece driveline model. It was constructed with the intent to further investigate the elasto-acoustic couplings that can occur when an impulsive torque is applied, and which then excites the higher frequency modal behaviour in parts of the driveline.

The three-piece driveline model had 5 DOF (see 4.4.4.7) and hence met the 'rules' for being a dynamic system. Dynamics considers the kinetics and kinematics of a system. It considers the forces and interactions that lead to system motion. The fundamental principles governing dynamics are based on Newton's three laws of motion

4.3.4.1. Gear mesh model assumptions

The 3-piece driveline model was more sophisticated than the 2-piece model. The impulse torque characteristic was delivered to the driveline by an impacting second gear set in the transmission. Gear mechanisms have found extensive application in modern power transmission systems, due to their considerable technical advantages. In many cases, the special geometrical characteristics of the gear teeth affect the dynamics and vibration behaviour of geared systems in a significant way. As a consequence, research in the area of dynamics of mechanical systems involving gear mechanisms has been intensive, especially over the last forty years. However, in the presence of gear backlash, which is either introduced intentionally at the design stages or caused by manufacturing errors and wear, the equations of motion of such systems become strongly non-linear. Another important complication arises from the variable number of gear teeth pairs that are in contact at a time, causing a variation of the equivalent gear meshing stiffness. These two factors introduce serious difficulties in the analysis and obscure the interpretation of the numerical results.

The dynamics of a gear-pair system involving both backlash and time-dependent mesh stiffness are being investigated using a dynamic model with the use of piecewise linear equations of motion with time-periodic coefficients and external forcing. In particular, this forcing is generated by either torsional moments or by errors in gear geometry. The centres of both gears are not allowed to move laterally. The stiffness of the model depends on the number and position of the gear teeth pairs that are in contact, and is a periodic function of the relative angular position of the gears. The ADAMS model takes into account the so-called static transmission error, which represents geometrical errors of the teeth profile and spacing. Since the mean angular velocities of the gears are constant, both the stiffness and the static transmission error quantities can approximately be considered as time-periodic functions. In addition, if the tooth-to-tooth variations (i.e. pitch errors and run out of teeth) are neglected, the fundamental frequency of both of these quantities equals the gear meshing frequency: $\omega_M = n_1\omega_1 = n_2\omega_2$, where the integers n_1 and n_2 represent the number of teeth for each gear. This implies that the meshing stiffness $k(t)$ and the static transmission error $e(t)$ terms can be expressed in a Fourier series form.

For instance, the model stiffness can be expressed in the following form

$$k(t) = k_0 + \sum_{s=1}^{\infty}\left[p_s \cos(s\omega_M t) + q_s \sin(s\omega_M t)\right] \quad (4.74)$$

The force developed between the pair of gears is given by the product: $k(t)h(x)$,

where, $x(t) = R_1\varphi_1(t) - R_2\varphi_2(t) - e(t)$ (4.75)

R_1 and R_2 represent the contact point radii of the gears, $\varphi_1(t)$ and $\varphi_2(t)$ are the two torsion coordinates (rotation angles of the gears)

and $h(x) = \begin{cases} x - b, & x \geq b \\ 0, & |x| < b \\ x + b, & x \leq -b \end{cases}$, where $2b$ represents the total backlash.

ADAMS is capable of representing free play or backlash in the driveline but it is easier to use code. It was therefore necessary to write some additional code in FORTRAN to control the forces and dynamics through the transmission gear lash. By comparison, MATLAB/SIMULINK for example, is a similar but different multi-body analysis package, which has the capability of representing, lash or extremely low rate stiffness regimes between impacting bodies by the use of library functions in conjunction with look-up tables.

The following assumptions were made when considering the impact of transmission helical gears in mesh:

- Backlash was defined as circumferential free play on the pitch circle diameter.
- The simulation was assumed to start with the driving gear tooth spaced equidistant between the two opposite adjacent teeth.
- The model was set to increment in extremely small time intervals through the contact condition, as the tooth contact moved from the heel to the toe.
- At each contact point, the circumferential movements of each gear were calculated and the resultant velocity was used to evaluate the local elastic deformation (once the lash had been taken up).
- The local contact force was evaluated from the deflection and stiffness values and used to calculate gear torque.

- As the contact point moved along the tooth flank, the local radius of curvature was evaluated and included in the torque estimation.

The following transmission gear mesh model assumptions were also made:

- No flexural deflection of the transmission main shaft and counter shaft whilst transmitting torque. Hence no dynamic increase in backlash due to shaft separation.
- No gear lateral tooth vibration under impact, and no forced response.
- Dry tooth contact. Elastic contact under Hertzian assumptions.
- Only torsion loadings were considered.
- However, global tooth bending deflection under load *was* included, the teeth were considered to be elastic cantilevers.

4.3.4.2. ADAMS 3-piece driveline model set up procedure:

The following procedure is used to create a 3-piece elasto-multi-body dynamics model of the drivetrain system:

- Import the tube parasolid CAD file into NASTRAN: Creation of the tube FEA model using 2D shell elements (6 DOF for every node). This was justified, because the cylinder wall thickness is very small compared to the radius of the hollow tube. The ratio is 23:1 (0.03751/0.00165)

Cylinder material properties (steel):
E=206 GN/m^2, density=7850 kg/m^3, v=0.3.

- Tube boundary conditions: Fully restrain the 3 orthogonal displacements of all nodes at the closing diameter. The imported cylinder tube is open-ended.

For stability, set the grid mesh such that the number of elements along each normal axis is of the similar order.

- Set the number of nodes along the tube length such that the higher frequency modes and their shapes from 1000 to 5000Hz may be captured and defined by the modal analysis.

Procedure:

- Create the FEA (Finite Element Analysis) model of tube in NASTRAN code.
- Create Super Element.
- Component Mode Synthesis – Craig Brampton Method (the number of modes is kept above 10 KHz).
- Import the tube Super Element model into ADAMS for elasto-multibody analysis.

4.3.4.3. *Parts description.*

Table 4.4 lists the **41** component parts of the driveline model, and their respective masses and moments of inertia.

THREE PIECE DRIVELINE MODEL MASS AND INERTIA PROPERTIES

Part Number Reference	Part name/description	Mass (kg)	Moments of Inertia kg.m^2		
			I_{xx}	I_{yy}	I_{zz}
1	Transmission input shaft	1.82	$9.16E^{-04}$	$7.59E^{-03}$	$7.59E^{-03}$
2	Transmission main shaft	1.79	$4.39E^{-04}$	$3.84E^{-03}$	$3.84E^{-03}$
3	Transmission countershaft	3.15	$8.11E^{-04}$	$1.85E^{-02}$	$1.85E^{-02}$
4	Transmission output shaft	1.83	$4.11E^{-04}$	$8.41E^{-03}$	$8.41E^{-03}$
5	Transmission output flange	1.02	$1.30E^{-03}$	$9.80E^{-04}$	$9.80E^{-04}$
6	SGF coupling	2.66	$7.54E^{-03}$	$3.96E^{-03}$	$3.96E^{-03}$
7	First shaft drive flange	1.04	$1.25E^{-03}$	$7.51E^{-04}$	$7.51E^{-04}$
8	Model dummy part (no inertia)	0.00	0.00	0.00	0.00
9	First drive shaft tube	1.88	$2.28E^{-03}$	$6.62E^{-02}$	$6.62E^{-02}$
10	Dummy	0.00	0.00	0.00	0.00
11	First shaft output flange	0.97	$5.27E^{-04}$	$9.63E^{-04}$	$9.13E^{-04}$
12	Flange yoke	0.85	$7.58E^{-04}$	$1.00E^{-03}$	$5.05E^{-04}$
13	Spider	0.29	$1.37E^{-04}$	$7.68E^{-05}$	$7.68E^{-05}$
14	Second shaft yoke	0.95	$1.09E^{-03}$	$5.51E^{-04}$	$1.00E^{-03}$

15	Dummy	0.00	0.00	0.00	0.00
16	Second shaft tube	1.29	$1.74E^{-03}$	$2.12E^{-02}$	$2.12E^{-02}$
17	Dummy	0.00	0.00	0.00	0.00
18	Second shaft output flange	0.97	$5.27E^{-04}$	$9.13E^{-04}$	$9.63E^{-04}$
19	Flange yoke	0.85	$7.58E^{-04}$	$5.05E^{-04}$	$1.00E^{-03}$
20	Spider	0.29	$1.37E^{-04}$	$7.68E^{-05}$	$7.68E^{-05}$
21	Yoke female slip spline	1.16	$8.72E^{-04}$	$3.37E^{-03}$	$3.00E^{-03}$
22	Male spline	1.76	$6.79E^{-04}$	$6.69E^{-03}$	$6.73E^{-03}$
23	Dummy	0.00	0.00	0.00	0.00
24	Third shaft tube	1.72	$2.33E^{-03}$	$4.99E^{-02}$	$4.99E^{-02}$
25	Dummy	0.00	0.00	0.00	0.00
26	Third shaft tube flange and yoke	0.80	$9.42E^{-04}$	$8.62E^{-04}$	$4.57E^{-04}$
27	Spider	0.35	$1.87E^{-04}$	$1.04E^{-04}$	$1.04E^{-04}$
28	Unknown part connection	???	???	???	???
29	Axle flange	1.24	$2.34E^{-03}$	$1.25E^{-03}$	$1.22E^{-03}$
30	Axle drive pinion shaft	2.63	$1.11E^{-03}$	$9.03E^{-03}$	$9.03E^{-03}$
31	Crown wheel driven gear	4.80	$2.00E^{-02}$	$3.93E^{-02}$	$2.00E^{-02}$
32	Axle differential case	5.62	$1.81E^{-02}$	$1.90E^{-02}$	$2.14E^{-02}$
33	LH Side gear (1)	0.57	$2.58E^{-04}$	$4.33E^{-04}$	$2.58E^{-04}$
34	RH Side gear (2)	0.57	$2.58E^{-04}$	$4.33E^{-04}$	$2.58E^{-04}$
35	Front Side gear (3)	0.25	$1.03E^{-04}$	$5.89E^{-05}$	$1.03E^{-04}$
36	Back Side gear (4)	0.25	$1.03E^{-04}$	$5.89E^{-05}$	$1.03E^{-04}$
37	Side gear shaft	0.36	$2.25E^{-05}$	$4.72E^{-04}$	$2.25E^{-05}$
38	Half shaft (1)	11.44	0.89	$1.49E^{-02}$	0.89
39	Half shaft (2)	11.44	0.89	$1.49E^{-02}$	0.89
40	Vehicle inertia (1)	Dependent on vehicle loading			
41	Vehicle inertia (2)	Dependent on vehicle loading			

Table 4.4: Parts in the 3-piece drivetrain model

4.3.4.4. *Constraints*

Table 4.5 defines the **42** component parts and constraint types in the driveline model.

It can be noted that the Total number of constraints = **235**

ASSEMBLY CONSTRAINTS IN THE VEHICLE MODEL

Part I	Part J	Constraint type	No of constraints
1 Transmission input shaft	Transmission main shaft	Fixed type	6
2 Transmission main shaft	Ground	Revolute joint	5
3 Transmission countershaft	Ground	Revolute joint	5
4 Transmission output shaft	Ground	Revolute joint	5
5 Transmission output shaft	Transmission output flange	Fixed joint	6
6 Transmission output flange	SGF coupling	Fixed joint	6
7 SGF coupling	First shaft drive flange	Fixed joint	6
8 First shaft drive flange	Dummy	Fixed joint	6
9 Dummy	First drive shaft tube	Fixed joint	6
10 First drive shaft tube	Dummy	Fixed joint	6
11 Dummy	First shaft output flange	Fixed joint	6
12 First shaft output flange	Flange yoke	Fixed joint	6
13 Flange yoke	Spider	Revolute joint	5
14 Spider	Second shaft yoke	Revolute joint	5
15 Second shaft yoke	Dummy	Fixed joint	6
16 Dummy	Second shaft tube	Fixed joint	6
17 Second shaft tube	Dummy	Fixed joint	6
18 Dummy	Second shaft output flange	Fixed joint	6
19 Second shaft output flange	Flange yoke	Fixed joint	6
20 Flange yoke	Spider	Revolute joint	5
21 Spider	Yoke female slip spline	Revolute joint	5
22 Yoke female slip spline	Male spline	Translation joint	5
23 Male spline	Dummy	Fixed joint	6
24 Dummy	Third shaft tube	Fixed joint	6
25 Third shaft tube	Dummy	Fixed joint	6
26 Dummy	Third shaft tube flange and yoke	Fixed joint	6
27 Third shaft tube flange and yoke	Spider	Revolute joint	5
28 Spider	Axle flange	Revolute joint	5
29 Axle flange	Ground	Revolute joint	5
30 Axle flange	Axle drive pinion shaft	Fixed joint	6

31 Axle drive pinion shaft	Crown wheel driven gear	Coupling joint	1
32 Crown wheel driven gear	Axle differential case	Fixed joint	6
33 Crown wheel driven gear	Ground	Revolute joint	5
34 Axle differential case	LH side gear (1)	Fixed joint	6
35 Axle differential case	RH side gear (2)	Fixed joint	6
36 Axle differential case	Side gear shaft	Fixed joint	6
37 Side gear shaft	Front side gear (3)	Fixed joint	6
38 Side gear shaft	Back side gear (4)	Fixed joint	6
39 RH side gear (2)	RH half shaft	Fixed joint	6
40 LH side gear (2)	LH half shaft	Fixed joint	6
41 RH half shaft	Vehicle inertia (2)	Fixed joint	6
42 LH half shaft	Vehicle inertia (1)	Fixed joint	6

Table 4.5: Constraints in the 3-piece drivetrain model

4.3.4.5. Compliances and restraints

A restraint resists movement by its compliance, i.e. it is not rigid.

Table 4.6 defines the 10 compliant component parts of the driveline model, and their respective stiffness and damping characteristics.

Reference Number	Parts/Areas of Application	Characteristics
1	First Driveshaft tube	Superelement - 142 Modes
2	Second Driveshaft tube	Superelement - 102 Modes
3	Third Driveshaft tube	Superelement - 122 Modes
4	Total Normal Backlash ~ fourth gear set	Experimental Data - 63μm
5	Total Normal Backlash ~ second gear set	Experimental Data - 75μm
6	First Driveshaft Tube Angle (around y axis)	Manufacturing Data - 4.5°
7	Second Driveshaft Tube Angle (around y axis)	Manufacturing Data - 4.9°
8	Third Driveshaft Tube Angle (around y axis)	Manufacturing Data - 2.8°
9	Third Driveshaft Tube Angle (around z axis)	Manufacturing Data - 1.5°
10	Axial and Torsional Coupling Stiffness	Experimental Data

Table 4.6: Restraints and Compliances in the Driveline Model

4.3.4.6. *Applied forces and torques*

A force or torque may be externally applied to a MBD system. It may also be considered as an internal force or torque arising from internal interactions.

Table 4.7 lists the external force in the driveline model. Also shown is the magnitude and duration for the force.

Reference Number	Type	Position	Magnitude	Duration
1	Ramp torque	Transmission input shaft	According to driving technique (80-180 ms) pulse	

Table 4.7: External applied force in the driveline model

There are other important internal restoring forces in the model. They are:

- Gear meshing force (assume Hertzian impact bending conditions) in 2^{nd} and 4^{th} gear.
- Bearing force (assume Hertzian impact forces)

4.3.4.7. DOF in the 3-piece MBD system model.

The number of DOF of the multi body driveline model is obtained using the Gruebler-Kutzbach expression: DOF = 6(number of parts – 1) - $\sum \text{constraints}$

Hence, the 3-piece driveline model has 240 – 235 = 5 rigid body degrees of freedom.

The 5 degrees of freedom are identified in figure 4.14

They are as follows:

- Transmission input shaft and main shaft rotation.
- Transmission counter-shaft rotation.
- Rotation of the three-piece drive shaft assembly including axle drive pinion.
- Translation motion of slip spline.
- Crown wheel rotation and all subsequent rotation parts to the wheels.

4.3.5. 3 piece driveline Elastodynamics modelling procedure

The driveshaft tube parasolid CAD files were imported into NASTRAN finite element code. The driveshaft tube FEA models were created, using 2D shell elements (six DOF for every node). This was justified, because the cylinder wall thickness was very small compared to the tube radius. The ratio was 0.03751/0.00165 = 23:1

The FEA meshing density for the three drive shafts was as follows (see figure 4.14):

Front tube (nearest engine)	3476 nodes	3444 shell elements
Centre tube	760 nodes	740 elements
Rear tube	1020 nodes	1000 elements

Cylinder material properties:

Youngs Modulus, E=206 GN/m^2, Density=7850 Kg/m^3, ν = Poisson ratio=0.3

Tube boundary conditions are:

The three orthogonal displacements of all nodes at the closing diameter were fully restrained. The open-ended imported cylinder tube was closed in the model. In other words the shaft could be considered as a fully built-in encastré beam with closed ends.

For computational stability, the grid mesh was set such that the number of elements along each normal axis was of a similar order.

The number of nodes along the tube length was set such that the model would capture and define the higher frequency modes and their shapes, from 1000 to 5000Hz.

Précis summary of the model set up procedure:

- FEA tube model creation in NASTRAN.
- Super element creation.
- Component Mode Synthesis – the Craig Brampton Method (number of modes kept above 10 KHz
- Tube super-element model was then imported into ADAMS for the elasto multi-body analysis. This meant that the impulse torque in the ADAMS model created by the gear mesh impact was transferred to the FE mesh model of the driveshaft tube.

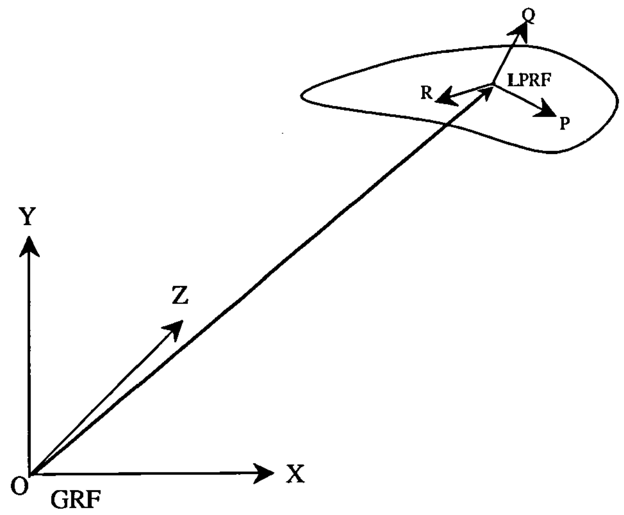

Figure 4.1 Definition of the direction vector of LPRF with respect to GRF

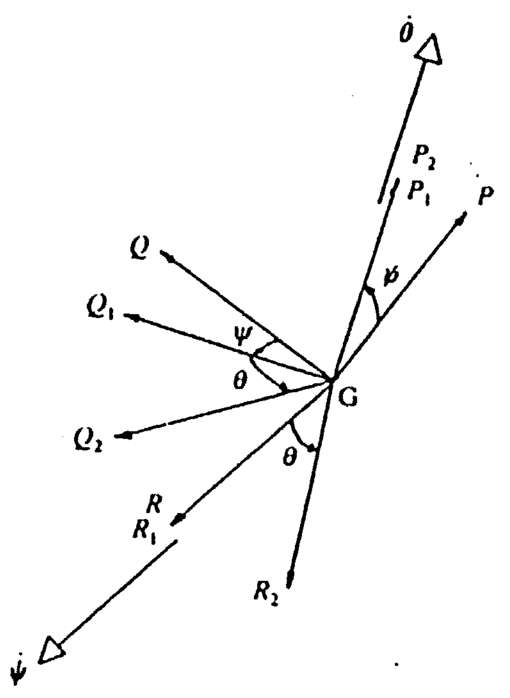

Figure 4.2 Time derivatives of Euler angles

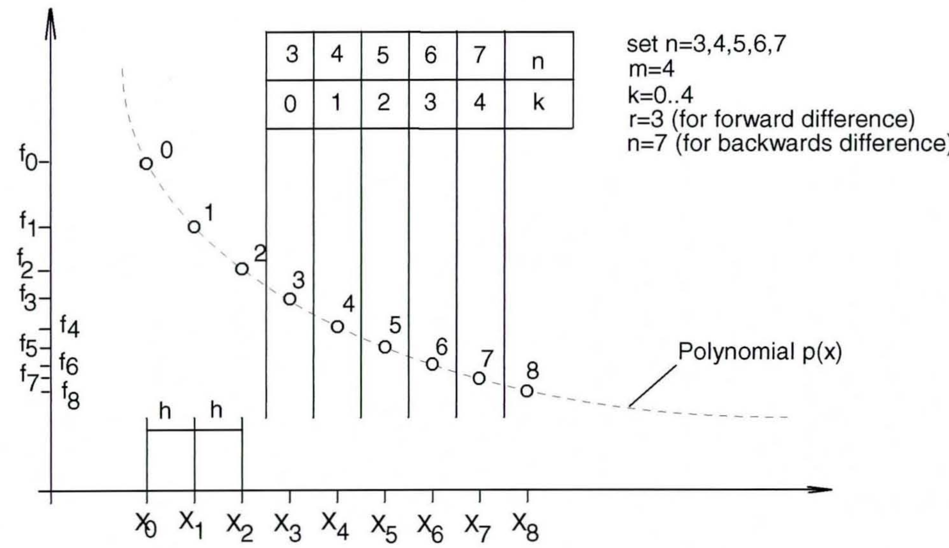

Figure 4.3 The interpolation polynomial

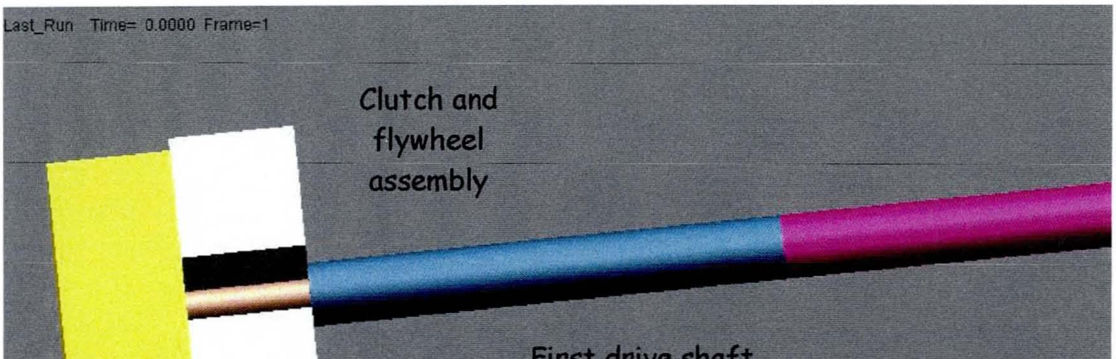

Figure 4.4 ADAMS representation of the flywheel and clutch and first driveshaft

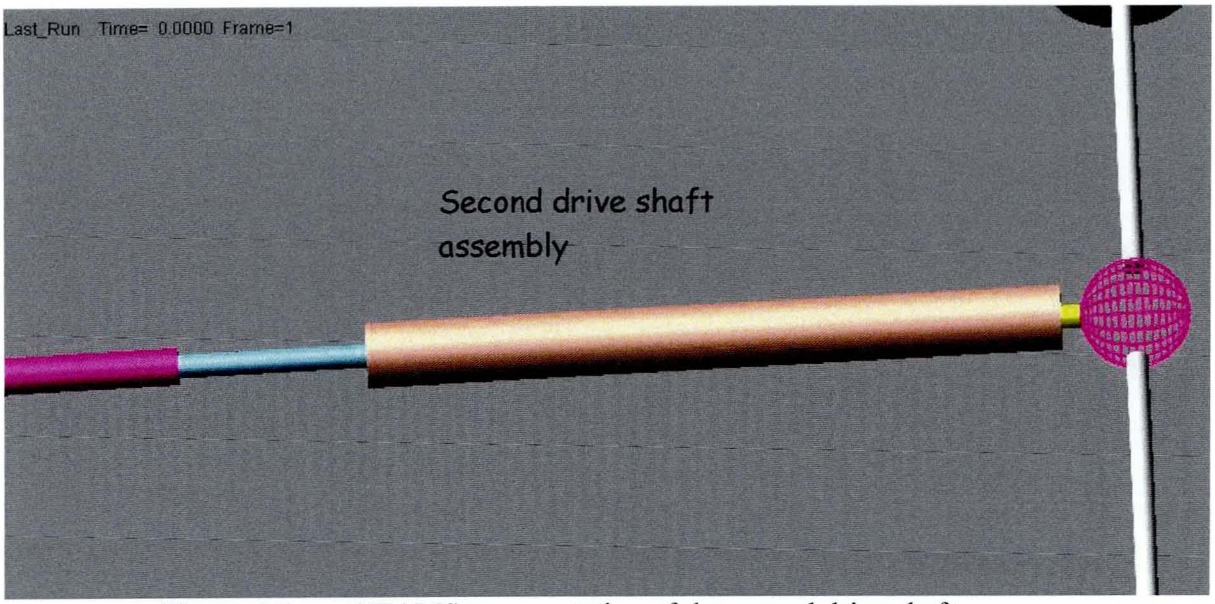

Figure 4.5 ADAMS representation of the second drive shaft

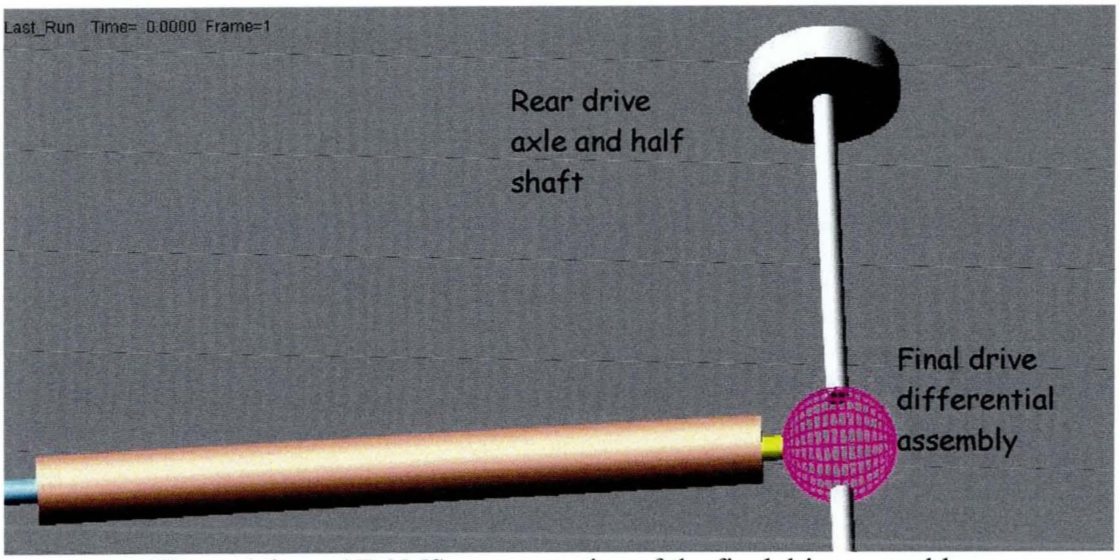

Figure 4.6 ADAMS representation of the final drive assembly

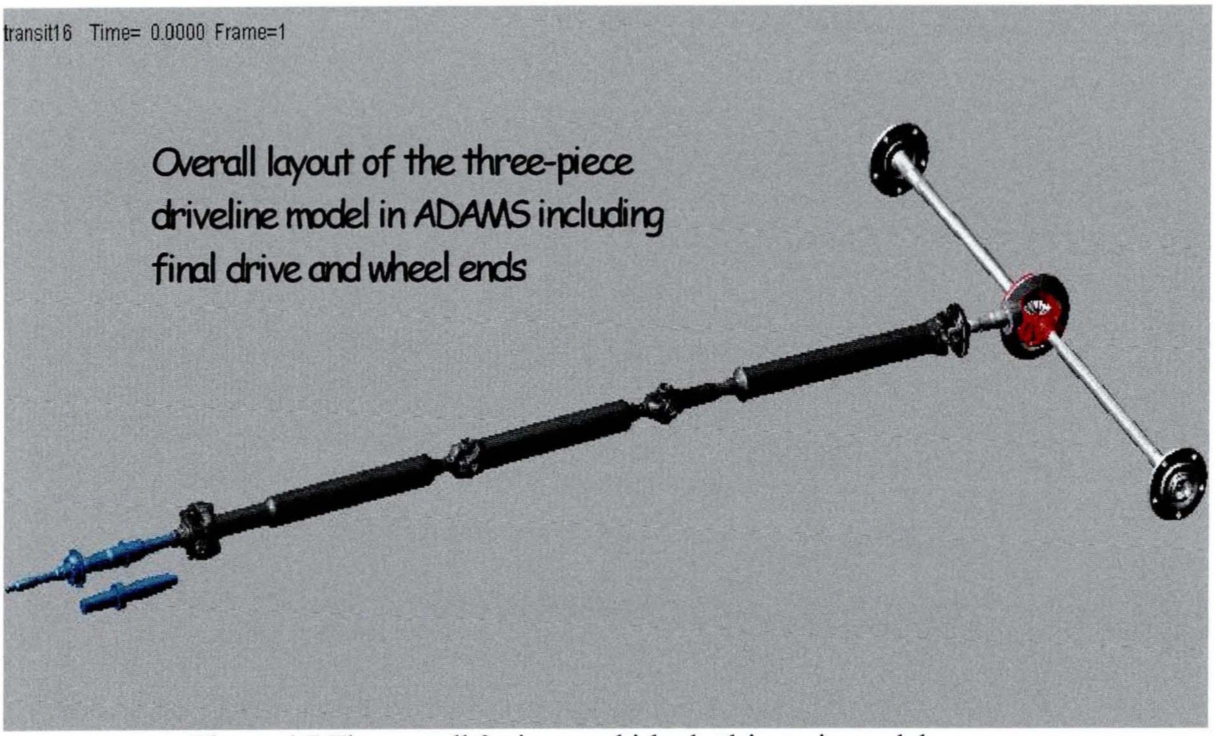

Figure 4.7 The overall 3-piece multi-body drivetrain model

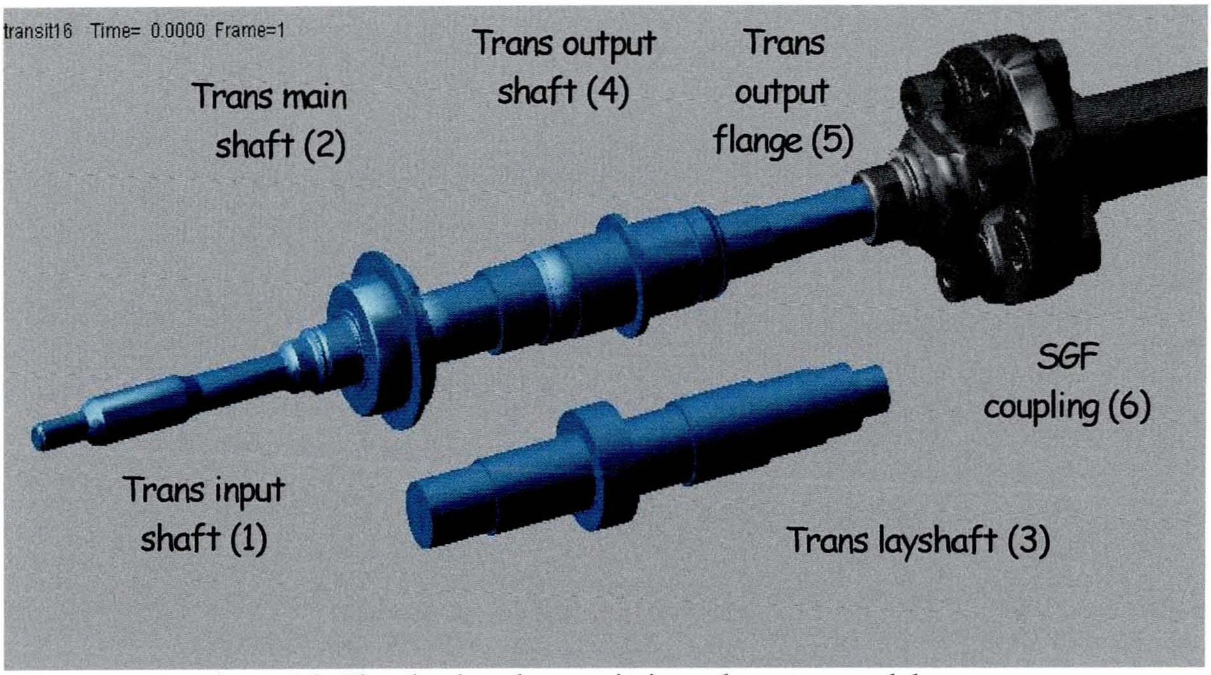

Figure 4.8: The clutch and transmission sub-system model

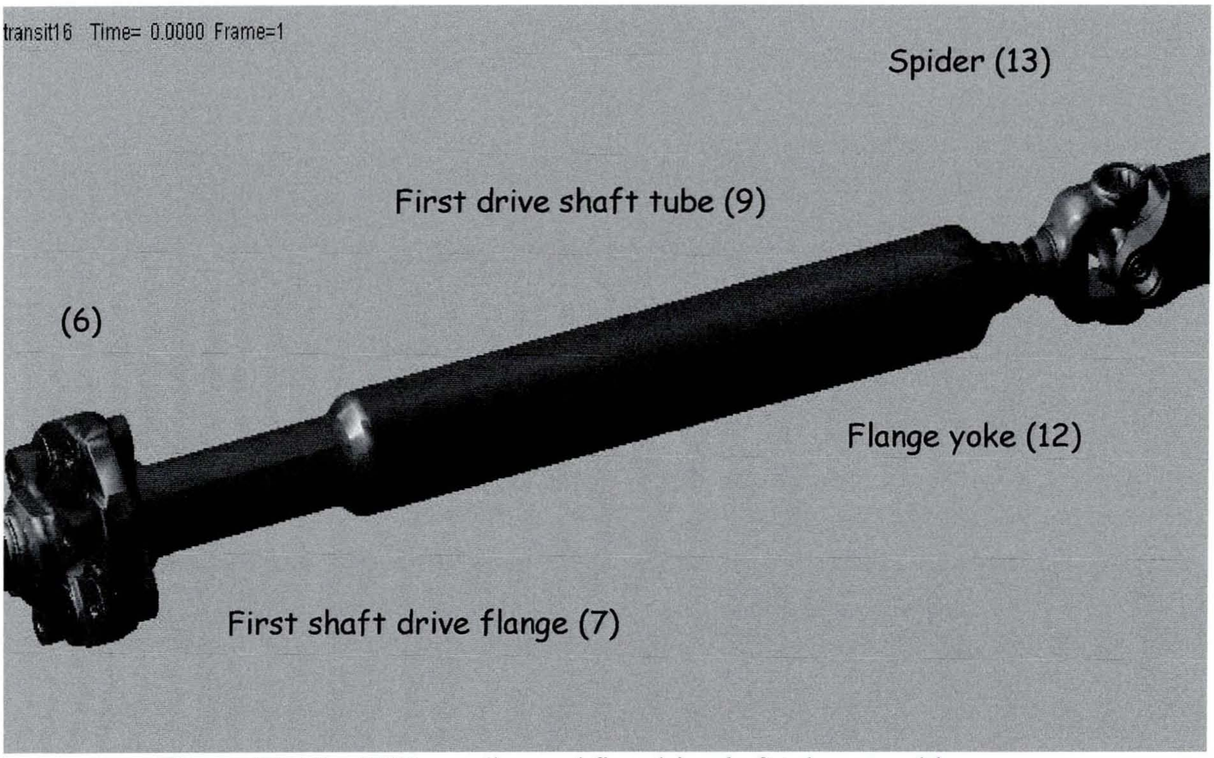

Figure 4.9: The SGF coupling and first driveshaft tube assembly

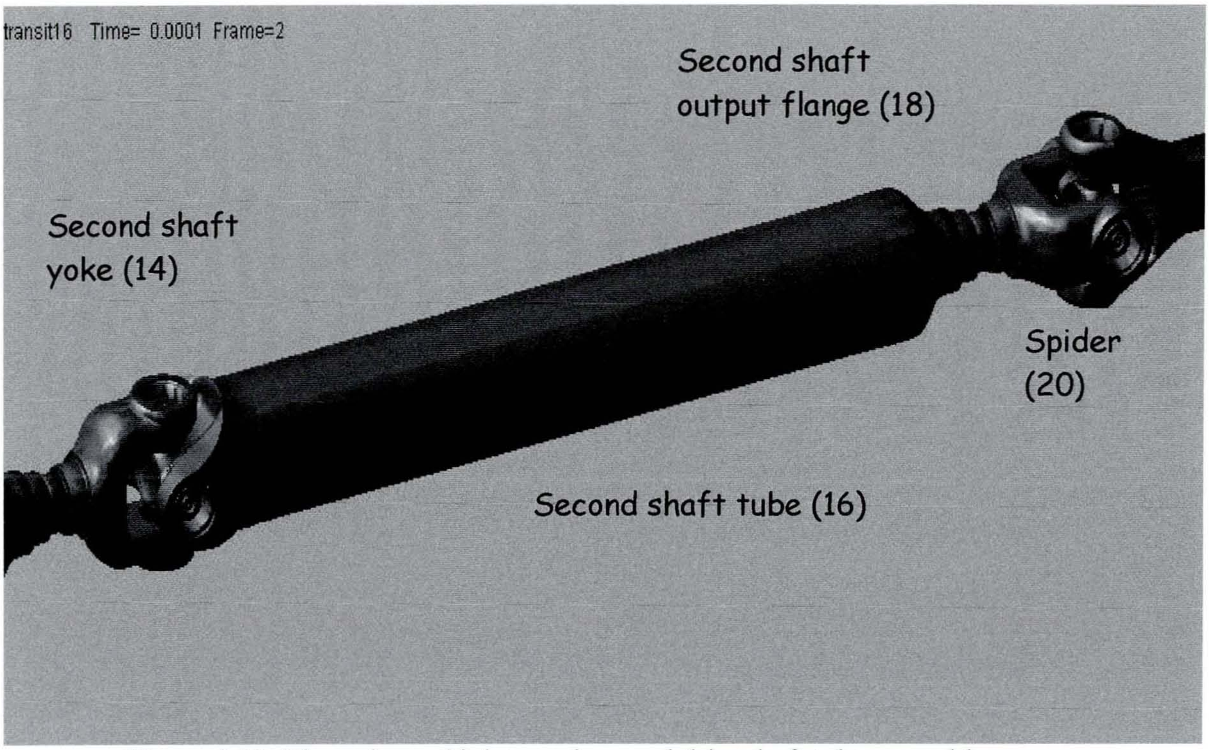

Figure 4.10: The universal joints and second driveshaft tube assembly

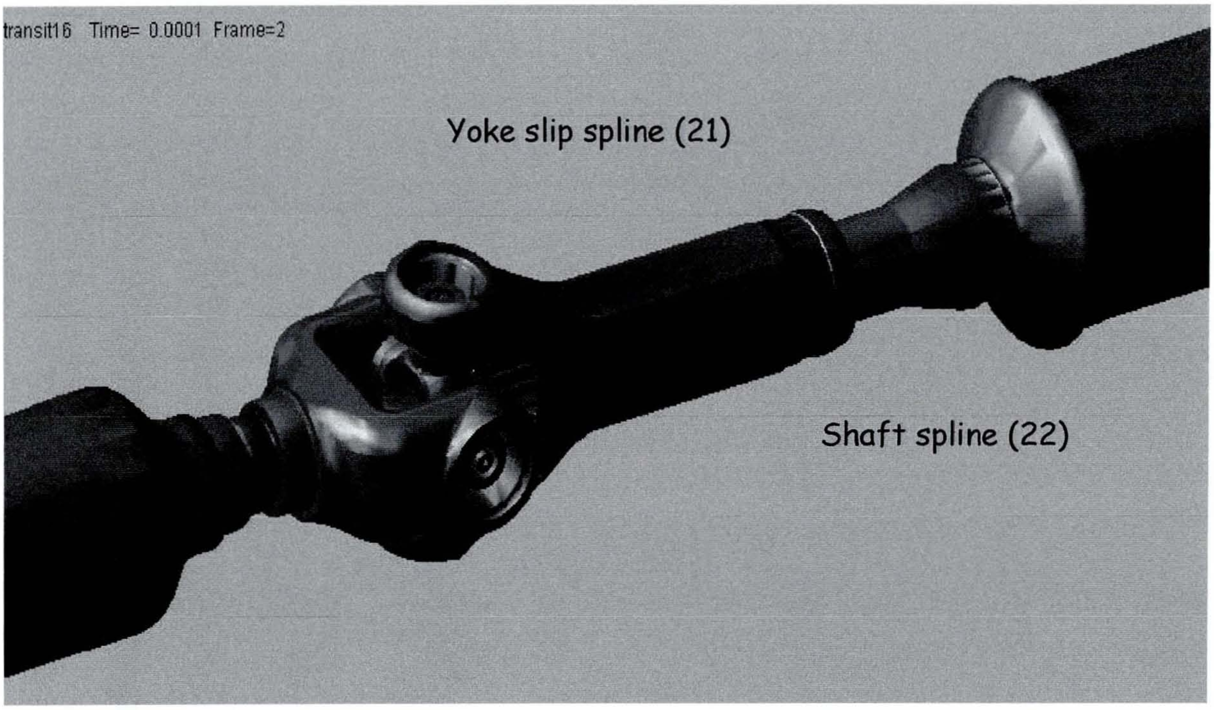

Figure 4.11: The universal joint and the spline joint in the driveline system

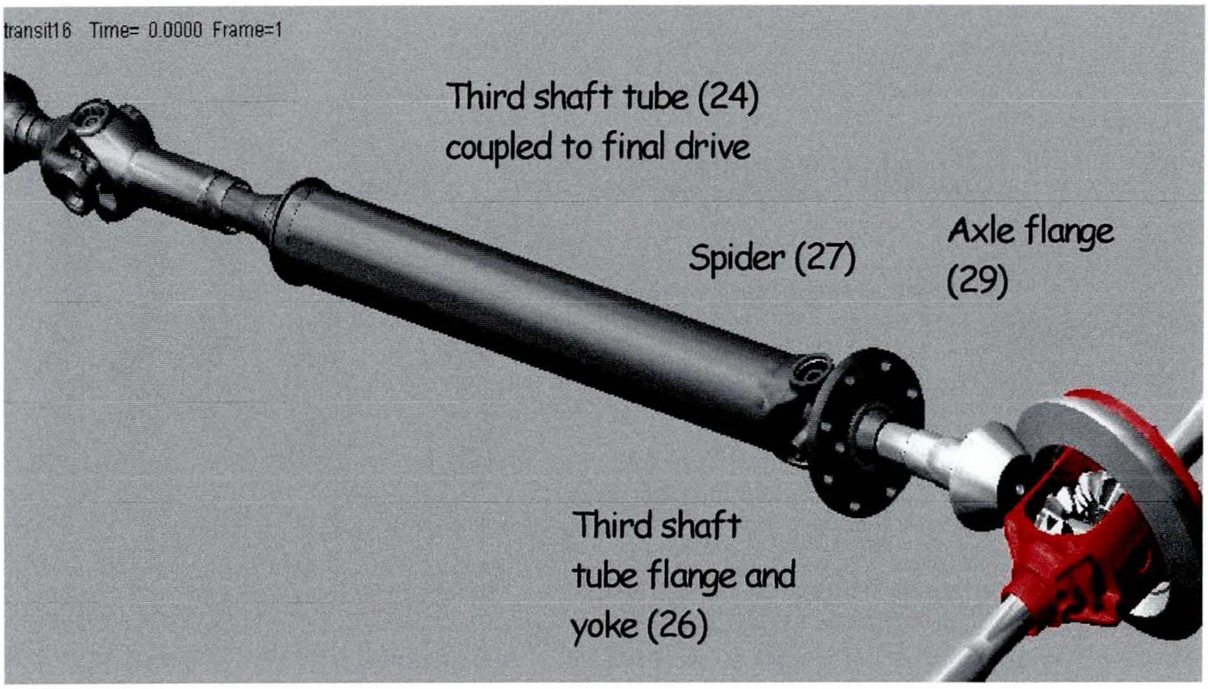

Figure 4.12: The rear driveshaft tube, pinion and differential subsystem

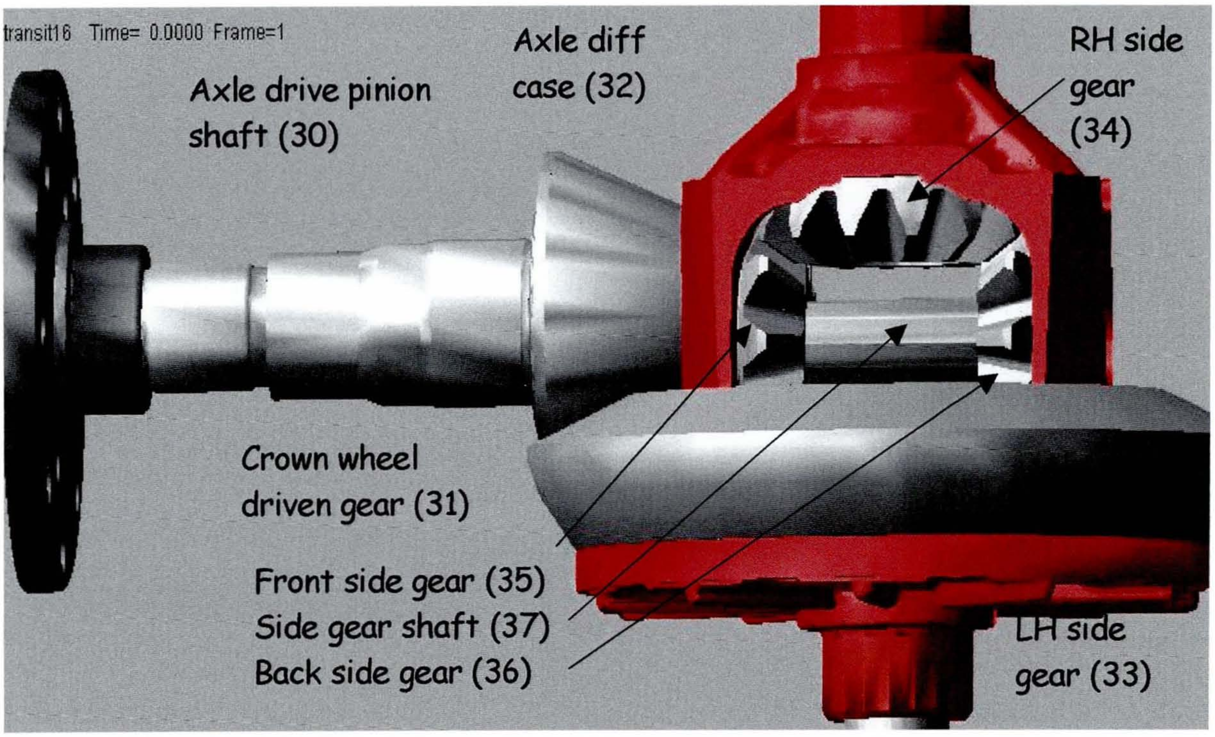

Figure 4.13: Pinion gear and differential system

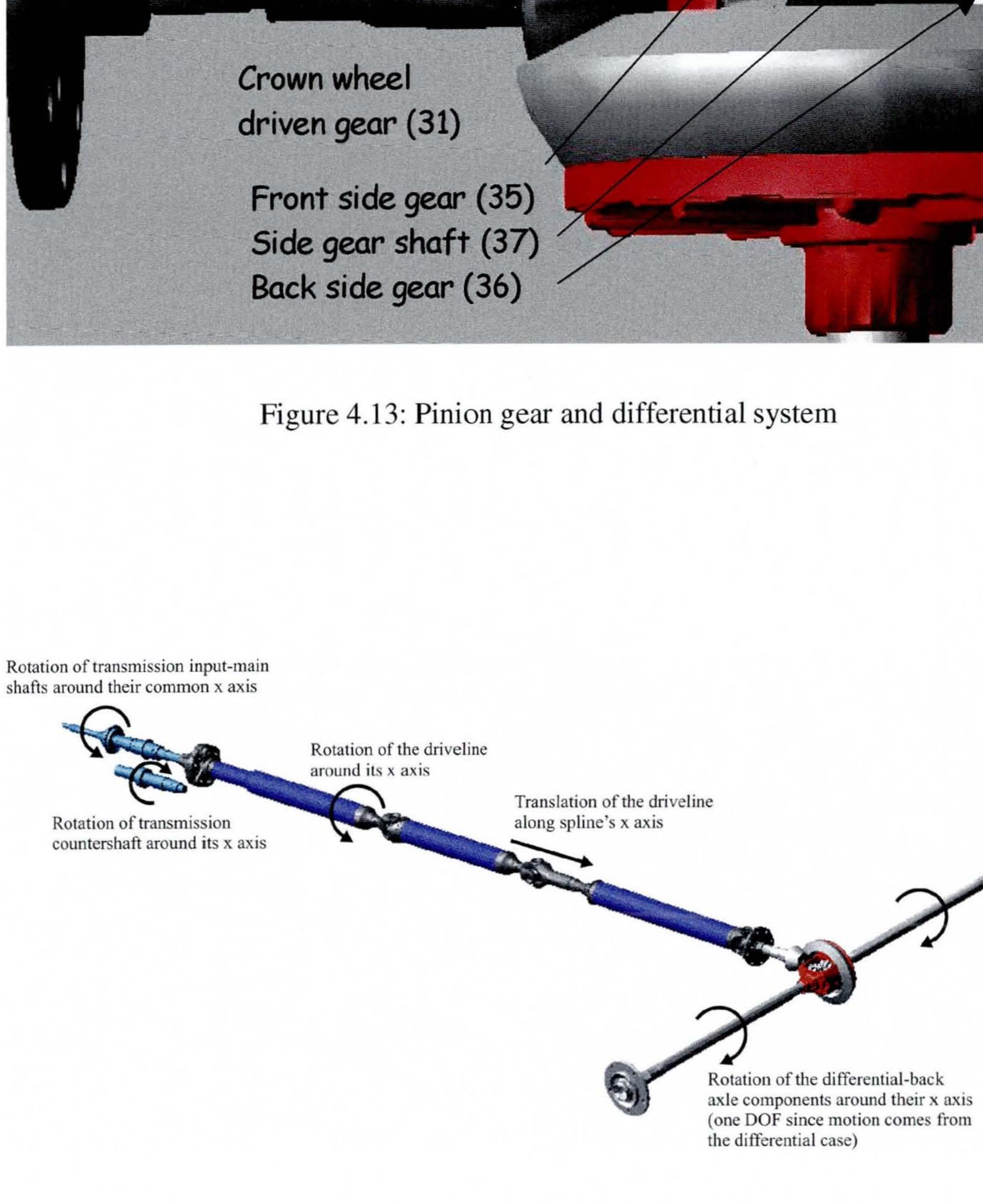

Figure 4.14: Three piece driveline simulation with 5 DOF.

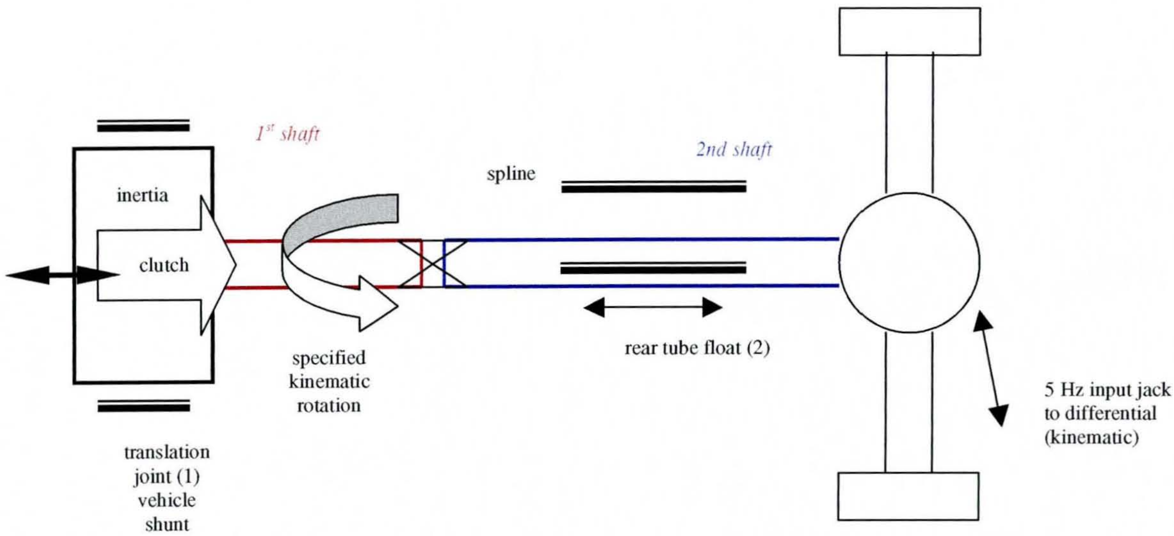

Figure 4.15: Two piece driveline schematic with 2 DOF.

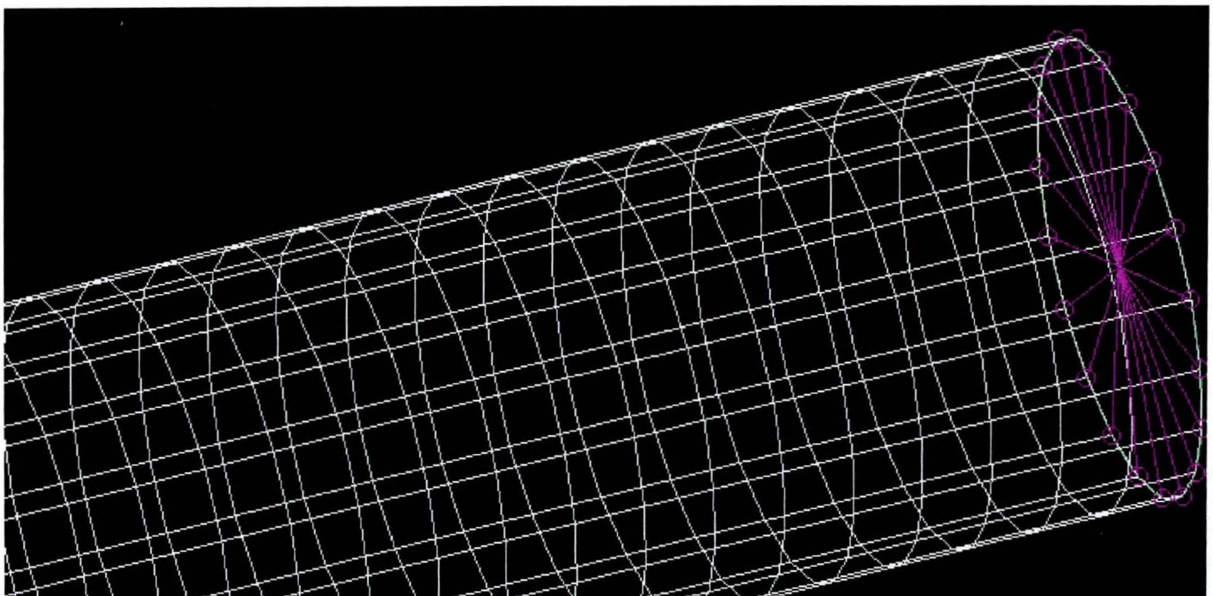

Figure 4.16: The computational mesh density for a hollow tube

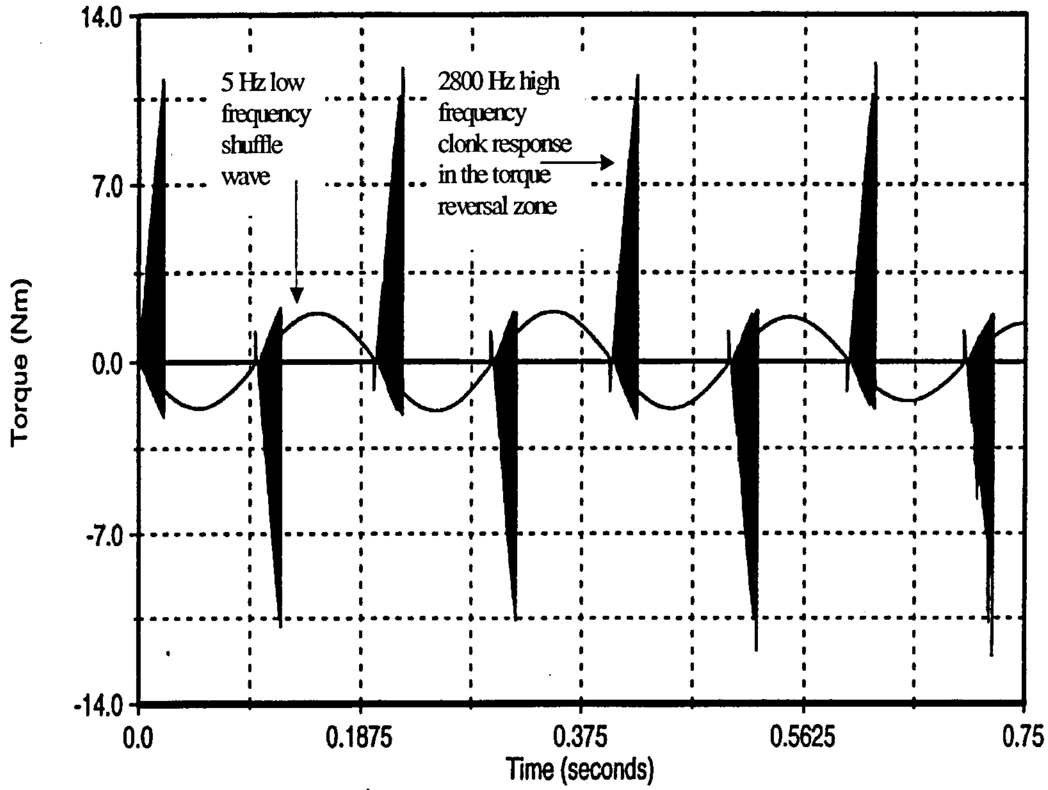

Figure 4.17: Showing high frequency clonk on low frequency shuffle.

CHAPTER 5

Elasto-acoustic coupling in the driveline.

5.1. Introduction to numerical analysis of driveline impact dynamics

Noise, vibration and harshness (NVH) are three important design issues in the automotive engineering quest for vehicle refinement to meet increasing customer expectations. NVH issues are compounded by the need to improve responsiveness through increased engine power and reduced body mass. Controlling and decreasing noise and vibration in vehicles is a difficult task for design engineers to accomplish. This is due to the existence of many noise and vibration sources and paths within the vehicle. One of them is the drivetrain system (flywheel, clutch, transmission, driveshafts and differential).

5.1.1. Clonk and impulse.

The absence of specific driveline clonk literature references meant that it was necessary to investigate the phenomenon of driveline impact in a non-specific way. It was necessary to consider the subject from first principles, to generate a plausible model of clonk, and then to apply available literature references and experimental verification, to the model that had been constructed.

The use of hollow, thin walled tubes adds to the NVH burden in the drive-train system. The following paragraphs provide some information regarding the noise mechanisms in these tubes and the efforts that are being made to connect them with the phenomenon of clonk.

Clonk is excited when a torsion impulse is supplied to the driveline in the presence of lash, and when the resulting impact energy is fed to any nearby lightly damped structure, which can then act as a loudspeaker.

Clonk is an audible high frequency response in a vehicular driveline system. As it gives an impression of bad quality to the vehicle passengers, it is a cause of concern to the automotive industry. Audible clonk is the result of metallic impact at several locations in the driveline, and in the presence of lash, it is also a matter of concern related to impact durability. The causes and the environments in which the clonk appears are summarised as follows:

- Clonk may occur with a rapid application of throttle from coast condition, or a rapid release of throttle from drive condition, especially in low gear and at low speeds when the concern is more audible.
- Clonk may be excited with rapid engagement /disengagement of the clutch.
- Clonk may occur in conjunction with a sudden torsion loading to the driveline that causes a low frequency longitudinal rocking motion in the vehicle, known as shuffle or shunt.
- Clonk may also be excited when a road input closes the driveline lash whilst the throttle is open.

Driveline clonk may be visualized as a series of almost coincidental impacts at each lash site along the driveline, when a torque is applied. The impact energies are fed into nearby elastic structures, which then emit radiated noise as a result of the wave propagation that follows the impact energy transfer. These events are shown in figure 5.1.

In this scheme, the inertias are separated in series by compliance. The scheme is not too dissimilar to the Newton Trolley or Cradle, where an external force impacts the first solid sphere and the final solid is accelerated away as a result of simultaneous force transfer through the chain.

The schematic shown above introduces the important driveline dynamics of the local elastic Hertzian impact conditions in the backlash zones, the sequential impacts that arise out of the multi-body compliant contacts, and the high frequency elasto-acoustic couplings between the impacted structures and their internal acoustic cavities.

The assumption of a time dependent series of impacts has been tested in the driveline rig (as described in the thesis) and shown to be true. It was also found that the incremental time gaps at each impact were not the same, due to the differences in compliance and inertia balances at each impact site.

The test data showed that local wave propagation was generated by the local impact, and the propagation was still in the development phase when the next impact in the chain occurred.

Clonk noise is radiated as a result of the wave propagation at each impact site, and each wave therefore makes an almost simultaneous but incremental contribution to the overall clonk phenomenon.

5.1.2 A brief historic review of impact.

The impact/contact of bodies plays an important role across the spectrum of dynamics problems, in engineering and physics. The kinetics (study of system force formulation) of the impact problem can be very complex indeed. The impact problem is related to the physical scale, the material properties of the bodies in impact, the duration of impact, the relative velocity at impact, and the medium in which such an impact takes place. These considerations determine the kinetics of the problem. Continuum mechanics is concerned with the motion of a large collection of particles in space and time, when they have been subjected to the forces that influence the motion.

The transition from free motion to a post impact condition is conceived through constrained multi-body dynamics, in which the unilateral constraint is envisaged as that imposed by the kinetics of impact as an impulse. This approach was initiated by Newton in the 17th Century and was perfected nearly a century later by Poisson (1781-1840). Newtonian impact assumed infinitely short contact times with infinitely large forces but with no deformation. In such an impact, the solution to the equations of motion must be undertaken in two distinct steps; firstly in free pre-impact motion to obtain the conditions prior to the infinitesimal impact time, and secondly for the post impact dynamics. The output of the first step acts as the initial condition for the second step and one should note that the second step should be regarded as an 'initial value' problem. The accelerated motion at the instant of impact gives rise to local body deformation, a fact that remained unaccounted for by both Newton and Poisson. This was realised in the 1880's by Hertz (1881,1896), who attributed local deformation effects to impacting ellipsoids of revolution. Of course the observations made with respect to the finite nature of the impact time is equally valid to any geometry of impacting region, but not necessarily within the Hertzian assumptions. The assumption of a unilateral constraint holds good, and the impact force operates over a finite impact duration (formulated by Hertz). The problem here is the severe non-linearity that is induced by the large impact force and the change in the "stiff" characteristics of the system equations. The deformation of solids in the Hertzian impact is considered to be local and in the domain of the contact, which is far smaller in size than the principal radii of curvature of contacting surfaces. In fact, Hertz developed his theory now referred to as the classical Hertzian contact theory, for the elastostatic concentrated *contact* of counterformal contiguous bodies and subjected to external forces, and not for the case of *impacting* solids. The Hertzian theory of contact was later extended for the case of impacts, in which he assumed no external forces were applied. He determined the contact pressures and the contact time as a function of the impacting velocity. In the Hertzian model the dissipation of impact energy and the resulting elastic wave motion in the impacting bodies is ignored. This assumption may not be considered as gross, when the solids of revolution have a *very small* contact area.

A good illustration of this assumption of nil energy dissipation is *Newton's trolley*, where the acoustic output of solid impacting spheres indicates that the dominant noise source is accelerative in nature. This is not true if the spheres in the trolley are hollow. The impact then gives rise to an elastic wave motion that is followed by a structural ringing noise of much longer duration than the accelerative noise. This phenomenon was of course realised by Helmholtz for hollow tubes, and even earlier by Daniel Bernoulli (1724) , Euler (1776) and D'Alembert in for strings (1761-1780). Such elastic contacts with a propagated elastic wave motion were indeed formulated by Saint-Venant for the general case of short duration impact. He assumed that the colliding bodies were elastic outside of the contact area during the contact time, and as a result high frequency low magnitude audible waves would propagate from the impact.

Therefore, one may consider two broad classes of impact problems in the engineering domain, if one is to ignore the idea of infinitesimally short Dirac type impact durations. These classes were proposed by Hertz in 1881 and Saint-Venant (1797-1886) and are associated with short contact times. This thesis considers these short contact times under localised conditions and localised deformation. Saint Venant proposed the high frequency wave propagation in elastic bodies that is associated with the driveline impacts particularly gear meshing.

By comparison, the highest energy is determined by the shortest impact time, according to the Hertzian proposal. The counterformal contact / impact of gear teeth due to the radii of curvature at the point of contact may be approximated by classical Hertzian elastic contact theory. This is justified later in 5.3.1.

5.2 Hertzian Contact Theory

Hertzian contact theory is based on the local elastic deformation of an ellipsoidal body indenting a semi-infinite elastic half-space under an external force. Viz, contact area <<body dimensions.

In the Hertz contact model, two elastic bodies are brought slowly into contact by the application of an external force. There is no lubricant between the surfaces in contact. The force is applied and released slowly, so that there is no loss of energy and there is a subsequent full recovery of elastic deformation. The force may be applied up to the elastic limit of either of the materials in contact. In the elastic regime, the materials are assumed to store the compression as mechanical energy (work done) with no energy dissipation. The theory does not apply in the plastic domain.

As the force is increased (within elastic bounds) the pressure at the centre of the contact patch is greater than that at the boundary. The pressure distribution and the elliptic contact patch must both be defined before a contact stress distribution may be evaluated. It is assumed that the elastic deformation is zero (for example, at the centre of gravity of the body) at a relatively large distance from the point of contact. Contact ellipticity occurs when the bodies in contact have different radii, the contact patch is circular for bodies with equal radii.

The force must be released at a rate that is slower than the natural frequency of vibration of either body. Hence, according to the Hertzian contact model, there will be no excitation of structural waves of vibration due to slow contact.

Once the applied force takes the material into the plastic region, the Hertzian contact assumptions no longer apply. Elastic energy losses are insignificant compared to plastic deformation losses.

When the applied forces are large enough to initiate plastic deformation, yielding will occur first in the material with the lower yield strength, and at a point in the material below the contact surface. The plastic zone will increase with the applied force and will then be surrounded by elastic material below the contact surface. Hence even after sub surface yield, deformation will be small in the elasto-plastic condition. Eventually with increasing load, the plastic region grows up to the surface and surrounds the contact zone, and the local condition is then said to be fully plastic.

The contact pressure distribution is semi-elliptical and has a maximum value at the origin equivalent to 1.5 times the average contact pressure in the contact zone.

In arriving at this classical theory, *On the contact of elastic solids* in 1881, Hertz made several assumptions. These are:

Assumption 1: The principal radii of curvature of the contiguous bodies in contact are considered to be large compared to the dimensions of the contact itself. When the contact dimensions are much smaller than the principal radii of the curvature, the elastic bodies in contact are referred to as semi-infinite elastic half-spaces.

The local contact area is elliptical in shape, with the eccentricity being determined by the relative magnitudes of the contacting curvatures.

Figure 5.2 shows the principal radii of a pair of bodies of revolution in counterformal contact. The counterformal contact refers to the low degree of conformity (contiguity) of the undeformed profile of bodies in contact. This applies to many engineering load bearing surfaces such as balls or rolling elements-to-raceway contacts, cam-follower pair and indeed the meshing of gears. In the case of helical gears, such as those in vehicular transmission, these achieve a better degree of conformity. Conformity increases the area of contact and reduces the contact stresses. Therefore, the use of classical theory becomes approximate, since the contiguous surfaces may not be strictly regarded as semi-infinite. The semi-infinite assumption also means that the local deformation of the solids is much smaller compared with their thickness or depth. This is of course true of local deformation of mating gear teeth, even under high loads.

The assumption that the loads are carried and transmitted through a very small contact area means that contact stresses and local deformations are invariably very high. This leads to premature component failure due to overloading, seizure, fatigue, fretting, and wear.

Assumption 2: The surfaces of the contacting members are assumed to be smooth and elastic, thus the contact condition is frictionless. Hence the transmitted forces are normal to the contact surface since there are no frictional forces induced between the smooth bodies in contact. This is not the case in practice as surface undulations always exist and can in certain circumstances, assist in reducing wear of contiguous members under lubricated conditions (as briefly described later). Hertz does not consider the sliding and rolling contact conditions.

Assumption 3: The deformation of the bodies is within their elastic limits (i.e. the strain must be within the elastic limits) and it may be calculated by treating the problem as a sphere contacting an elastic flat half-space.

The gap h (or the clearance caused by the deformed profiles) between the undeformed surfaces may be approximated by an expression of the form:

$$h = Ax^2 + By^2 \tag{5.1}$$

which defines the geometric profile of spheres, cylinders and ellipsoids prior to contact.

Hertz (1881, 1896) gives the expressions for maximum elastic deformation, maximum contact force, maximum contact width, and maximum contact pressure. He was able to very neatly combine these variables with the applied load, the geometry, and the elastic modulus.

5.3 Hertzian impact theory

Thus far, the Hertzian contact model is assumed to be an extremely slow quasi-static loading process due to external forces.

By contrast, under Hertzian *impact* loading one needs to consider extremely fast loading rates, as well as the associated dynamic effects. There are no externally applied forces, only those inter-body forces that arise from impact. Elastic deformation between the impacting bodies is assumed to be localized. In fact, it is assumed that under dry impact conditions the deflection between solid bodies is wholly taken up in a fictitious non-linear *Hertzian spring.*

From the Theory of Elasticity by Timoshenko and Goodier (1934), one may consider two elastic spheres of masses m_1 and m_2 approach the other with velocities v_1 and v_2 and impact at O with a compressive force F

Applying Newton's 2nd law of motion to each mass in turn,

$$-F = m_2 \frac{dv_2}{dt} \text{ and } -F = m_1 \frac{dv_1}{dt} \tag{5.2}$$

Consider a local elastic Hertzian depression of δ at O due to the impact.

Let $\dot{\delta} = v_1 + v_2$ is the relative velocity just before impact.

Substituting from the above: $\ddot{\delta} = -F\dfrac{m_1 + m_2}{m_1 m_2}$ where: $F = k\delta^{3/2}$

$\therefore \ddot{\delta} = -k\delta^{3/2}$

Multiply both sides by $\dot{\delta}$

$$\therefore \frac{1}{2} d(\dot{\delta})^2 = -k\delta^{3/2}.d\delta \tag{5.3}$$

By integration:

$\frac{1}{2}(\dot{\delta}^2 - v^2) = -\frac{2}{5}k\delta^{5/2}$ where v=velocity of approach at start of impact

Now substitute: $\dot{\delta} = 0$ in this equation, then $\delta_1 = \frac{5}{4}\left[\frac{v^2}{k}\right]^{2/5}$ (5.4)

Thus: $dt = \dfrac{d\delta}{\sqrt{v^2 - \frac{4}{5}k\delta^{5/2}}}$ (5.5)

And: $dt = \dfrac{\delta}{v}\dfrac{dx}{\sqrt{1-x^{5/2}}}$ (5.6)

Therefore: $t = \dfrac{2\delta}{v}\displaystyle\int_0^1 \dfrac{dx}{\sqrt{1-x^{5/2}}}$ which is resolved to $t = \dfrac{2.94328\delta}{v}$ (5.7)

This is the contact time for two elastic spheres of same material and dimensions. In this case the contact duration time is proportional to the elastic deflection and inversely proportional to the velocity of approach.

Using back substitution, $t = 2.87(m^2/RE^{*2}v)^{1/5}$ (5.8)

Where: $1/m = (1/m_1 + 1/m_2)$

And: $1/E^* = (1 - \nu_1^2)/E_1 + (1 - \nu_2^2)/E_2$

$1/R = 1/R_1 + 1/R_2$, v = velocity of approach $(v_2 - v_1)_{t=0}$

For the case of impacting spheres, the time of contact is very long compared to the lowest mode of vibration of the spheres (subject to elastic properties) and after elastic compression the impacting bodies regain their original shapes. Hence, under these conditions local wave propagation may be ignored.

In summary the salient expressions for classical Hertzian elastic impact for circular point contacts under a contact force F are given below (from Johnson, 1985):

Maximum elastic deformation:
$$\delta^* = \left(\frac{15mv^2}{8\sqrt{R}E^*} \right)^{2/5} \quad (5.9)$$

Maximum generated contact force:
$$F_{max} = \frac{2}{3}\sqrt{R}E^*\left(\delta^*\right)^{3/2} \quad (5.10)$$

Semi-contact width (radius)
$$b_{max} = \left(\frac{3}{2} \frac{F_{max} R}{E^*} \right)^{1/3} \quad (5.11)$$

Maximum contact pressure:
$$P_{max} = \frac{3}{2} \frac{F_{max}}{\pi b_{max}^2} \quad (5.12)$$

Total impact time:
$$T_{max} = 2.94\frac{\delta^*}{v}, \text{ where } \delta^* = \left(\frac{15mv^2}{8\sqrt{R}E^*} \right)^{2/5} \quad (5.13)$$

Hertz (1881,1896) obtained the above expressions analytically, using the principle of conservation of momentum for an elastic impact. The kinetic energy of a falling sphere transforms to strain energy without any losses. Under lubricated impact dynamic conditions, such as the impact loading of meshing gears, some of the energy is lost due to the viscous shearing of the fluid and some in the form of heat due to tractive action. Therefore, the principle of conservation of momentum does not hold for this inelastic impact.

The Hertzian impact dynamic model described above is incorporated into the multi-body model of the drivetrain system in order to generate the impact loads that occur, when the drivetrain system is subjected to sudden torsional oscillations.

It is found that the impact time for *dry* contact increases in the presence of a lubricant due to viscous resistance of the fluid film, whilst the depth of penetration also increases. The impact load is higher in the case of lubricated impact, but because of the viscous losses the energy transferred to elastic wave propagation is decreased. Therefore, the dry impact energy condition represents the worst-case scenario in terms of energy conversion to wave propagation, and thus the reason for its implementation in this thesis. Furthermore, the study of lubricated impact dynamics is a fundamental subject in its own merit, and a significant body of literature already exists. These include elastohydrodynamic impact analysis by Dowson and Wang (1994), Larsson and Hoglund (1995, 1996) and Al-Samieh and Rahnejat (2002). Experimental verification for the above observations were made in a pioneering experiment using miniature micro-transducers by Safa and Gohar (1986).

The above equations are useful in determining the size of the computation domain, in evaluating the magnitude of the pressures likely to be achieved during the impact, and in the normalization of the governing equations in numerical calculation as shown by Dowson and Wang (1994). They also enable interesting comparisons to be made between the results of both dry and lubricated impact conditions, when compared with numerical lubricated contact dynamic results, see for example Dowson and Wang (1994).

5.3.1. A brief introduction to modal analysis

As a very brief introduction to modal analysis, one must start with Galileo 1564-1642 who set out the relationships between vibration, pitch and sound. Even earlier, Pythagoras 582-507 BC had identified the relationship between string length and tone. Sauveur 1653-1716 identified the fundamental wave frequency for a string and the succeeding harmonics. It was clear that a discretised string would have an infinite number of degrees of freedom with an infinite number of natural frequencies. Bernoulli 1700-1782 first proposed the principle of linear superposition of harmonics, that for any string configuration of free vibration the mode shape was made up of modal harmonics acting on it. In 1822 Fourier published the doctrine of harmonic analysis, a principle of superposition that could also be applied to plates and structures. The subject of vibrating strings led to the wave equation, which was expressed as a differential equation of partial derivatives.

In 1676 Hooke's law of elasticity enabled the wave equation for strings and acoustics, to be applied to the study of structural vibration of beams. Euler initiated the analysis of such wave motions in 1744. Von Helmholtz and his assistant Heinrich Hertz expanded the theories for other thin walled structures and membranes. Lord Rayleigh addressed the problem, and the solution methodology is known today as Rayleigh's method.

In more modern times the Bernoulli principle of superposition and Brooke Taylor's discretisation methods in 1713 such as Taylor series, have resulted in the use of finite element analysis in elasto-acoustic investigations. In this thesis, finite element and boundary element analysis are employed to study elastic wave motion and sound pressure radiation of thin walled structures.

The result of the pioneering work on waves, vibration, and harmonic analysis, has been the emergence of modal or eigenvector analysis, and the necessary use of matrix structural analysis.

The application of this theoretical background is the post impact dynamics in the drivetrain system when an impact has been applied, and the resulting propagation of elastic waves along the structural elements of the system such as the driveshaft tubes even after the impact has subsided.

5.3.2. St Venant theory and implications for driveline clonk analysis

St Venant's postulation in 1855 dealt with the effects of applied forces on the equilibrium of an elastic body. He stated that if a balanced system of forces was applied to any part of a body it would induce stresses in the body that would very rapidly diminish with distance from the point of application.

In other words, the stress field in a body at a sufficient distance from the applied force system is insignificantly affected by the method of force application. He considered a force is applied to a small surface area that is insignificant compared to the overall body dimensions. Furthermore, he stated that provided the resultant force system is statically equivalent then there would be no significant change to the stress field remote from the force system.

This thesis considers wave propagation resulting from impact zones in the driveline. Some of the zones are free of lubrication, but some are grease packed, and some are oil filled. Each impact site therefore has its own force characteristic. If one considers lubricated transient impact then we must apply elastohydrodynamic (EHL) analysis. However, this would involve the simultaneous solution of elasticity and Reynolds equations for time increments of normal impact, and this would be a major theoretical consideration. Alternatively, one may consider wave propagation from non-lubricated impact sites and applying the Hertz and St Venant models of impact, thereby avoiding EHL considerations.

One may, therefore, compare Hertzian type impacts and St Venant conditions, to test if driveline impact causes local (Hertz) or global (St Venant) wave distortion, and then to justify if the forces of dry impact are so high that it represents the worst-case for wave propagation. In addition we need to test if the impact pulse is synchronized with the local structural natural period of vibration.

With consideration of the Hertz relationship: $T_{max} = 2.94\frac{\delta^*}{v}$ for contact time, it has been shown by several authors that for a lubricated contact, the local elastic deformation increases and the relative velocity at impact decreases due to viscous shearing. As a result the overall effect due to lubrication is that the contact time increases and energy levels are reduced. Hence, the thesis considers the 'worst-case' scenario by ignoring the EHL contact condition. Additionally, the frequency spectrum for increased (lubricated) contact time will have a smaller effect on clonk excitation.

5.3.3. Inclusion of impact simulation in the multi-body model

As mentioned earlier, the Hertzian dynamic impact model was incorporated into the multi-body simulation of the drive train system in order to generate the impact loads that occur, when the drivetrain system is subjected to sudden torsional impulse.

Gear mechanisms have affected the dynamics and torsional behaviour of geared systems in a significant way. As a consequence, research in the area of dynamics of mechanical systems involving gear mechanisms has been intensive, especially over the last forty years. However, in the presence of gear backlash, which is either introduced intentionally at the design stage or caused by manufacturing errors and wear, the equations of motion of such systems become strongly nonlinear. Another important complication arises from the variable number of gear teeth pairs that are in contact at a time, causing a variation of the equivalent gear meshing stiffness. These two significant non-linearities introduce serious difficulties in the analysis and may obscure the interpretation of the numerical results.

The dynamics of a gear-pair system involving backlash and time-dependent mesh stiffness are investigated by the use of piecewise linear equations of motion with time-periodic coefficients and external forcing. In particular, this forcing is generated by either torsion moments or by errors in gear geometry. The centres of both gears are not allowed to move laterally. The stiffness of the gear mesh model depends on the number and position of the gear teeth pairs, which are in contact, and is a periodic function of the relative angular position of the gears. The model also takes into account the so-called transmission error, which represents geometrical errors of the teeth profile and spacing. Since the mean angular velocities of the gears are constant, both the stiffness and the static transmission error quantities can be assumed to be time-periodic functions. In addition, if the tooth-to-tooth variation (i.e. pitch errors and run out of teeth) is neglected, the fundamental frequency of both of these quantities equals the gear meshing frequency: $$\omega_M = n_1\omega_1 = n_2\omega_2 \qquad (5.14)$$

where the integers n_1 and n_2 stand for the teeth number of each gear. This implies that the meshing stiffness $k(t)$ and the static transmission error $e(t)$ terms can be expressed in a Fourier series form. For instance, the model stiffness can be expressed in the following form:

$$k(t) = k_0 + \sum_{s=1}^{\infty}[p_s \cos(s\omega_M t) + q_s \sin(s\omega_M t)] \tag{5.15}$$

The force developed between the pair of gears in contact is given by the product $k(t)h(x)$

where, $x(t) = R_1\varphi_1(t) - R_2\varphi_2(t) - e(t)$ (5.16)

R_1 and R_2 represent the contact point radii of the gears,

$\varphi_1(t)$ and $\varphi_2(t)$ are the two torsional coordinates (rotation angles of the gears)

and $h(x) = \begin{cases} x-b, & x \geq b \\ 0, & |x| < b \\ x+b, & x \leq -b \end{cases}$, where $2b$ represents the total backlash (5.17)

5.4 Elastodynamics

Here, the elastic/flexible component behaviour of a multi-body system is considered, which is subjected to a dynamic set of conditions that is induced by impact. There are several approaches that can be undertaken. They include lumped-mass modeling techniques, making use of point mass/inertial elements, interspersed with Euler/Bernoulli type beams. The approach is referred to as transfer matrix method. Alternatively, non-linear stiffness matrices may be specified due to elastic members, such as in dynamic stiffness matrix method.

Finite element analysis is a more comprehensive approach, including the effect of various modal characteristics. Selected range of modes can be used for the spectrum of interest, using component mode synthesis. To reduce the size of matrices, the initial finite element models of flexible members make use of *super-elements*, described later on. The alternative approach is boundary element method, which is quite suitable for elastic, as well as acoustic studies. This approach is also applied in this thesis to obtain modes of cavities.

5.4.1- Beam Elements for Flexible Dynamics

The first step for inclusion of elasticity of flexible members in a multi-body system is through Bernoulli-Euler type beams. In such a case, the thin hollow driveshaft pieces may be represented as distributed elements, comprising point mass/inertial members and interconnected by a three-dimensional elastic field element. The latter appears as a combination of field element stiffness and damping matrices. The field element matrices provide the forces/moments at a marker i due to a relative displacement at a marker j, these representing the positions of the lumped inertial elements. The three-dimensional field element requires an initial alignment of the two markers, having a co-directed x-axis. Thus:

$$\begin{bmatrix} F_x \\ F_y \\ F_z \\ T_x \\ T_y \\ T_z \end{bmatrix} = \begin{bmatrix} \frac{EA}{L} & 0 & 0 & 0 & 0 & 0 \\ 0 & \frac{12EI_{zz}}{L^3} & 0 & 0 & 0 & \frac{-6EI_{zz}}{L^2} \\ 0 & 0 & \frac{12EI_{yy}}{L^3} & 0 & \frac{6EI_{yy}}{L^2} & 0 \\ 0 & 0 & 0 & \frac{GI_{xx}}{L} & 0 & 0 \\ 0 & 0 & \frac{6EI_{yy}}{L^2} & 0 & \frac{4EI_{yy}}{L} & 0 \\ 0 & \frac{-6EI_{zz}}{L^2} & 0 & 0 & 0 & \frac{4EI_{zz}}{L} \end{bmatrix} \begin{bmatrix} x-L \\ y \\ z \\ \theta \\ \phi \\ \psi \end{bmatrix} - [D] \begin{bmatrix} \dot{x} \\ \dot{y} \\ \dot{z} \\ \dot{\theta} \\ \dot{\phi} \\ \dot{\psi} \end{bmatrix} \tag{5.18}$$

where: $[D]$ is the structural damping matrix, the elements of which are taken to be 1%-5% of the stiffness matrix.

The problem with this approach is that a flexible part may have to be discretised into many lumped masses, interspersed by such beam elements in order to obtain the higher frequency responses. Although the approach can lead to the evaluation of such modal contributions, the amplitudes at higher modes cannot be relied upon.

The result of the integration of a flexible rear tube in a two-tube configuration with a multi-body model is described later.

5.4.2- Elastodynamics through Super-Element Modal Analysis

Finite element analysis is employed in this thesis to introduce component flexibility into the multi-body dynamics model of the drive train system. By comparison, multi-body dynamics theory is valid for constrained rigid body interaction. The combined analysis is referred to as elasto-multi-body dynamics or simply as *elastodynamics*. The multi-body component is essential in order to provide the dynamic loads that the flexible structures are subjected to, and then analysed by the use of finite elements. This approach allows the investigation of small high frequency displacements of elastic members relative to a local frame of reference, whilst at the same time the local reference frame is subjected to a lower frequency larger displacement global motion.

5.4.3. The Finite Element Method

The use of FEA has the following advantages:

FEA increases the fidelity of the multi-body dynamics model.
The realistic loads - initial conditions that are required for an analysis in the FEA domain may be obtained in a natural way by incorporating the flexible structures inside the multi-body model, prior to detailed simulation studies.

The input and output shafts of the transmission, the driveshaft pieces (front, middle and rear tubes) and the rear axle half-shafts, are major components of the driveline which behave in a flexible manner. By incorporating FEM models instead of rigid bodies for the representation of these components, it is feasible to determine the principal stresses that are generated during the simulation exercise. Furthermore, the initial conditions of the driveshafts (displacements, velocities etc.) that are required in an acoustic analysis may be extracted which enables the determination of the acoustic sound pressure field both within and external to each tube.

5.4.4. Component Mode Synthesis (Elastic modal analysis)

Finite element and finite difference methods are often used in structural dynamic analysis. In this methods, the structure is divided into a number of elements, which are defined by nodes. The elements are in the form of prescribed shape functions. An equation of motion is applied to each and every node in the final mesh, and every node will have three degrees of freedom DOF so a very large matrix equation will be necessary to represent the structure, with a correspondingly large computation time.

The matrix equation must be solved and as many structural eigenvalues (modes) will then be found, in line with the same number of nodes in the structure.

The process is tedious, if a time dependent solution is required for any node in the structure. If a solution in the high frequency domain is required then a high nodal mesh density will be needed. In addition, it is often the case that a solution in a frequency band is required, and the finite element method is not suitable for this. Hence, for these reasons, finite element computational times will be high, and it will be seen that the method is not suitable for the high frequency clonk investigations.

Here, the concept of Component Mode Synthesis (CMS) is introduced. This method of analysis greatly reduces the computational time by using a model reduction technique, and it is more efficient.

CMS uses a linear combination of shape functions to represent a complex structure, by reducing the structure to an assembly of functional components. CMS uses a much smaller set of functional equations than that needed for a finite element simulation.

The application of *superelements* in structural analysis to replace the more conventional finite element model approach has dramatically reduced computation effort without a significant loss of accuracy. A *superelement* is a component made up of many finite elements and comprises inner degrees of freedom DOF and boundary DOF's. The forces at the interior DOF's are set to zero, the boundary DOF's are located at the attachment points of the *superelement*. The *superelement* has a reduced number of behavioural DOF, which allows the computation improvement.

It is important that suitable shape functions are chosen to represent the characteristic dynamic behaviour of the structure under consideration.

The most important assumption behind the FEA procedure is the consideration of small, linear body deformations relative to a local reference frame, whilst it is undergoing large, non-linear global motion. The discretization of a part into a finite element model attempts to represent an infinite number of degrees of freedom, albeit with a very large number of finite element degrees of freedom. The linear deformations of the nodes of a finite element mode u, may be approximated as a linear combination of a smaller number of shape vectors (or mode shapes) ϕ,

$$u = \sum_{i=1}^{M} \phi_i q_i \qquad (5.19)$$

where M is the number of mode shapes. The scale factors of amplitudes, q, are the modal coordinates.

The main concept of ***modal superposition*** (as originally expounded by Bernoulli) is that the behaviour of a component with a very large number of nodal degrees of freedom (NOF) can be captured with a much smaller number of modal degrees of freedom (DOF). Thus, the finite element modes can be rewritten in the matrix form as:

$$u = \Phi q \qquad (5.20)$$

where q is the vector of modal coordinates and the modes ϕ_i are included in the columns of the modal matrix, Φ. This matrix is the transformation from the small set of modal coordinates, q, to the larger set of physical coordinates, u.

The determination of the modal shape matrix M can be achieved by the *Craig-Brampton* method, which is one of the most general methods of CMS techniques. The summary of this method is described as follows.

- A set of *boundary* degrees of freedom (u_B) is defined, which is not to be subject to modal superposition and is preserved exactly in the modal basis.
- A set of *interior* degrees of freedom (u_I) is defined.

Additionally, two sets of mode shapes are defined, as follows:

- The *constraint modes* (q_C) are static shapes that are obtained by giving each of the boundary degrees of freedom a unit displacement, while holding all other boundary degrees of freedom fixed. There is a one-to-one correspondence between the modal coordinates of the constraint modes and the displacement in the corresponding boundary degrees of freedom, $q_C = u_B$.
- The *fixed boundary normal modes* (q_N), which are obtained by fixing the boundary degrees of freedom and computing a solution of the eigenvalue problem. These modes define the modal expansion of the interior degrees of freedom. The quality of this expansion is proportional to the total number of modes.

According to the aforementioned, the relationship between the physical degrees of freedom, the Craig Brampton modes, and their modal coordinates is expressed as

$$u = \begin{pmatrix} u_B \\ u_I \end{pmatrix} = \begin{pmatrix} I & 0 \\ \Phi_{IC} & \Phi_{IN} \end{pmatrix} \begin{pmatrix} q_C \\ q_N \end{pmatrix} \qquad (5.21)$$

where

$I, 0$ are the unity and zero matrices respectively

Φ_{IC} are the physical displacements of the interior degrees of freedom in the constraint modes, and

Φ_{IN} are the physical displacements of the interior degrees of freedom in the normal modes.

The generalized stiffness and mass matrices are obtained through the following transformations:

$$\hat{K} = \Phi^T K \Phi = \begin{pmatrix} \hat{K}_{CC} & 0 \\ 0 & \hat{K}_{NN} \end{pmatrix}, \qquad \hat{M} = \Phi^T M \Phi = \begin{pmatrix} \hat{M}_{CC} & 0 \\ 0 & \hat{M}_{NN} \end{pmatrix}$$

where $\hat{M}_{NN}$, $\hat{K}_{NN}$ are diagonal matrices, and $\hat{K}$ is a block diagonal.

Since the Craig-Brampton modes are not an orthogonal set of modes, a mode shape ortho-normalization procedure is applied. By solving the eigenvalue problem,

$$\hat{K}q = \lambda \hat{M} q$$

the obtained eigenvectors are arranged in a transformation matrix N, that transforms the Craig-Brampton modal basis to an equivalent, orthogonal basis with modal coordinates q^*, where

$$Nq^* = q \tag{5.22}$$

Thus, the effect on the superposition formula is,

$$u = \sum_{i=1}^{M} \phi_i q_i = \sum_{i=1}^{M} \phi_i N q^* = \sum_{i=1}^{M} \phi_i^* q^*$$

where ϕ_i^* are the orthogonal Craig-Brampton modes.

5.5- Elasto-acoustic Coupling

Here, one is concerned with the high frequency interaction between vibrating flexible members and the associated spatial distribution of sound pressure that follows.

5.5.1- Introduction

One would be concerned with coupling in the frequency domain, between elastic structural vibration behaviour and the attached acoustic waves.

Norton (1989) reported the pioneering work on impact by Richards *et al* (1979a) as:

When two bodies were impacted together, sound could be created by two distinct processes:

> *Acceleration noise*, which was due to a rapid change in velocity of the moving part during the impact and which gave rise to a pressure perturbation. This was not dependent on damping or vibration isolation.

Acceleration noise arising from impact is a function of impact duration, size factor, area in contact, and impact velocity.

The dominating acceleration noise mechanisms are those which relate to very short impact times, and in association with backlash. The shorter the contact time the greater the radiated noise energy. Acceleration noise is only developed during the contact time.

> *Ringing noise*, which was due to sound radiation from vibrating modes of the attached structure. This continued long after the initial impact, until all the impact energy had been radiated as sound or had been absorbed in the structural damping system (Richards *et al*, 1979b).

Ringing noise is a complex function of structural damping, the rate of propagation of vibration energy, Young's elasticity modulus of the structure, radiation efficiency of the structural panels liable to vibrate flexurally, surface areas and velocities, and vibration amplitudes (White and Walker, 1982).

Richards *et al* (1979a, 1979b) developed empirical formulae for the prediction of noise generated by impact, so that design action could be taken early in a programme to avoid costly palliation later on.

For solid bodies with sufficiently compact dimensions it was found that acceleration noise and structural ringing noise were of similar order (Richards, 1981, Richards and Cuscheri, 1983). However, if local resonant flexural modes were excited by the impact, the radiation energy was significantly higher than the accelerative energy radiated during the time of impact. The reason for this was the longer time taken for the lightly damped structure to radiate the noise energy by ringing, or for the ringing to be structurally damped, or for the vibration energy to be channeled to other parts of the structure (Richards, Carr and Westcott, 1983).

In a bell type structure (like the aluminium clutch housing for example), very little energy would convert into heat through structural damping, and most of the impact energy would radiate as sound until the energy had been fully dissipated.

The impact in the lash zone generates a short (1 to 2 ms) pulse of airborne noise, which is dependent on contact conditions. The energy is dissipated into the surrounding structure and supporting structure, and this may take 30 to 50 ms dependent on structural damping and on the vibration paths.

The following figure 5.3 schematically shows one of many possible pulse exchanges in the driveline due to lash.

The driveline surrounding structures - clutch bell housing, driveshaft tubes for example - are thin walled and lightly damped and may be readily excited into resonance by internal impact. The transmission bell housing is cast in Aluminium, which has intrinsically much lower levels of structural damping than cast iron (transmission housings were originally produced in cast iron).

When both acceleration and ringing noises are present in an impact process, it is necessary to confirm which is the dominant source in order to take appropriate design action. The fraction of ringing energy radiated as structure borne sound will depend on the ratio of acoustic to structural damping and on the rate of propagation into the floor and other parts of the surrounding structure.

The impulsive noise from impacts must, therefore, necessarily consider in more detail, the structural response characteristics associated with the impact pair. Structural modes may be responsible for most of the sound radiation. Non-resonant forced modes are much less effective noise radiators. When structural modes are coupled to acoustic cavity modes by frequency and by modal shape then it has the potential for maximum noise radiation.

If *no* internal structural damping or leakage of vibration energy to ground can occur, then all the vibration energy must be radiated acoustically. Normally, structural and interfacial damping is present and would absorb impact vibration energy; the question therefore remains how much of this energy is radiated as sound or as heat during the structural absorption following an impact.

Richards and Cischeri (1983) and Richards and Lenzi (1984) concluded that effective impact noise reduction primarily depends on a *reduction in excitation levels* and on *increased impact duration*, which has the effect of achieving *lower radiation efficiencies at lower response frequencies.*

Softening impacts was generally a more effective way of reducing impact noise than the addition of structural damping. This is an important conclusion for driveline impact analysis.

In any case, irrespective of the nature of the impact and the resulting elastic waves, a cause of concern when dealing with acoustic cavities such as drive shaft tubes or the transmission bell housing, is the mechanism of structural-acoustic coupling. This of course like any other resonating phenomenon depends on the natural modes of the cavity itself. A method of determining such modes is through the solution of the acoustic wave equation for various forms of sound pressure propagation. The established method for this is boundary element discretisation of the Helmholtz equation (i.e. the acoustic wave equation).

5.5.2 The Boundary Element Method

One may now consider the dynamics acting between the acoustic enclosure of a thin walled hollow driveshaft and the acoustic radiation from the surfaces of the tube, when the tube is subjected to external transient excitation.

On the one hand, the driveshaft tube which is a cylindrical closed cavity, will resonate with internal standing sound pressure waves when subjected to structural excitation. The *acoustic* modes will be of lower frequency in the longitudinal direction, and of much higher frequency in the radial direction. They may be excited by flexural or radial structural vibration.

On the other hand, one must also consider the extremely complex and active drive shaft tube *structural* modes of vibration, which are very lightly damped and have a very high modal density in the high frequency clonk range. The driveshaft tubes will radiate sound very effectively, especially at critical structural frequencies, and particularly from flexural modes of vibration.

This dynamic interactive system calls for a coupled structural-acoustic analysis in the frequency range 1000 to 5000 Hz. However, a very large mesh density and a massive number of interface elements would be required for an FEA of such elasto-acoustic models. One solution is to employ the *boundary element method* for the acoustic analysis. In many cases, FEA of structures may be fed into the acoustics BEM for a sufficiently accurate uncoupled analysis to be carried out. The aim is to observe any excitation of acoustic response induced by natural structural modes, this being adequate to identify the troublesome structural modes.

The propagation of small amplitude waves within an enclosure may be represented by the Helmholtz wave equation when the applied sound pressure, as a function of time and space, is considered as a harmonic function (Rooke *et al*, 1995).

$$(\nabla^2 + k^2)p = 0 \tag{5.23}$$

$$\text{where: } \nabla^2 = \frac{\partial^2}{\partial^2 x} + \frac{\partial^2}{\partial^2 y} + \frac{\partial^2}{\partial^2 z}$$

$k = \dfrac{\omega}{c}$ = the wave number.

ϖ = angular frequency.

c = speed of sound within the medium (344 m/sec)

p = sound pressure where p = p (x, y, z, t)

For a finite volume with closed ends, the boundary surface may be represented by a series of outward normals (n). The normal outward component of the air velocity for each structural mode ω is given by $ve^{i\omega t}$, providing the following boundary condition for the solution of equation (5.23):

$$\frac{\partial p}{\partial n} = -i\rho\omega v \tag{5.24}$$

where n represents the outward boundary surface normal at any field location and ρ is the fluid density (in this case, that of air).

In conventional boundary element analysis, the Helmholtz differential equation is reduced to a boundary integral equation over the surface of the structure. This is solved by a set of linear algebraic equations, the drawback being a repetitive calculation procedure for each of the structural modes. This shortcoming has been overcome by an improved BEM by extracting the frequency terms from the integrals such that the influence coefficient matrices are independent of the structural modal frequencies. This procedure is highlighted by Hussain (1993). This improved BEM method is employed here.

This BEM methodology can provide a method of determining the interior sound pressure distribution of the drive shaft tube. The eigenvalues using this method compare well with the results obtained from experimental tests, as in the case of the drive shaft tube subjected to torsional vibration as described earlier. Modifications to the basic equations can allow both free and forced response problems to be addressed.

A weighted residual form of the Helmholtz equation is used as follows:

$$\int_V w_i(\nabla^2 + k^2)p\,dV \tag{5.25}$$

where in this case:

V = volume of the cavity in question,

$w_i = \dfrac{1}{4\pi r_i}$

r_i is the position of a field point from the source of excitation for which $c_i = 0, \frac{1}{2} or 1$ depending on the position of the source point (see figure 5.4).

If one takes Γ as the boundary surface of Ω and n being the normal vector at the field point under consideration, a double integration may then be performed, leaving

$$k^2 \int_V w_i p dV = c_i p_i + \int_S p(\nabla w_i . n) dS - \int_S w_i p dS \tag{5.26}$$

where the volume to be investigated is bounded by N nodes and contains L nodes within the boundary, in which the pressure can be calculated as follows:

$$p = \sum_{j=1}^{N+L} f(\beta_j, \alpha)\Omega_j \tag{5.27}$$

where: $f(\beta_j, \alpha) = 1 - r(\beta_j, \alpha)$ is an approximating function that satisfies the condition:

$$f(\beta_j, \alpha) = -\nabla^2 v(\beta_j, \alpha) \tag{5.28}$$

Now replacing (5.28), (5.27) and (5.26) into a discretised version of equation (5.25), the final matrix relation (5.29) results, from which the particle velocity v can be obtained for all the frequencies in the spectral source content.

$$([A] - k^2[B])\{\Omega_j\} = -i\omega\rho[H]\{v\} \tag{5.29}$$

The solution procedure is highlighted by Hussain (1993)

5.5.3 Acoustic Analysis

The mechanism of generation of sound by structural high frequency vibration of the tube surface and the acceleration of fluid/air in contact with this surface is common in all the previous conditions. What changes is the effectiveness of sound radiation in relation to the amplitude of vibration. In order for a vibrating surface to radiate sound effectively, it must not only compress or change the density of the fluid with which it is in contact, but also in a manner as to produce significant changes in the density of the fluid that is remote from the surface.

In the case of thin walled hollow tubes that may be characterised as finite length cylindrical shells, the techniques that are being considered for the definition of their acoustic properties in a light medium such as air, may be categorized into two groups, the *statistical approach* and the *deterministic analysis* (Richard and Cuscheri, 1983, Richards and Lenzi, 1984).

SEA *Statistical Energy Analysis* is a statistical approach, which may be used when resonant frequencies are characterised by dense packing in a limited frequency band. By comparison, the driveshaft tube will also have a high modal density at high frequencies, due to the tube length (L) and radius (α) to thickness (h) ratios. In such cases of high modal density, it is not practical to examine each individual mode and the SEA method considers the energy levels in the spectrum. The SEA method has the disadvantage that it is only appropriate in high frequency areas (above 400 Hz) with a high modal density.

On the other hand, in deterministic analysis the velocity distributions of each mode that could be affected by the boundary conditions and the excitation are individually considered. This is a rather time consuming but accurate method for the determination of the acoustic radiation efficiency of each mode. Specifically for shell structures, the influence of the curvature on sound radiation derives from its effect on the flexural wave characteristics, which are mainly in low wave numbers. Cylinder curvature increases the flexural wave phase velocities through the mechanism of mid-plane strain with a consequent increase in radiation efficiency [33, 34]. Simultaneously, a reduction in the density of natural frequencies is observed, compared to the acoustic efficiency of flat panels. The parameter that indicates the frequency range for which curvature effects are important is the so-called ring frequency f_r, which is defined as the frequency when the wavelength of extensional (axial) waves in the shell is equal to the shell circumferential waves:

$$f_r = \frac{1}{2\pi a}\sqrt{\frac{E}{\rho}}$$

(5.30)

where α is the radius of the tube, E is the modulus of elasticity of the material, and ρ is the density.

In coupled elasto-acoustic analysis there is another parameter that is important, the so-called critical frequency or coincidence frequency f_c, which is defined as the frequency at which the acoustic wave-length in the medium is equal to the acoustic wave-length in the shell structure material, or alternatively it is the frequency at which the speed of sound in the fluid equals the bending wave velocity in the structure:

$$f_r = \frac{c_o^2}{2\pi h}\sqrt{\frac{12\rho\left(1-\nu^2\right)}{E}} \tag{5.31}$$

where c_o is the speed of sound in the medium (such as air), ν is the Poisson's ratio, and h is the thickness of the tube. The critical frequency is a characteristic magnitude of flat plates (Richards and Carr, 1986, Richards, 1984, and Roy and Ganesan, 1995).

The aforementioned two characteristic frequencies determine whether a cylindrical shell is classified as acoustically *thin* when $f_r < f_c$, or acoustically *thick* when $f_r > f_c$. At this point it is quite interesting to make the distinction that a shell structure can be characterised as thin from a geometric point of view (when $h << \alpha$), but as thick from an acoustic classification (when $f_r > f_c$). The acoustically thin shells are associated with a high modal density. This means that the statistical approach methods for the determination of the acoustic radiation properties may give quite accurate results. However, in many engineering applications acoustically thick shells are used, in which case the modal density is high only in the high frequency band. Consequently, an individual analysis of each mode is required for the extraction of accurate conclusions, with regard to the acoustic radiation efficiency that is also strongly dependent on the geometric properties and boundary conditions of the shell. Generally, it has been observed that the radiation efficiency of acoustically thick shells reaches unity at high frequencies, in which case the elasto-acoustic coupling of the structure and the medium should be especially considered. The acoustic behaviour is also influenced by the nature and type of excitation. For example, road surface excitations on the vehicle and the sudden engagement of the clutch could produce different acoustic responses in the driveshafts.

The natural modes of a cylindrical shell structure (i.e. the hollow vehicle drive-shafts) may be categorised into two main groups, acoustically fast or acoustically slow.

The so-called acoustically fast *supersonic* modes have structural wave numbers that are smaller than the corresponding acoustic wave numbers of the external medium.

The so-called acoustically slow or *subsonic* modes have structural wave numbers that are greater than the corresponding acoustic numbers.

The subsonic modes are not as efficient in sound radiation when compared to the supersonic modes. For flat plates the critical frequency identifies the distinction between the supersonic and the subsonic modes in the frequency domain. For cylindrical shells there is not such a critical frequency. This means that below the critical frequency there is a mixed frequency area, where supersonic and subsonic modes will coincide due to the influence of the shell curvature in the characterisation of a mode as being acoustically fast or slow.

As has been mentioned before, structural supersonic modes are usually effective acoustic radiators of noise. Therefore, as a first step, an investigation is required for the separation of the driveshaft modes into the supersonic and subsonic ranges. Figures 5.5-5.7 show the separation between supersonic and subsonic modes for each tube of the three-piece driveline. The distinction between them has been achieved by calculating the quantity:

$\Delta L(m,n) = k - k_s$, where, k and k_s are the acoustic and structural wave-numbers, respectively.

5.6 Coincidence of Higher Acoustic and Structural Modes

The disturbances that occur in the connections of the shafts during torque transmission through the driveline, can lead to the propagation of internal sound standing waves in the medium (air), The vibration response of the cylindrical tube walls to these types of excitation and hence the externally radiated sound power, are mainly determined by the possible coincidence of the higher order acoustic modes inside the shell and the resonant flexural modes of the walls. At this point, a few details about the definition of the term "coincidence" are also pertinent.

Sound waves in the axial direction inside a cylindrical shell (tube) demonstrate a continuous variation of axial wave number with frequency (travelling waves) compared with the circumferential waves that appear fixed, due to the boundary conditions that are introduced by the tube walls (stationary waves). Structural waves in the circumferential direction have discrete wave-number values. The axial waves also have discrete wave numbers because they have a finite length, but they would vary with frequency if the tubes had infinite lengths.

Definition of the higher order acoustic modal configuration is self evident by the (p, q) wave number are shown in figure 5.8.

Definition of higher order structural modal configuration is by the (m, n) wave number (Norton, 1989), when m is the number of half structural waves in the axial direction, and n is the number of full structural waves in the circumferential direction. For each circumferential mode order (n=1, 2, 3, etc) there is a large number of axial orders, and a correspondingly large modal density.

External sound radiation is predominantly determined by coincidence of the higher order acoustic modes and the resonant structural modes. *Complete coincidence* requires that *wave number* matching in axial and circumferential directions, and also *frequency matching,* occurs (Richards and Cuscheri, 1983, and Richards and Carr, 1986). In general terms, coincidence is deemed to occur when the (m, n) structural modes and the (p, q) acoustic modes, match by wave number. Hence, coincidence will be achieved when the (m, 1) structural modes are matched with the (1, 0) and (1, 1) and (1, 2) acoustic modes, and so on.

It should be borne in mind that although it is essential for acoustic coupling to be well understood, the mechanism is transient and modal densities of both cavity and structure are extremely high. Hence, any palliation should necessarily be assessed over a wide frequency band.

Figures 5.9 and 5.10 show the coincidence between the (m,1) and (1,q) modes, and between the (m,2) and (2,q), when referring to the middle driveshaft tube with the simply supported closed ends.

5.7 Closure

Having already separated the "dangerous" modes from the acoustic point of view based on the existence of subsonic and supersonic regimes, and having defined the frequency bands where the medium of the tubes could interact with the structure, the investigation may be directed to the calculation of the (averaged) radiation efficiency. This target may be achieved by the use of analytical models or more accurately by using *Finite Element* or *Boundary Element* techniques. FEA is rather time consuming and complicated, because the computation of the radiated noise power is required for the complete surrounding area to the structure.

On the contrary, BEM can give accurate results for specific locations in space around the structure-radiator (Roy and Ganesan, 1995). This procedure must be applied for the different *types of excitation* and *boundary conditions* for each tube in the driveline, because these two factors can alter the behaviour of a mode and transform it from subsonic to supersonic and vice-versa (Shope *et al*, 1984, Junger and Fett, 1972). Then, the averaged radiation efficiency of each mode may be compared with experimental results that have been obtained during the operation of the driveline in anechoic rooms.

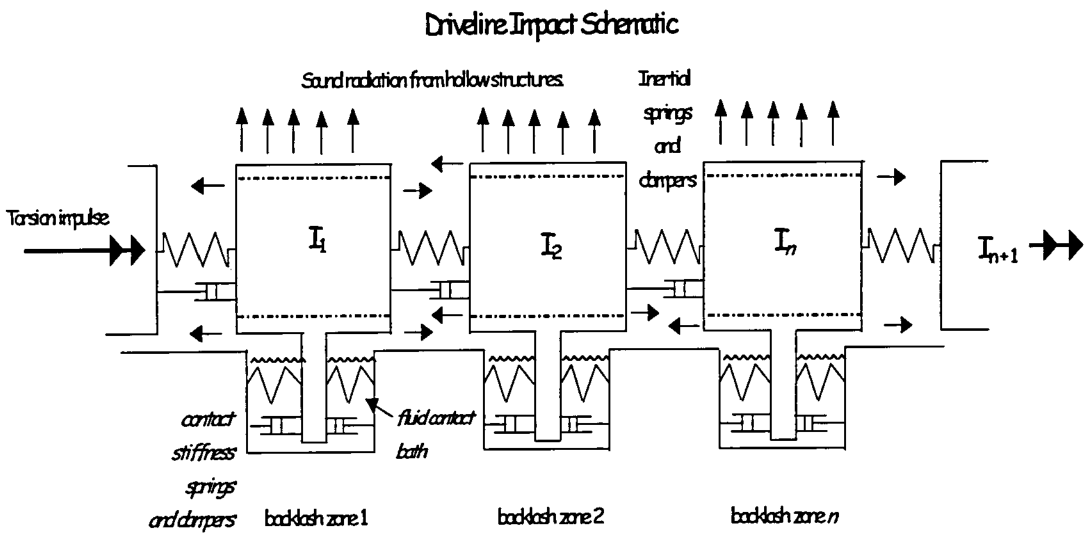

Figure 5.1 Driveline schematic of the sequential impact mechanism

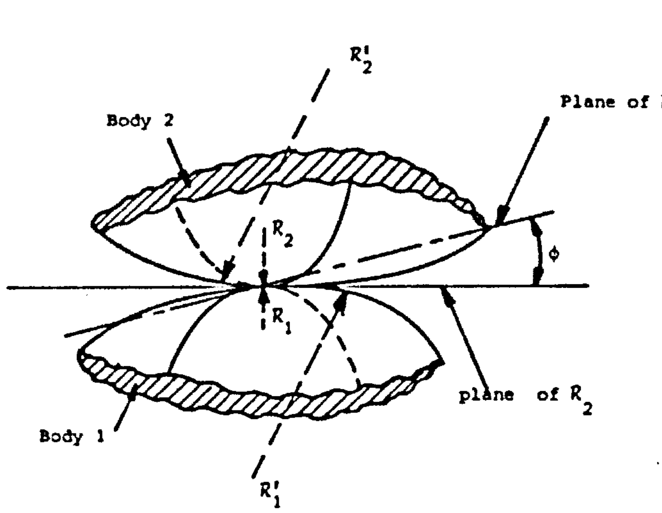

Figure 5.2 Principal radii of a pair of bodies of revolution in counterformal contact.

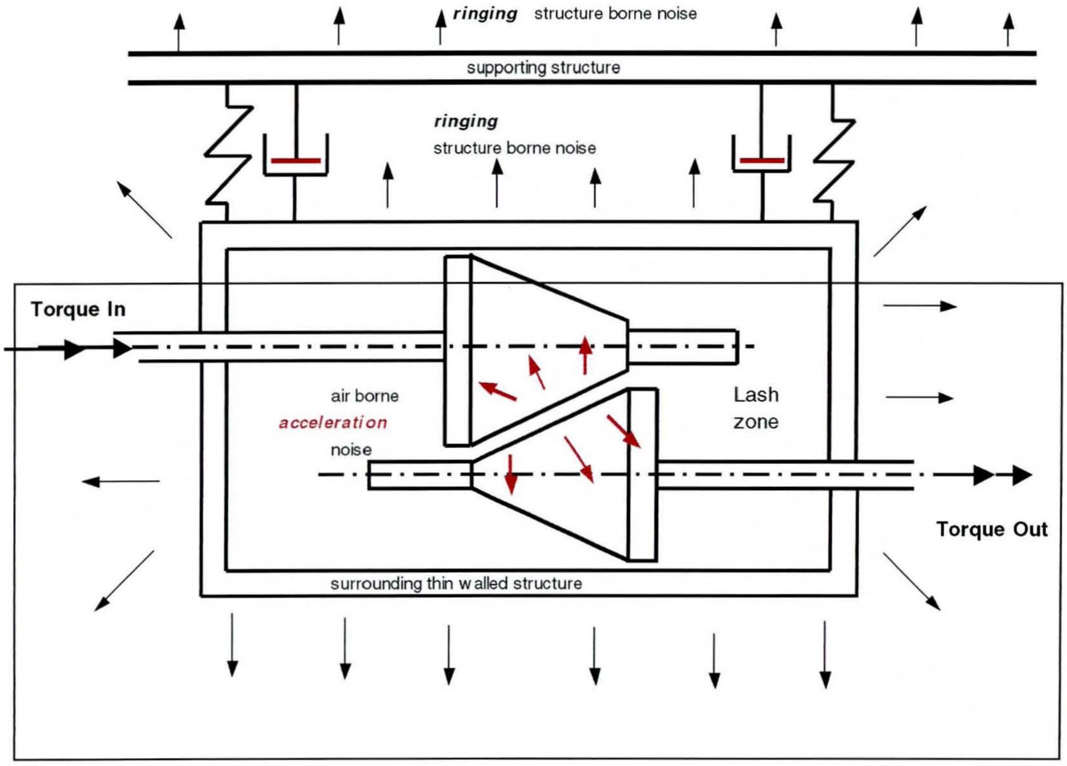

Figure 5.3 The impact mechanism and the dissipation of impact energy into the surrounding structure

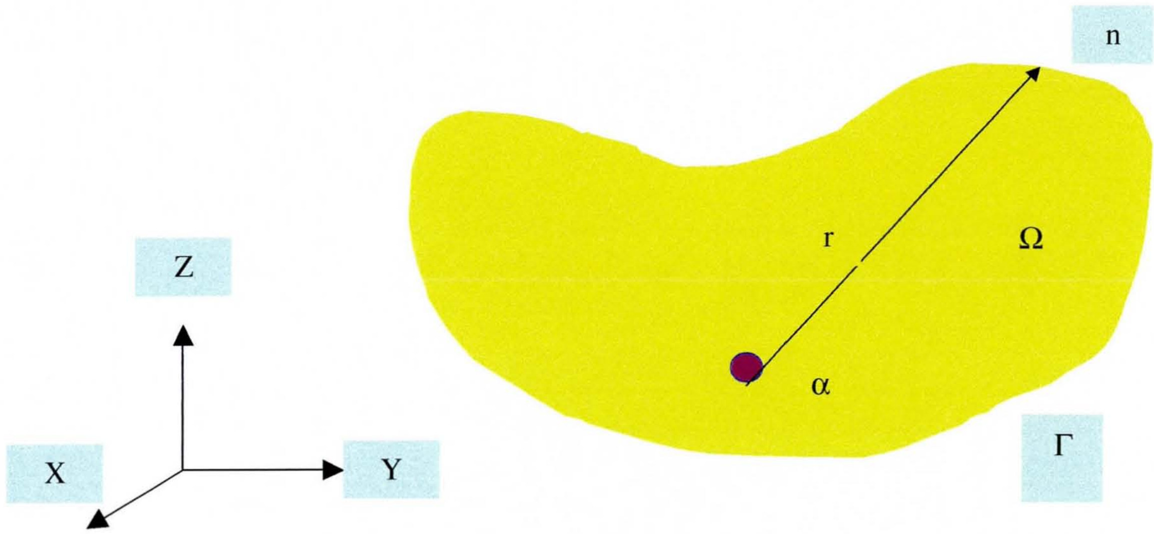

Figure 5.4 Pressure at a distance from a source

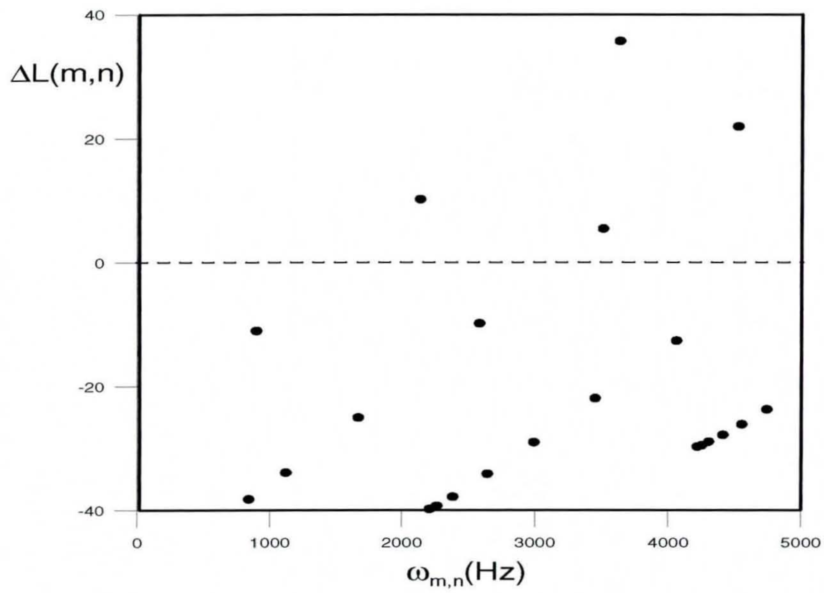

Figure 5.5 Front tube subsonic and supersonic modes

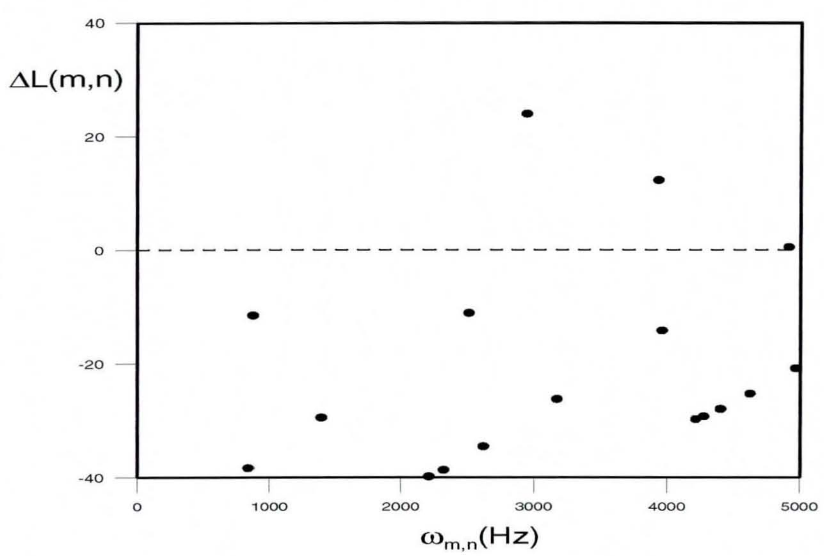

Figure 5.6 Middle tube subsonic and supersonic modes

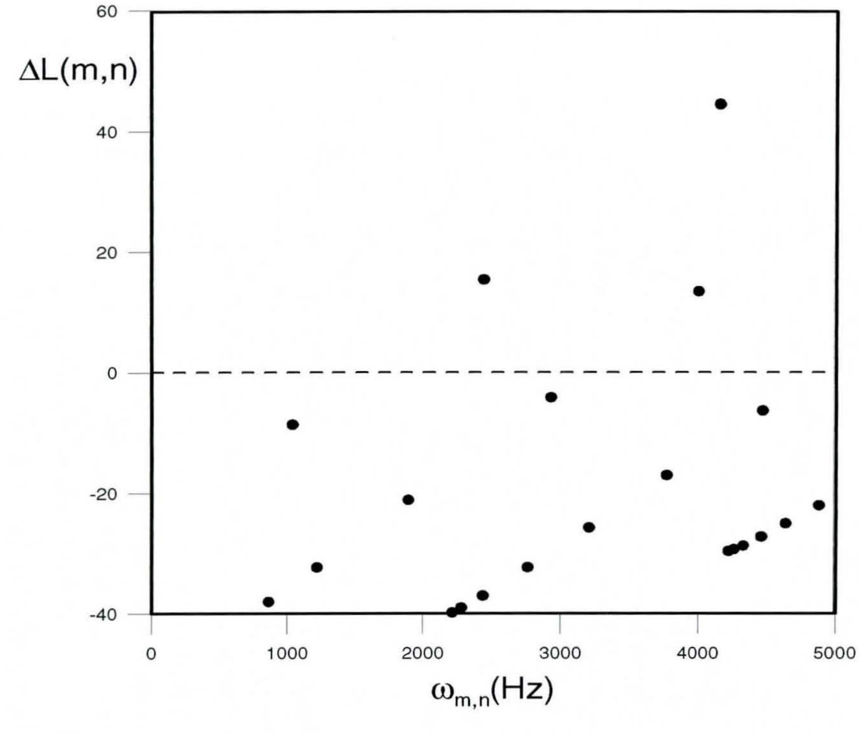

Figure 5.7 Rear tube subsonic and supersonic modes

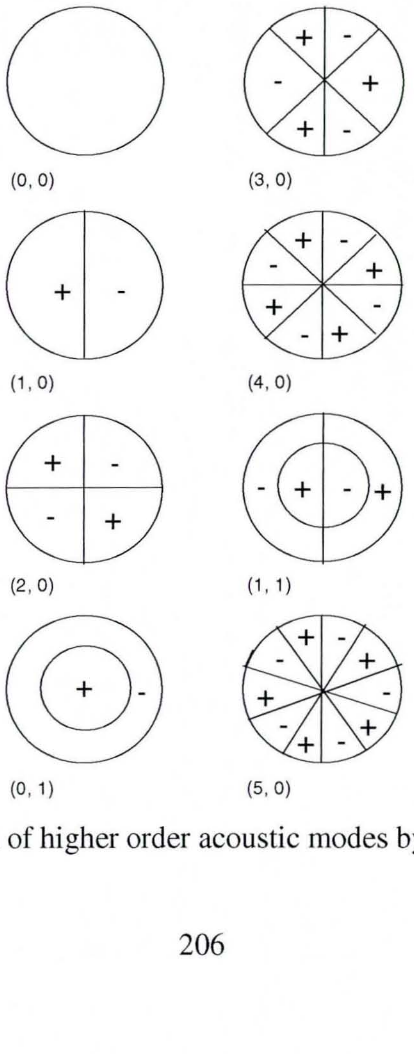

Figure 5.8 Definition of higher order acoustic modes by (p,q) nomenclature

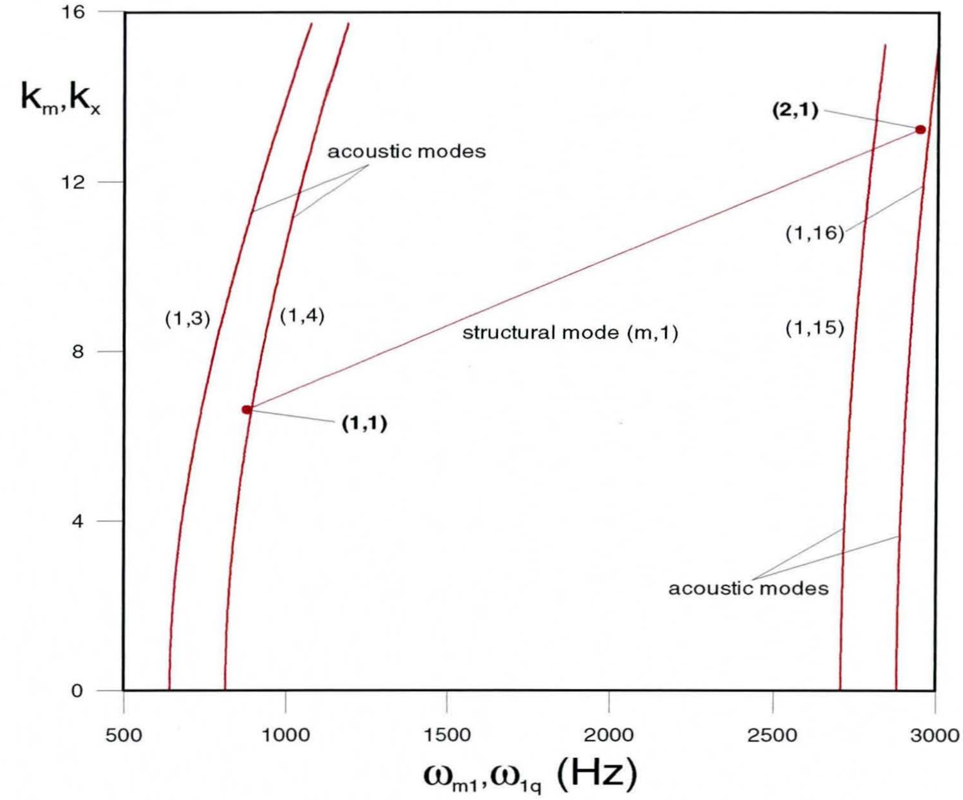

Figure 5.9 Coincidence of (m, 1) structural tube modes and internal acoustic modes.

Centre driveshaft tube.

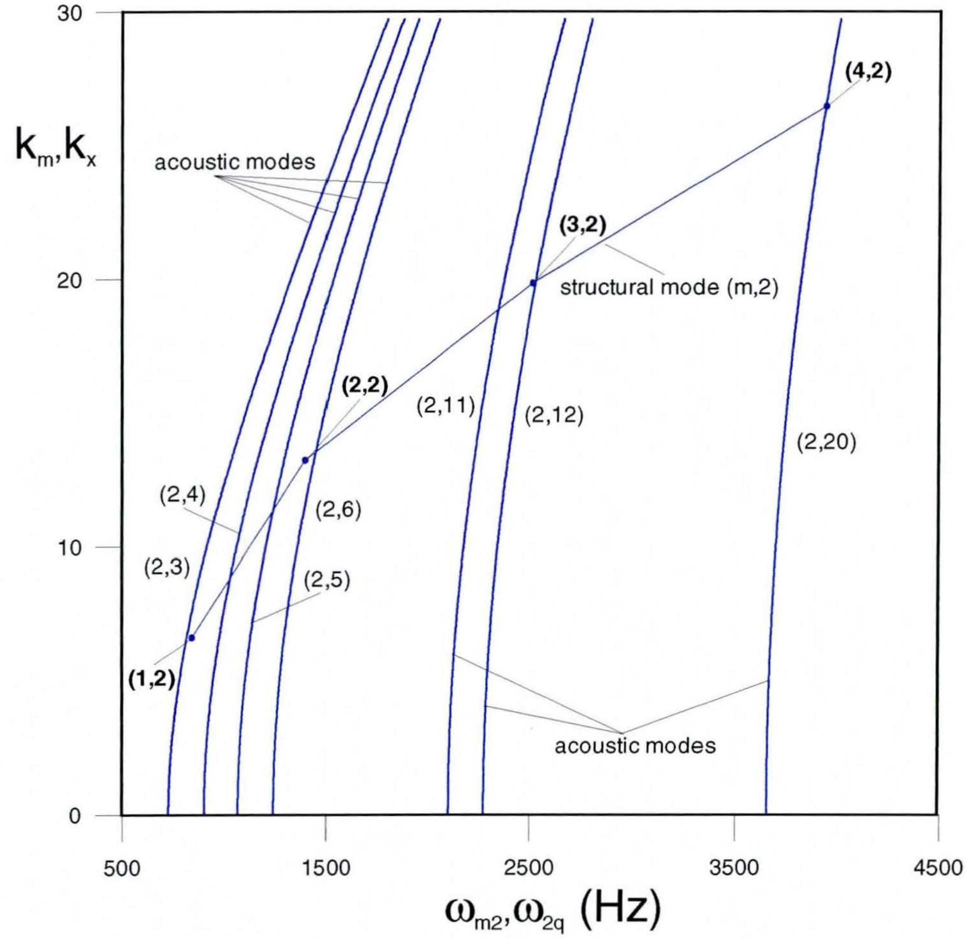

Figure 5.10 Coincidence of (m, 2) structural tube modes and internal acoustic modes: Centre driveshaft tube.

Chapter 6

Numerical results and comparison with experimental investigations

This chapter highlights the comparative studies between numerical predictions and experimental findings, to gain or explain fundamental understanding of the physics of the problem, and the major contributory causal factors using FE and DOE techniques.

6.1. 2-piece ADAMS RWD driveline model-results

The ADAMS model set up procedure for the 2-piece driveline was described in Chapter 4. The longitudinal vibrations of the model were investigated and the model simulation was run for 4 seconds at 2.67 milliseconds time intervals. Since the model was effectively a two-lumped mass model, two natural modes of vibration would be expected from the simulation. These modes would be evident when an FFT transform of the time response had been performed. In fact, two frequencies were observed in the frequency spectrum at 3Hz and at 20 Hz.

The 3 Hz mode was related to the vehicle tip-in or shuffle. The 20 Hz mode was related to an oscillatory motion of axle/differential/rear tube assembly under driveline angulations or axial float. Both resonant modes were confirmed by a parallel study into a functionally similar two mass system with the same parameters as used in the MBD model.

6.2. 2-piece Finite Element (FE) RWD driveshaft tube model-results

Driveshaft tubes and transmission housings are lightly damped thin walled structures, having a very wide frequency range of response. The driveshaft structural modes have an extremely high modal density (modes per frequency band) and they increase with shape complexity as the frequency of response increases.

The study of driveline clonk was focussed on the structural modal behaviour of the driveshaft tubes when impacted, and this may be accomplished using FE codes such as ABAQUS or NASTRAN.

The diameter-to-wall thickness ratio of the driveshaft tube was sufficiently large to allow ABAQUS shell elements to be used. These elements are four noded curvilinear elements, with a node at each corner.

The tube structural modes are excited at a high frequency, and a high element mesh density is required to accurately capture the modal frequencies (eigenvalues) and the modal shapes (eigenvectors).

In the event, 106 shell elements were employed for the FE analysis along the length of the tube, and there were 32 elements at each cross-section of the tube. In addition, 100 elements were added to each end, giving a total of 3592 elements per tube. This mesh density was necessary to catch the high frequency surface vibrations in the tubes.

The mesh patterns were created using PATTRAN, and then exported to ABAQUS for modal analysis.

Front tube: The first eigen-mode was a low frequency flexural bending mode at 24 Hz. As a further example, the third mode of the first tube occurred at 44 Hz and this was the first axial buckling mode.

Rear tube: The first eigen-mode occurred at 7 Hz, which was known to be close to the shuffle frequency. Another mode was noted at 20 Hz, which had been earlier identified in the MBD study as an axial system mode. This was a reassuring coincidence between the FE analysis and the MBD study, since it had been identified that combined axial and torsion modes occurred. The FE analysis identified the first combined torsion and bending mode at this frequency.

The consequence of the high mesh density made it difficult to conduct a high frequency sweep of the structure. However, a limited sweep was conducted on the first tube and it was noted that structural modal density was extremely high in the frequency bands 1000 to 1250 Hz, 2000 to 2500 Hz, and around 3500 Hz (see figure 3.14).

It was, therefore, decided to concentrate on the known areas of modal interest that had already been identified on the rig. Hence, small computational excursions were made around known frequency poles of interest. These were centred at 1750, 2450 and 3250 Hz, although there were many other 'hotspots' of modal activity. These are shown for the frequencies 1757 Hz, 2445 Hz, and 3257 Hz in figures 6.1 and 6.2 for the front tube respectively.

Figure 6.2 show the mode shapes for 1751 Hz, and 3246 Hz for the rear tube respectively. These modes were found to be quite complicated shapes, typically of combined torsion and axial compression, and torsion and flexure, and resulting in surface circumferential waves. Some of these would be powerful noise emitters, others not so, dependent on the surface wave phase angle to the outer noise field.

A particularly interesting mode pattern was observed at 2445 Hz, where a large number of axial spikes in the waveform were noted (see figure 6.1). Such a modal condition would be an effective radiator of noise and would be best suppressed by damping placed around the diameter (see figure 6.1 for the 2445 Hz mode showing the circumferential motion).

6.3. 2-piece driveline rig experimentation

The driveline rig was constructed as described in Chapter 3. A maximum torque was applied to the clutch springs and then locked. This meant that the backlash at every point in the driveline was open. When the impulse was required, the clutch torque lock was abruptly released. The torque flow passed through every backlash zone and was reacted at the rear wheels, which were fixed to the floor. Simultaneously with torque release the acoustic and structural driveline responses were measured by three microphones and nine accelerometers stationed along the driveline, to capture the modal behaviour.

The data sampling frequency was 12500 Hz, with a corresponding time increment of 0.08 ms. Application of the Nyquist sampling theorem indicated that modal data up to 6250 Hz could be obtained with this sampling rate. This was necessary, because it had already been established from the road testing that the clonk audible frequency range extended to 5000 Hz.

It would have been preferable to generate a compliant tyre to road contact condition with the rig. This would have improved the realism, particularly for the shuffle response mode. Another desirable feature would have been a road impulse through a tyre contact. These conditions would have helped further understanding of the high frequency propagated and reflected wave motions. In the event, the correlation between the rig and road results was very good and the rig design was justified (see figure 3.4). In any case, by limiting the angular motion of the system it was possible to use accelerometers, which would otherwise have been impossible. Another advantage was the elimination of tyre noise under traction.

The investigation followed a well-defined Design of Experiments test array (see Table 6.1). The purpose of the DOE plan was to investigate causal factor effects on clonk and also to provide verification test data for the CAE models that have already been referred to.

6.3.1. 2-piece driveline rig DOE-results

Multi-body dynamics is the study of motion of a number of components in a system, each having interactions, which ultimately affect the output response of the system, when subjected to a given set of externally applied forces.

Importantly, it is for this reason that this thesis considers the application of DOE (Design of Experiments) methodology to an MBD system. DOE is an analytical tool, which considers the contribution of factors and factor interactions in a multi-body system in terms of the system output response.

The outline 16 run 2^4 DOE plan involving 5 factors set at 2 levels, is shown in Table 6.1
This schedule ensured that every factor and factor interaction was not confounded.

The 5 factors chosen were as follows:

Factor A	Torque preload	A+	150 Nm
		A-	75 Nm
Factor B	Driveshaft type	B+	Damped prototype shaft
		B-	Baseline shaft
Factor C	Clutch type	C+	Disc without predamper spring
		C-	Disc with predamper spring
Factor D	Axle type	D+	Axle without pinion gear lash
		D-	Axle with maximum gear lash
Factor E	Flywheel type	E+	Baseline inertia
		E-	Minimum inertia

From the table 6.1, it can be seen that acceleration time histories were simultaneously measured at 9 driveline locations. The table shows the peak-recorded values at impact for each test run.

Figure 3.10 in Chapter 3 showed a typical input torque ramp profile against the first shaft response. In particular, the initial impact of 2ms was followed by a ringing period of about 50 ms during which the tube vibration decayed due to structural damping.

Figure 6.3 shows a typical time history, for the acceleration measured at the centre of the 2nd driveshaft for test run 3.

Figure 6.4 shows the frequency transform of the time history in figure 6.6, and the shaft modal activity.

Figure 6.5 shows that noise at the transmission during rig testing was consistently higher than at the rear axle location in the clonk frequency range.

Figure 6.6 shows the nine driveline pick-up responses and the input torque. All signals are on the same scale for direct comparison. The low inertial axle flange and transmission flange have the highest response levels.

Figure 6.7 illustrates the predominant effects of lash on the acceleration responses. For 8 test runs with the same 150 Nm input torque, ***all*** of the responses associated with a clutch and predamper, were more responsive than ***all*** of the responses for a clutch without predamper, measured at the transmission flange.

Similarly, ***all*** of the responses associated with an axle with maximum lash, were more responsive than ***all*** of the responses for an axle with minimum lash, measured at the axle.

The figure shows the lash effect from the clutch on the right hand side, and that due to the axle on the left hand side.

Figure 6.8 shows the DOE result summary for all the factors and factor interactions that were considered in the testing.

From this investigation, the main factor contributing to clonk was the clutch disc. The low rate predamper spring was effectively a major source of lash in the driveline. This conclusion was also evident in Figure 6.7. The second ranked factor was the flywheel inertia. By comparison, the factor interactions were clearly not effective in this study.

The same findings were also reported when a SIMULINK lumped-mass model simulation was carried out, using a genetic algorithm for optimisation process. This work was carried out in conjunction with the author, and was reported by Farshidianfar *et al* (2002).

6.3.2. 2-piece driveline coupled structure-acoustic model

An uncoupled and a coupled analysis of the structural and internal acoustic modes of both front and rear shaft tubes were investigated.

Four noded two-dimensional shell elements were used for the tube walls. Eight-noded three-dimensional elements were used for the acoustic volume. The grid density for both was identical with node coincidence at the boundary between wall and fluid. In the coupled analysis there is a direct connection between wall and fluid with no allowance for rotational fluid motion. The FEA code NASTRAN was used.

Clamped-clamped conditions were assumed for the tube edges, to simulate the vehicle condition. The coupled analysis showed very little differences in frequency, when compared to those predicted by the uncoupled analysis.

The front tube was of a constant diameter, and was smaller in both diameter and length than the rear tube (see figure 6.9). The rear tube was flanged with two larger diameters and was much longer than the front shaft (see figure 6.10). The wall thickness and material was the same for both tubes.

The result is that the front tube had fewer structural and acoustic modes in the clonk-frequency range than the rear tube although the frequency spacing was different. Hence, there was a sensitivity difference between the tubes, in response to impulsive impact.

ARMA spectral analysis was conducted on the test signals taken from both the front and rear tubes during the DOE test programme. Several critical structural eigenmodes were extracted between 3000 and 3500 Hz for the front tube (see figure 6.11), and between 3500 and 4000 Hz for the rear tube (Figure 6.12).

The results obtained from ARMA for driveshaft tubes lowest flexural modes (see figure 6.13) agreed well with the acoustic cavity modes obtained through boundary element method. Figure 6.14 shows that the fundamental mode for the standing pressure wave for the same tube occurs at 390 Hz (the equivalent having been extracted by ARMA from the experimental signal in between 350-375 Hz). The BEM method indicates multiples of the fundamental for the acoustic cavity of the tube. It is clear that these include contributions at 2340 Hz which is the 6^{th} order of the 390Hz fundamental, and is very close to the FEA answer at 2445 Hz. (Figure 6.1). There is another contribution at 3120 Hz which is the 8^{th} order of the fundamental, close to the FEA prediction of 3257 Hz. (also figure 6.1) The contribution at 3900 Hz (see figure 6.12) is close to the ARMA monitored values at 3700 Hz and 4000Hz, where coincidence is obtained for this front tube between the structural and acoustic modes (see section 6.3.2.1).

The acoustic mode analysis for the tube cavity was conducted using FEA and CMS, as shown in the Table 6.2.

6.3.2.1. Front driveshaft tube results

Figure 6.15 shows the structural and acoustic modes in the frequency plane, and some of these are in regions of coincidence. By explanation, full coincidence is said to occur between structure and acoustic cavity, when the wave number (mode configuration) and the mode shape (eigenvector) are in agreement. Under these conditions there would be a maximum propensity for acoustic emission.

Figure 6.15 provides a graphical representation of elastic and acoustic coincident modes.

6.3.2.2. Rear driveshaft tube results

For the flanged rear driveshaft tube, figure 6.16 shows the low and high modal density regimes. The lower regime in the lower frequency range up to 2000 Hz, relates to the axial standing waves in the tube, which change with position in the tube.

The higher density regime refers to the higher order acoustic modes above 2000 Hz, which do not change with axial location but with tube radius. These modes have extremely rapid sound pressure gradients across the tube diameter. Table 6.2 shows, in bold type, the areas of coincidence for the rear tube between 3700 and 4000 Hz, when the structure and high pressure gradients move in phase at coincidence frequency and produce a maximum sound radiation.

Figure 6.17 shows the structural modal frequency behaviour for the flanged tube. There is a high modal density at ca 3000 Hz and generally the modal density increases with frequency.

For both shafts, it is clear that there is a heavy concentration of (undamped) structural modes in the clonk frequency range, which alone would generate a significant noise problem. The problem is fully exacerbated by the accompanying acoustic modes, which are closely coupled in a very similar frequency domain.

There are several other pertinent observations that may be made from the mode predictions:

- The two driveshafts have different dimensions and this leads to different eigen families. One is more sensitive to clonk impact frequency than the other. This has in fact been borne out by an impromptu vehicle test. The first shaft only, was shielded by a loose cover and a significant subjective noise improvement was achieved.
- The degree of overlap between the structural and acoustic behaviours is so great that a significant 'uncoupling' exercise would be required.
- The tube structural responses will be resonant, when they are aligned with the torque pulse frequency content. The dynamic variability will be highly dependent on the *matching* that arises from the engine and the road inputs to the driveline.

Figures 6.18 and 6.19 show the end view of an acoustic mode at 3947 Hz and a neighbouring structural mode at 3946 Hz respectively. Note that amplitudes are exaggerated for demonstration purposes only.

The circumferential phase matching, and the eigenmodal complexity, between the tube and the air may be clearly seen.

6.4. 3-piece driveline ADAMS RWD multi body model

A three-piece driveline model was constructed, with the intent to further investigate the elasto-acoustic couplings that can occur when an impulsive torque is applied, and which then excites the higher frequency modal behaviour in parts of the driveline.

6.4.1. 3 piece driveline multi body model set up procedure

The driveshaft tube parasolid CAD files were imported into NASTRAN. The driveshaft tube FEA models were created using 2D shell elements (6 DOF for every node). This was justified, because the cylinder wall thickness was very small compared to the tube radius. The radius-to-wall thickness ratio was 0.03751/0.00165 = 23:1

The FEA meshing density for the three driveshafts.

Front tube (nearest engine)	3476 nodes	3444 shell elements
Centre tube	760 nodes	740 elements
Rear tube	1020 nodes	1000 elements

The mesh is shown in figure 6. 20.

Cylinder material properties, E=206 GN/m^2, density=7850 Kg/m^3, ν = Poisson ratio=0.3

The tube boundary conditions used were as follows:

- The three orthogonal displacements of all nodes at the closing diameter were fully constrained.
- The open-ended imported cylinder tube was closed in the model. In other words the shaft could be considered as a fully built-in encastré beam with closed ends.

For computational stability, the grid mesh was set such that the number of elements along each normal axis was of a similar order.

The number of nodes along the tube length was set such that the model would capture and define the higher frequency modes and their shapes from 1000 to 5000Hz.

Tube super-element model was then imported into ADAMS for the elasto-multi-body dynamic analysis.

6.4.2 3-piece driveline elasto-multi-body dynamics results

The following are some predicted structural and acoustic modes in the clonk frequency range: They serve to demonstrate the complexity of each resonant mode shape, and the modal similarities at similar frequencies, when coincident coupling is likely to occur.

They also demonstrate how much the modal shapes can change with only a small change in frequency. Although the modes are relatively undamped, there will be high levels of inter-modal coupling.

The acoustic modes cannot be experimentally verified at this time due to the difficulties of using a miniature microphone in a small enclosed tube, and the adverse effects on the internal sound pressure gradients. One solution would be to use a much larger cavity with the same dimensions in proportion, so that the intrusive effects of a microphone could be minimised.

Figure	View	Type	Frequency	Front or rear tube
6.21	End	Acoustic	3748 Hz	Rear
6.22	End	Structural	3782 Hz	Rear
6.23	Longitudinal	Structural	3782 Hz	Rear
6.24	End	Structural	3856 Hz	Rear
6.25	Longitudinal	Structural	3856 Hz	Rear
6.26	End	Acoustic	3899 Hz	Rear
6.27	Longitudinal	Acoustic	3899 Hz	Rear
6.28	End	Structural	3946 Hz	Rear
6.29	Longitudinal	Structural	3946 Hz	Rear
6.30	End	Acoustic	3993 Hz	Rear
6.31	Longitudinal	Acoustic	3993 Hz	Rear
6.32	End	Structural	4008 Hz	Rear
6.33	Longitudinal	Structural	4008 Hz	Rear
6.34	End	Acoustic	3233 Hz	Front
6.35	Longitudinal	Acoustic	3233 Hz	Front
6.36	End	Acoustic	3268 Hz	Front
6.37	Longitudinal	Acoustic	3268 Hz	Front
6.38	Longitudinal	Acoustic	3468 Hz	Front

The elasticity of the tubes is included in the multi-body, and the driveline impact induces structural wave motion which propagates through the driveshaft tubes. The research commenced with the postulate of wave motion, and this has been axiomatically proved by the results shown in figure 6.39, in this case depicting the middle tube. This is the combination of a number of such modes, as described in figures such as those in figures 6.21-6.38.

6.5 FWD passenger car – clonk test programme

Figure 6. 40 shows a schematic of the Front Wheel Drive (FWD) powertrain assembly layout.

No modelling was conducted for the FWD configuration.

The experimental testing programme was conducted in the following areas:

- Drive shaft component testing
- Road testing
- Chassis dynamometer testing with a DOE format

All test were both subjective and objective.

The purpose of the experimentation was to build on the knowledge gained on RWD vehicles and to examine whether the same clonk mechanism also applied for FWD.

6.5.1. FWD road testing

A series of road tests were conducted on a complaint FWD passenger vehicle. Clonk was readily excited by clutch engagement alone and with no throttle.

It also became clear that two drive condition prerequisites were necessary to induce unacceptable clutch engage clonk in the FWD vehicle:

- A rapid clutch engagement, and
- The engine speed just before clutch engagement had to be close to the idle engine speed of about 800-900 rpm,

With both of these conditions satisfied, the clonk rating was poor. With neither satisfied, the rating was good. Figure 6.41 shows a comparison of fast clutch engagement at low road speed compared with slow clutch engagement at a higher road speed with the same vehicle.

In addition the drive clonk with clutch fully engaged, was unacceptable with throttle application from coast to drive. It was totally acceptable, and even inaudible, with tip-in from drive. In other words, when the backlash had been taken up before the pulse had been applied.

Another observation, and one that would be further investigated on the chassis dynamometer, was the significant clonk difference when running at very low speeds. Figure 6.41 shows this difference, between 10 kph and 22 kph.

A proximity microphone was used under the bonnet to pick up the airborne clonk noise. It was helpful that clonk was most audible at low speeds, with low background engine and tyre noise levels to corrupt the signals. The clutch was quickly engaged five times with a very short time interval in order to maintain the speed conditions throughout. This was to check for repeatability and to examine the noise trace. The results are shown in Figure 6.42. The airborne pulse interval was approx 300 ms.

It was necessary to understand the frequency content of these recordings. When the car was later tested on the chassis dynamometer, the same sequence of testing was repeated. This not only confirmed that the clonk problem could be reproduced on the 'rolling road', but also that the better testing environment would allow a frequency analysis of the noise recordings. The results are shown in figure 6.41 for a single clutch engagement condition at low speed as before.

Figure 6.43 is a wavelet diagram for the single clonk (i.e. a frequency-time display). The diagram has been edited to show:

- That the clonk frequency range is 1500 to 5000 Hz, following a hard impact,
- There is a total clonk time of 100 ms,
- The wavelet has identified three successive lower frequency noise impacts following the single clutch engagement. This calculates to be ca. 6.3 Hz, which is the shuffle

frequency. At the time of test, the shuffle was not felt. The system was in shuffle mode, but on this occasion it was not transferred to the driver. An alternative explanation could be the result of reflected wave motion.

- There was a lower (ca 800 Hz) content as well as the high frequency content in the first impact. The figure 6.44 also indicates that the FWD and RWD clonk frequency ranges are similar, and both share the 1000 to 5000 Hz range.

It was, therefore, necessary to examine the driveshaft mobility and to evaluate the shaft dynamics contribution to the noise results.

6.5.2. Component level modal testing

Figure 6.44 shows the result of an impact response on each of the driveshaft pieces. A lightweight clamp with small rigid bracket was attached to each shaft, in turn. A metallic hammerhead impact was applied at the centre of each shaft at the clamp bracket. In other words, a torsion impulse was applied to the shaft in *situ*. The vehicle was left in gear. The shaft acceleration was recorded with an accelerometer in the hammerhead. Each shaft was resonant in the 3000 and 5000 Hz domains. Some allowance must be made for the compliance in the bracket that was used, but in general the results supported the noise recordings taken on the chassis dynamometer.

These results were backed up with component testing of the shafts (not on the vehicle), again by using a clamped rigid bracket as the impact area. This is shown in Figure 6.45, which uses a linear vertical axis to indicate the dramatic rise in amplitude near the resonant conditions. The signals become erratic beyond 5000 Hz, because the energy input from the hammer head impact is insufficient to drive the structure without some distortion.

Figure 6.46 shows the spectra of interior noise under clonk condition with solid and hollow driveshafts. This figure provides comparison of interior noise profiles for tubular shaft (green) versus solid shaft (red). This test was conducted in 2^{nd} gear at 800 rpm with a quick clutch pedal engage rate. The clonk is clearly more detectable with the tubular shaft due to its noise emitting efficiency, especially in the so-called clonk frequency range.

6.5.3. Chassis dynamometer testing

Vehicle examination on a chassis dynamometer (rolling road) allows controlled and repeatable testing procedures to be conducted against a known set of environmental conditions. This was particularly important when considering a DOE test programme. The vehicle is mounted on large diameter rollers, which absorb the tractive driving efforts from the vehicle. Alternatively, the rollers may be used to drive the vehicles. Both front and rear vehicle wheels may be coupled to the rollers. Any road surface may be applied to the rollers. The chassis dynamometer may also be located in a noise free room for anechoic testing.

A major consideration with DOE testing, and most experimentation, is the necessity to determine whether the analysis is a true reflection of the factor changes that are made during testing, and the errors that may otherwise occur. In other words is the result statistically significant?

The conclusion must be robust to the errors or variation that could occur during test due to:

- Variance due to time.
- Variance due to the use and accuracy of the measurement equipment.
- Variance due to production and piece-to-piece differences.
- Variance due to the environment.
- Other factors

In addition to the above, transient audible sounds also represent a major difficulty in subjective and objective measurements. For example, some time may elapse between each run of the DOE and subjective ratings would then be greatly at risk of being inconsistent. Ultimately, clonk is a perceptive judgement of quality and the testing needs to reflect an improvement in that metric. The measurements taken during test need to be clearly linked to the subjective nature of the problem. In any case, the long term deliverable of a sound quality investigation must be a usable design metric. This could be driveline lash, for example, although this is probably simplistic and it could be far more difficult to define.

6.5.4. Clonk DOE testing on FWD

The selection of DOE factors to be tested on the chassis dynamometer, was based on prior knowledge with RWD variants, and also on the lessons learnt during road testing the FWD. In general, the effectiveness of DOE is enhanced with a certain amount of *apriori* knowledge.

The five factors selected were as follows:

- Engine speed at 700 and at 900 rpm, when clutch is engaged.
- Transmission filled with low and high viscosity lubricant.
- Driveshaft to be solid or tubular.
- Clutch disc to be with or without predamper low rate springs.
- Clutch pedal engagement rates to be fast or slow.

It can be seen that most of the factors were fairly easy to change during testing, and having a minimum effect on the vehicle integrity. The exception was the clutch disc and this required a significant change to the system.

Table 6.3 outlines the DOE test array. There was some confounding between factors and factor interactions. This was an agreeable compromise due to the lack of time available with the test facility. For every run the interior and exterior (proximity microphone) clonk noise was recorded.

It was considered that personal ratings taken for every test configuration would not be reliable, as already discussed. However, this element was considered to be extremely important. It was decided to record every internal and external clonk time history for later subjective evaluation, when all the noise traces could be reviewed in the same rating session. In the event, this transpired to be a very useful method, and the correlation between subjective and objective data was found to be good, given the highly transient nature of the problem. This is discussed later.

6.5.5. Results of DOE testing on FWD clonk

With reference to figure 6.47 (DOE run 3), and figure 6.48 (DOE run 10).

It can be seen that these two test runs represented the worst and best conditions for clonk respectively, out of the 16 test runs.

Subjectively, Run 3 was rated *unacceptable,* and Run 10 was rated as *good* by a jury panel of 8 people.

Figure 6.47 diagrammatically represents bad clonk, and this is symbolised by the crank speed differential following clutch engagement as evidenced by the exterior and interior noise recordings shown. It is clear that six successive clutch engagements in 25 seconds were made for the purposes of repeatability comparison.

The external proximity microphone recorded an initial local audible pulse (which was not recorded in the vehicle) followed by the main transient ringing, which was time aligned with the interior signal. The crank speed had fallen to 700 rpm, whilst the clonk audible transient decayed for almost 2 seconds.

Figure 6.49 shows an overall frequency-time wavelet for a single clutch induced clonk. The active frequency range is from 500 to 5000 Hz.

Figure 6.50 shows a close up of the clonk in the impact frequency region. There is a clear region of structural ringing, following the hard impact, taking up to 25ms. The FWD solid shaft has a shorter decay time than the thin walled RWD shaft tube.

Figure 6.48 showed good clonk (subjectively acceptable) and this was characterised by a small crank speed differential, following clutch engagement. The clonk was almost inaudible. Even in the presence of lash, the low speed differential negated the effects of impact, leading to audible clonk. The Hertzian impact relationship is thus held, so that as the differential approaches zero, the contact time is infinitely long, and there is negligible impact energy supplied to the system.

To compare the test conditions for Runs 3 and 10, which yielded such dramatically different results:

Factor and setting	Run 10	Run 3
A: Engine speed setting	900 rpm	700 rpm
B: Transmission oil viscosity	Low	High
C: Drive shaft type	Tubular	Tubular
D: Clutch disc	Nil predamper spring	With predamper
E: Clutch engage rate	Slow	Fast

See also Table 6.4: The DOE run table.

The three factors which had most clonk effect; namely engine speed setting, clutch disc configuration, and clutch engage rate, were at opposite setting levels for runs 3 and 10. Factors B and C were found to have much lower contribution effects. However, a deeper investigation of the data showed that factor A had the most significant effect on clonk.

Figure 6.47 has already shown that when engine speed coincident with clutch engagement was ca 700 rpm, the speed differential during clonk was high and clonk was poor. Conversely Figure 6.48 showed that when engine speed was ca 900 rpm at engagement, the speed difference was low, and clonk was good.

Figure 6.51 shows the clear difference in the data, when all the readings are considered and taken from the 16 DOE test runs. Below a 400-rpm speed differential, the clonk is poor. Above a 600-rpm speed differential, the clonk is good. There is no overlap, the difference is quite clear. Clonk below a 400-rpm differential and clonk above a 600-rpm differential are mutually exclusive events.

The ramp of engine speed below idle rpm is a characteristic of the engine management system.

In order to accurately compare the subjective clonk ratings for all test runs, to avoid the effects of time between each test run set-up, and to avoid driver factors, the interior and exterior noises were recorded and a jury play-back session was arranged, when all 16 runs could be heard simultaneously. In the event, the correlation between jury ratings and internal measured noise was reassuringly good (see figure 6.52). This opens up the very useful possibility that if a subjective rating method using recorded noise is adopted for transient audible signals, this could obviate the need for other objective measurements.

This clearly vindicates the impact theories that were generated in the earlier chapters of this thesis. That when resultant velocities at impact are high, the contact time is short and in the limit the energy spectrum is infinite and able to excite a range of undamped structural activity.

It is, therefore, clear from this exercise that the resultant speed (the speed differential) is the major cause of clonk and the clutch predamper and clutch engagement speeds are major aggravating factors.

6.5.6. Summary of DOE analysis on FWD clonk testing

Several outputs (metrics) were measured for each test run. A factor analysis may be used for each metric. Similar but different factor effects may be identified for each metric. It depends on what metric best describes the problem, whether the measured data is reliable, and other reasons.

This shows that clonk correlation between measured interior noise and exterior noise is not reliable, $R^2 = 0.465$ (see figure 6.53), therefore, a DOE factor analysis must reflect this lack of agreement.

There are several choices available:

- Interior noise is the objective measure of clonk to the driver, but the signal has been corrupted between the source and the driver's ear.
- Exterior clonk noise directly from the shaft proximity microphone is perhaps more reliable, but has airborne noise content only.
- Perceived clonk transient noise by jury is highly subjective.

All the above have some limitations, when deciding on which to use for the factor analysis.

Figure 6.54 shows the driveline factor effects attributable to clonk by using the *subjective* opinion data alone.

Figure 6.55 shows the driveline factor effects attributable to clonk, by using the *exterior noise* data alone. This clearly shows the dominance of crank differential speed.

As already mentioned, the conclusion on factor effects using objective data is slightly different to that based on the subjective data. The shaft response to torsional impact, as picked up by the proximity microphone was primarily sensitive to Factor A; the speed differential at clutch engagement. By comparison, the jury evaluation was equally sensitive to Factor E; the clutch engagement rate and Factor A the speed differential.

A factor interaction calculation was also conducted to establish if factors in combination were responsible for clonk. The results are shown in figure 6.56, which shows that only the crank speed multiplied by clutch pedal speed interaction was effective, followed by the clutch lash multiplied by pedal speed interaction.

Figure 6.57 shows the factor, and factor interaction contributions, to clonk in order of significance. The figure shows that factor A is significant using a confidence level of 95%, indicated by the dotted line. In this case, it would be normal to continue the analysis by removing the lower order factors and submitting for a further contribution analysis, to identify other potential significant factors.

6.5 Closure comments

- DOE study was based on a RWD 2-piece driveline rig.
- ARMA signal analysis of experimental driveshaft acceleration data, identifying high frequency structural modal behaviour.
- Coupled analysis of 2-piece driveline and driveshaft modal behaviour. Correlation with test data.
- Evidence of coincidence coupling in clonk frequency range for both front and rear tubes. More modal activity in rear tube.
- Very high modal density (structural and acoustic) especially above 2000 Hz
- ABAQUS FE analysis of structural and acoustic modes and the mode shapes.
  Low and high density rates in the flanged tube.

	L16 orthogonal array															Peak tangential acceleration responses in m/s2									
Run number	**A** 75 or 150 Nm inputtorque	**B** Driveshaft	A*B	**C** Clutch with/without predamper	A*C	B*C	D*E	**D** Axle min / max backlash	A*D	B*D	C*E	C*D	B*E	A*E	**E** Flywheel min/max inertia	Axle ring gear	Axle flange	2nd shaft rear	2nd shaft centre	2nd shaft front	1st shaft rear	1st shaft centre	1st shaft front	Transmission flange	
1	-	-	+	-	+	+	-	-	+	+	-	+	-	-	+	139	233	67	55	47	47	66	48	162	864
2	+	-	-	-	-	+	+	-	-	+	+	+	+	-	-	199	242	121	117	99	89	113	117	511	1608
3	-	+	-	-	+	-	+	-	+	-	+	+	-	+	-	199	240	134	114	91	85	92	101	242	1298
4	+	+	+	-	-	-	-	-	-	-	-	+	+	+	+	171	206	104	111	79	113	118	77	270	1249
5	-	-	+	+	-	-	+	-	+	+	-	-	+	+	-	132	232	81	80	43	33	48	42	65	756
6	+	-	-	+	+	-	-	-	-	+	+	-	-	+	+	195	243	111	117	79	68	78	91	90	1072
7	-	+	-	+	-	+	-	-	+	-	+	-	+	-	+	121	236	44	42	56	20	37	23	47	626
8	+	+	+	+	+	+	+	-	-	-	-	-	-	-	-	198	235	114	94	106	79	87	53	97	1063
9	-	-	+	-	+	+	-	+	-	-	+	-	+	+	-	53	232	34	58	32	40	55	69	316	889
10	+	-	-	-	-	+	+	+	+	-	-	-	-	+	+	63	285	36	38	47	74	108	106	271	1028
11	-	+	-	-	+	-	+	+	-	+	-	-	+	-	+	9	45	8	10	10	16	26	21	86	231
12	+	+	+	-	-	-	-	+	+	+	+	-	-	-	-	57	301	43	83	40	71	99	89	286	1069
13	-	-	+	+	-	-	+	+	-	-	+	+	-	-	+	2	42	12	9	9	19	24	21	73	211
14	+	-	-	+	+	-	-	+	+	-	-	+	+	-	-	50	98	29	33	23	68	49	49	220	619
15	-	+	-	+	-	+	-	+	-	+	-	+	-	+	-	25	63	12	12	8	15	35	23	39	232
16	+	+	+	+	+	+	+	+	+	+	+	+	+	+	+	25	40	21	18	9	21	32	23	42	231
																1638	2973	971	991	778	858	1067	953	2817	Sums

Table 6.1 Orthogonal test array with response

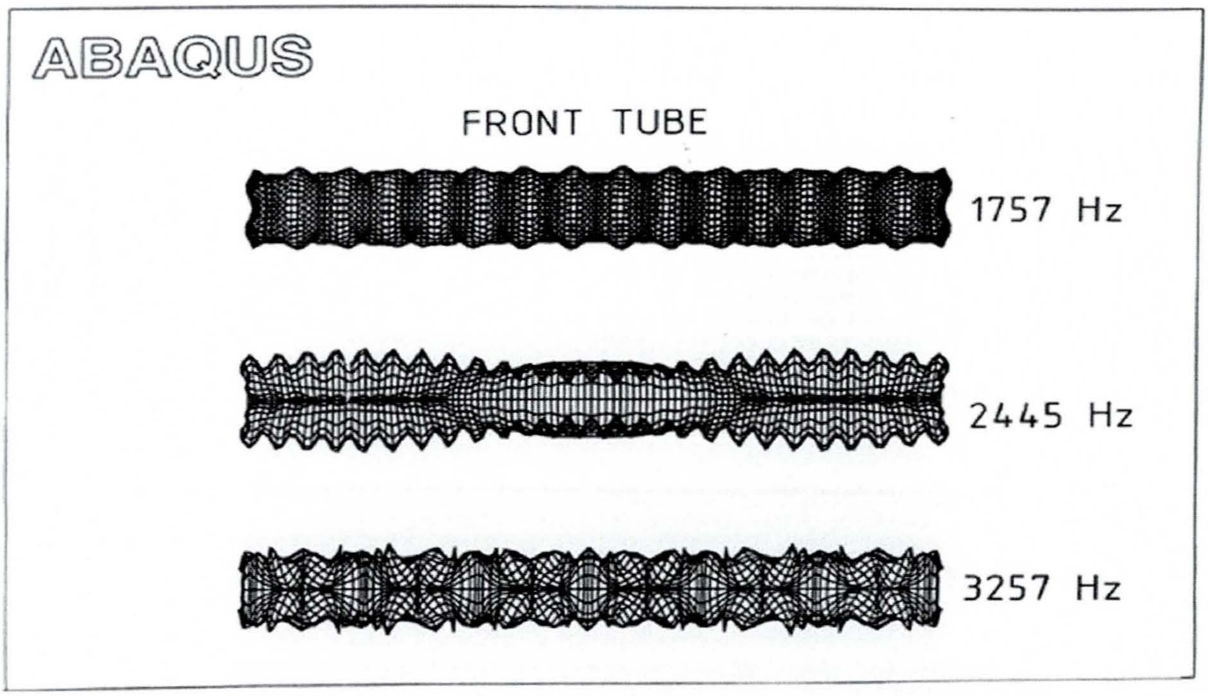

Figure 6.1 High frequency of structural modes of the front tube

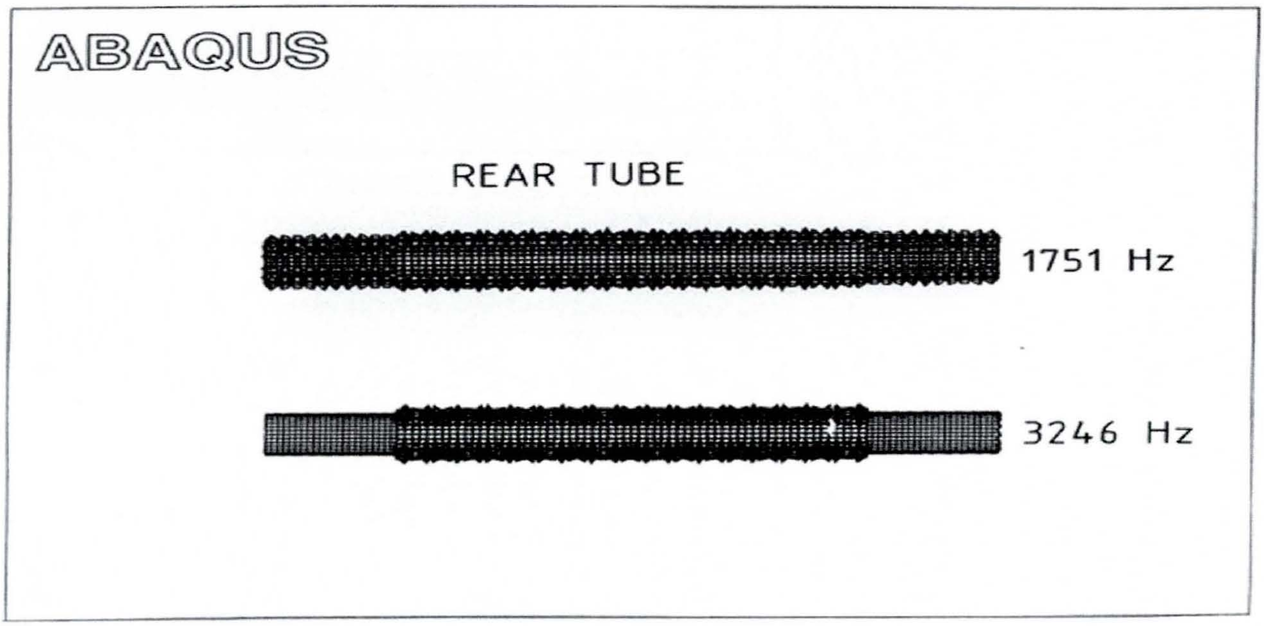

Figure 6.2 High frequency of structural modes of the rear tube

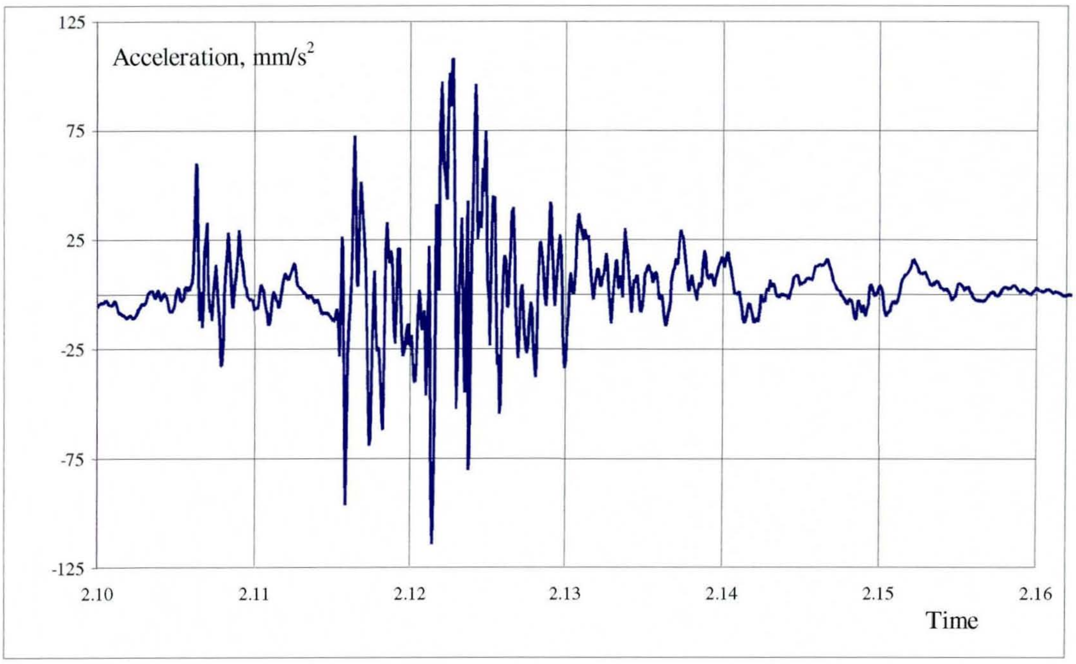

Figure 6.3 Time history of the 2nd shaft centre location for Run 3

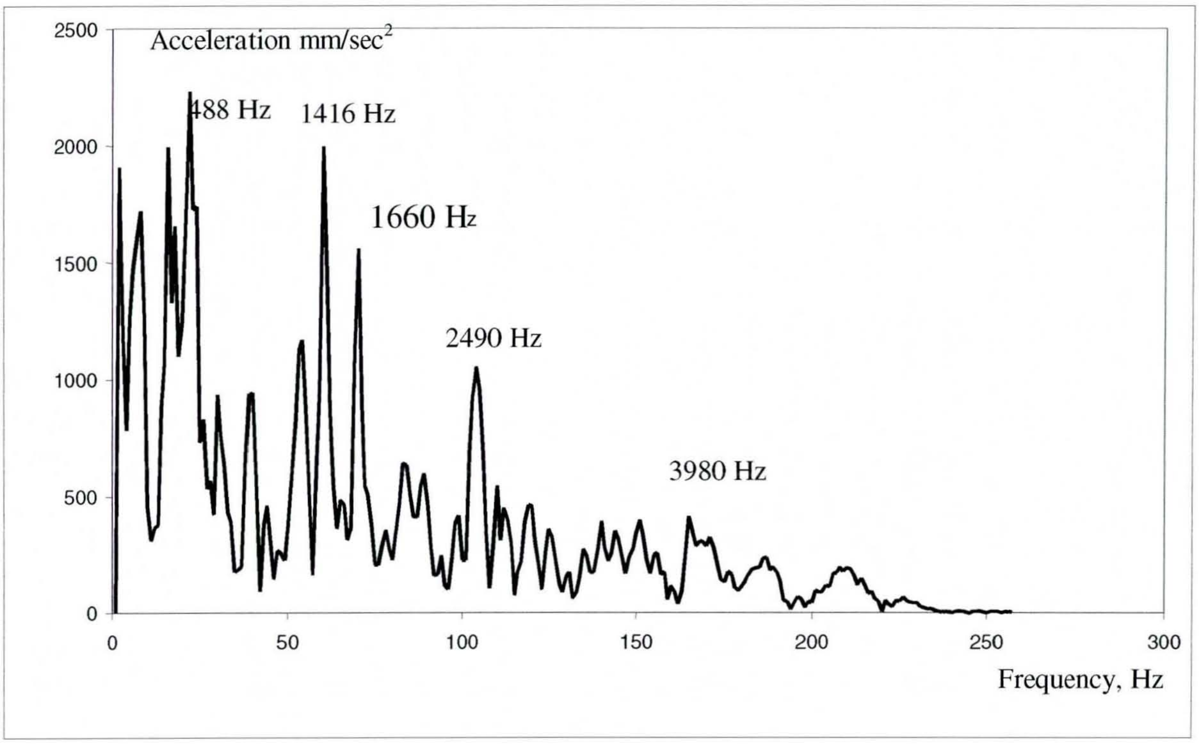

Figure 6.4 Frequency response of the 2nd shaft centre Run 3

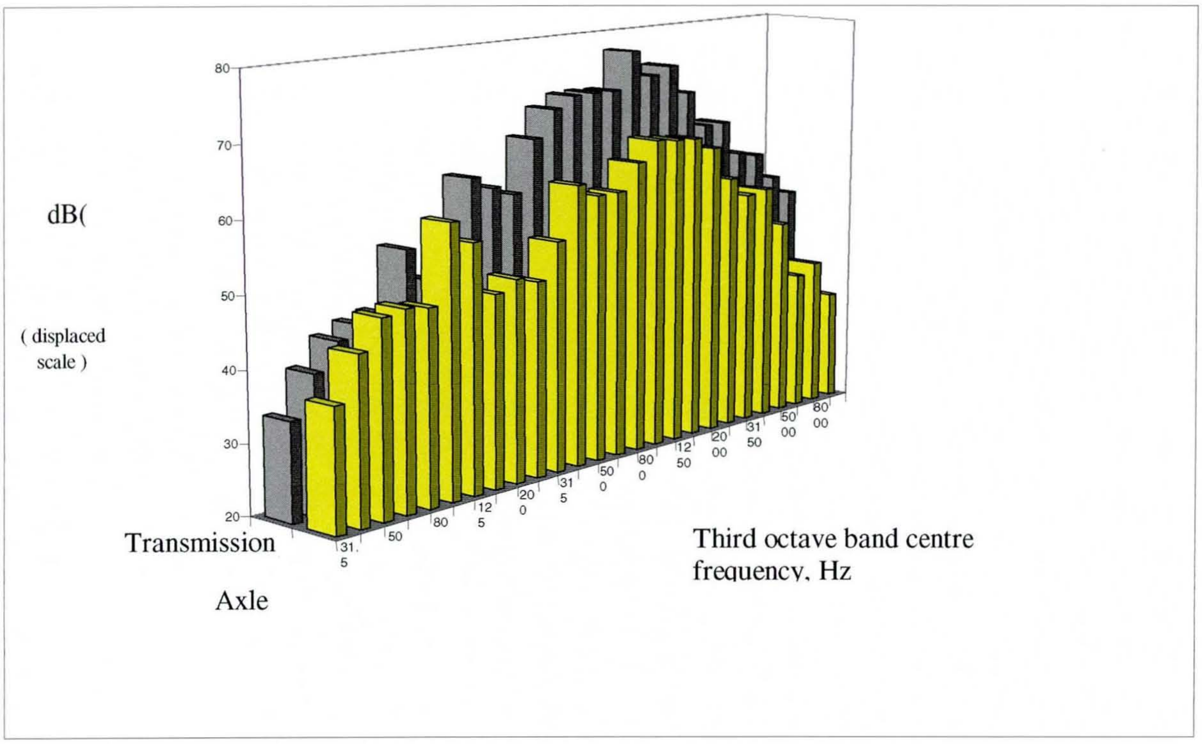

Figure 6.5 Comparison of clonk noise at transmission and rear axle

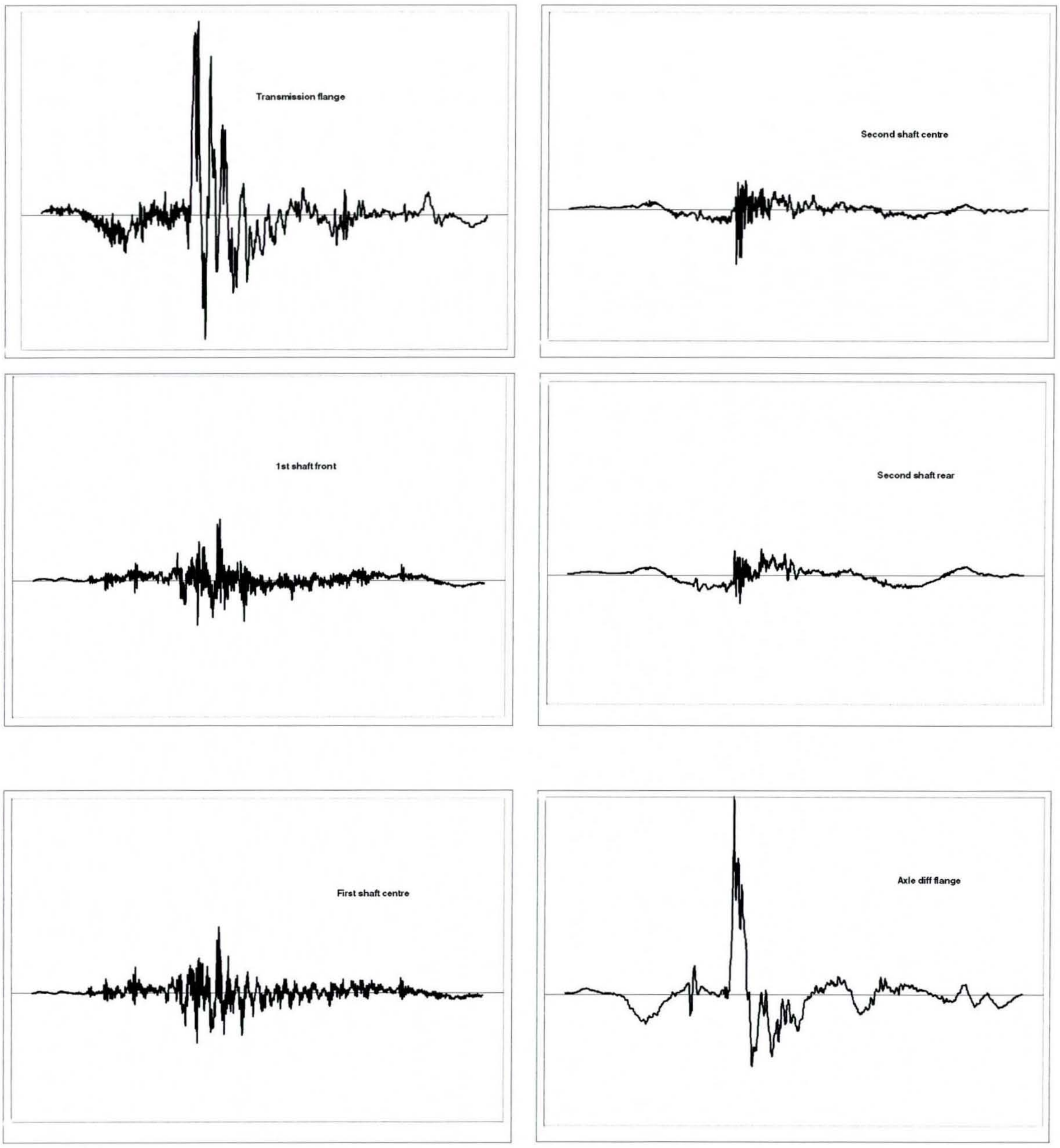
Transmission flange
Second shaft centre
1st shaft front
Second shaft rear
First shaft centre
Axle diff flange

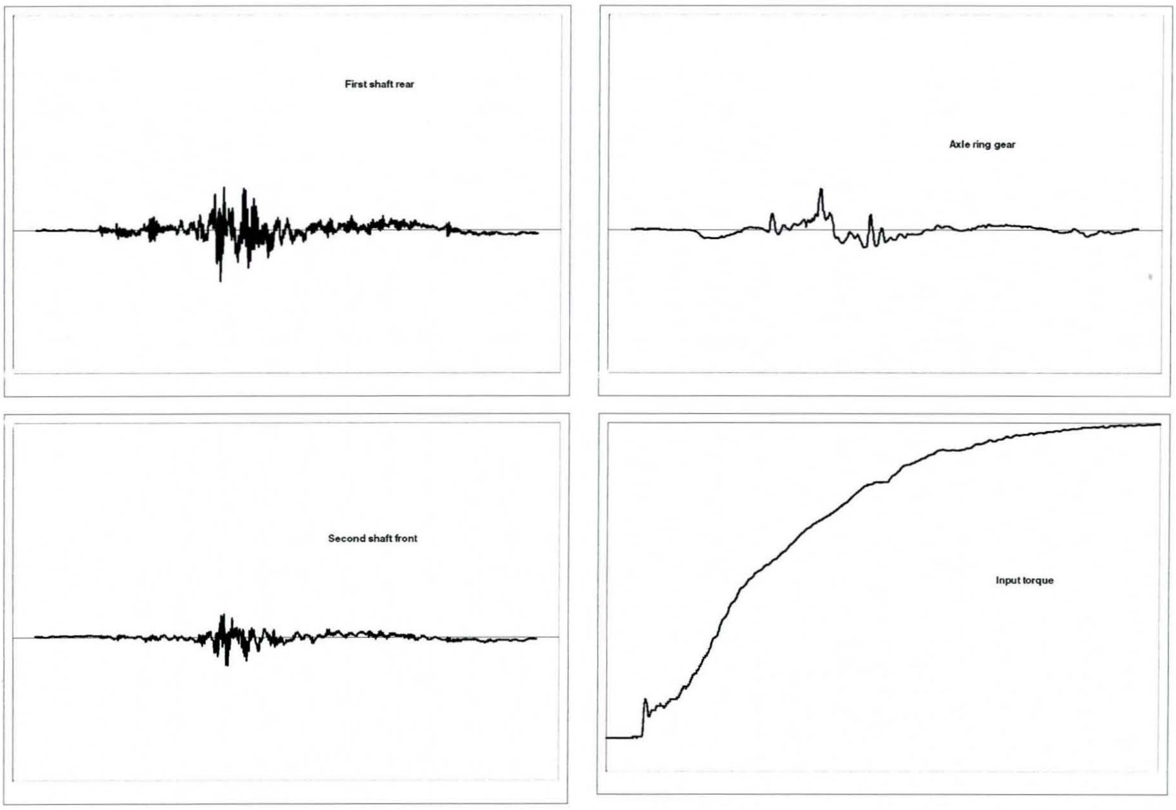

Figure 6.6 Driveline pick-up acceleration responses versus time, and input torque profile

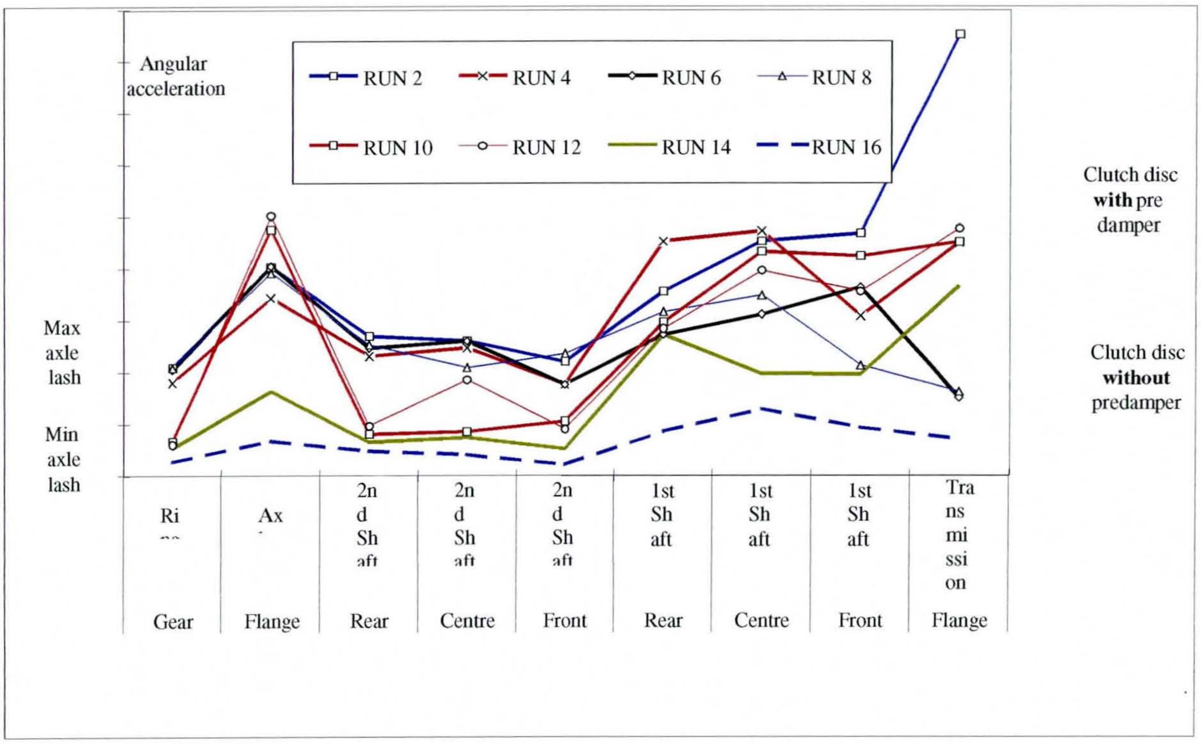

Figure 6.7 Peak acceleration responses for each driveline pick-up at 150 Nm impulse torque, showing clutch pre damper and axle lash effects

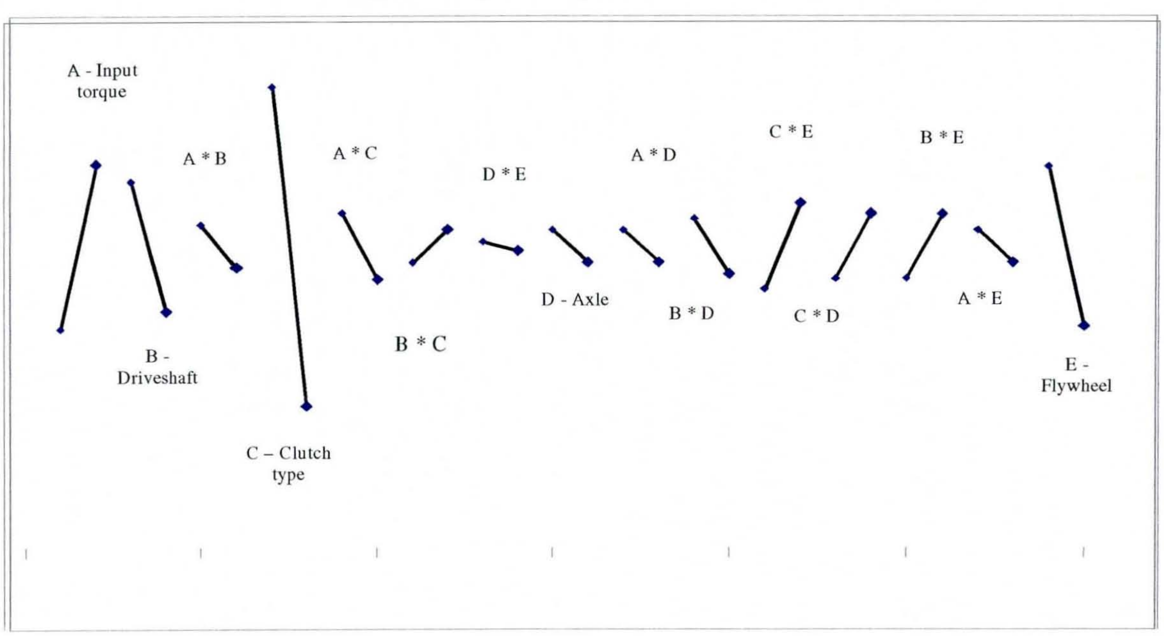

Figure 6.8 Factor effects plot response at transmission flange

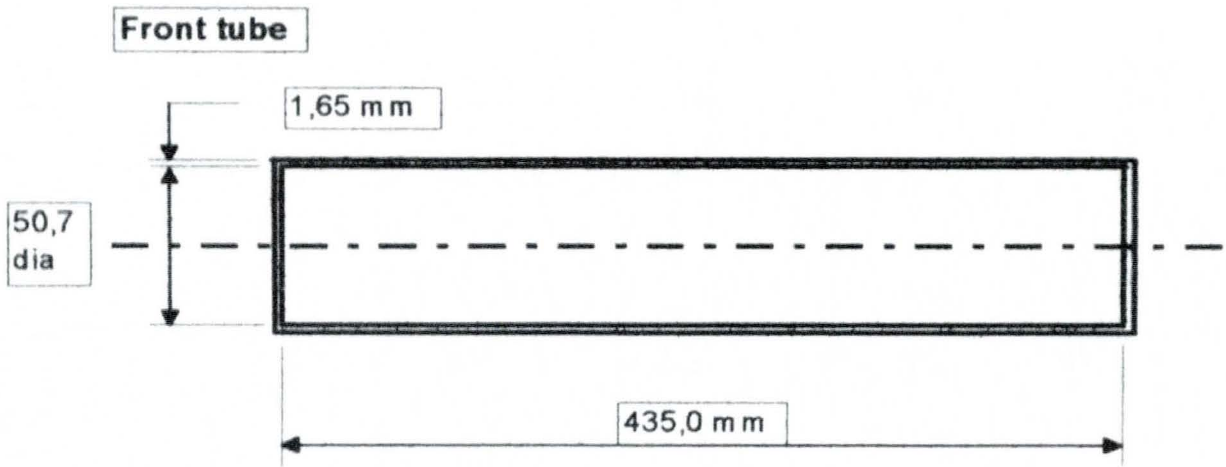

Figure 6.9 Front drive shaft parallel tube main dimensions

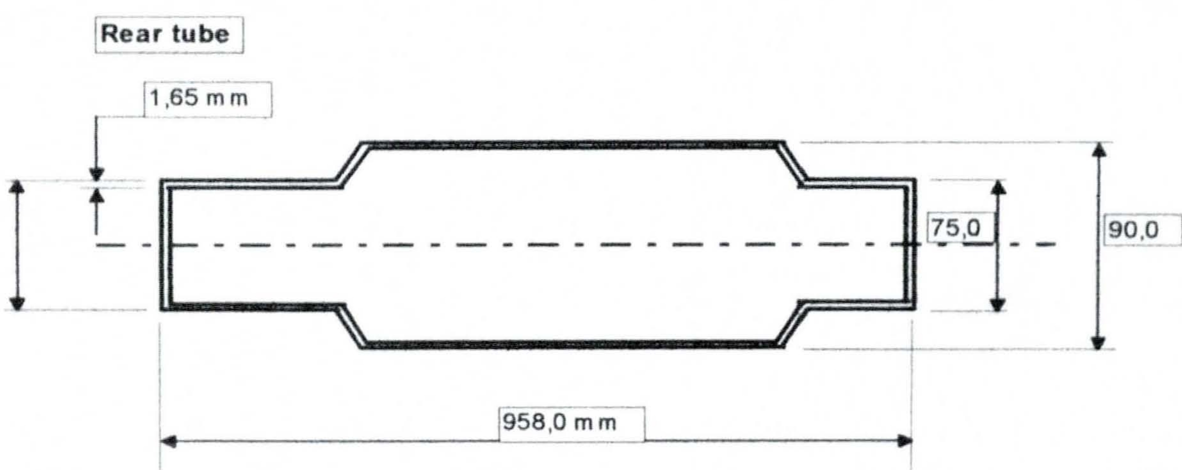

Figure 6.10 Rear driveshaft swaged tube main dimensions

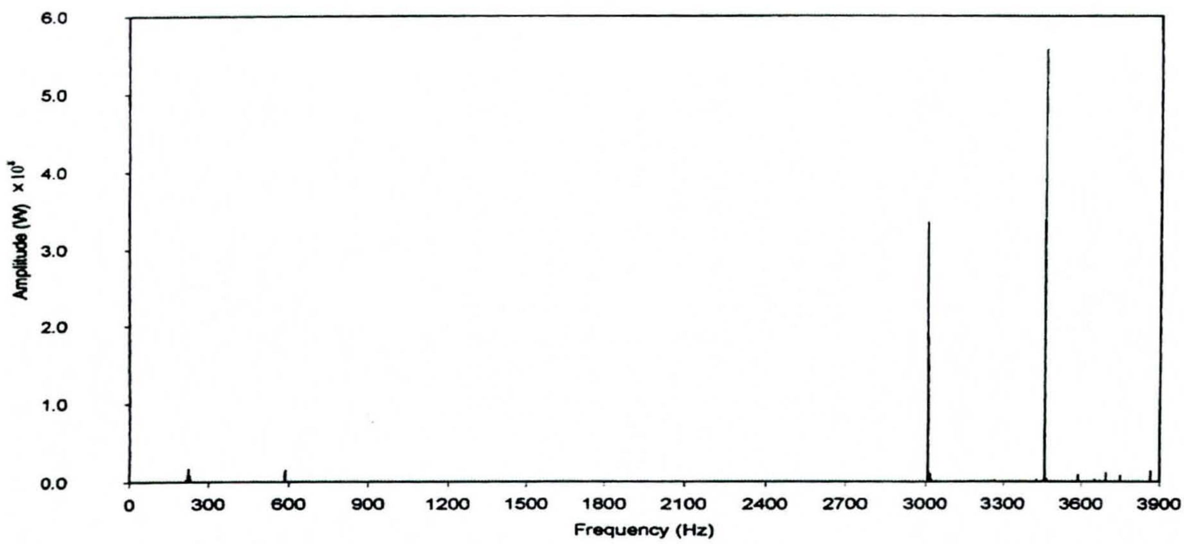

Figure 6.11 Structural response spectrum of the front driveshaft tube

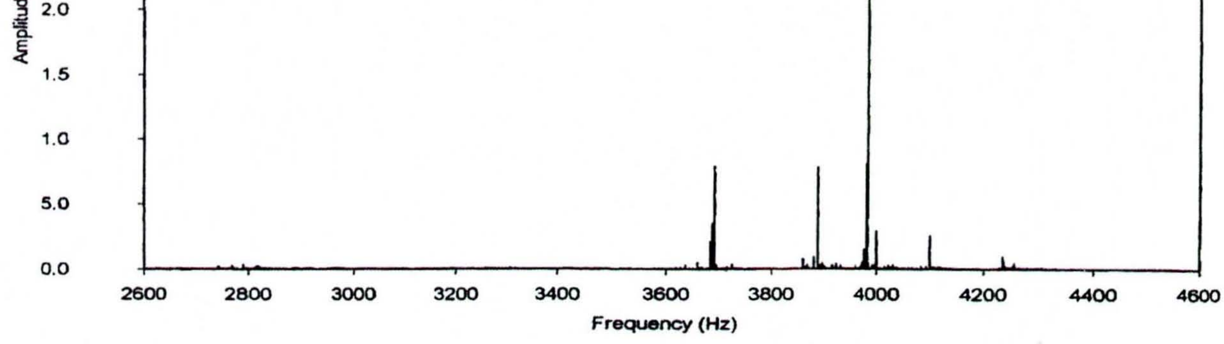

Figure 6.12 Higher mode in Structural response spectrum of the rear driveshaft tube

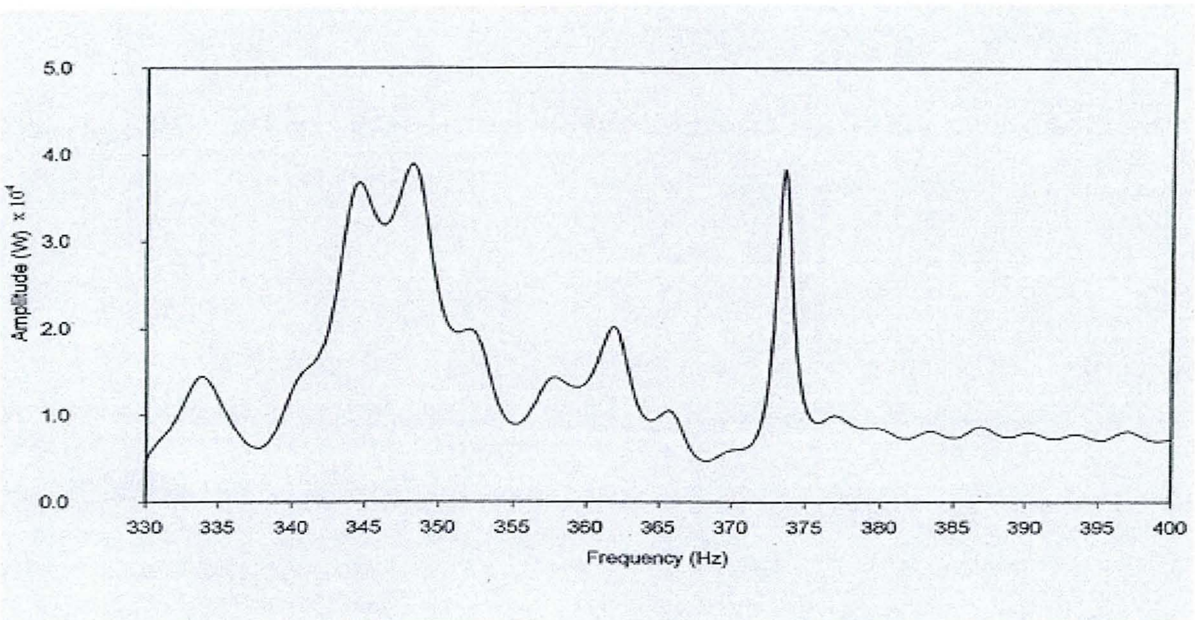

Figure 6.13 Low frequency spectrum of a driveshaft tube

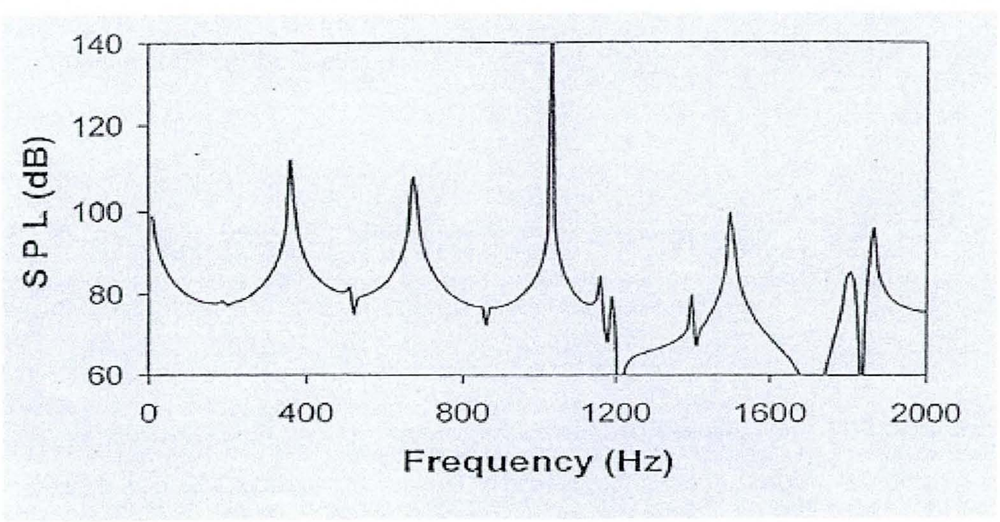

Figure 6.14 Predicted acoustic modes in planar sound propagation in a driveshaft tube

FRONT DRIVESHAFT		REAR DRIVESHAFT			
STRUCTURE	FLUID	STRUCTURE	FLUID	STRUCTURE	FLUID
1393.6	0.0	487.2	0.0	2995.4	2940.7
1393.7	381.1	487.2	190.8	3070.4	2941.5
1949.6	764.2	610.6	360.0	3070.6	2990.1
1950.5	1151.1	610.6	510.4	3074.8	**3016.7**
2357.5	1544.0	934.3	671.3	3212.3	**3016.8**
2357.9	1944.6	943.0	856.8	3215.1	3152.1
3233.8	2355.2	1165.4	1050.5	3216.1	3157.4
3234.3	2777.5	1184.0	**1228.5**	3216.3	3160.7
3302.5	2875.6	**1209.4**	1382.9	3454.6	3301.0
3302.8	2900.7	**1210.8**	1538.1	3455.0	3304.1
3373.5	2975.4	1365.6	1717.5	**3464.2**	3324.7
	3097.4	1378.5	1912.3	**3467.6**	3432.0
	3213.5	1387.6	2099.3	3533.6	3433.3
	3263.9	1557.2	**2176.9**	3562.9	3508.9
	3471.4	1557.2	**2178.1**	**3782.7**	**3537.4**
	3664.8	1631.8	2212.6	**3792.6**	**3539.4**
	3717.0	1632.0	2213.5	**3798.4**	3652.0
	3997.9	1855.7	2262.1	**3799.1**	3658.8
		1855.7	2275.0	**3855.9**	3697.7
		2034.9	2275.6	**3946.8**	3704.2
		2035.6	2359.7	**4007.9**	3705.5
		2069.7	2360.1		3714.5
		2073.7	2416.5		3719.1
		2206.0	2467.6		**3748.6**
		2278.3	2469.2		3761.0
		2279.3	2583.3		**3805.5**
		2855.3	2583.9		**3822.5**
		2855.7	2592.6		3844.2
		2876.7	2630.7		3848.8
		2881.0	2632.3		**3888.1**
		2895.7	2649.0		**3899.6**
		2904.8	2650.9		3918.8
		2921.8	2746.4		3981.0
		2922.3	2747.0		**3993.8**
		2963.9	2793.8		4010.8
		2964.1	2864.8		
		2995.2	28676.5		

Table 6.2 Table of structural and acoustic eigen-modes for front and rear tubes

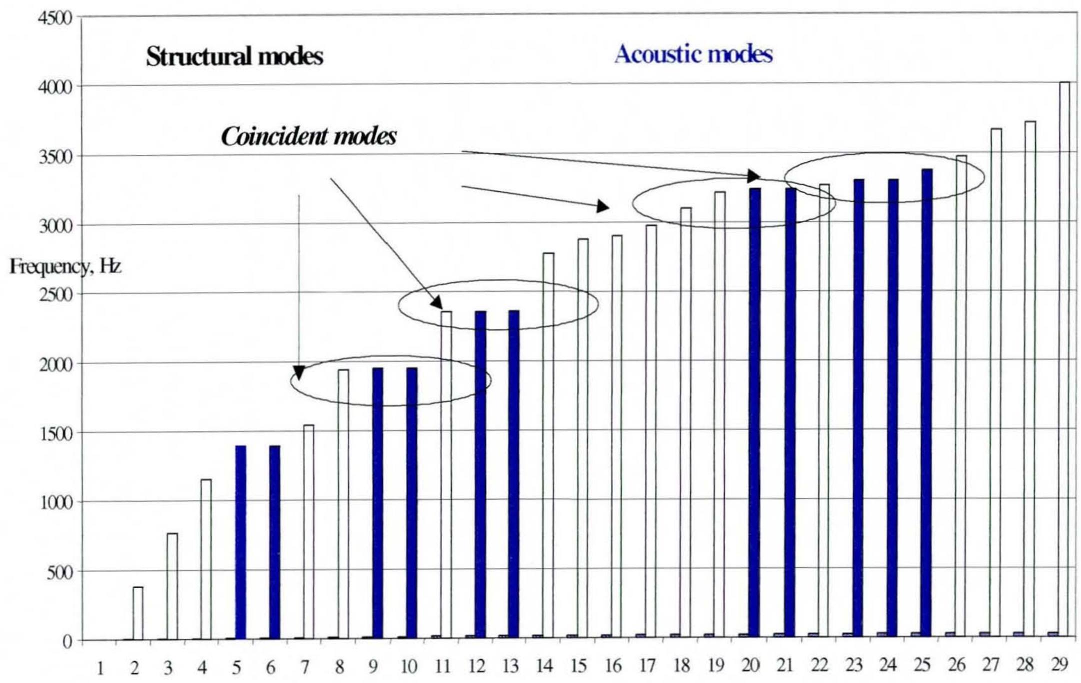

Fig 6.15 Front driveshaft tube structural and acoustic modes and coincidence.

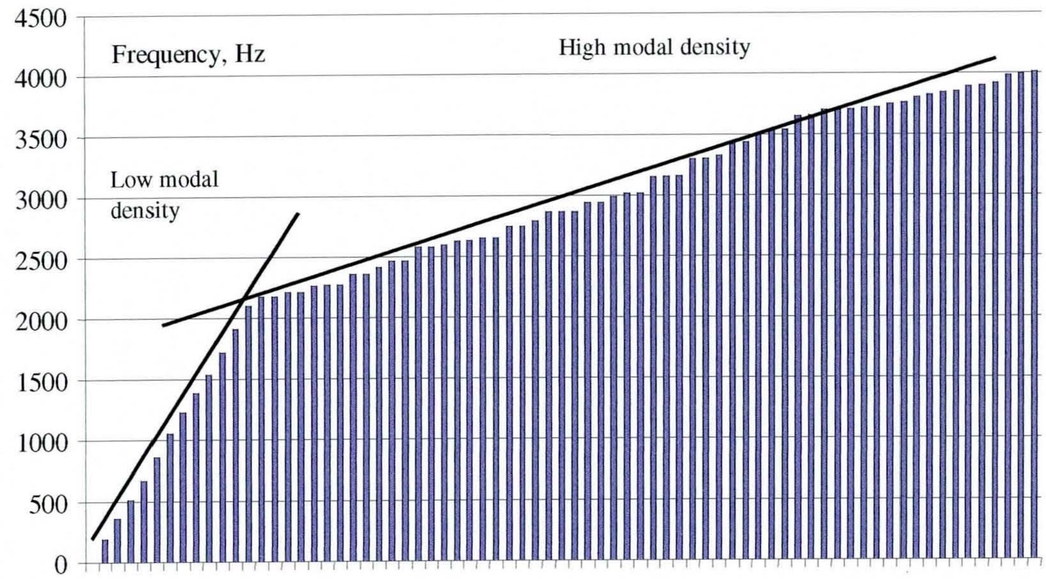

Figure 6.16 Rear shaft acoustic modes

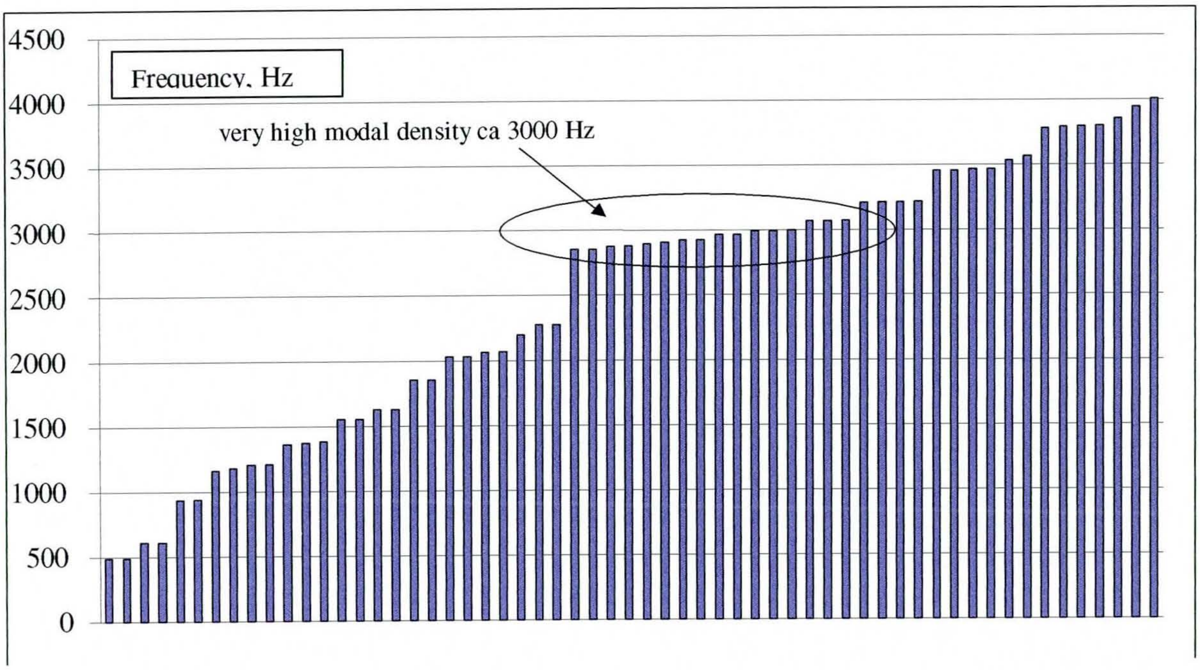

Figure 6.17 Structural modes – rear tube

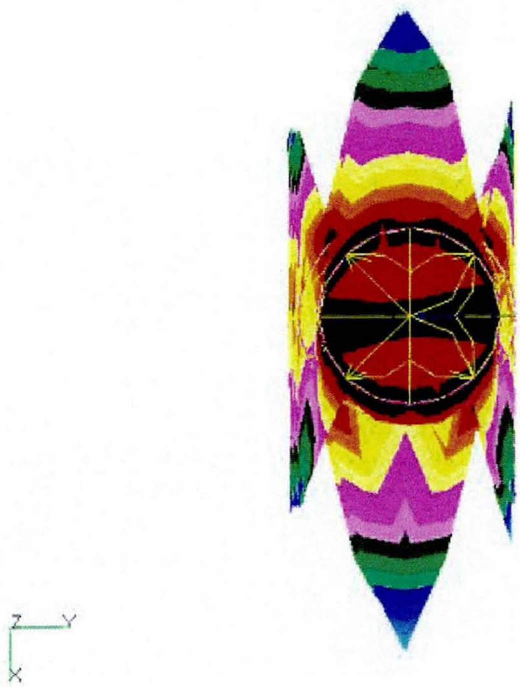

Figure 6.18 End view of acoustic mode at 3947 Hz

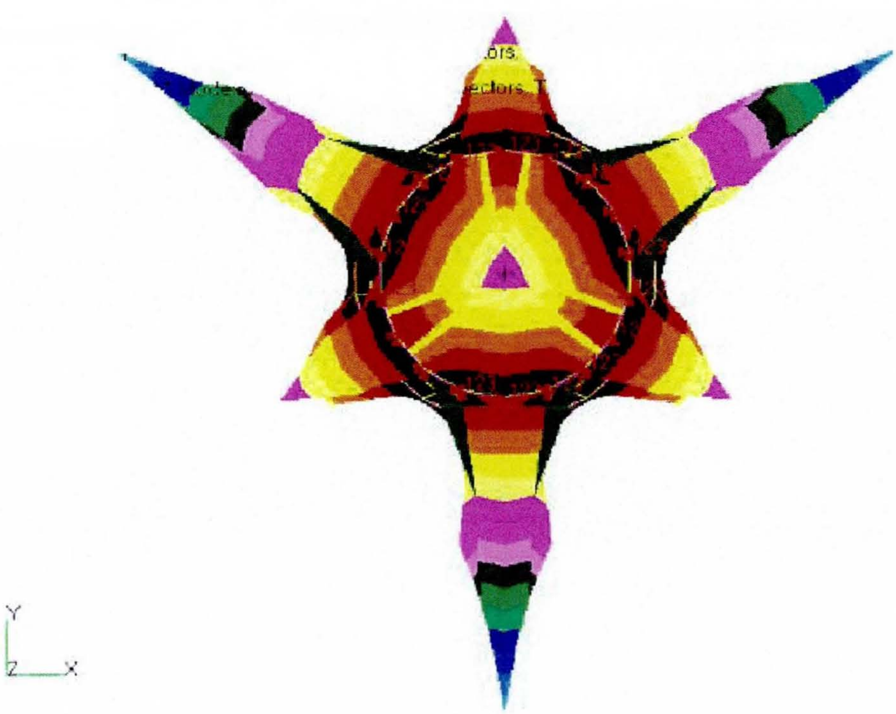

Figure 6.19 End view of structure mode at 3946 Hz

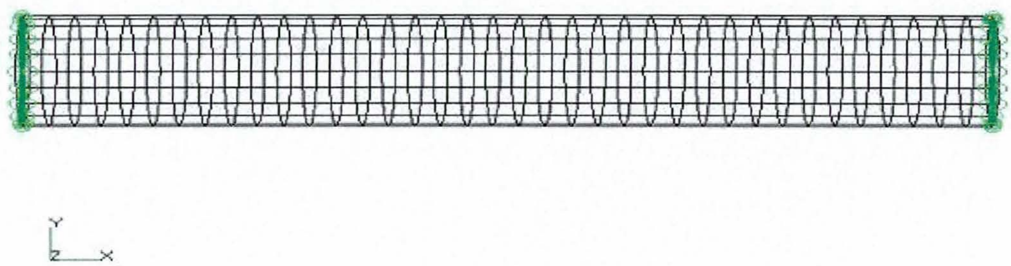

Figure 6.20 Drive shaft tube mesh – longitudinal view

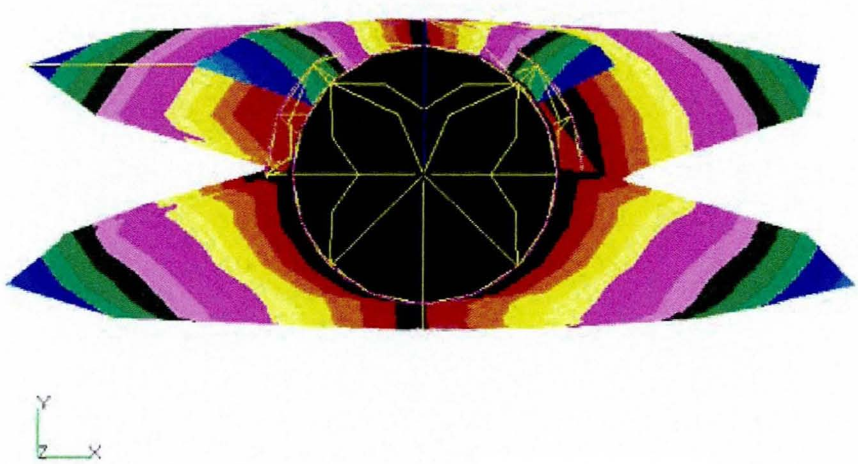

Figure 6.21 End view of acoustic mode at 3748 Hz (rear tube)

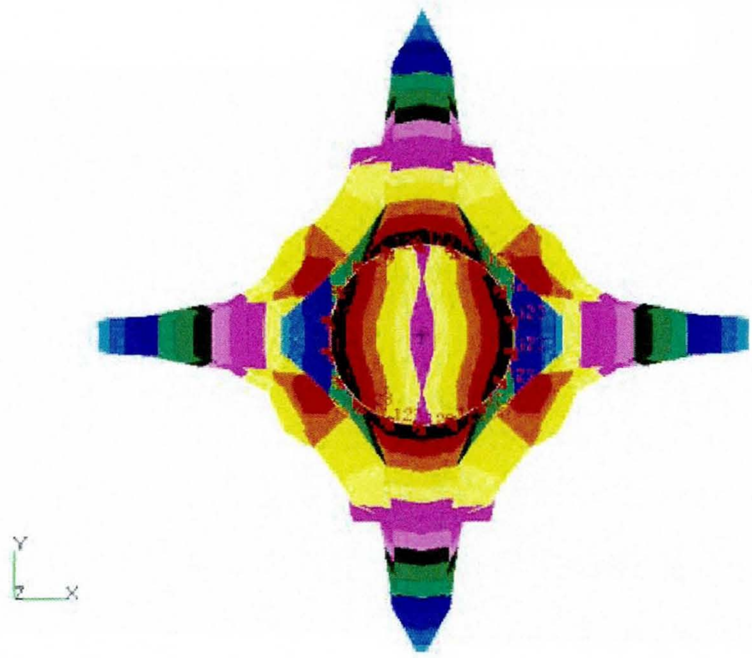

Figure 6.22 End view of structural mode at 3782 Hz (rear tube)

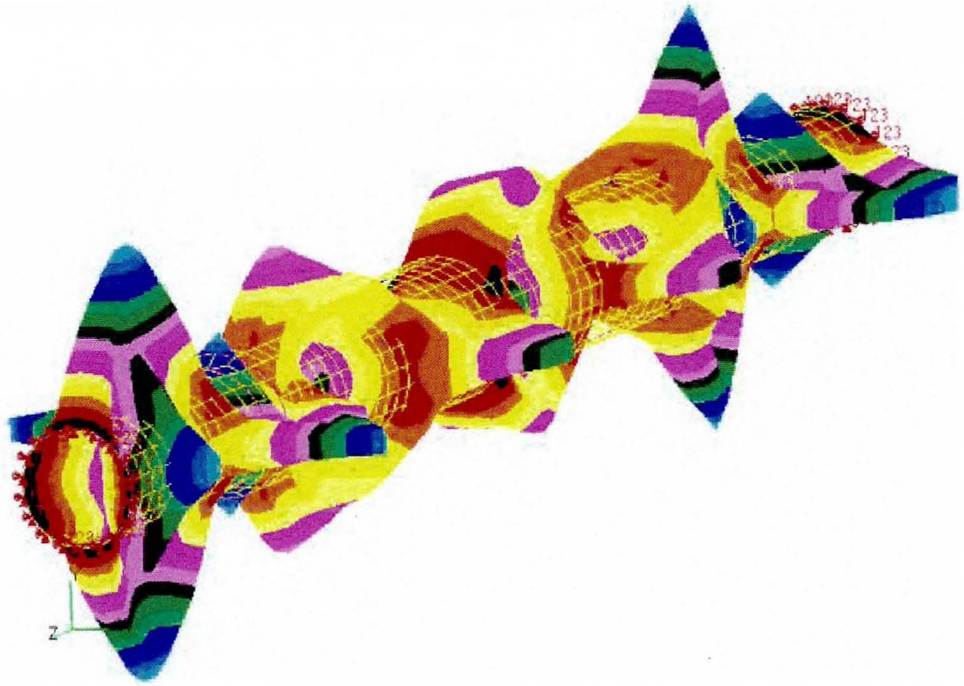

Figure 6.23 Longitudinal view of structural mode at 3782 Hz (rear tube)

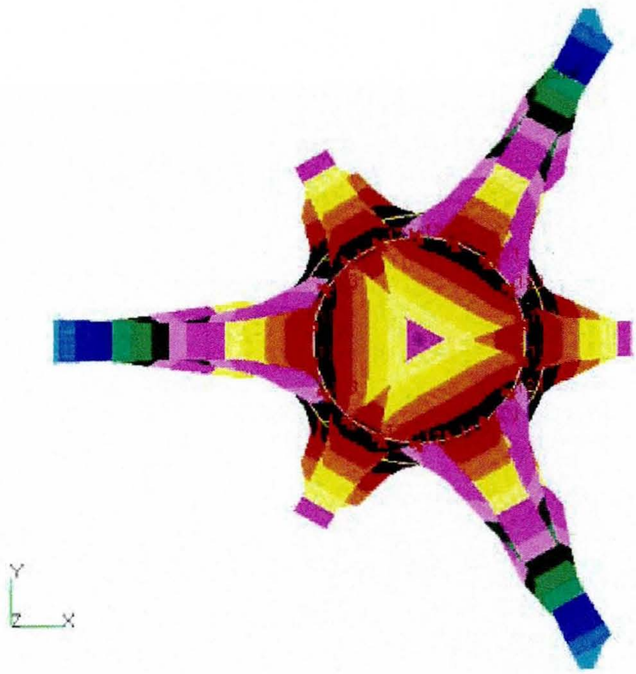

Figure 6.24 End view of structural mode at 3856 Hz (rear tube)

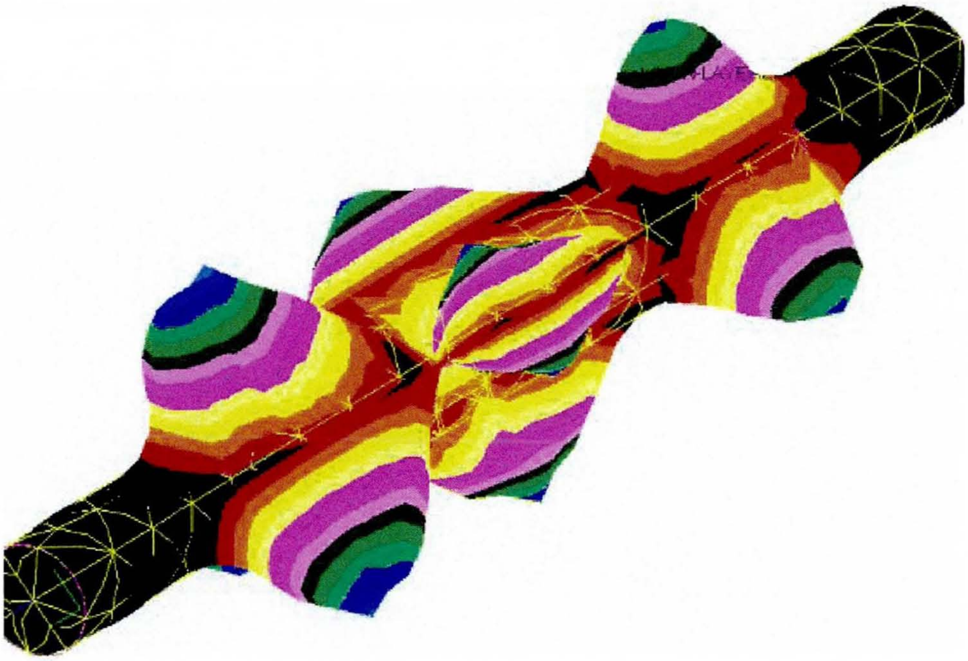

Figure 6.25 Longitudinal view of structural mode at 3856 Hz (rear tube)

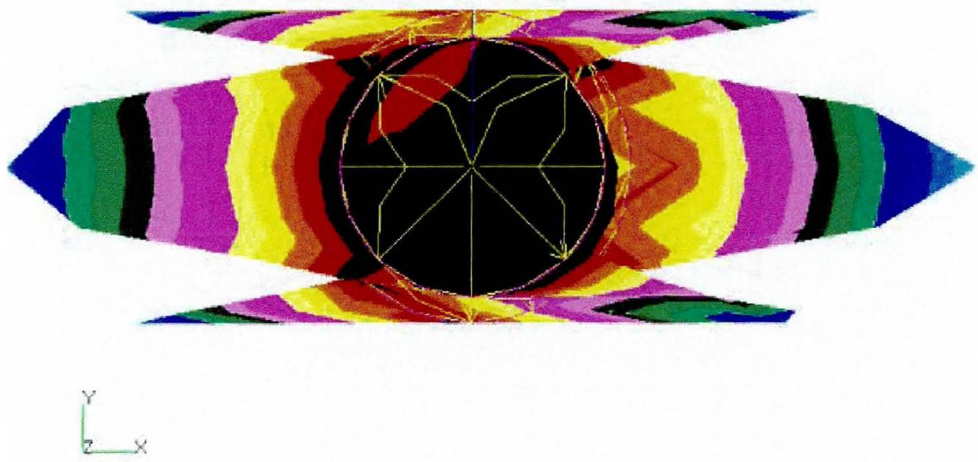

Figure 6.26 End view of acoustic mode at 3899 Hz (rear tube)

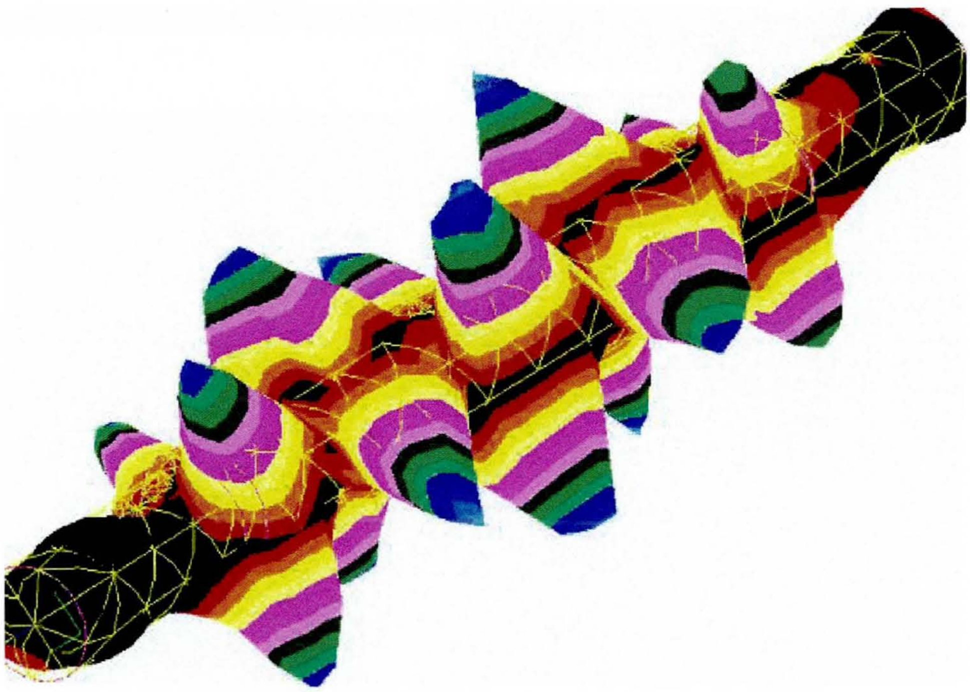

Figure 6.27 Longitudinal view of acoustic mode at 3899 Hz (rear tube)

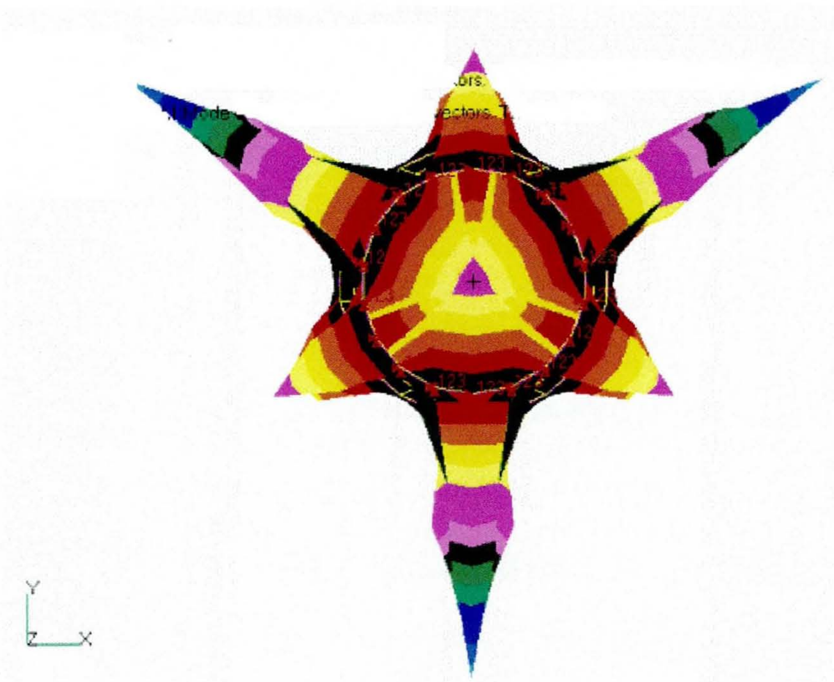

Figure 6.28 End view of structural mode at 3946 Hz (rear tube)

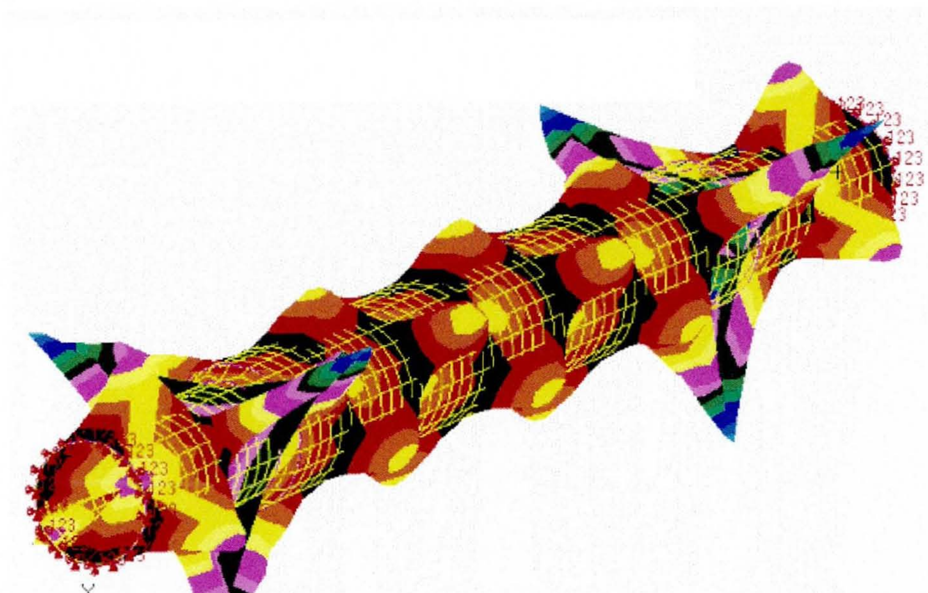

Figure 6.29 Longitudinal view of structural mode at 3946 Hz (rear tube)

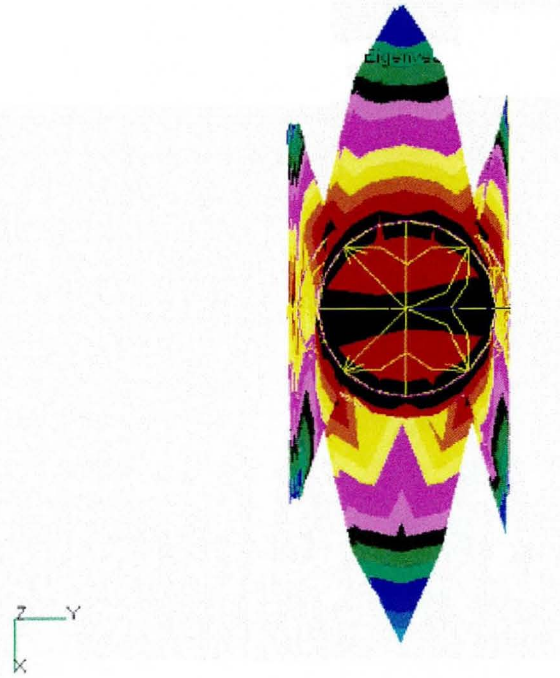

Figure 6.30 End view of acoustic mode at 3993 Hz (rear tube)

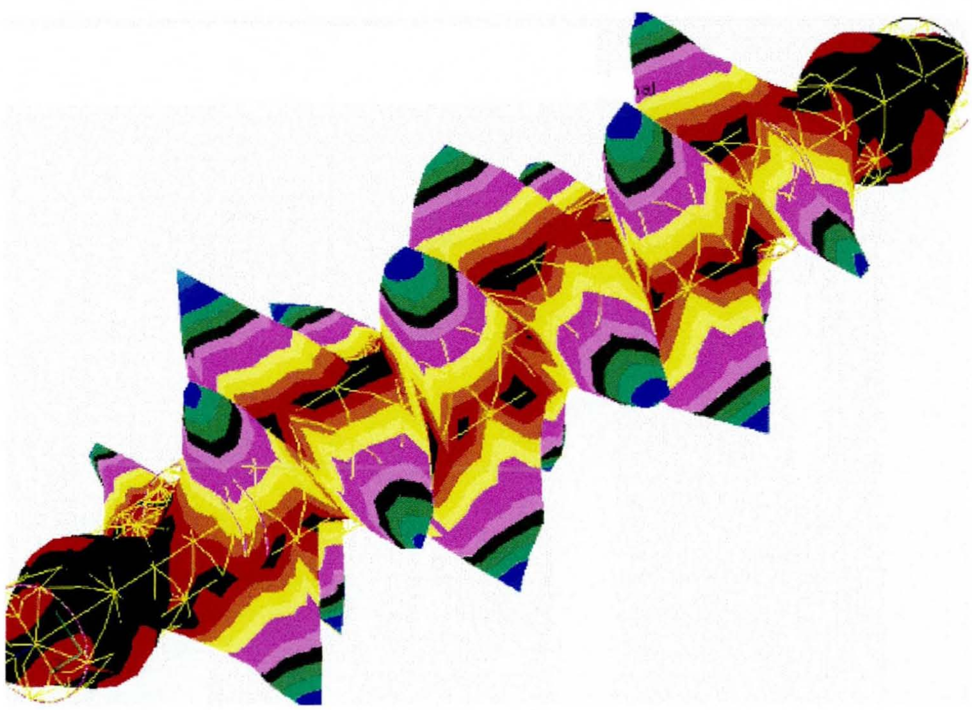

Figure 6.31 Longitudinal view of acoustic mode at 3993 Hz (rear tube)

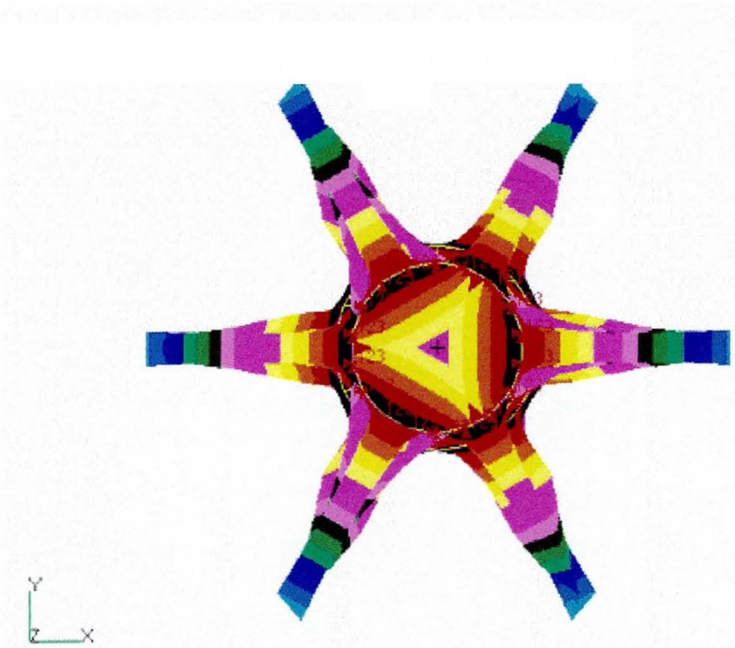

Figure 6.32 End view of structural mode at 4008 Hz (rear tube)

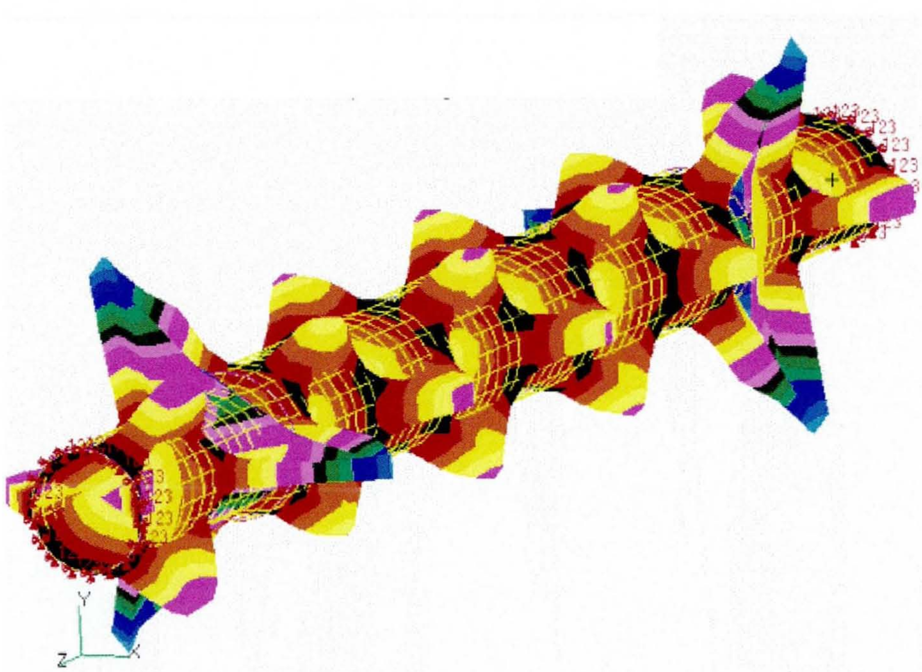

Figure 6.33 Longitudinal view of structural mode at 4008 Hz (rear tube)

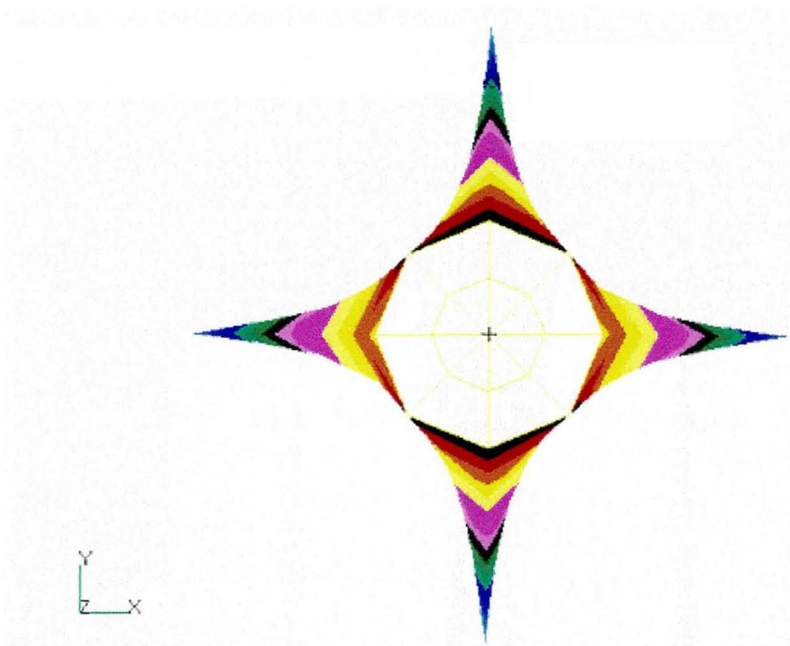

Figure 6.34 End view of acoustic mode at 3233 Hz (front tube)

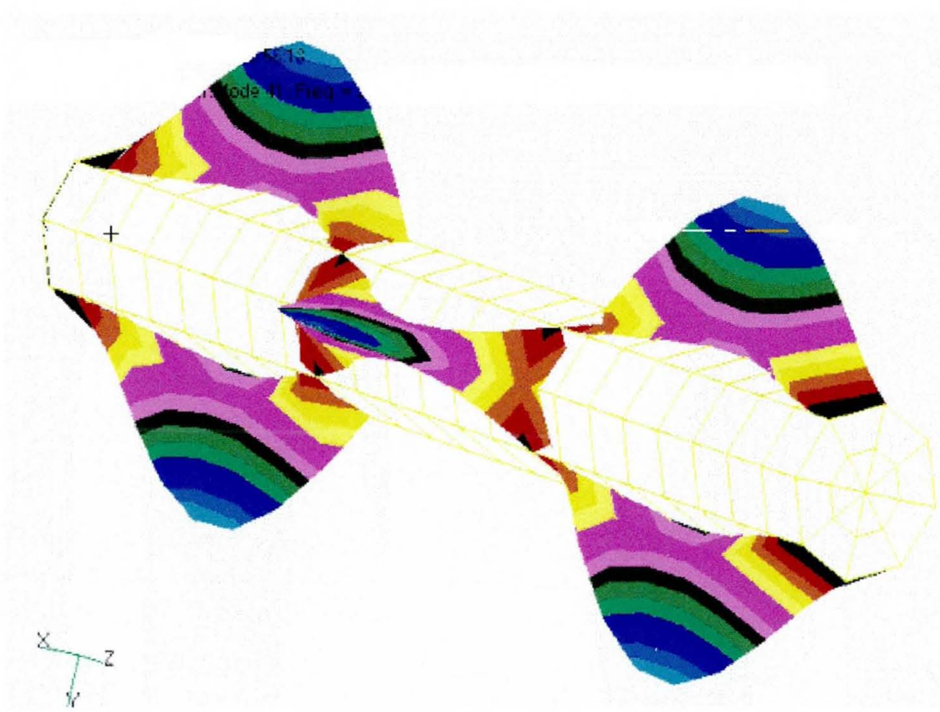

Figure 6.35 Longitudinal view of acoustic mode at 3233 Hz (front tube)

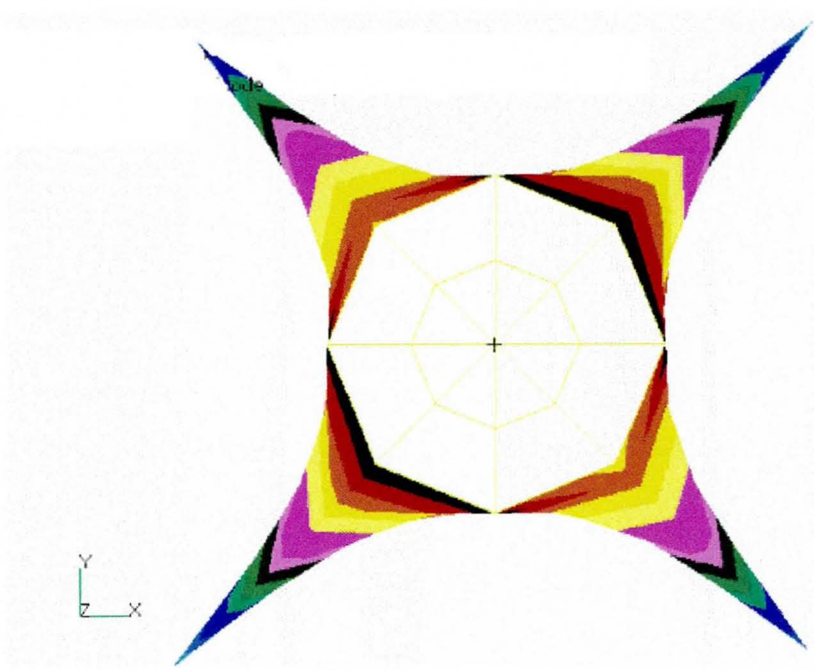

Figure 6.36 End view of acoustic mode at 3268 Hz (front tube)

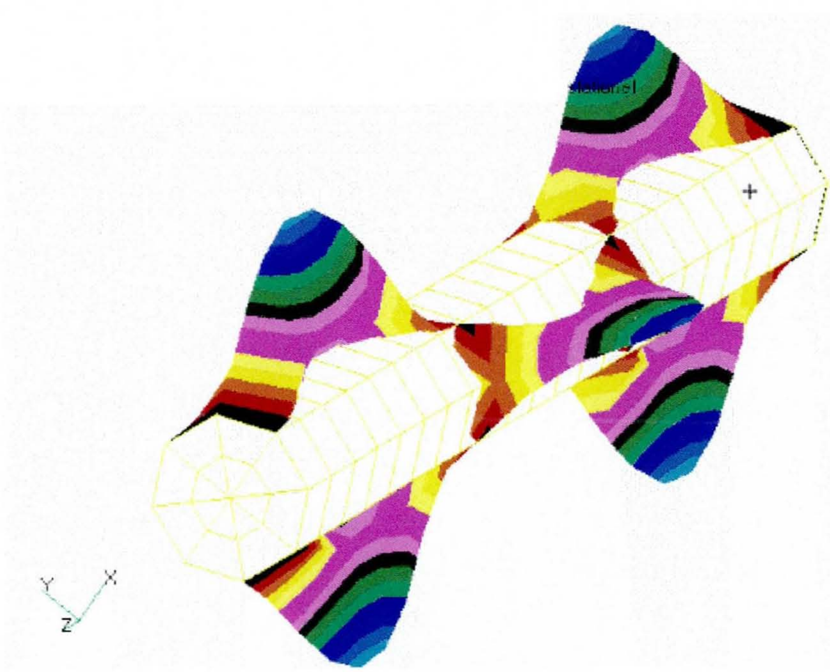

Figure 6.37 Longitudinal view of acoustic mode at 3268 Hz (front tube)

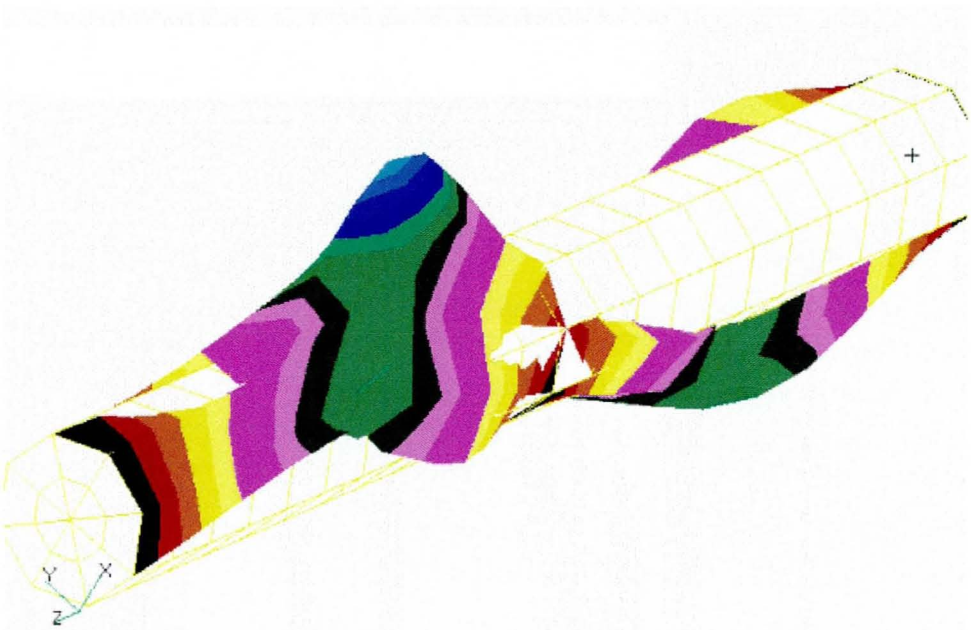

Figure 6.38 Longitudinal view of acoustic mode at 3468 Hz (front tube)

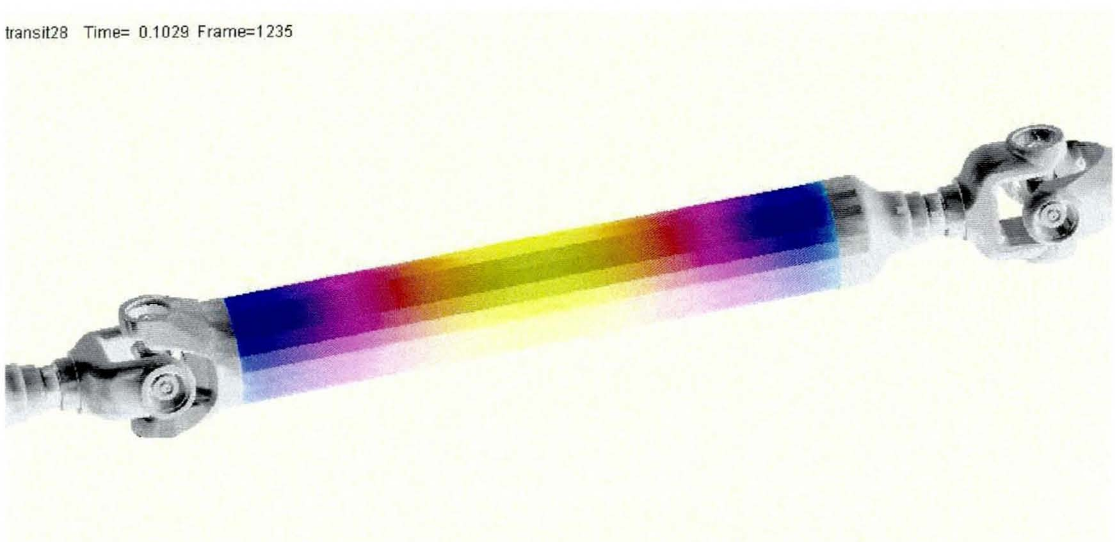

Figure 6.39 Wave propagation in the middle driveshaft tube

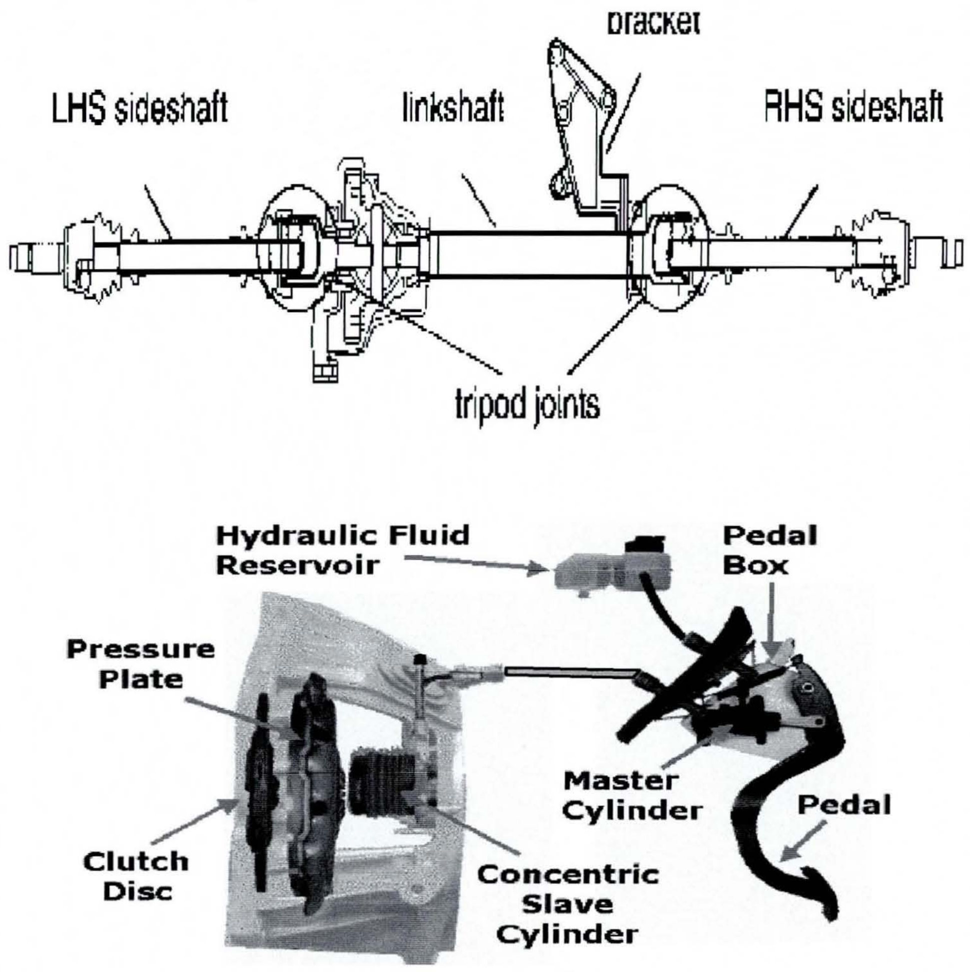

Fig 6.40 Schematics of FWD powertrain layout

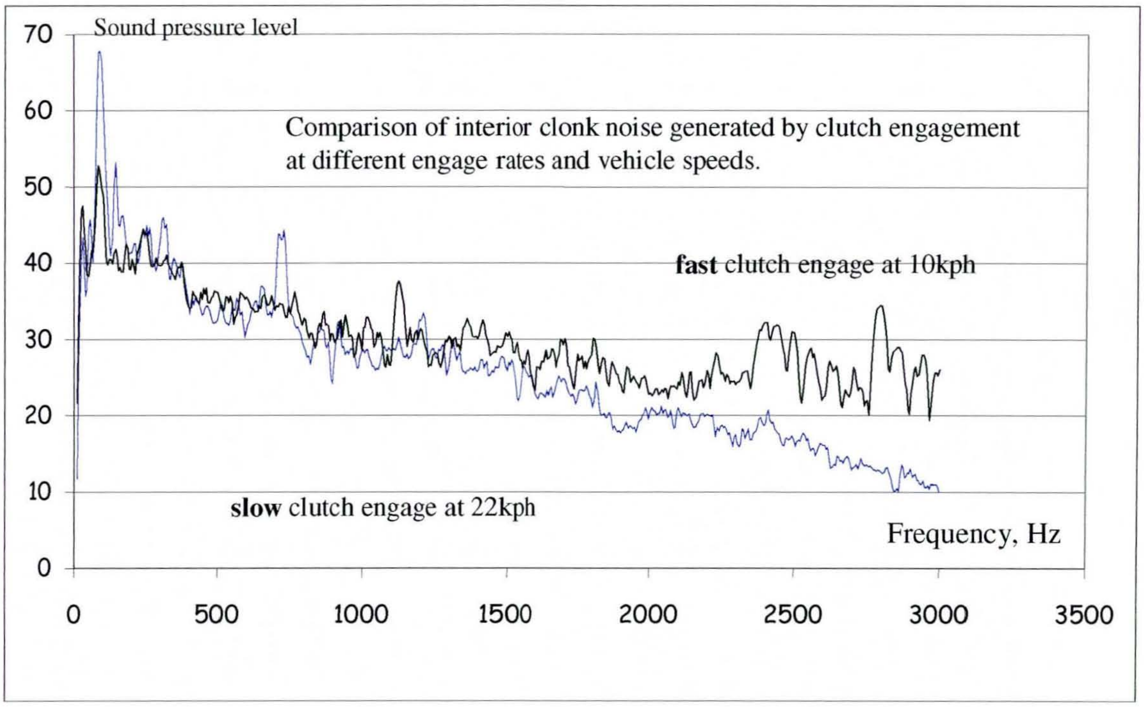

Figure 6.41 Interior clonk noise with two drive conditions

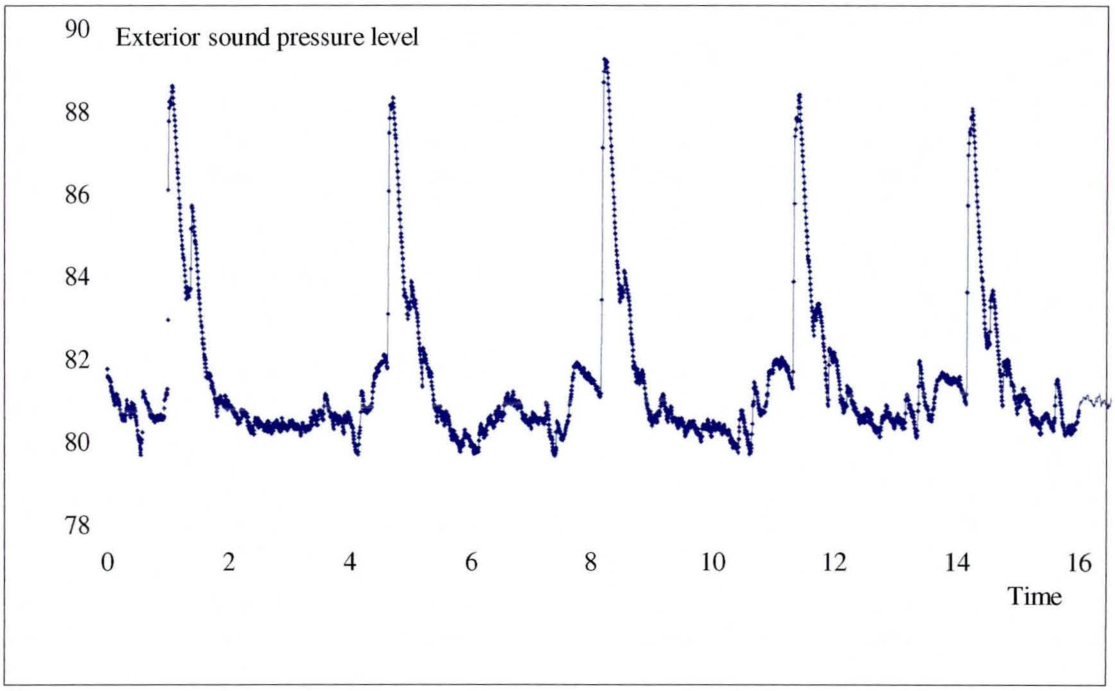

Figure 6.42 Five consecutive clonk

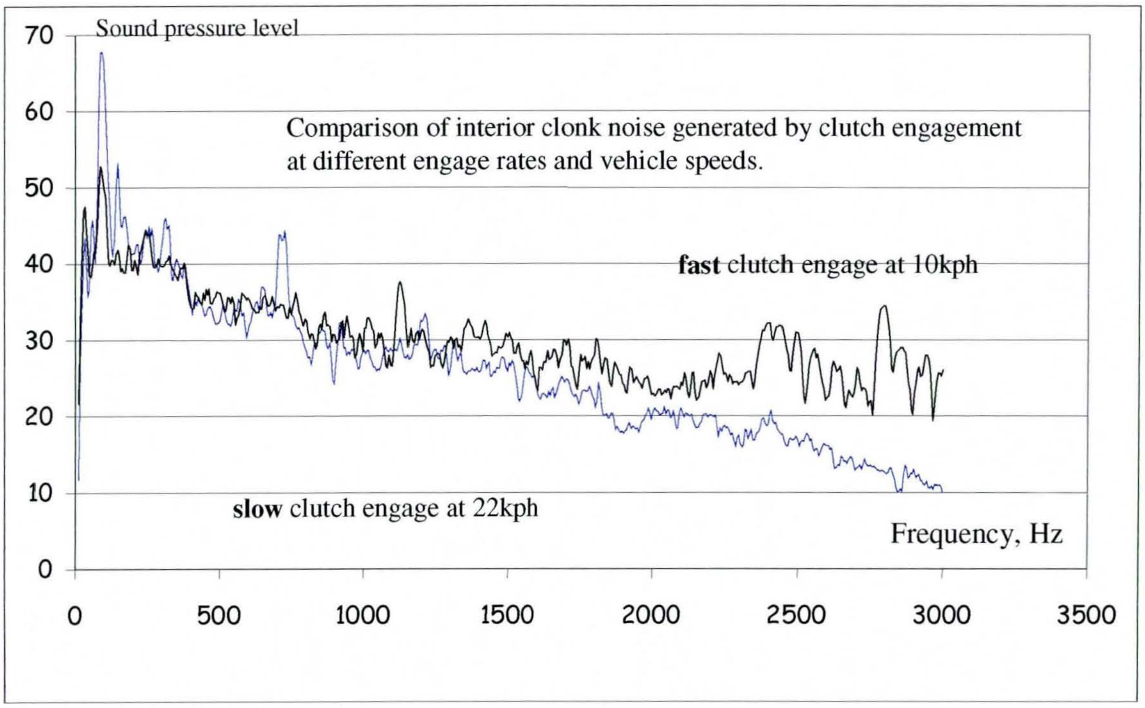

Figure 6.41 Interior clonk noise with two drive conditions

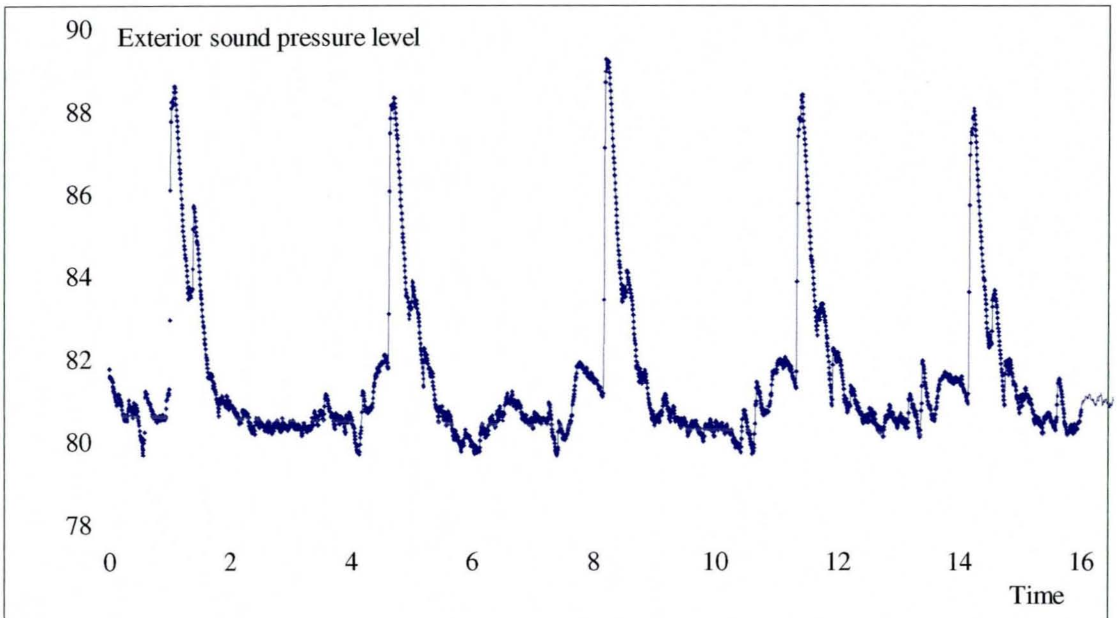

Figure 6.42 Five consecutive clonk

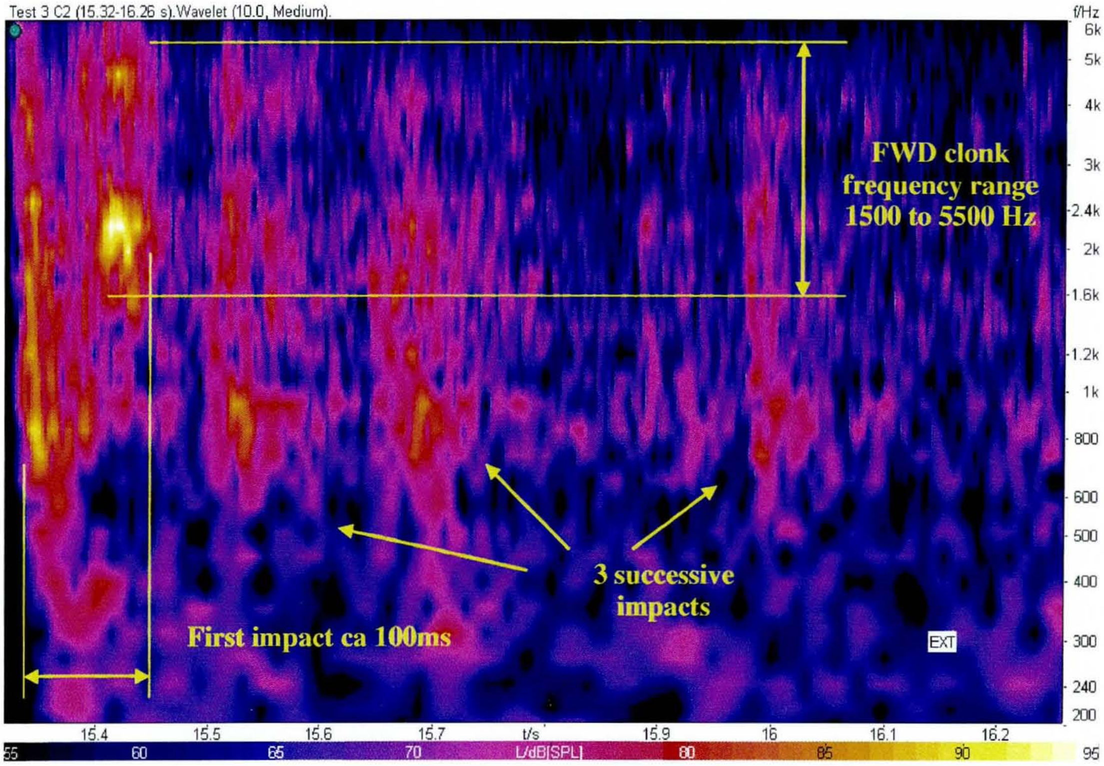

Figure 6.43 Wavelet display of a single clonk in frequency:time

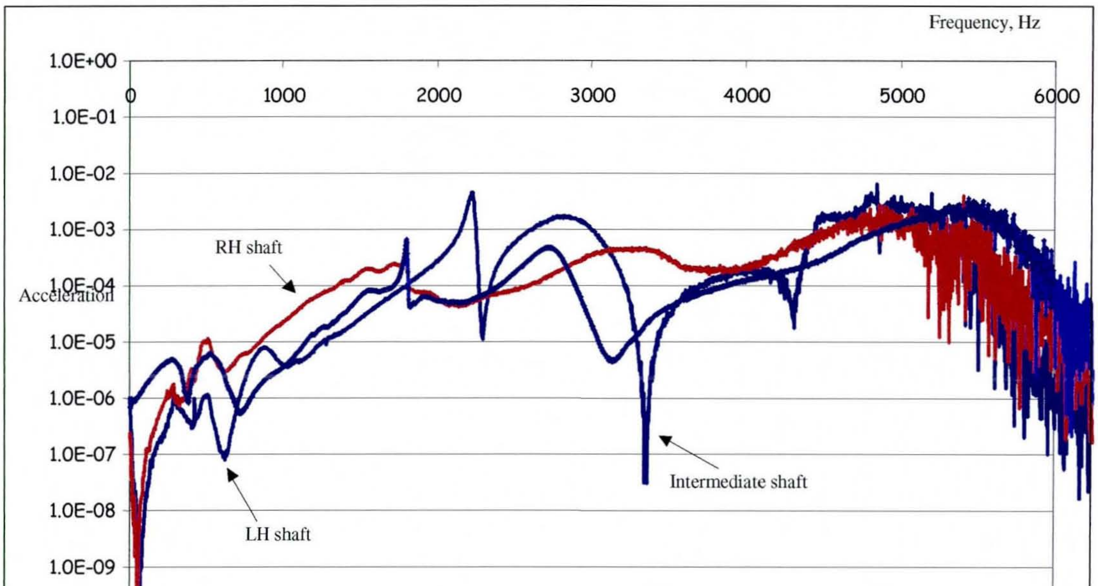

Figure 6.44 FWD drive shaft modal response

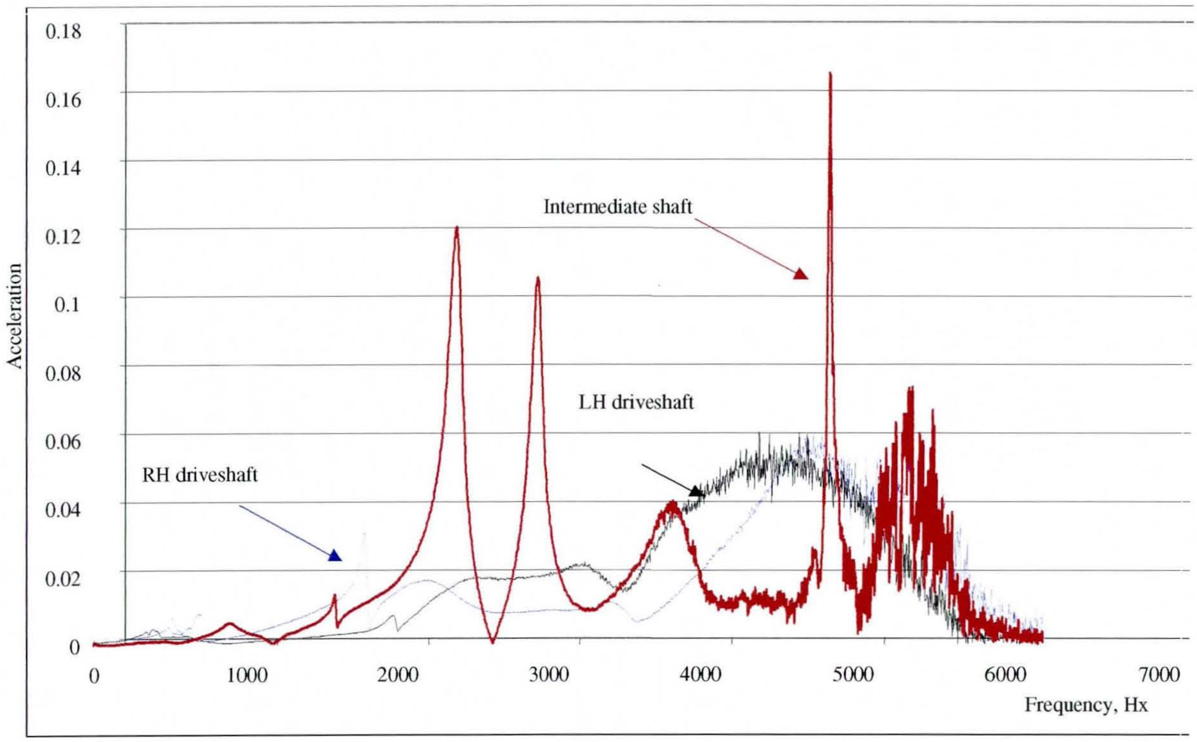

Figure 6.45 Component impact test

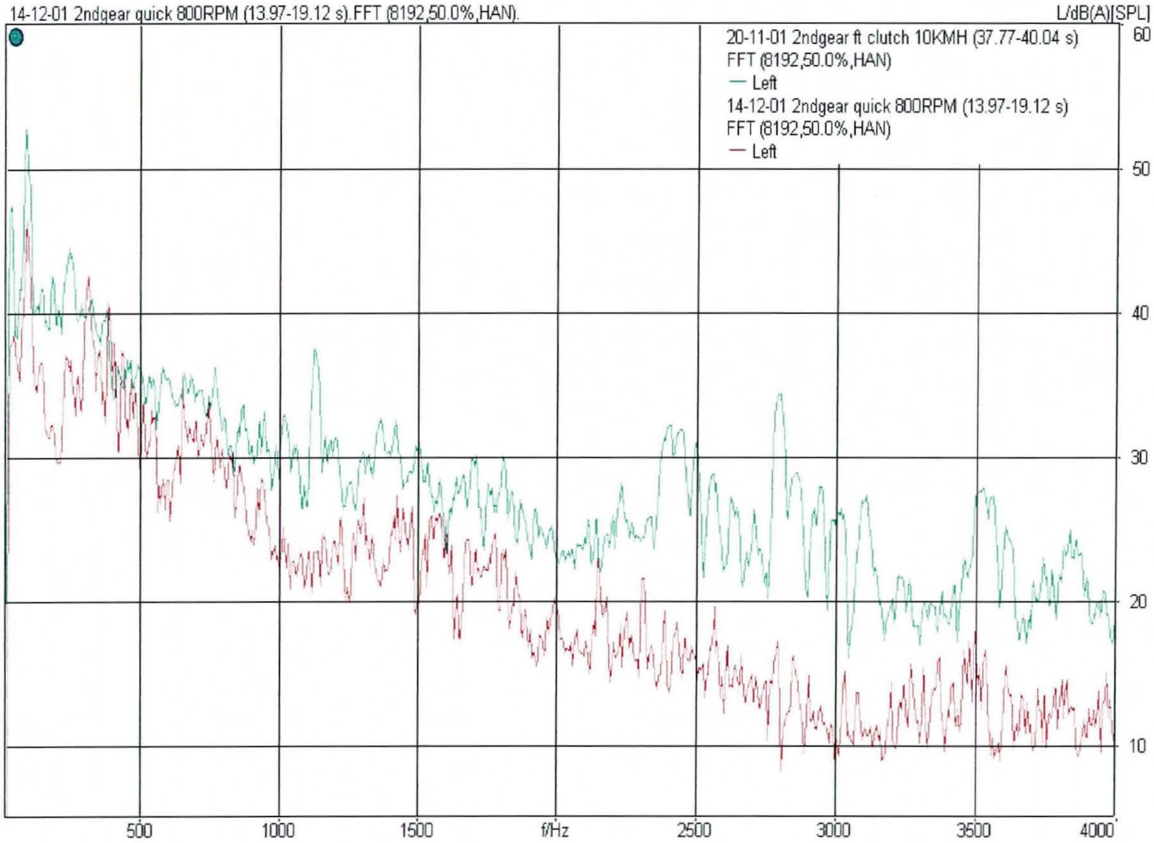

Figure 6.46 Comparison between interior clonk noise with tubular shaft (green trace) versus noise with solid shaft (red trace).

RU	A	B	C*D*E / A*B	C	A*C	B*C	A*B*C / D*E	D	A*D	B*D	A*B*D / C*E	C*D	B*E	B*C*D / A*E	A*B*C*D / E	Output: Internal noi	Output: External noi	Output: Subjective rating
1	-	-	+	-	+	+	-	-	+	+	-	+	-	-	+			
2	+	-	-	-	-	+	+	-	-	+	+	+	+	-	-			
3	-	+	-	-	+	-	+	-	+	-	+	+	-	+	-			
4	+	+	+	-	-	-	-	-	-	-	-	+	+	+	+			
5	-	-	+	+	-	-	+	-	+	+	-	-	+	+	-			
6	+	-	-	+	+	-	-	-	-	+	+	-	-	+	+			
7	-	+	-	+	-	+	-	-	+	-	+	-	+	-	+			
8	+	+	+	+	+	+	+	-	-	-	-	-	-	-	-			
9	-	-	+	-	+	+	-	+	-	-	+	-	+	+	-			
10	+	-	-	-	-	+	+	+	+	-	-	-	-	+	+			
11	-	+	-	-	+	-	+	+	-	+	-	-	+	-	+			
12	+	+	+	-	-	-	-	+	+	+	+	-	-	-	-			
13	-	-	+	+	-	-	+	+	-	-	+	+	-	-	+			
14	+	-	-	+	+	-	-	+	+	-	-	+	+	-	-			
15	-	+	-	+	-	+	-	+	-	+	-	+	-	+	-			
16	+	+	+	+	+	+	+	+	+	+	+	+	+	+	+			

Chosen factors and factor

A	+	Engine speed 900
	-	Engine speed 700
B	+	High viscosity
	-	Low viscosity
C	+	Solid drive
	-	Tubular drive
D	+	Clutch disc without predamper
	-	Clutch disc with predamper
E	+	Slow clutch engagement
	-	Fast clutch engagement

Table 6.3 DOE table for FWD

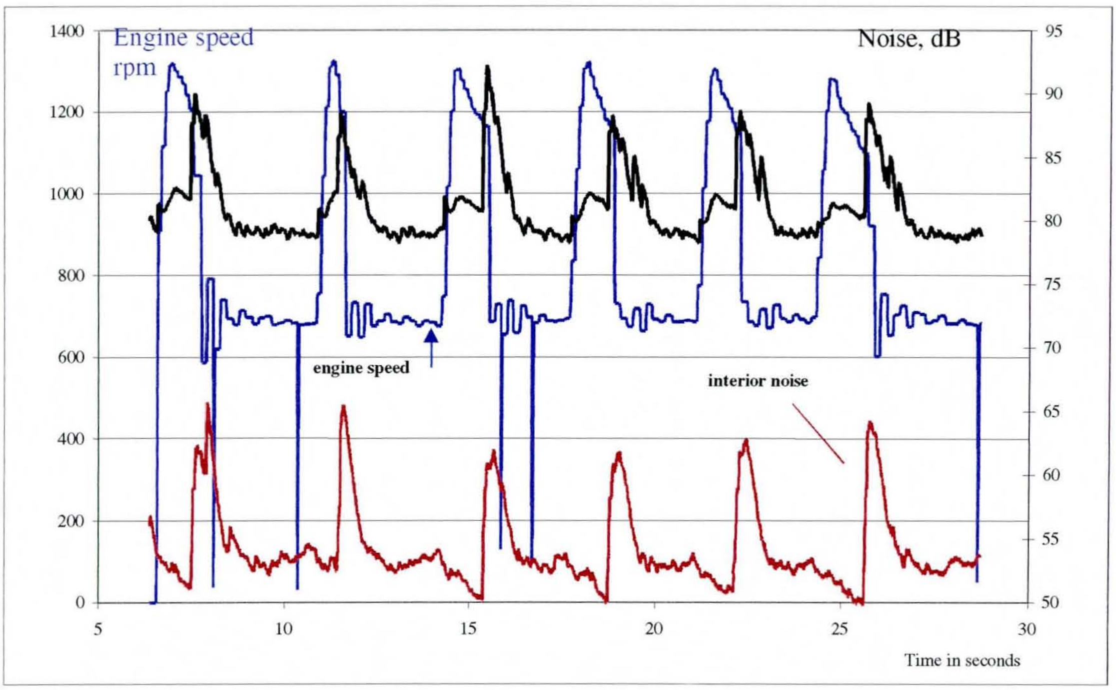

Figure 6.47 Test run 3 of DOE: Worst-case clonk

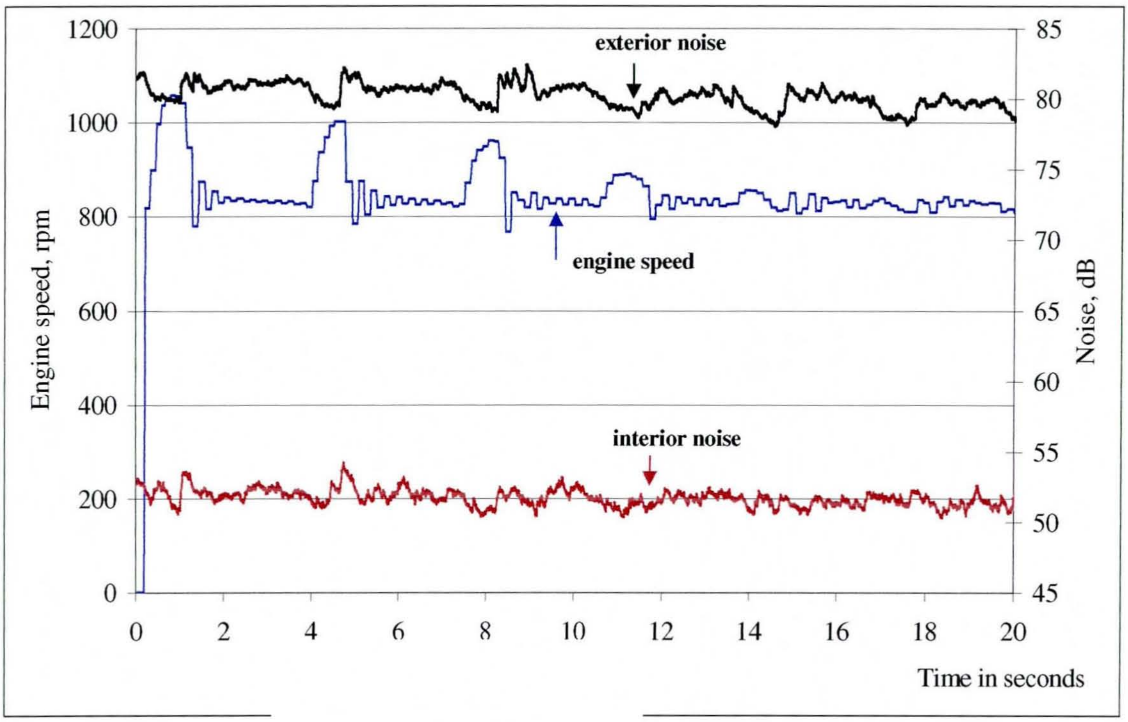

Figure 6.48 Test run 10 of DOE: Best-case clonk

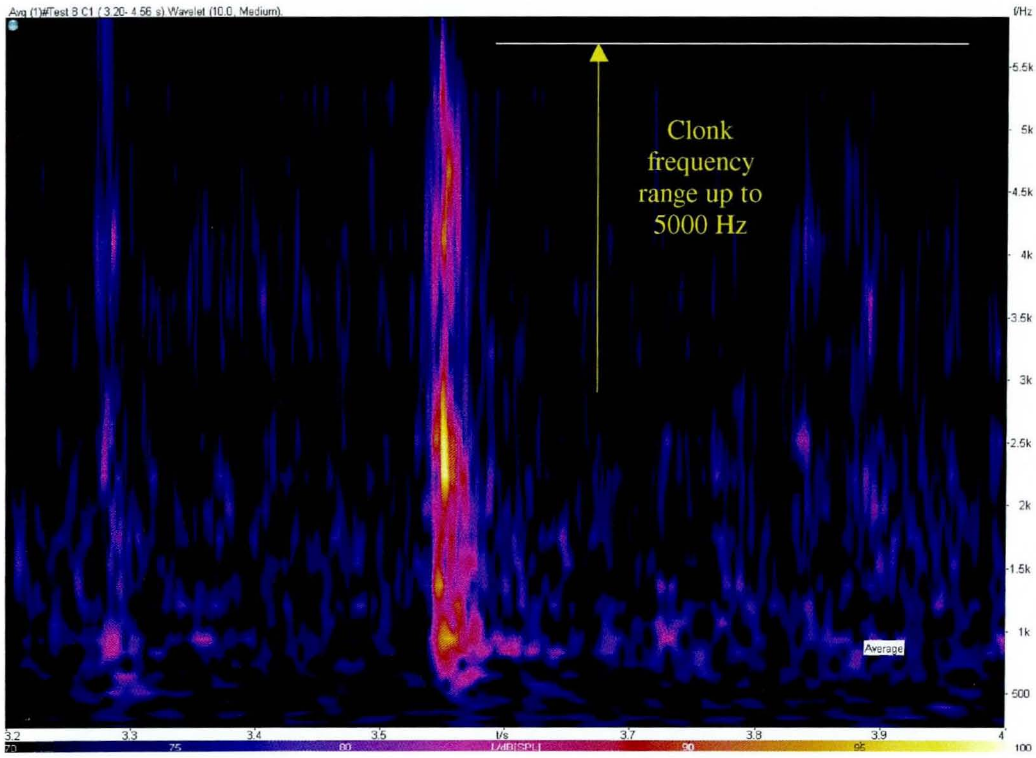

Figure 6.49 Overall frequency: time Wavelet for a single clutch induced clonk

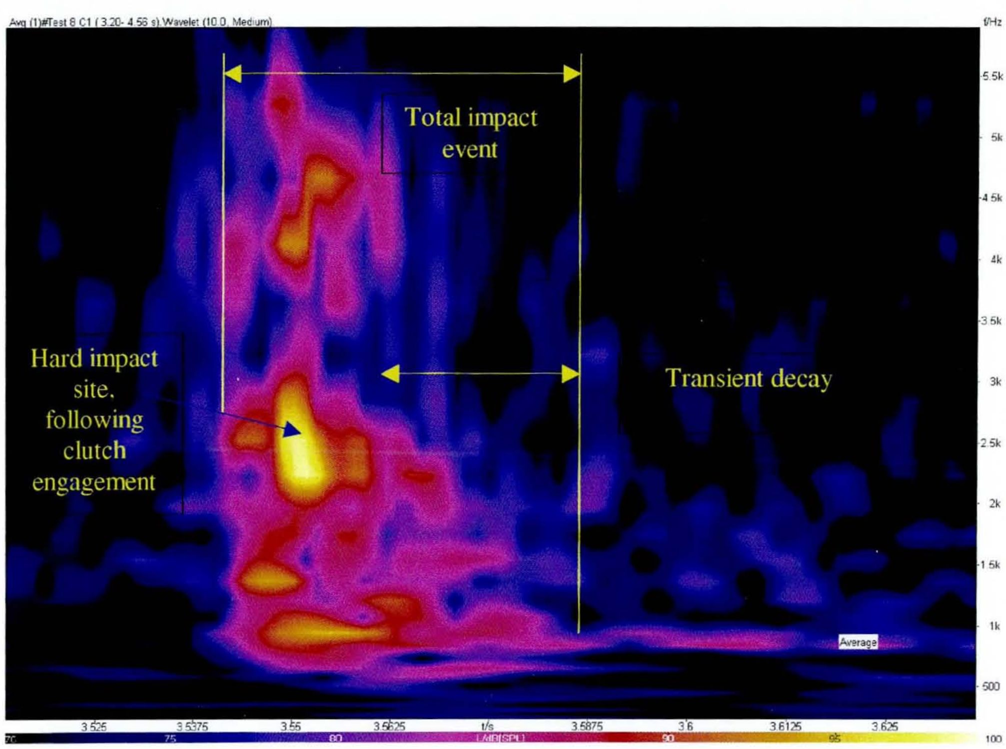

Figure 6.50 Close up of the impact region.

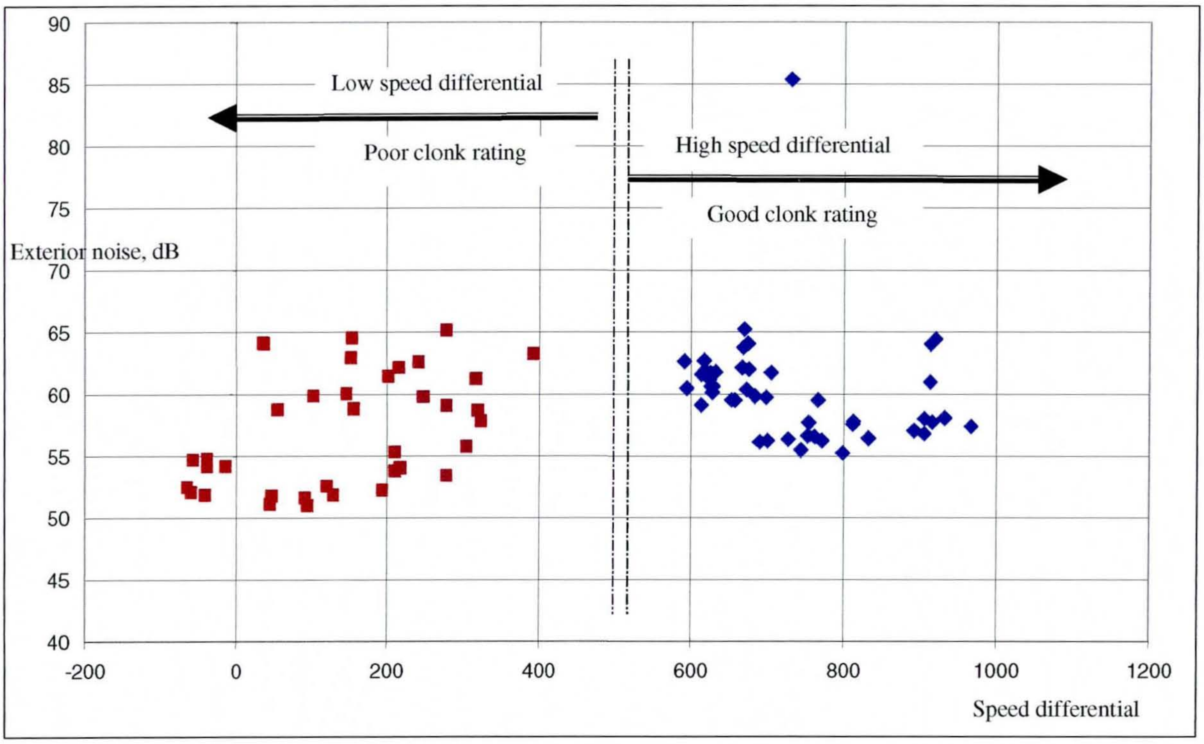

Figure 6.51 Effects of engine speed on clonk by DOE

	FACTORS					OUTPUTS				
	A	B	C	D	E					
Run number	Engine speed	Transmission oil	Shaft type	Clutch disc	Clutch pedal speed	Peak interior noise	Average jury rating	Subjective rating	Peak exterior noise	Mean speed difference
1	700 rpm	Thin	Tubular	With predamper	Slow	59.6	3.6	Poor	90.67	930
2	900 rpm	Thin	Tubular	With predamper	Fast	63.54	4.2	Poor	87.34	285
3	700 rpm	Thick	Tubular	With predamper	Fast	66.74	2.4	Not acceptable	89.29	656
4	900 rpm	Thick	Tubular	With predamper	Slow	53.73	7.4	Good	79.25	-45
5	700 rpm	Thin	Solid	With predamper	Fast	60.22	4.2	Poor	88.23	648
6	900 rpm	Thin	Solid	With predamper	Slow	51.8	8.1	Good	79.94	45
7	700 rpm	Thick	Solid	With predamper	Slow	56.2	4.7	Border line	85.27	742
8	900 rpm	Thick	Solid	With predamper	Fast	57.33	6.3	Acceptable	87.33	287
9	700 rpm	Thin	Tubular	Without predamper	Fast	61.98	2.6	Not acceptable	86.06	648
10	900 rpm	Thin	Tubular	Without predamper	Slow	52.67	7.5	Good	81.1	196
11	700 rpm	Thick	Tubular	Without predamper	Slow	58.57	5.1	Border line	86.38	854
12	900 rpm	Thick	Tubular	Without predamper	Fast	61.37	3.6	Poor	80.55	77
13	700 rpm	Thin	Solid	Without predamper	Slow	56.37	5.6	Acceptable	85.33	772
14	900 rpm	Thin	Solid	Without predamper	Fast	61.27	4.1	Poor	84.68	197
15	700 rpm	Thick	Solid	Without predamper	Fast	60.57	3.7	Poor	85.81	646
16	900 rpm	Thick	Solid	Without predamper	Slow	52.26	7.9	Good	80.9	117

Table 6.4 DOE run table

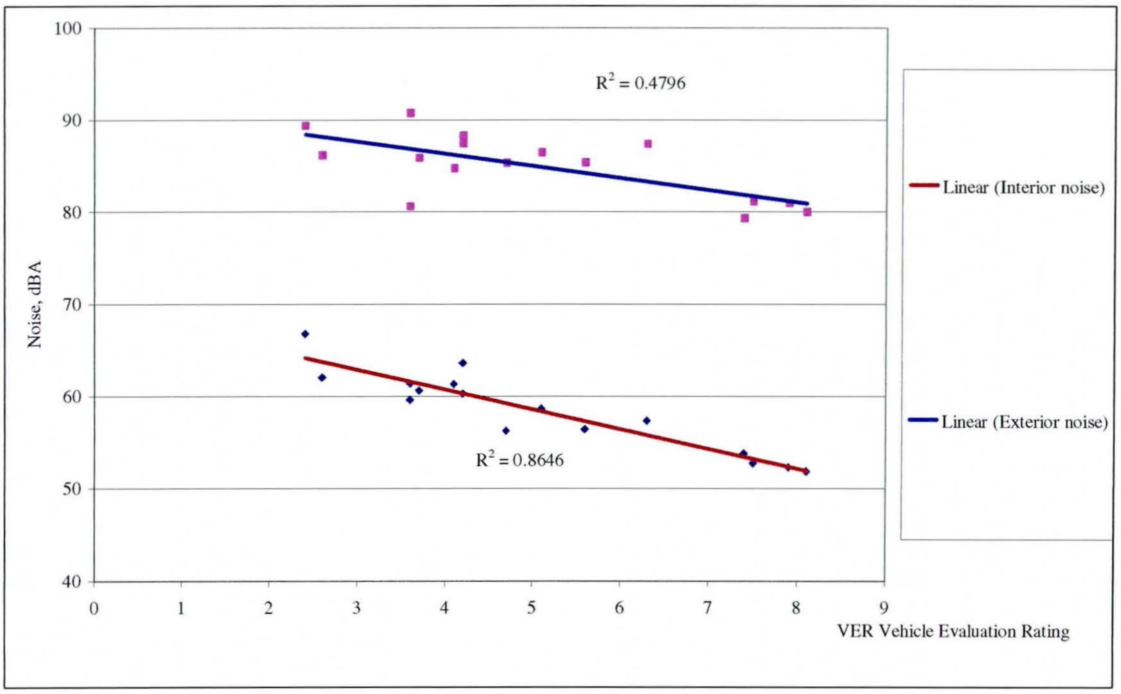

Figure 6.52 Correlation between jury ratings and measured noise

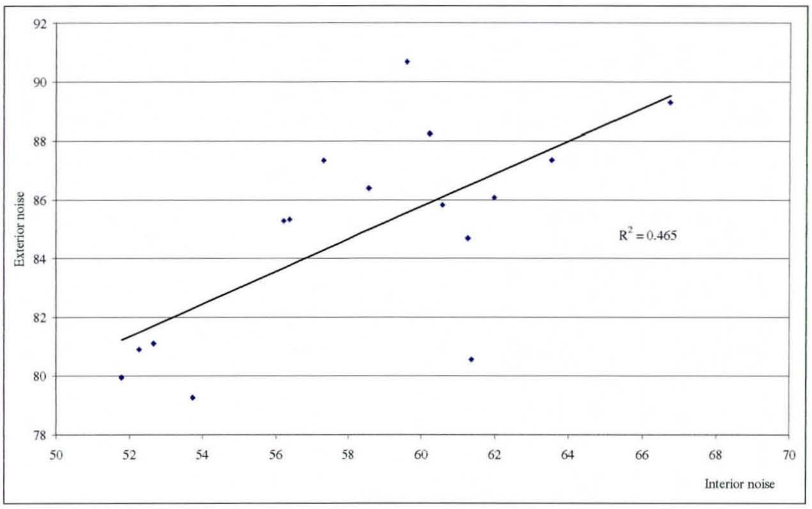

Figure 6.53: Interior-exterior noise correlation

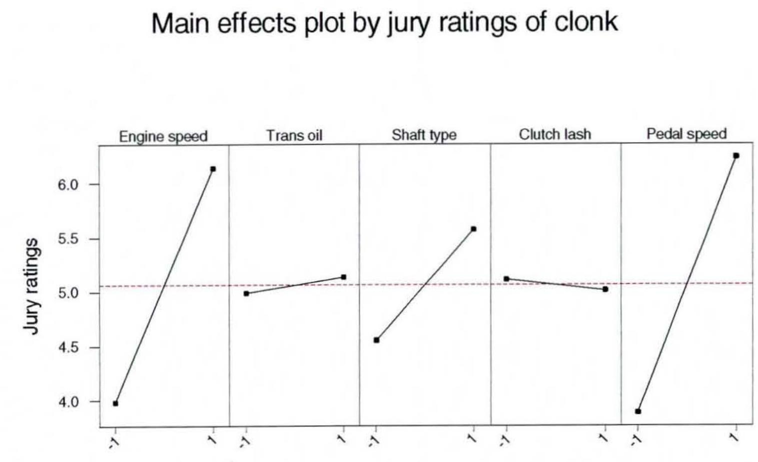

Figure 6.54: Subjective effects plot (by Jury)

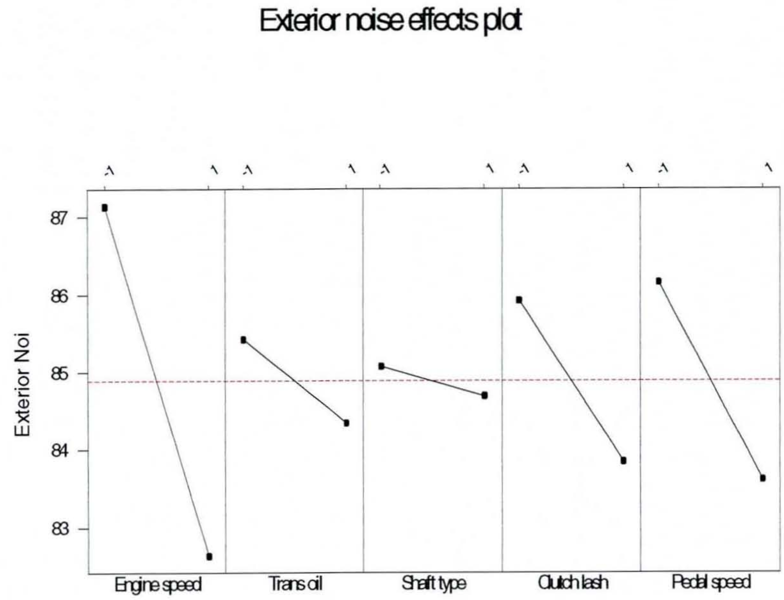

Figure 6.55: Objective effects plot (through measurements)

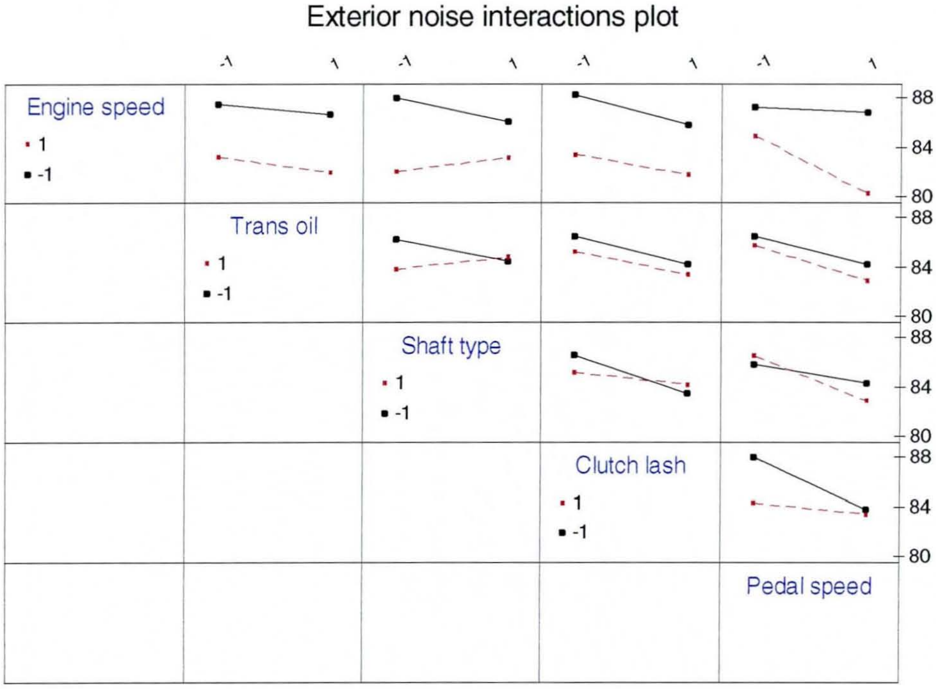

Figure 6.56 Plot of factor interactions based on exterior noise.

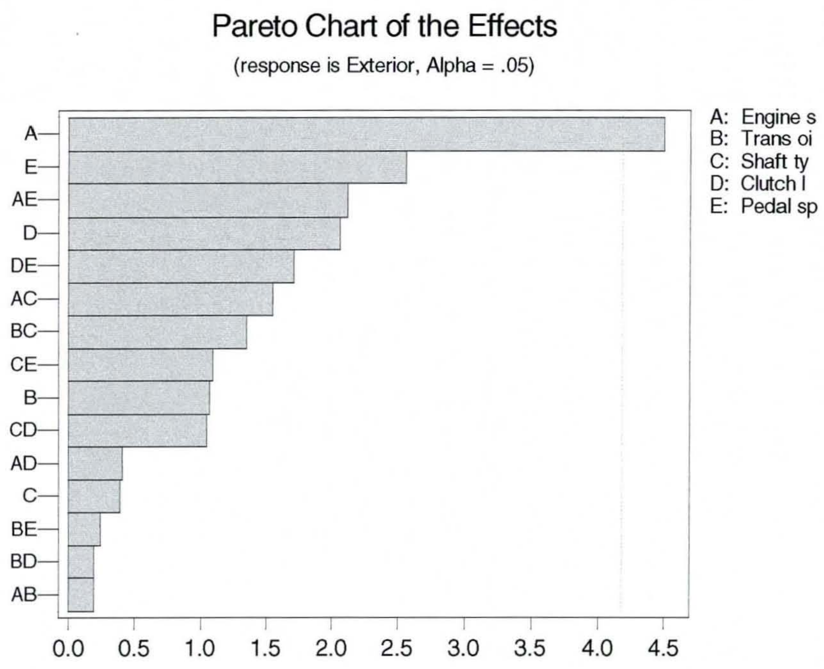

Figure 6.57 The Pareto chart of the DOE factor effects.

Chapter 7

Conclusions and Suggestions for Future Work

7.1- Overall Conclusions

There are a significant number of findings that form the overall conclusions of this research. These include the following:

- The mechanism that is responsible for the *clonk* phenomenon is an abrupt change in torque requirements/demand in the presence of backlash. The change in torque can result from a number of actions. These include throttle tip in from coast or back out in an abrupt manner, often associated for example, with the negotiation of a speed bump. Other causes of torque impulse include clutch engagement, as described in previous Chapters. Torque rise rates are engine sourced and are dependent on driver behaviour, but there are also road induced torsional inputs that may result in the same driveline torque ramps.

- The thesis has shown the direct interaction between drivetrain *shuffle* mode (being the first rigid body torsional mode of the drivetrain system) and the clonk response. Shuffle may be induced by the torque applications as described above, and also during the modulation of clutch slip torque during a pull away manoeuvre. In this case the shuffle excitation is related to the clutch friction disc characteristics. Shuffle and clonk are independent events, but worst-case clonk will occur during a shuffle manoeuvre with a high torque rise rate, and in association with driveline lash between transmission meshing teeth, the differential, and the shaft spline joints. In the extreme case there may be a series of clonk impacts with each cycle of the shuffle mode.

- The root cause of clonk is the dynamic impact phenomenon in the driveline lash zones that have been described. The backlash allows a sudden impact of the meshing pairs causing local deflection of the contiguous bodies, which as a first approximation may be considered to be a Hertzian impact. For highly loaded conformal contacts of helical type gear teeth pairs, an elliptical point contact condition will result. An extremely high force will develop at the contact zone. This does not take into account the lubricant behaviour in the contact, which leads to elastohydrodynamic conditions. It has been found that when lubricated conditions are considered, the elastic deformation is increased due to lubricant resistance, whilst the energy and momentum transferred to the rest of the structure is attenuated due to viscous dissipation. Therefore the severity of impact for the case of dry contact is the worst for structural wave propagation from the impact site, and this is the fundamental clonk mechanism. Apart from the wet transmission and final drive gear mesh conditions, the splined teeth engagements in the clutch and drive shafts are anyway dry or at least starved. This justifies the assumption of the Hertzian approach in this thesis, which relates to the worst-case condition for clonk excitation, and it also means that the impact analysis does not need to consider finite line contact under transient elastohydrodynamic fluid lubrication, which is a major study area in its own right.

- The transferred impact energy from the initial torque overshoot travels as a structure-borne wave along the drivetrain components, and excites numerous high frequency circumferential and axial waves on the thin-walled hollow driveshaft tubes. These have a high modal density in the clonk frequency range. Clonk readily occurs due to the coincident frequency coupling between the impact forces (which have a high frequency content) and the structural modal responses of the transmission housing and the driveshaft tubes, which are resonant in the same frequency range. This signifies that an appropriate approach to the clonk problem would be to uncouple the input pulse frequency spectrum from the elastic wave frequencies, with an increase in structural damping. There are several attractive methods of achieving clonk reduction by frequency separation between impulse signal and drivetrain resonances:

- Lower the impulsive frequency content (so-called pulse tailoring).
- Increase the drive train elastic wave frequency range.
- Dampen the wave response.
- Uncouple the inner acoustic cavity modes from the containing structural modes.

- During the vehicle testing, clonk was seen to be closely related to the shaft speed through the lash, when clonk was induced. This is further borne out by the Hertz contact relationship:

$$\Delta t = \frac{2.94\delta}{v}$$

where δ = local elastic deformation at impact,

Δt = duration of contact,

v = relative velocity of impacting parts,

and therefore, it is clear that an increase in velocity at impact will reduce the contact duration and then increase the high frequency content of the exciting signal, which then increases the radiated clonk.

- Fluid-structure modal interactions take place over a wide frequency range (fluid referring to the cavities such as the internal volume of the driveshaft tubes and the transmission bell housing). At certain frequencies structure-acoustic coupling or *coincidence* takes place between the structure-borne waves and the standing sound pressure waves in the fluidic medium (this being air in the untreated driveshaft tubes with closed ends. It is found that acoustic radiation, referred to commonly as the clonk phenomenon, is most sensitive when the coincidence leads to a wave motion in the fluidic medium that reaches supersonic speed. This is a major finding of the investigations.

- The numerical predictions have shown remarkable agreement with the experimental findings, thereby confirming the clonk generation hypothesis in the sequence of events that lead to the clonk phenomenon. Good agreement has been found between experimental findings and the numerical predictions for structural frequencies of significant power spectral density. AR|MA signal analysis methods have been applied to extract the high frequency transients from the measured data taken from the driveshaft tubes. Among the significant structural frequencies are those that, according to detailed analysis for fluid-structure interactions, lead to the clonk phenomenon. This analysis also includes wave motion prediction by the boundary element method.

- The experimental investigations spanned component testing, rig-based and vehicle-based work under controlled conditions. The numerical predictions have involved multi-body simulation, based on constrained Lagrangian dynamics (using ADAMS). All of these approaches have shown a high degree of correlation.

- An extremely attractive NVH potential has arisen out of the clonk study. Since transmission gear rattle has a different but similar mechanism to clonk, there should be an opportunity to resolve both clonk and rattle problems with similar treatments, thus, avoiding the compromise resolutions that have been adopted in the past.

7.2- Novel Approaches and Contributions to Knowledge.

Clonk is a very short-term transient response with a complexity of potential causal factors. It was considered necessary to take a number of different approaches to the problem to fully verify the noise mechanism as described above. These included Lagrangian dynamics for a multi-body analysis in ADAMS. Therefore, one of the overall contributions of the thesis has been the development of detailed constrained inertial dynamic models for vehicular drive train systems.

Component flexibility yields high frequency oscillations of structural members. The incorporation of these effects through the use of non-linear elastic fields, either by transfer matrix method or by dynamic stiffness matrices into the multi-body model has been another contribution of the reported research. A particularly novel aspect of the work is the inclusion of component flexibility for driveshaft tubes into the multi-body dynamic analysis, using the super-element finite element method in NASTRAN and the component mode synthesis in ADAMS/Flex. The resulting combined solution of large displacement low frequency carrier wave motion (shuffle) with superimposed small amplitude elastodynamic high frequency vibration (clonk) driven by an impulsive shock force, is the first ever reported detailed model for vehicular drivetrain systems.

The above mentioned drivetrain model was extended to include the acoustic cavity response, using the same super-element technique. This resulted in the creation of elasto-acoustic models of thin hollow driveshaft tubes, which then clearly indicated the coincidence between some of the structural modes excited by impulsive loading of the system, and the acoustic modes of the cavities. It has been shown that elasto-acoustic coupling leading to high levels of sound wave propagation takes place when frequency coincidence occurs, resulting in travelling waves of supersonic nature. This is a main novel finding of the thesis and a significant contribution to knowledge in terms of the mechanism of propagation of noise in impulsive loading of drive train systems, a fact not hitherto established in open literature.

Subsequently, the use of a modified boundary element method to obtain the natural acoustic eigenmodes of enclosed volumes in hollow driveshaft tubes, has verified the findings reported in the previous paragraph.

The numerical investigations by themselves could not provide verification of the clonk mechanism, and could not identify the remedial actions that need to be undertaken for a cost effective solution within the constraints of the mass volume automobile engineering environment. Consequently, it was necessary to carry out a comprehensive programme of testing at component, rig-and vehicle level. The combination of experimental investigations and numerical predictive studies on such a scale has also not been reported in the literature. In particular, the novel use of signal processing methods has been made with the use of Auto-Regression Moving Average (ARMA) method, hitherto not used for high frequency short transient signals and in particular for automotive drivetrain NVH studies. The findings of ARMA and Wavelet analysis have corroborated with those obtained through numerical predictions using the elasto-acoustic multi-body model. Similar agreement has also been found with the noise propagation and boundary element analysis findings. The conformance of numerical predictions with the experimental rig based results accounts for a significant contribution to knowledge in this thesis. The concordance of rig-based results having very good degree of correlation with vehicle tests is also regarded as a contribution.

A series of vehicle tests were conducted on a chassis dynamometer/rolling road to assess the causal factor contribution to driveline clonk in a realistic environment. The trials were conducted against a Design of Experiments orthogonal test matrix of control factors. It was conducted in order to evaluate the ranking order of potential causal factors that contribute to the excitation of driveline clonk.

Several output parameters were measured and recorded as each factor combination was tested in turn. At the conclusion of the testing, an analysis was conducted on the test data and appropriate consideration was given to the statistical significance of the result. This is believed to be the first report of the application of the DOE methodology to the analysis of transient time dependent data taken from a non-linear system in open literature.

The results of the analysis were also compared with the subjective ratings that had been taken during the course of the test program, and an encouraging correlation was subsequently found. This suggested that much quicker subjective DOE tests may be employed, and certainly a subjective clonk DOE may be used as a preliminary filter before a final objective confirmation testing.

7.3 A critical assessment of the approach taken.

The ideal approach in a multi-physics analysis such as that reported in this thesis (i.e. a coupled multi-body dynamics, elastodynamics and acoustic analysis), would encompass the determination of applied dynamic loads through a multi-body analysis, and subsequent structure-borne vibration by the boundary element method. The same method would apply to the determination of acoustic response at a field point, without needing to compute the intervening field points within the same medium. Although this approach has been used in the thesis, it was indirectly related to the multi-body analysis, through surface velocity vector of the thin shell tubes. A super-element FEA on the other hand has been fully integrated which is computationally more intensive. Thus, integrated BEM and multi-body analysis would normally be favoured. Furthermore, for the investigation of outer noise fields external to the tubes the finite element method is not suitable.

A boundary element approach, as highlighted above, would be more suitable than the super-element FEA. Another, perhaps better option, would be the use of Statistical Energy Analysis (SEA) for very high frequency modal behaviour of such thin tubes. SEA is concerned with the high modal density grouping that occurs at high frequency and is not suitable for discrete modal shape definition. Since the clonk phenomenon is active over a fairly wide spectrum of elasto-acoustic coincident response, the modification of driveshaft tube in terms of length/diameter/wall thickness, to shift the modal response would not be a practical option. This means that the use of SEA is of limited benefit, but that of BEM would be desired in order to investigate the noise out-field as well as the in -field in computationally acceptable time frames.

The floor mounted experimental rig described in Chapter 3, provided good correlation with road vehicle behaviour, and was very useful in the verification of numerical findings, as well as completing a fundamental physical approach in the investigation of clonk in conjunction with the numerical work. Although it lacked the dynamic characteristics of a running drive train, it recreated the transient conditions which caused the impact induced impulsive loading and reflection of the drive train system. In addition the mounted rig was fully repeatable and reliable. By comparison, it is accepted that a rotating rig input with a transient impulse would represent the conditions in a slightly more realistic manner.

It would have been desirable to apply the developed ARMA methodology to the frequency acoustic response of the entire driveline system, with measurements taken from a battery of microphones placed around the transmission bell housing and at the differential. The transmission bell housing is particularly active in the clonk frequency range, and has low levels of structural damping (i.e. it is Aluminium housing). It also has an internal cavity that will resonate in frequency with the structure. There is no doubt that the bell housing would make a significant contribution to radiated noise in addition to that radiated by the driveshaft tubes. But in order to find correlation with the numerical predictions of the elasto-acoustic couplings within the acoustic boundary, it would be necessary to accurately locate very small microphones in the cavity to pick up the standing wave patterns and the very high pressure gradients.. It is recognised that placement and isolation of microphones within the tubes and bell housing would be quite difficult and their presence would interfere with the standing sound pressure wave.

In order to predict the radiated noise from vibrating shells, SYSNOISE may be used. This is an important general acoustic FE/BEM code, which could be used to calculate radiated sound pressure from the drive shaft tubes and the transmission housing, driven by the vibrating body panels into the external 3D sound field.

SYSNOISE would run an FE model of the structure with a BEM of the fluid field and boundary as a coupled pair, to predict the radiated sound at discrete points in the 3D external field as a time dependent solution. The coupled model could then be used to conduct 'what-if' palliative studies, with a specific focus on the drive shaft tubes.

The predicted results would be compared to experimental evidence derived from impact excitation on a static driveline assembly and with a battery of microphones placed in the near field to capture the sound pressure gradients.

This activity was beyond the scope of the reported work but it is planned to follow up this challenge.

7.4 Suggestions for future work.

There are a number of issues that may be investigated in order to further confirm the findings of this thesis, as well as to quantify the responsible mechanisms and sources that contribute to the clonk problem. The study carried out in this thesis is fundamental and objective, although the actual quantification of the sources of the problem requires further investigation. For example, the impact mechanism used in the multi-body model is based upon dry impact dynamics of a pair of highly loaded low conforming gear teeth pair, where one can assume Hertzian conditions. The justification for such an assumption is made, but in reality the presence of a lubricant film causes viscous dissipation and reduces the effect of impact energy that in turn causes elastic wave propagation in the structural elements of the system. This necessitates investigation of the elastohydrodynamic EHL impact problem under transient conditions. This aspect of the work is being undertaken under a recent Vehicle Foresight funded project at Loughborough University (OPTRAREF), which is co-ordinated by the author of this thesis.

Another important issue is the development of a rotating rig rather than a fixed static rig reported in Chapter 3, as highlighted in the previous section. This experimental action is also undertaken under the OPTRAREF project.

Changes in the engine speed due to engine management strategy can cause sudden variation in contact deformation due to impact as shown by the Hertzian analysis in chapter 5. It should be noted that the contact stiffness non-linearity is dependent on the duration time. The contact time reduces as the impact velocity increases and can lead to variable conditions, some of which may lead to clonk. A detailed analysis beyond that employed in this thesis is suggested.

It is proposed that the boundary element method be employed in an elasto-acoustic multi-body model, instead of a super-element finite element analysis This will enable simultaneous study of the elasto-acoustic coupling inside, as well as outside, of the hollow driveshaft tubes at any particular field location. The work should also be extended to other regions such as the transmission bell housing, where preliminary ARMA results have indicated multiple elastic modal responses of breathing modes to bending and flexural responses. The results of such an analysis may be compared with experimental findings in the frequency domain by signal processing of the noise signal output from microphones that can be placed in the external sound field and also those that may be placed within the tubes, to achieve the transfer function. As already indicated, the accurate measurement of interior sound pressure waves would be very difficult to achieve due to the potential for wave disturbance and the extremely high sound pressure gradients at clonk frequency. The use of hot wire probes or hot film anemometry to measure the velocity of the airwave and hence deduce sound pressure distribution is a possible method of experimentation (see Bruun, 1995). The solution to this problem is beyond the scope of this project.

The most important suggestion for future work, one that is also being investigated under the aforementioned OPTRAREF project, is to find a robust solution to the problem from an industrial viewpoint. Clearly, a root cause solution will have to be sought at the point of impulsive action, this being in the impacting conjunction of mating gear teeth pair through backlash. However, it is clear that some amount of backlash is always required for a functional transmission (i.e. backlash cannot be eliminated). Furthermore, manufacturing control of the backlash and backlash variation is not feasible and probably not required. Therefore a possible root cause approach would be to control the impulsive input that occurs for example in throttle tip in condition.

There are a number of possible solutions that can extend from the findings of this thesis. A practical approach would be pulse tailoring for frequency separation, between the impulse content and system modal response. For example, it is more important and more effective to control lash drag than to control lash travel. This will increase the contact time, which is very desirable. Also a pre-loaded clutch disc would remove lash effect and attenuate clonk response, although this may lead to other NVH problems, such as rattle. It would be useful to include such features on a future multi-body model.

Another approach to the problem may be taken at the point of clonk manifestation (i.e. at the transmission housing and the driveshaft tubes) rather than at the source of the problem described above. This approach may be regarded as palliative. There are many possible approaches, one being the inclusion of an internal baffle or a membrane to break the continuity of the acoustic waves (see SAE 841697). Another approach may be to reduce the speed of acoustic wave motion in the cavity by foam filling or by introduction of absorbent materials. It is clear from the findings of this thesis that if the speed of propagation is reduced below supersonic levels, then mere coincidence of structural and acoustic waves will attenuate the clonk problem. Another approach may be to alter the driveshaft torsion stiffness thus altering the structural modes. These proposals, some of which are highlighted in this thesis, have certain beneficial effects, but may not be entirely effective over the wide range of audible frequencies involved. For instance, inclusion of membranes to the tubes will effectively change the dimensions of the active cavity. This may alter both the structural and acoustic characteristics but it may not be sufficient to move it outside the audible range. However, it may achieve significant attenuation when used in conjunction with pulse tailoring to ensure that the resulting dominant modes are not fully excited. These ideas point to the need for a fundamental experimental analysis of elasto-acoustic coupling for controllable experiments with input pulse tailoring and combined with boundary element analysis.

It is clear that lash and clonk are not linearly related. However, the tests conducted thus far have been with new parts. The adverse effects on clonk due to increased lash and reduced lash drag, in combination with lubrication contamination and degradation through wear in service, should therefore be investigated.

It is also very clear that clonk is not fully attributable to build variation alone. Clonk and clonk variation occur only when certain vehicle conditions occur in combination. Clonk is very sensitive to these drive conditions (gear, speed, clutch and throttle actuation, etc). The challenge is to apply the 'lessons learnt' to all drive modes and hence achieve robustness.

It should be possible to preload the driveline through the clutch disc and thereby eliminate backlash by the application of sufficient torque to overcome drag at all the locations where lash occurs. This technique requires investigation through the use of numerical or experimental methods, to explore the disadvantages of such an approach.

The contents of this thesis have already resulted in 17 publications in learned scientific journals, and an MSc by research in the same field of study (see Appendix)

REFERENCES

AL-SAMIEH, M., F., and RAHNEJAT, H., *Physics of lubricated impact of a sphere on a plate in a narrow continuum to gaps of molecular dimensions,* J.Phys. Appl Physics Vol 35, 2002

AMBROSSI, G., and OROFINA, L., *Automotive Driveline Dynamic behaviour Simulation*, 2nd Int. Conference on New Developments in Powertrain and Chassis Engineering, Strasbourg, 14-17th June 1989, ImechE pap. C382/117, Mech. Eng. Pub. Ltd., 1989, pp. 159-170.

AMBROSI, G., and OROFINO, L., *Driveline vibration simulation of a 4WD vehicle*, I.Mech Eng Symposium Report C389/154, 1992

ARNOLD, R., and WARBURTON, G., *Flexural vibrations of the walls of thin cylindrical shells having freely supported ends*, Proceedings of the Royal Society (London), 1949

BERNOULLI. D., *Exercitationes quaedam mathematicae*, Venice, 1776

BIERMANN, J., and HAGERODT, B., *Investigation of noise emission - clonk - of drivelines caused by load changes*, Aachen University Report, Ford Motor Company Confidential Report, 1995

BIERMANN, J., and HAGERODT, B., *Investigation of the clonk phenomenon in vehicle transmissions – measurement, modelling and simulation*, Proc Instn Mech Engrs Vol 213 Part K, 1999, pp53-61

BIERMANN, J., W., and HAGERODT, B., *Investigation into the clonk phenomenon in vehicle transmissions - measurement, modelling and simulation.* Multibody Dynamics Monitoring and Simulation Techniques, MEP Publications, 1997

BOYSAL, A., *Virtual prototyping applied to the robust design of engine components*, M. Sc. Dissertation, University of Bradford, 1995

BROCH, J.T., *Acoustic noise measurements*, Bruel and Kjaer, 1969

BROCH, J.T. *Mechanical vibration and shock measurements*, Bruel and Kjaer 1984

CHACE, M., A., *Methods and experience in computer aided design of large-displacement mechanical systems*, Computer aided analysis and optimisation of mechanical system dynamics, NATO ASI Series, Vol. F9, Springer-Verlag Berlin Heidelberg, 1984, pp. 233-259.

CHAN, E., and CROSSLEY, P., *The effect of engine torque and driveline backlash on vehicle shuffle*, Ford Motor Company Internal Report, Confidential Internal Report, 1993

CHENG, Z., *Analysis of automobile crash responses using wavelets*, SAE 2002-01-0183, 2002

CHISOLM, C., and WORTHINGTON, P., *Static and dynamic analysis of machine drivelines*, J. Agricultural Engineers, 1987

CLARKSON, B., and POPE, R., *Modal density and loss factors of flat plates and cylinders*, Journal of Sound and Vibration Vol 19, 1981

COOK, P., A., *Non linear dynamical systems*, Prentice Hall, 1986

D'ALAMBERT, J., le R., *Traité de dynamique*, Paris, 1743

DOWELL, E., GORMAN, G., and SMITH, D., *Acoustoelasticity: General theory, acoustic natural modes and forced response to sinusoidal excitation including comparisons with experiments*, Journal of Sound and Vibration Vol 52, 1977

DOWSON, D., and WANG, D., *An analysis of the normal bouncing of a solid elastic ball on an oily plate,* Wear, 1994

EULER, L., *Nova methods motum corporum rigidarum determinandi*, Novi Commentarii Academiae Scientiarum Petropolitanae, 20, 1776

FARSHIDIANFAR, A., EBRAHIMI, M., RAHENJAT, H. and MENDAY, M., T., *Optimization of the high-frequency torsional vibration of vehicle driveline systems using genetic algorithms,* Proc Instn Mech Engrs Vol 216 Part K, 2001, pp 249-262

FORSBERG, K., *Influence of boundary conditions on the modal characteristics of thin cylindrical shells*, AIAA, 1964

FOTHERGILL, D., J., and SWIERSTRA, N., *The application of non-linear displacement modelling techniques to an automotive driveline for the investigation of shunt*, VDI Berichte NR 1007, 1992

GEAR, C., W, *Simultaneous numerical solution of differential – algebraic equations,* IEEE Transactions on circuit theory, 1971, Vol. 1, pp 89-95

GEAR, C., W, *The numerical solution of problems which may have high frequency componets*, Pron. NATO ASI on Computer Aided Analysis and Optimisation of Mechanical System Dynamics, Springer-Verleg, 1984

GEARHART, C., *Applications of wavelet based signature analysis in designing for crashworthiness*, Proceedings of ASME Technical Conference Las Vegas, 1999

GIZARD, M., VILLATA, G., and LABARRE, G., *Slipping clutch and transmission vibration reduction*, SAE 905187, 1990

GROVE, D., and DAVIS, T., *Engineering quality and experimental design*, Longman Scientific and Technical Press, 1992

GRUBIN, A., N., Central Scientific Research Institute for Technology and Mechanical Engineering, Book No 30, Moscow. 1949

HACKENBROICH, D., *Reduction of the commercial vehicle noise level using numerical optimisation of the structure borne sound and sound radiation behaviour of a driveshaft*, SAE 947122, VDI Report No 1153, 1994

HECKL, M., *Vibration of point driven cylindrical shells*, J.Acoustic Soc.America Vol 34, 1962

HAWTHORN, J., *A mathematical investigation of driveability*, I.Mech Eng Report C420/003, 1995

HERTZ, H., *On the contact of elastic solids*, J.Reine Angew Math 92, 1881

HROVAT, D., *Influence of drive train / chassis dynamics on tip in and back out driveability*, Ford Motor Company Internal Report 1989. Internal Ford Motor Company Confidential Report

HUTCHINS, C., *A study of the cavity resonances of a violin and their effects on its tone and playing qualities*, JASA, 1990

HUSEIN, K., *Boundary Element Analysis of Vehicle Interior Noise*. PhD Thesis, University of Loughborough

JOHNSON, K., L., *Contact mechanics*, Cambridge University Press, 1985

JUNGER, M., and FEIT, D., *Sound structures and their interaction*, MIT Press, 1972

KIM, K., *Vibration analysis of driveline*, University of Southampton ISVR M.Sc Thesis, 1987

KIM *et al*, *Modelling of airborne tyre noise transmission into car interior by using the vibro-acoustic reciprocity and the boundary element method,* SAE 972046, Noise and Vibration Conference, Michigan, 1997

KRENZ, R., *Vehicle response to throttle tip in / tip out*, SAE 850967, 1985

LARSSON, R., and HOGLUND, E., *Elastohydrodynamic lubrication at impact loading,* ASME Journal of Tribology, Vol 116 1994

LARSSON, R., and HOGLUND, E., *Numerical simulation of a ball impacting and rebounding a lubricated surface*, ASME Journal of Tribology, Vol 117, 1995

LASCHET,A. *Computer simulation of vibrations in vehicle powertrains considering non linear effects in clutches and manual transmission*, SAE 941011, 1994

Li, C.J and Ma, J, "Wavelet decomposition of vibrations for detection of bearing–localized defects," NDT & International, Vol.30, No.3, 1997, pp.143-149.

LOOS, H., and LAERMANN, F-J, *Simulations and measurements of car driveability phenomena*, Ford-Werke AG, Cologne. Internal Ford Motor Company Confidential Report.

LOVE, A., E., *A treatise on the mathematical theory of elasticity*, New York Dover Publications, 1892

LUK BUHL, *Torsional vibrations in the drive train*, 4th LUK Clutch International Symposium, 1990

MALLET, S., *A theory for multi-resolution signal decomposition: the wavelet representation*, IEEE Trans. Pattern Anal. and Machine Intell.,Vol.11, 1989, pp.674-693.

MISITI, M., MISITI, Y., OPPENHEIM, G., and POGGI, J., M., *Wavelet Toolbox for use with Matlab*, 1997.

MO, C.Y., BEAUMOUNT, A.J., and POWELL,N.N., *Active control of driveability*, SAE 960046, 1996

MORIMURA,H., MINAMI,H.,and TSUCHIYA,M., *Effects of engine output torque and driveline non linear characteristics on vehicle driveability*, SAE 865122, 1985

Nakamura, S., *Applied Numerical Methods with Software*, Prentice-Hall Inc, USA, 1991

NORTON, M.P., *Fundamentals of noise and vibration analysis for engineers*, Cambridge Univ Press, 1989

ONSAY, T., *The use of wavelet transforms and frames in NVH applications*, SAE 951364, 1995

ORLANDEA, N., CHACE, M., A., and CALAHAN, D., A., *A Sparsity-Oriented Approach to the Dynamic Analysis and Design of Mechanical Systems*, Part 1, J. Engng. Ind., 1978, pp. 1-7.

ORLANDEA, N., V., A study of the effects of the lower index methods on ADAMS sparse tableau formulation for the computational dynamics of multi-body mechanical systems, Proc Instn Mech Engrs Vol 213 Part K, 1999, pp1-10

PATES, C., S., *et al*, *Coupled boundary and finite element method for analysis of composite structure-acoustic interaction problems*, SAE 951343, 1995

RAHENJAT, H., *Multibody Dynamics: Vehicles, machines and mechanisms*, Professional Engineering Publications and Society of Automotive Engineers (Co-publishers), July 1998.

PETRI, H., and HEIDINGSFELD, D., *The hydraulic torsion damper – a new concept for vibration damping in powertrains*, SAE 892477, 1989

PETRUSEVICH, A., I., *Fundamental conclusions from the contact-hydrodynamic theory of lubrication*, Izv.Uzbekist.FilAkad, 1951

RENNISON, D., and BULL, M., *On the modal density and damping of cylindrical pipes*, Journal of Sound and Vibration Vol 54, 1977

REYNOLDS, O., *On the theory of lubrication and its application to Mr Beauchamp Towers experiments*, Phil Trans Vol 177, 1886

RICHARDS, E.J., WESTCOTT, M., and JEYAPALAN, R., *On the prediction of impact noise: Part 1. Acceleration Noise*, Journal of Sound and Vibration Vol 162, 1979

RICHARDS, E.J., WESTCOTT, M., and JEYAPALAN, R., *On the prediction of impact noise: Part 2. Ringing noise,* Journal of Sound and Vibration Vol 65, 1979

RICHARDS, E.J., *On the prediction of impact noise: Part 3. Energy accountancy in industrial machines*, Journal of Sound and Vibration Vol 76, 1981

RICHARDS, E.J., and CUSCHERI, J.M., *On the prediction of impact noise: Part 4. Estimation of noise energy radiated by impact excitation of a structure*, Journal of Sound and Vibration Vol 86, 1983

RICHARDS, E.J., CARR, I., and WESTCOTT, M., *On the prediction of impact noise: Part 5. The noise from drop hammers,* Journal of Sound and Vibration Vol 88, 1983

RICHARDS, E.J., and CUSCHERI, J.M., *On the prediction of impact noise: Part 6. Distribution of acceleration noise with frequency, with application to bottle impacts*, Journal of Sound and Vibration Vol 90, 1983

RICHARDS, E.J., and LENZI, A., *On the prediction of impact noise: Part 7. The structural damping of machinery*, Journal of Sound and Vibration Vol 97, 1984

RICHARDS, E.J., and CARR, I., *On the prediction of impact noise: Part 10. The design and testing of a quietened drop hammer*, Journal of Sound and Vibration Vol 104, 1986

RICHARDS, E.J., and SUN, J.C., *Prediction of total loss factors of structures, theory and experiments*, Journal of Sound and Vibration Vol 103, 1985

RICHARDS, E.J., *The identification and systematic elimination of sources of noise from an experimental drop hammer*, Noise Control Engineering Journal Vol 23, 1984

ROOKE, G., CHAN, E., and CROSSLEY, P., *Computer modelling of a vehicle powertrain for driveability development*, I.Mech Eng Report C462/31/035, 1995

ROY, P. and GANESAN, N., *Transient response of a cantilevered beam subjected to an impulse load*, Journal of Sound and Vibration Vol 183, 1995

RYAN, R., R., *ADAMS multi-body system analysis software*, in Multibody Systems Handbook, Werner Schielen (Ed.), Springer-Verlag, 1990, pp. 361-402.

RYAN, R., R., and STEIGERWALD, M., F., *ADAMS: theory and application*, Proceedings of the 1988 ADAMS Software Theory Seminar, Mechanical Dynamics Inc., Ann Arbor, Michigan, 1988.

SAFA, M., M., A., and GOHAR, R., *Pressure distribution under a ball impacting a thin lubricant layer*, ASME Journal of Tribology, Vol 108, 1986

SANTIAGO, J., and WISNIEWSKI, H., *Convergence of finite element frequency predictions for a thin walled cylinder*, Computers and Structures, 1989

SHEARER, J., MURPHY, A., and RICHARDSON, H., *Introduction to system dynamics, Addison-Wesley Pubs*, 1967

SHOPE, W., ARDISANA, L., and MAZZOLA, S., *Aerostar powertrain and chassis isolation technology*, SAE 841695, 1984

SOI, A., and HERPE, F., V., *Numerical prediction of a whole car vibro-acoustic behaviour at low frequencies*, SAE 2001-01-1521, 2001

STEINEL,K., *Shuffle : Analysis and optimisation by measurement and computer simulation*. Fichtel and Sachs Test Report 910839. Internal Ford Motor Company Confidential Report,1990

STOKER, J., *Nonlinear vibrations*, InterScience Pubs, 1950

STRANG, G., and NGUYEN, T., *Wavelets and filter banks*, Wellesley-Cambridge Press 1995.

SZECHENYI, E., *Modal densities and radiation efficiencies of unstiffened cylinders using statistical methods*, Journal of Sound and Vibration Vol 19, 1971

TIMOSHENKO, S., P., and GOODIER, J., N., *Theory of Elasticity*, McGraw Hill 1934

TOBLER, W. and TSANGERIDES, M. *Dynamic behaviour of a torque convertor with centrifugal bypass clutch*, SAE 850461, 1985

TOBLER, W. *Modelling of ATX powertrain ; application to clunk and shuffle*. Ford Motor Company Internal Report 1983. Internal Ford Motor Company Confidential Report

TSANGERIDES, M., TOBLER, W., and HEERMAN, C., *Interactive computer simulation of drive train dynamics*, SAE 850978, 1985

VAFAEI, S., MENDAY, M. and RAHENJAT, H., *Transient High Frequency Elasto-acoustic Response of Vehicular Drivetrain to Sudden Throttle Demand*, Proc Instn Mech Engrs Vol 215 Part K, 2001, pp35-52

APPENDIX

ARRUNDALE, D, HUSSAIN, K, RAHNEJAT, H, and MENDAY, M, *Acoustic response of driveline pieces under impacting loads (clonk).* Proc. 31st ISATA, Dusseldorf, June 1998, pp319-331.

ARRUNDALE, D, RAHNEJAT, H, and MENDAY, M, *Multi-body dynamics of automobile drivelines: an investigation into the interaction between shuffle and clonk.* Proc 32nd ISATA, Vienna, Austria, June 1999, pp 397-405

CENTEA, D, RAHNEJAT, H, and MENDAY, M, *The influence of the interface coefficient of friction upon the propensity to judder in automotive clutches,* Proc. Inst Mech Engrs. Part D, Journal of Automotive Engineering, Vol. 213, 1999 pp 245-258.

FARSHIDIANFAR, A, EBRAHIMI, M, RAHNEJAT, H, and MENDAY, M, *High frequency torsion oscillation of vehicular driveline systems in clonk.* Heavy Vehicle Systems, Int Journal of Veh Design, Vol 9, No 2, 2002

FARSHIDIANFAR, A, RAHNEJAT, H, EBRAHIMI, M, and MENDAY, M, *Low frequency torsional vibration of vehicular driveline systems in shuffle.* In Multi-body Dynamics: Monitoring and Simulation Techniques (Ed H. Rahnejat), 2000 pp 269-282 (MEP Publications)

FARSHIDIANFAR, A, RAHNEJAT, H, EBRAHIMI, M, MENDAY, M, and MOAVENIAN, M, *Optimisation of the high frequency torsional vibration of vehicle driveline systems using genetic algorithms.* SAE 2001-01-1502

FARSHIDIANFAR, A, RAHNEJAT, H, EBRAHIMI, M, MENDAY, M, and MOAVENIAN, M, *Optimisation of the high frequency torsional vibration of vehicle driveline systems using genetic algorithms.* Proc Inst Mech. Engrs, Part K, Journal of Multi-body Dynamics Vol 216 2002. pp 249-262.

GNANAKUMARR, M, MENDAY, M, THEODOSSIADES, S, and RAHNEJAT, H, *Impact induced high frequency vibration of vehicular driveline systems with elasto-acoustic waves coincidence.*

MENDAY, M, *Torsional impact in an automotive vehicle driveline.* MSc Thesis, University of Bradford, 1997.

MENDAY, M, and M., EBRAHIMI, M., *The application of dynamic modelling using parametric design methods for an automotive driveline system.* Multibody Dynamics Monitoring and Simulation Techniques, MEP Publications, 1997

MENDAY, M, RAHNEJAT, H, and EBRAHIMI, M, *Clonk: an onomatopoeic response in torsional impact of automotive drivelines.* Proc. Instn. Mech. Engrs. Part D: Journal of Automobile Engineering Vol. 213 (D3), pp 349-357 1999.

MENDAY, M, and EBRAHIMI, M, *The application of dynamic modelling using parametric design methods for an automotive driveline system*, Proceedings of Inst Mech Engrs Conference on Multi-body dynamics Monitoring and Simulation Techniques, 1997. pp 67-69 (MEP Publications)

MENDAY, M, and RAHNEJAT, H, *Spectral resolution of highly coupled non-linear drive train elasto-acoustic vibration,* Proc ISATA-2000, Dublin, September 2000, pp 495-503.

RAHNEJAT, H., EBRAHIMI, M., and MENDAY, M., *The investigation of driveline clonk in a Ford Transit van,* Internal Ford Report, 1996

RAHNEJAT, H, KELLY, P, and MENDAY, M, *Powertrain refinement: A combined experimental and multi-body dynamics analysis approach.* Proc. 8th Aachener Kolloquium, Ika, Aachen, Germany, 4 – 6th October 1999.

VAFAEI, S, MENDAY, M, and RAHNEJAT, H, *Transient high frequency elasto-acoustic response of vehicular drive train to sudden throttle demand,* Proc Inst Mech Engrs, Part K, Journal of Multi-body Dynamics Vol 215, 2000

VAFAEI, S, RAHNEJAT, H, EBRAHIMI, M, and MENDAY, M, *Monitoring of impact induced high frequency vibrations in vehicular drive train systems,* Proc Int Conf. On Gearing, Transmission and Mech systems, Nottingham, 2000 PEP (I.Mech Eng), pp 853-860.